SEX DIFFERENCES IN THE PROGRESSION FROM CARDIAC HYPERTROPHY TOWARDS HEART FAILURE

Ph.D thesis

Myocardial Function Section, National Heart and Lung Institute, Imperial College London

Dr Hsiang-Yu Yang MD

Cardiovascular Surgery, Tri-Service General Hospital, National Defense Medical Center, Taipei, Taiwan, Republic of China

SUPERVISOR

Professor Kenneth T. MacLeod

Professor of Cardiac Physiology, National Heart and Lung Institute, Imperial College London

Abstract

This thesis aims to investigate differential changes in Ca^{2+} and Na^{+} regulation during the development from cardiac hypertrophy to heart failure (HF) between sexes. Clinical evidences show females are more resistant to the development of cardiac hypertrophy and have better survival in HF than males. Oestrogen is postulated to provide cardioprotection although this is still under debate. This work used guinea pigs (GPs), a species with electrophysiology akin to human, that were subjected to aortic constriction (AC) to study the progression from pressure-overload cardiac hypertrophy to HF between sexes. Selected female animals underwent ovariectomy (OVx), mimicking postmenopausal status, to examine the effects of long-term deprivation of ovarian hormones. The effect of oestradiol supplementation was also investigated.

Ventricular myocytes isolated from hearts at cardiac hypertrophy had prolonged action potential duration (APD), increased Ca^{2+} transient amplitudes and SR Ca^{2+} content, reduced Na^{+}/K^{+} ATPase (NKA) function and increased late sodium current ($I_{Na,L}$). Fractional shortening (FS) remained unchanged in these hearts. Compromised FS with detrimental Ca^{2+} handling, more reduced NKA function and enhanced $I_{Na,L}$ were noted at HF. Males showed earlier declined NKA function, more compromised FS and more detrimental Ca^{2+} handling than females at HF.

Ventricular myocytes from OVx animals showed increased L-type Ca^{2+} channel current with gating shifts and larger window current, larger Ca^{2+} transient amplitudes, greater SR Ca^{2+} content, and increased Ca^{2+} sparks and waves. OVx myocytes showed more early and delayed afterdepolarisations (EADs and DADs) with DAD-induced extrasystoles following β-adrenergic stimulation. AC with OVx GPs showed more reduced FS, more dysregulated Ca^{2+} handling, more reduced NKA function and larger $I_{Na,L}$ than AC females.

In conclusion, females were more resistant to pressure-overload. Long-term deprivation of ovarian hormones abolishes the slower onset of HF in females, and provides pro-arrhythmic substrates to females. Oestradiol supplementation offered protective effects on OVx GPs.

Table of Contents

Front matter

Declaration of Originality

All work and data presented in this thesis are my own work. Any contributions from others are clearly stated where applicable (Acknowledgements, page 13).

Copyright declaration

Acknowledgments

Firstly, I would like to thank my supervisor, Professor Ken T. MacLeod, for his full and kind support and supervision during the last four years. As an overseas student, I really appreciate his availability and open door policy that helped me a lot when I needed it. I would also like to thank my colleagues, Dr. Anita Alvarez-Laviada and Dr. Markus B. Sikkel who guided and helped me at the beginning of my Ph.D. Specific thanks to Dr. Alvarez-Laviada for helping me in the immunocytochemical staining and confocal imaging, and to Dr. Sikkel for offering me his self-coded ImageJ plugin for Ca^{2+} wave analysis which I think is a genius design. I would also like to thank Dr. Jahn M. Firth and Miss Alice J. Francis, who were new comers in our lab in the last year of my Ph.D, for their full support and help from every angle. Especially thank you to Dr. Firth for the experimental work for our scientific paper and the proofreading of my Ph.D thesis, which was not an easy task. A special thank you to Miss Francis for carrying out most of the Western blot work of Na^+/K^+ ATPase and phospholemman, which really helped me a lot. I would also like to thank my Cardiovascular Sciences BSc student Mr. Harishanan Surendran. We had a great time doing his BSc project together. His work was marked first place among his classmates and has made an important contribution to my Ph.D thesis and our Na^+/K^+ ATPase paper.

I am grateful to my boss in Taiwan, Professor Chien-Sung Tsai, for offering me the precious opportunity to study a Ph.D aboard. My deep thanks go to my father- and mother-in-law, for their wise advice and for believing in me.

The work is funded in part by the Taiwan government and the British Heart Foundation grant.

My Ph.D work is dedicated to my dear parents and sisters, for their sincere encouragement and giving without asking for any return in my life. Lastly, to my wife, Nancy. I could not live and study without her love and company here in London.

List of Figures

List of Tables

Abbreviations

AC	Aortic Constriction
ACTB	β-actin
ACOVx	Aortic Constriction combined with Ovariectomy
AHA	American Heart Association
AM	Acetoxymethyl ester
APD	Action Potential Duration
APD_{10}	Time to 10 % repolarisation of action potential
APD_{90}	Time to 90 % repolarisation of action potential
ATP	Adenosine Triphosphate
βAR	β-Adrenergic Receptor
BSA	Bovine Serum Albumin
BW	Body Weight
Ca	Calcium (refers to ionic form Ca^{2+} unless otherwise stated)
$[Ca^{2+}]_i$	Intracellular Ca^{2+} concentration
CaM	Calmodulin
CaMKII	Ca^{2+}/calmodulin-dependent protein kinase II
cAMP	cyclic Adenosine Monophosphate
CDI	Ca^{2+}-Dependent Inactivation
CHF	Congestive Heart Failure
CICR	Ca^{2+}-Induced Ca^{2+} Release
CPVT	Catecholaminergic Polymorphic Ventricular Tachycardia
CRU	Ca^{2+} Release Unit
*C*t	Cycle threshold
CVD	Cardiovascular Disease
D	Days
DAD	Delayed After Depolarisation
DAPI	4',6-diamidino-2-phenylindole
DHPR	Dihydropyridine Receptor
DMEM	Dulbecco's modified Eagle's Medium (solution)
DMSO	Dimethyl Sulfoxide
DTT	Dithiothreitol
E2	17β-oestradiol
EAD	Early After Depolarisation

ELISA	Enzyme-Linked Immunosorbent Assay
E-C	Excitation-Contraction
ECG	Electrocardiogram
E_m	Membrane potential
ES	Enzyme Solution
ER	Oestrogen Receptor
F	Female
FDHM	Full Duration at Half Maximal amplitude
F/F_0	Peak fluorescence in relation to baseline fluorescence
FKBP12.6	FK506 binding protein 12.6
FWHM	Full Width at Half Maximal amplitude
FS	Fractional Shortening
G	Conductance
GAPDH	Glyceraldehyde-3-phosphate Dehydrogenase
GPCRs	G Protein-coupled Receptors
GPER	G Protein-coupled Oestrogen Receptor 1
GP	Guinea Pig
HCM	Hypertrophic Cardiomyopathy
HEPES	*N*-2-hydroxyethylpiperazine-*N*'-2-ethanesulphonic acid
hERG	Human Ether-a-go-go Related Gene
HF	Heart Failure
HRT	Hormone Replacement Therapy
HW	Heart Weight
ID	Internal Diameter
I-V	Current-Voltage relationship
$I_{Ca,L}$	L-type Ca^{2+} channel current
I_{to}	Transient outward K^+ current
I_{K1}	K^+ current flows through the inward rectifying K channel $K_V7.1$
I_{Kr}	K^+ current flows through the channel $K_V11.1$, r for rapid
I_{Kur}	K^+ current flows through the channel $K_V1.5$, ur for ultra-rapid
I_{Ks}	K^+ current flows through the channel $K_V7.1$, s for slow
I_{Na}	Na^+ current
$I_{Na,L}$	Late Na^+ current
I_{NCX}	Na^+/Ca^{2+} Exchange current

$I_{to,f}$	Fast transient outward K^+ current
$I_{to,s}$	Slow transient outward K^+ current
I_p	Na^+/K^+ ATPase current
I/R	Ischaemic/Reperfusion
ISO	Isoprenaline
K	Potassium (refers to ionic form K^+ unless otherwise stated)
K_d	Dissociation constant
K_m	The Michaelis constant
KH	Krebs-Henseleit
LC	Low Ca^{2+} (solution)
LQTS	Long QT Syndrome
LV	Left Ventricle
L-VDCC	L-type Voltage-Dependent Ca^{2+} Channel
LVIDd	Left Ventricular Internal Diameter in Diastole
LVIDs	Left Ventricular Internal Diameter in Systole
LW	Lung Weight
M	Male
MAPK	Mitogen-Activated Protein Kinase
MI	Myocardial Infarction
mRNA	messenger RNA
Na	Sodium (refers to ionic form Na^+ unless otherwise stated)
$[Na^+]_i$	Intracellular Na^+ concentration
NCX	Na^+/Ca^{2+} Exchanger
NO	Nitric Oxide
NOS	Nitric Oxide Synthases
n/s	not significant
NT	Normal Tyrode's (solution)
NTA	Nitrilotriacetic Acid
OD	Outside Diameter
O.D.	Optical Density
OVx	Ovariectomy
OVx+E	OVx with 17β-oestradiol supplement
PBS	Phosphate Buffer Saline
PFA	Paraformaldehyde

PKA	Protein Kinase A
PLB	Phospholamban
PLM	Phospholemman
PLM-Ser^{68}	Phosphorylated phospholemman at Ser-68
PMCA	Plasma Membrane Ca^{2+} ATPase
PMSF	Phenylmethansulphonyl Fluoride
Pre-op	Pre-operation
PTFE	Polytetrafluoroethylene
PVDF	Polyvinylidene Difluoride
ROI	Region Of Interest
RT	Room Temperature
RVOT	Right Ventricle Outflow Tract
RyR	Ryanodine Receptor (refers to RyR2 unless otherwise stated)
RyR2	Ryanodine Receptor 2 (cardiac form)
sc	subcutaneous
SDS	Sodium Dodecyl Sulphate
SERCA	Sarcoplasmic/Endoplasmic Reticulum Ca^{2+} ATPase
SHR	Spontaneously Hypertensive Rat
SOICR	Store-Overload-Induced Ca^{2+} Release
SR	Sarcoplasmic Reticulum
R_{50}	Time from the peak to the 50 % amplitude
R_{90}	Time from the peak to the 90 % amplitude
τ	Tau (time constant)
TBST	Tris-Buffered Saline and Tween-20
TEA	Tetraethylammonium
TTP	Time-To-Peak
T-Tubule	Transverse Tubule
TTX	Tetrodotoxin
UK	United Kingdom
UW	Uterine Weight
VDI	Voltage-Dependent Inactivation
VPB	Ventricular Premature Beat
VT	Ventricular Tachycardia
WT	Wild Type

1 Introduction

1.1 Excitation-contraction coupling

Ca^{2+} plays an important role in cardiac excitation-contraction (E-C) coupling (the process from electrical excitation of the myocytes to contraction of the heart) and relaxation[1] (Fig. 1)[2]. Ca^{2+} influx occurs through L-type voltage-dependent Ca^{2+} channels (L-VDCC), which are located primarily at transverse tubules (T-tubules) and in close contact with the sarcoplasmic reticulum (SR). Ca^{2+} influx through L-VDCCs triggers Ca^{2+} release from the SR Ca^{2+} release channels, ryanodine receptors (RyRs), a process known as Ca^{2+}-induced Ca^{2+} release (CICR). This raises the intracellular Ca^{2+} concentration ($[Ca^{2+}]_i$), allowing Ca^{2+} to bind to the myofilaments and produce contraction. For relaxation to occur, $[Ca^{2+}]_i$ must be rapidly removed from the cytoplasm, causing Ca^{2+} dissociation from the myofilaments. Among the routes involved in the removal of Ca^{2+}, the sarcoplasmic reticulum Ca^{2+} ATPase (SERCA), sequesters Ca^{2+} into the SR, and the sarcolemmal Na^+/Ca^{2+} exchange (NCX) extrudes Ca^{2+} from the cell, contributing about 70 % and 25 % towards relaxation, respectively. This dynamic increase and decrease in $[Ca^{2+}]_i$ is generally referred to as the Ca^{2+} transient and in steady-state conditions, the amount of Ca^{2+} leaving the cell is equal to the amount entering. Ca^{2+} regulation is linked with Na^+ regulation via NCX. Positive membrane potentials and high $[Na^+]_i$ favour Ca^{2+} influx by reversing the mode of NCX which moves Na^+ out in exchange - so called reverse mode.

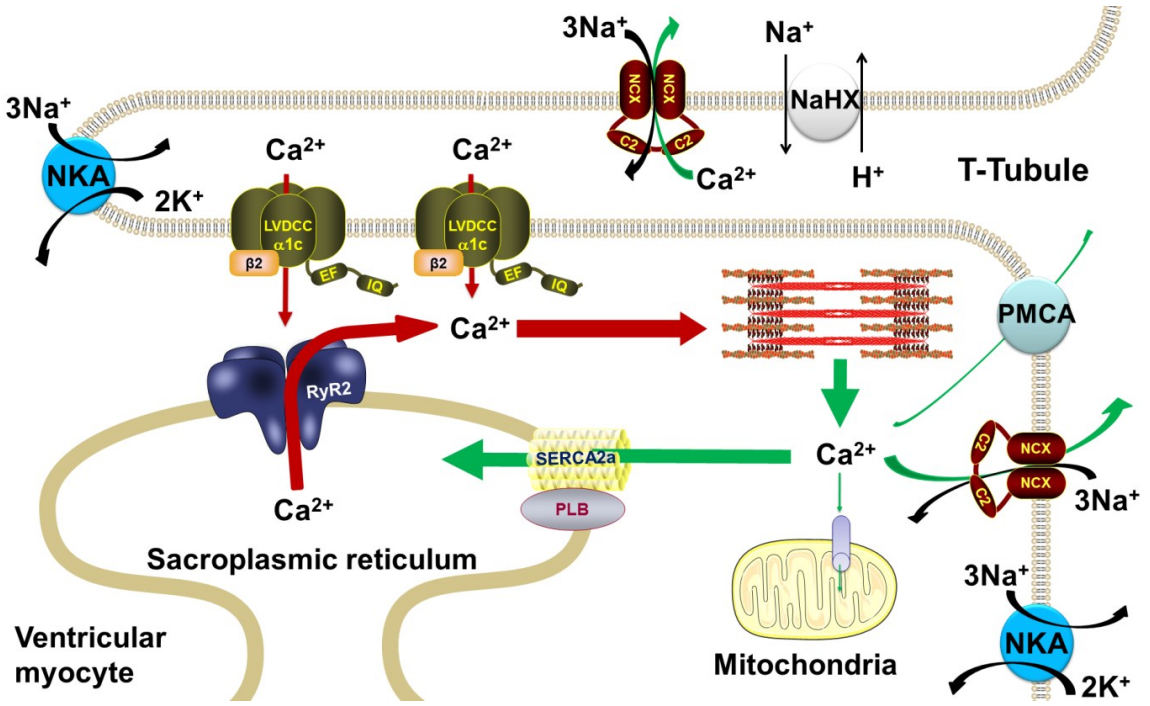

Figure 1-1. E-C coupling in a ventricular myocyte.

1.1.1 Action potential in ventricular myocytes

The action potential, determined by interactions of ion channels and transporters, initiates E-C coupling[1]. The shape of action potential represents the influx and efflux of mainly Na^+, K^+, Ca^{2+} and Cl^- ions mediated by ionic channels and transporters. The action potential in ventricular myocytes has a longer plateau phase than that in pacemaker cells or atrium cells[1].

The action potential in ventricular myocytes consists of 5 phases[3] (Fig. 1-2) with different major contributing currents (Table 1-1):

- Phase 4: resting potential.
- Phase 0: rapid depolarisation of the membrane potential.
- Phase 1: early rapid repolarisation producing a "spike" shape on the action potential.
- Phase 2: plateau phase marking the phase of Ca^{2+} entry.
- Phase 3: slow then rapid repolarisation that restores the membrane potential to its resting value to enter phase 4.

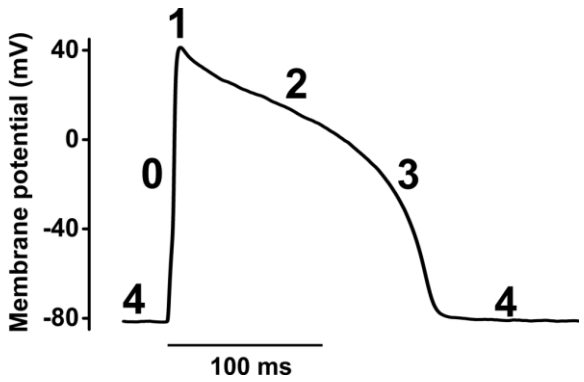

Figure 1-2. Action potential in a ventricular myocyte from GP.

The 5 phases of action potential in a ventricular myocyte from GP.

	Inward current		Outward current	
Phase 0	I_{Na}	Na^+ current	I_{NCX}	NCX outward current
Phase 1	$I_{Ca,L}$	Ca^{2+} current, L-type	$I_{to,f}$	Transient outward current, fast
			$I_{to,s}$	Transient outward current, slow
			I_{NCX}	NCX outward current
Phase 2	$I_{Ca,L}$	Ca^{2+} current, L-type	I_{Kr}	Delayed rectifier, fast
	I_{NCX}	NCX inward current	I_{Ks}	Delayed rectifier, slow
Phase 3	I_{NCX}	NCX inward current	I_{Kr}	Delayed rectifier, fast
			I_{Ks}	Delayed rectifier, slow
			I_{K1}	Inward rectifier
Phase 4	I_{NCX}	NCX inward current	I_{K1}	Inward rectifier

Table 1-1. Cardiac action potential major contributing ion currents in mammalian ventricular myocytes.

1.1.1.1 Phase 0

The rapid upstroke depolarisation in phase 0 is driven by Na^+ influx through Na^+ channels. The $Na_V1.5$ channel, encoded by the gene *SCN5A*, is the dominating Na^+ channel in the human heart, and is much less sensitive to block by tetrodotoxin, which blocks many neuronal Na^+ channels. The positive feedback of regenerative activation of Na^+ channel produces a very fast depolarisation. The depolarisation also inhibits I_{K1}, which sets and stabilise the rest membrane potential in the phase 4. The transient increase in Na^+ influx lasts only 1 to 2 ms. As the $[Na^+]_i$ and positive intracellular charges increase, the driving force for Na^+ decreases, so when the membrane potential reaches equilibrium potential of Na^+, there is no more Na^+ influx. However, Na^+ channels can also exhibit some persistent slow inactivation which would contribute to prolongation of APD[4]. Type 1 antiarrhythmic agents, including 1A: quinidine, procainamide, 1B: lidocaine, dilantin, mexiletin and 1C: flecanide, propafenone, which prolong, shorten or do not change APD, respectively, inhibit the cardiac Na^+ channel. Mutations in the gene that encodes the channel (*SCN5A*) are associated with long QT syndrome (LQTS), Brugada syndrome, primary cardiac conduction system disease, and dilated cardiomyopathy[5-7].

1.1.1.2 Phase 1

The phase 0 depolarisation is followed by a small and early repolarisation which is caused by inactivation of Na^+ channels and activation of transient outward K^+ currents, I_{to} ($I_{to\,1}$ and $I_{to\,2}$). I_{to} is the major contributor to this early repolarisation which also called the action potential "notch". Functionally, the early repolarisation in phase 1 contributes to increasing the driving gradient for Ca^{2+} into the cardiac myocytes. Atrial myocytes, rat and mouse ventricular myocytes have relatively larger I_{to}; and consequently, larger early repolarisation and shortening of their action potentials in comparison with the GP[8-10]. The I_{to} quickly inactivates and is also overcome by inward Ca^+ currents flowing through L-type and T-type Ca^{2+} channels. Reduction in I_{to} causes the notch to disappear in phase 1 and a more positive membrane potential in early phase 2, and usually a prolonged APD, which affects Ca^{2+} handling.

1.1.1.2.1 Ca^{2+} influx via Cardiac L-VDCC

The L-type voltage-dependent Ca^{2+} channels, which mediate Ca^{2+} influx, play an essential role in regulating APD and triggering myocyte contraction. The L-type Ca^{2+} channels (L stands for "L"ong lasting) are historically termed dihydropyridine receptors (DHPR) due to their sensitivity to various 1, 4-dihydropyridines, such as nifedipine (antagonist) and Bay K 8644 (agonist), which inhibit or enhance Ca^{2+} current through L-type Ca^{2+} channels.

1.1.1.2.1.1 Molecular characterization of cardiac L-VDCC

There are four protein subunits found to constitute the cardiac L-VDCC (α_1, α_2, δ and β). The α_1 subunit is the primary structure of the pore-forming element, which is composed of 4 repeating domains (I - IV), each with 6 transmembrane helices (S1 - S6). Four isoforms for the α_1 subunit have been identified: $Ca_v1.1$ (α_{1S}), 1.2 (α_{1C}), 1.3 (α_{1D}) and 1.4 (α_{1F}). The primary cardiac α_1 subunit isoform is α_{1C} and is highly expressed in cardiac muscle[11]. c-AMP mediated protein kinase A (PKA) phosphorylation of α_1 plays an important regulatory role. Several potential phosphorylation sites near the C terminal tail of α_{1C} by cAMP-dependent PKA have been discovered[12]. The β subunit of the channel complex has four isoforms (β_1 - β_4), is on the intracellular part of the protein and can be phosphorylated. The β_2 subunit is the main cardiac isoform[13]. It can interact with α_1 to modulate channel activity and gating[12]. Co-expression of β_2 and α_{1c} produces increased calcium currents with accelerated activation and inactivation of the channel[14].

1.1.1.2.1.2 L-VDCC regulation

β-adrenergic stimulation activates cardiac L-VDCC via a classic c-AMP/PKA-mediated channel phosphorylation pathway, in which the cAMP-dependent PKA is activated by increased cAMP concentration[11]. The β-adrenergic receptors (βAR) are G protein-coupled, and stimulate adenylyl cyclase (AC) to increase cAMP. The binding of cAMP to the regulatory subunit of PKA liberates the catalytic subunit of PKA to phosphorylate various substrates, including the cardiac L-VDCC. This PKA-mediated phosphorylation of cardiac L-VDCCs results in a 2 - 4 fold increase in basal $I_{Ca,L}$, and shifts the voltage-dependence of activation and inactivation of the L-type channel to more negative E_m[15,16]. The PKA-dependent phosphorylation of the α_{1C} pore-forming occurs at residue Ser-1928[17] and Ser-1700[18]. In addition, PKA phosphorylates the auxiliary β_2 subunit of the Ca^{2+} channel at three sites, Ser-459, Ser-478, and Ser-479[19].

The decay of $I_{Ca,L}$ during depolarisation is both Ca^{2+}- and voltage-dependent. In cardiac myocytes voltage-dependent inactivation (VDI) was thought to occur slowly and the Ca^{2+}-dependent inactivation (CDI) (resulting from CICR) provided an automatic negative feedback mechanism to limit Ca^{2+} entry and the contribution of $I_{Ca,L}$ to the action potential. Biphasic decay of $I_{Ca,L}$ in cardiac myocytes has been traditionally assigned to the separate processes of CDI (fast decay) and VDI (slow decay). CDI signalling is predominantly mediated by CaM binding to an IQ motif at the proximal C-tail of the α1c subunit of $Ca_v1.2$. However, there are studies reporting that rapid VDI inactivates $Ca_v1.2$ before CDI can become effective. Rapid VDI can be turned on by membrane depolarisation and can be turned off by β-adrenergic stimulation[20].

1.1.1.3 Phase 2

The long-lasting depolarised plateau in phase 2 is caused by a close balance between outward I_K (I_{Kr}, I_{Kr}, and I_{Ks})[21,22] and inward I_{Ca} (mainly $I_{Ca,L}$). I_{Kr} increases as repolarisation progresses, and I_{Ks} activates more slowly on depolarisation. Mutation in *hERG* or *KCNQ1*, the I_{Kr} and I_{Ks} coding genes respectively, cause congenital LQTS in human[21,23-25]. The Ca^{2+} influx via L-type Ca^{2+} channels initiates CICR from SR, triggering muscle contraction. Depending on the $[Na^+]_i$, the Ca^{2+} influx in the very early part of phase 2 can also be contributed by NCX. Phase 2 is terminated by a voltage- and Ca^{2+}/calmodulin (CaM)-dependent slow inactivation of $I_{Ca,L}$ combined with the simultaneous activation of K^+ currents. L-type Ca^{2+} channels will be discussed in later section.

1.1.1.4 Phase 3

Phase 3 represents the repolarisation from the plateau phase to the resting membrane potential. I_{Kr}, I_{Ks}, and I_{K1} mediate this repolarisation. I_{Kr} activates relatively slowly, but more rapidly than I_{Ks}, followed by a fast inactivation in the end of phase 3[26]. I_{Ks} opens at membrane potentials positive to -20 mV, and activates and inactivates very slowly. I_{K1} is important for setting the resting membrane potential and is responsible for shaping the final repolarisation of the action potential[27]. Ventricles with high I_{K1} expression have a resting potential of -80 mV, while the maximum diastolic potential in pacemaker cells which lack I_{K1} is about -50 mV. The NCX transports Ca^{2+} out of the cell creating an inward current (forward-mode) in phase 3 and phase 4. The NCX can also bring Ca^{2+} into the cell creating an outward current (reverse mode) in phase 0/1, and can expel Ca^{2+} out of the cell creating an inward current (forward-mode) in phase 2 and 3.

1.1.2 Ca^{2+} transient

Ca^{2+} transient is the dynamic increase and decrease of $[Ca^{2+}]_i$, consisting of CICR from SR and Ca^{2+} removal from cytoplasm by various transporters.

1.1.2.1 CICR

A microdomain architecture exists between the T-tubules and SR, constituting the so-called dyadic cleft that forms a highly efficient region for CICR. The SR Ca^{2+} release ryanodine receptor (RyR) is a homotetrameric channel that is situated in close proximity to adjacent L-VDCCs in the T-tubules, forming a functional Ca^{2+} release couplon. Ca^{2+} influx through L-VDCCs causes a local increase in $[Ca^{2+}]_i$ within the dyadic cleft micro-domain between L-VDCCs and RyRs. The Ca^{2+} influx activates and rapidly opens RyRs, inducing a large release of stored Ca^{2+} from the SR into the cytoplasm, termed CICR. In this way a small influx of Ca^{2+} produces an amplification of its signal and creates a large release of Ca^{2+} into the cytosol. If each couplon activates at the same time there is an efficient global (cell-wide) increase in cytosolic $[Ca^{2+}]$ that initiates cardiac contraction. The gain of the amplification

mechanism can be described as the amount of Ca^{2+} released from the SR divided by the amount of required Ca^{2+} entering through the L-VDCCs.

1.1.2.2 Removal of intracellular Ca^{2+}

The increased intracellular Ca^{2+} is removed from the cytoplasm by SERCA, NCX and other slower transporters such as the plasma membrane Ca^{2+} ATPase (PMCA) and mitochondria Ca^{2+} uniporter, causing Ca^{2+} dissociation from the myofilaments and subsequent muscle relaxation .

1.1.2.2.1 SERCA

SERCA is the major relaxation contributor, and generally accounts for about 70 % of relaxation although there are variations between species[28]. SERCA2a is the cardiac isoform, in which two Ca^{2+} ions are transported for each ATP consumed. In contrast to skeletal muscle SERCA, SERCA2a activity is modulated by a regulatory protein, phospholamban (PLB), which tonically inhibits the protein. The concentration of PLB is comparable to the concentration of the SERCA. PLB can be phosphorylated by PKA at Ser-16, which reverses the tonic inhibition of SERCA, thus increasing the SR Ca^{2+} uptake rate. PLB can also be phosphorylated by CaMKII and PKA at Thr-17 and Ser-10 to enhance or decrease the function of SERCA, respectively[29].

1.1.2.2.2 NCX

In cardiac myocytes, NCX is located mostly in the T-tubules. NCX can account for up to 30 % of the decay phase of the Ca^{2+} transient[30]. The "downhill" energy gradient provided by the high extracellular $[Na^+]$ allows the efflux of Ca^{2+} from the cell against its large electrochemical gradient. The stoichiometry of NCX is 3 Na^+: 1 Ca^{2+}. Thus, NCX is directly involved in the regulation of both intracellular Ca^{2+} and Na^+ and is sensitive to E_m. NCX operates in reverse-mode (ie Ca^{2+} in/Na^+ out when the membrane potential is more positive than its reversal potential. Usually, NCX works in forward-mode when membrane potential is more negative than the reversal potential. Both Ca^{2+} influx and Ca^{2+} efflux activate NCX transport dynamically. When $[Ca^{2+}]_i$ is relatively high, Ca^{2+}-dependent activation stimulates Ca^{2+} extrusion by NCX. However, Ca^{2+}-dependent activation can also stimulate greater Ca^{2+} influx via NCX when conditions favour this direction, such as higher $[Na^+]_i$[31], in which the increased Ca^{2+} influx via NCX could in turn increase SR Ca^{2+} content[32,33]. Although Na^+-dependent inactivation could prevent Ca^{2+} influx via NCX, the mechanism requires very high $[Na^+]_i$ to observe, which rarely occurs in physiologically-relevant conditions[34].

1.1.3 Ca^{2+} sparks and waves

Ca^{2+} sparks are visualised microscopic Ca^{2+} release events that occur generally at couplons and arise through the spontaneous or triggered release of Ca^{2+} from RyRs. Sparks were first observed by Cheng *et al*[35] and, although still the subjects of fierce debate, are thought to represent the combined

openings of several RyRs. The number of RyRs in a cluster act in unison to constitute the functional unit of Ca^{2+} release (the so-called Ca^{2+} release unit (CRU)). These CRUs create the "building block" of E-C coupling because their combined activation produces a synchronised global release of Ca^{2+} - the Ca^{2+}-transient.

For reasons that are unclear at present, clusters of RyRs can activate in unsynchronized ways and cause local increases in $[Ca^{2+}]_i$ that, under certain conditions, cause CICR from neighbouring CRUs which propagate through the cells rather like a cluster bomb eventually forming Ca^{2+} waves. The amount of Ca^{2+} release during a Ca^{2+} wave may induce sufficient inward current via the activation of Ca^{2+}-sensitive currents, particularly forward-mode NCX. These currents produce delayed afterdepolarisations (DADs) of the cardiac cell membrane that may produce triggered beats under certain conditions[36]. Alterations in RyR function can affect the occurrence of spontaneous Ca^{2+} release and the propagation of Ca^{2+} waves, promoting triggered arrhythmias. Mechanisms including hyperphosphorylation of RyRs by PKA or CaMKII and regulation of RyRs at luminal or cytoplasmic sites have been reported to alter RyR function[37-40]. The frequency of spontaneous Ca^{2+} sparks and waves may increase when the SR Ca^{2+} is overloaded[41]. Excessive SR Ca^{2+} load is proposed to alter RyR2 Ca^{2+} sensitivity at luminal regulatory sites[38] or directly at the store-sensing gate in RyR2[39], and underlies a potentially arrhythmic mechanism termed store-overload-induced Ca^{2+} release (SOICR)[42].

1.1.4 Na^+/K^+ ATPase

1.1.4.1 Subunits and isoforms

The Na^+/K^+ ATPase is composed of three subunits, α, β, and ϒ[43] (Fig. 1-3). The α subunit is a 10 transmembrane α-helix structure, containing binding sites for Na^+, K^+, ATP and cardiac glycosides. The smaller β subunit spans the membrane only once and forms a large extracellular structure that sits on top of the external surface of the α subunit. The β subunit helps the insertion and stabilisation of the pump in the membrane, and facilitates ion-binding and transport. The ϒ subunit is one of the FXYD family proteins (FXYD1). This regulatory protein affects the Na^+ affinity of Na^+/K^+ ATPase. The α-subunit has 4 isoforms, namely α1, α2, α3, and α4. The β subunit has 3 isoforms, β1, β2 and β3. Table 1-2 shows species variation of Na^+/K^+ ATPase α-subunit isoform expression. Human heart expresses α1, α2 and α3 isoforms, together with the β1 isoform of the β subunit[44]. Rat heart expresses α1, α2 and α3 isoforms (α1 and α3 in neonatal rat, and α1 and α2 in adult rat) but GP and mouse hearts express α1 and α2 isoforms[45,46]. In dog hearts, the α1 and α3 isoforms are present[44]. In humans the α1, α2, and α3 isoform ratio is 55 - 62 % : 15 - 18 % : 23 - 27 %, respectively[32,47]. In GP, the α1 and α2 ratio is 50 - 82 % : 18 - 50 %[32,45]. The α1 isoform has been reported to be evenly distributed over the sarcolemma, while α2 isoforms have been shown to be more localised in the T-

tubules[48,49]. Both α1 and α2 have been suggested to be co-localised with NCX[50,51], which may indicate that α1 or α2 isoforms can locally regulate the function of NCX by modulating the local $[Na^+]$.

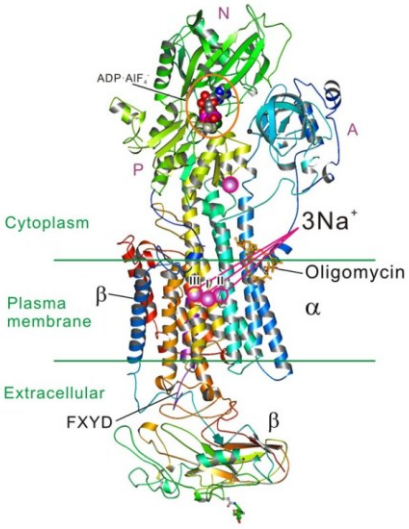

Figure 1-3. Crystal structure of the Na^+/K^+ ATPase.

The Na^+/K^+ ATPase consists of α- and β- subunits, and a FXYD protein. Three Na^+ ion-binding sites (I-III) are identified in the transmembrane region (Toyoshima et al, 2013).

	α1	α2	α3
Human	✓	✓	✓
Guinea pig	✓	✓	
Dog	✓		✓
Rat (adult)	✓	✓	
Rat (neonatal)	✓		✓
Mouse	✓	✓	

Table 1-2. Species variation of Na^+/K^+ ATPase α subunit isoform expression.

1.1.4.2 Function of Na^+/K^+ ATPase

The Na^+/K^+ ATPase maintains the ionic gradients of Na^+ and K^+ across the myocyte surface membrane that determine the resting membrane potential by pumping Na^+ out of cell and K^+ into cell against their concentration gradients. The coupled movement of the ions occurs with a stoichiometry of $3Na^+:2K^+$ and an energy consumption of 1 molecule of ATP. The Na^+/K^+ ATPase is therefore not electroneutral because each cycle produces a net outward positive charge that creates a pump current. The main regulators of Na^+/K^+ ATPase are $[Na^+]_i$ and $[K^+]_o$. The activating K_ms for $[Na^+]_i$ and $[K^+]_o$ are about 10 mM and 1.5 mM, respectively. With 6 mM $[K^+]_o$ or 30 mM $[Na^+]_i$, the Na^+/K^+ ATPase is almost maximally activated[52-55]. Inhibition or reduction of the Na^+/K^+ ATPase leads to an accumulation of $[Na^+]_i$.

1.1.5 Transverse tubules

T-tubules are highly branched invaginations of the sarcolemma, which are rich in ion channels and transporters and account for up to 21 - 33 % of total sarcolemma area[56]. The T-tubules penetrate from sarcolemma deep into the centre of the cell, which develop around myofilaments, anchoring to Z-discs through costameres[57]. These structures not only run in the transverse direction (perpendicular to myocyte longitudinal edges) but stretch in the axial direction[58] leading to the term transverse-axial tubular system (TATS)[59]. Soeller *et al* reported the ratio between transverse and axial elements is up to 60 to 40 %[60]. Organised T-tubules structure is critical for normal E-C coupling and cardiac function[61]. L-type Ca^{2+} channels are located primarily on T-tubule membrane, which are in close proximity to the RyRs on the SR terminal cisternae, forming dyadic cleft where CICR takes place.

T-tubule invaginations are not only formed by straight and smooth sarcolemma but have layered membrane microfolds[62]. The BIN1, a membrane scaffolding protein, generated microfolds, which are mainly located at the neck of the T-tubules. The BIN1-dependent microfolds are enriched with L-type Ca^{2+} channel-RyRs dyads, which imply the role of BIN1 in organising cardiac dyads[63]. Caveolae, organised by the plasma membrane binding protein caveolin-3, are flask-shaped membrane invaginations, which are found in sarcolemma and also in T-tubules at the neck. It has been postulated that caveolae may not only be developmental precursors of T-tubules but were critical in concentrating β_2AR signalling for the reason that β_2ARs were reported to localise predominantly in caveolae[64]. The T-tubules structure also plays an important role in Ca^{2+} removal from the cytoplasm. Another membrane scaffolding protein, ankyrin B, has been reported to be essential in the formation of the complex of Na^+/K^+ ATPase, NCX and inositol trisphosphate receptor (InsP3). Within T-tubules, Na^+/K^+ ATPase co-localises with NCX at the ankyrin B microdomains, contributing to the regulation of CICR by removing Ca^{2+} from the luminal clefts between the T-tubules and junctional SR membrane through NCX, facilitating Ca^{2+} transient decay during muscle relaxation[65].

1.2 E-C coupling in cardiac hypertrophy and HF

HF remains a leading cause of death among an aging population worldwide, especially in industrialised nations[66]. The estimated prevalence of HF in people > 45 years old is 2.2 % and 8.8 % in a population > 65 years old[67]. The median survival following diagnosis with HF is less than 3 years, and 5-year survival is only 32 % in patients with systolic dysfunction and 35 % in patients with HF but with preserved ejection fraction[67]. Generally, there are two fatal pathways in patients with heart failure: 1) pump failure due to progressive decline in contractility and 2) sudden cardiac death due to arrhythmias[68]. The underlying causes of HF are gradually being pieced together but are still not well

understood. The failing heart attempts to compensate for its poor function by various mechanisms, such as increasing the size of its myocytes producing myocardial hypertrophy, increasing its filling pressure, and enhancing whole body neurohumoral signals. Cardiac hypertrophy can be initially viewed as an adaptive process, maintaining strength of contraction, and allowing the cardiac output to meet the needs of the body. For unclear reasons the hypertrophy response becomes inadequate and the heart enters a decompensated stage that signals the progression towards HF[69]. The signalling pathways involved in the hypertrophic remodelling response include mitogen-activated protein kinase (MAPK) pathways[70] and calcineurin pathways[71]. The hallmark features of HF are mechanical dysfunction and arrhythmias, in which defective E-C coupling plays a crucial role.

1.2.1 Remodelling of electrophysiology in hypertrophy and HF

1.2.1.1 Prolongation of APD leading to arrhythmogenesis

Prolongation of the APD has been widely shown in both human and animal models of cardiac hypertrophy and HF[72-78]. The changes in action potential profile result from alterations in the functional expression of inward and outward currents. Therefore, increases in inward currents, such as $I_{Ca,L}$, $I_{Na,L}$ and I_{NCX}, promote the prolongation of the APD. On the contrary, a reduction in outward currents, including I_{to}, I_{kr} and I_{K1}, can also contribute to the prolongation of APD[79]. Increased inward NCX current may occur in response to an increased $[Ca^{2+}]_i$ and decreased Ca^{2+} uptake of SERCA in HF[80], which contribute to prolongation of APD and is related to arrhythmogenesis.

There is good evidence for enhanced $I_{Na,L}$ in HF and prolongation of APD, which we will discuss in a later section. EADs, a pro-arrhythmic substrate, are likely to develop with prolonged APD due to the long action potential plateau favouring reactivation of Ca^{2+} channels[81]. Decreased density of I_{to} plays an important role in the prolongation of APD in cardiac hypertrophy and HF[82]. Reduced I_{to} also results in reduced phase 1 early repolarisation, which in turn decreases the driving force for Ca^{2+} influx. However, there is species variation of the density of I_{to}. While mice and rats have noticeable I_{to}, human, dog and GP have smaller I_{to}, which may have a relatively small effect on APD in HF. I_{K1} is responsible for shaping the final repolarisation of the action potential. While decreases in I_{K1} may contribute to action potential prolongation, it would be mainly in the very late phase of final repolarisation. Since the I_{K1} play an important role in stabilising rest membrane potential, alteration of I_{K1} may increase the probability of arrhythmogenesis[27].

1.2.2 Na^+ and Ca^{2+} homeostasis in hypertrophy and HF

1.2.2.1 Ca^{2+} handling in cardiac hypertrophy and HF

Dysregulation of Ca^{2+} is the basis of contractile dysfunction and arrhythomogenesis in HF (Fig. 1-4). Smaller Ca^{2+} transients contribute to systolic dysfunction in HF. Studies have reported that reduced SR Ca^{2+} content may be responsible for the decline in Ca^{2+} transient size, because the triggered L-type Ca^{2+} current has been generally found to remain unaltered[83-85] though there are some studies that do not fit this consensus[86]. There are three major possible factors that may explain a reduction in SR Ca^{2+} content in HF: (a) reduced SERCA function, (b) increased expression and function of NCX, and (c) enhanced diastolic SR Ca^{2+} leak. Studies show varied relative contributions of each factor[87,88]. While NCX was shown to be unaltered or up-regulated in HF studies[89-91], the most consistent finding is a down-regulation of the SERCA.

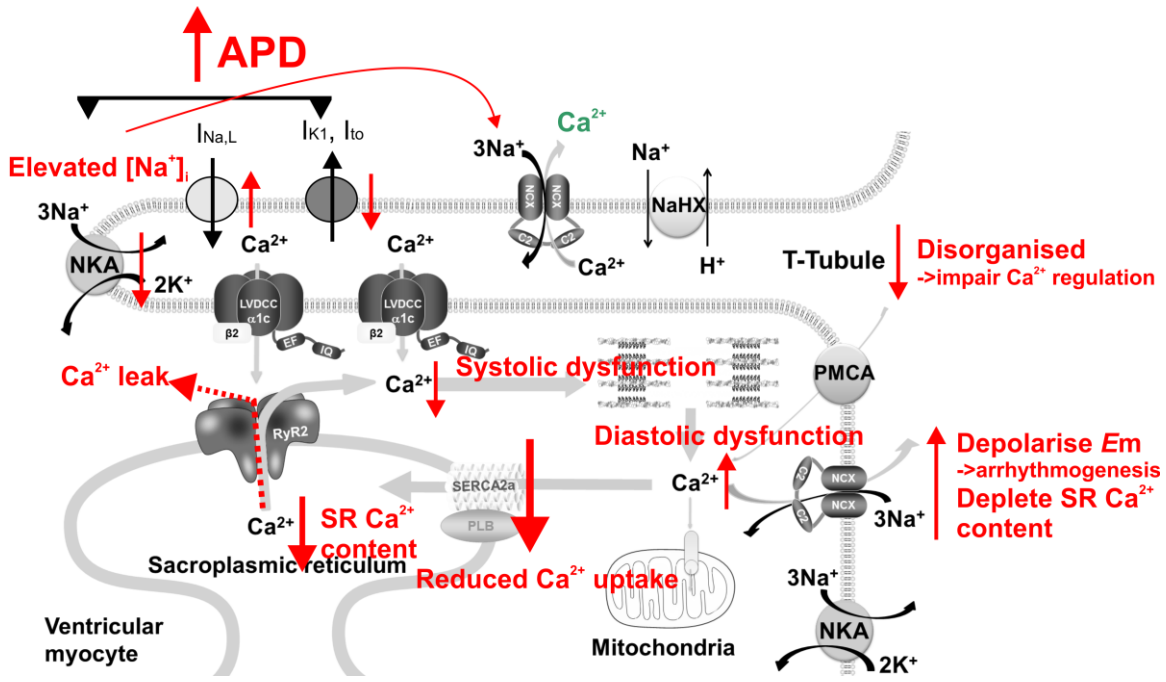

Figure 1-4. Dysregulation of Ca^{2+} handling in HF.

In early HF, elevated $I_{Na,L}$ not only contributes to the prolongation of APD but may increase Ca^{2+} influx via NCX. The reduced function of SERCA and increased Ca^{2+} leak from RyR2 can lead to depletion of SR Ca^{2+} content and reduced Ca^{2+} transient, causing systolic dysfunction. Diastolic dysfunction results from inefficient Ca^{2+} removal from cytoplasm. The elevated $[Ca^{2+}]_i$ is attributed to reduced Ca^{2+} uptake by SERCA and Ca^{2+} leak into cytoplasm from SR. Up-regulated NCX transports the excess $[Ca^{2+}]_i$ out of cell, which causes further depletion of SR Ca^{2+} and depolarisation of the membrane potential, leading to arrhythmogenesis.

1.2.2.1.1 Reduced SERCA function

The expression and function of SERCA, and its mRNA are decreased in most animal HF models[92-95]. The SERCA mRNA, however, was found to be unaltered or even up-regulated in cardiac hypertrophy followed by down-regulation in HF, and this switch may mark the transition from hypertrophy to HF[95,96]. Not only may the SERCA protein itself be down-regulated but there is also evidence suggesting that the amount of its regulatory protein phospholamban may be diminished or its phosphorylation state reduced in HF[92,97]. The reduced SERCA function slows the Ca^{2+} transient decay and myocyte relaxation and this poor function can be rescued by adenoviral gene transfer of SERCA into myocytes. This increases SERCA expression and the result is an acceleration of Ca^{2+} reuptake and myocyte relaxation[94,98,99]. Modifying cellular Ca^{2+} regulation by overexpressing SERCA also reduces ventricular arrhythmias[100] and improves haemodynamic, echocardiographic and molecular biology assessments of cardiac function[94].

Rescuing SERCA function has been achieved by adenoviral gene transfer of SERCA into cardiac myocytes isolated from failing human hearts and into whole hearts *in vivo* and this therapy underwent phase II clinical trials[99]. However, the phase IIb trial did not confirm the beneficial clinical outcomes that were initially reported in phase I trial[101]. While the exact reason for this outcome is not fully understood, further studies are required, including assessing the efficiency of intracoronary delivery of the AAV1 vector, which may not have resulted in efficient transduction of cardiomyocytes[101,102].

1.2.2.1.2 Roles of NCX in HF

Increased NCX mRNA has been reported in rodent models of HF and in human HF[84,87,103] and there is evidence of increased expression of the exchange protein[104-106]. As detailed earlier, when $[Na^+]_i$ is elevated, the amount of Ca^{2+} influx increases through reverse-mode NCX, which can improve the cellular and SR Ca^{2+} content and result in larger Ca^{2+} transients and therefore enhanced contractility[31]. However, in the face of poor SERCA function in HF the SR loading effect may be compromised leading to an increase in cytosolic $[Ca^{2+}]$. If NCX increases in amount this may exacerbate the formation of large delayed after-depolarisations and intensify pro-arrhythmic events.

1.2.2.1.3 Ca^{2+} leak from the SR

Diastolic SR Ca^{2+} leak contributes to depletion of SR Ca^{2+} content in HF[107]. The hyperadrenergic state in failing hearts may cause RyR2 hyperphosphorylation at Ser-2808 via the PKA pathway[108], resulting in dissociation of the FK-506 binding protein (FKBP12.6) which stabilises RyRs in the closed state. As a result, the open probability of RyRs increases, augmenting the normal random spontaneous SR Ca^{2+} leak from RyRs during diastole[109]. Increased SR Ca^{2+} leak can also result from phosphorylation of

RyR2 at Ser-2814 by CaMKII, a kinase that can be activated by an increase in diastolic $[Ca^{2+}]_i$. CaMKII blockade was shown to reduce SR Ca^{2+} leak and increase SR Ca^{2+} content in a HF rabbit model[110].

1.2.2.2 Na^+ regulation in cardiac hypertrophy and HF

Both down-regulated Na^+/K^+ ATPase and increased $I_{Na,L}$ have been shown in HF[68,111-113]. The combination of these changes will tend to increase $[Na^+]_i$ and may decrease Ca^{2+} efflux (or increase Ca^{2+} influx) via NCX and result in an increased SR Ca^{2+} content in early stage of HF[33]. An increase in $[Na^+]_i$ is a general finding associated with cardiac hypertrophy[114,115] and HF[116-119]. Na^+/K^+ ATPase inhibitors like cardiac glycosides have a positive inotropic action on cardiac muscle. Indeed, glycosides like digoxin were the among the earliest treatments for the failing heart following the work of Withering[120,121] who, in 1785, described the advantages of administering extracts of the foxglove, *digitalis purpurea*, to patients with HF. However, as described earlier in this chapter, an increase in $[Na^+]_i$ may also encourage the formation of DADs and so the ventricular cell is presented with an interesting predicament in which an increase in $[Na^+]_i$ can provide compensatory support for contraction yet encourages the evolution of a pro-arrhythmic substrate.

1.2.2.2.1 Na^+/K^+ ATPase

1.2.2.2.1.1 Expression and function of Na^+/K^+ ATPase in HF

There is little consensus about what happens to protein expression of Na^+/K^+ ATPase isoforms in HF. The expression of α1, α3 and β1 isoforms appears to be reduced in human HF[90] while the mRNA coding for the α1, α2, and α3 isoforms remains unaltered[122]. The α1, α2, and α3 isoforms also showed reduced expression in myocytes from a HF rabbit model[123]. In contrast in rat HF models, α1 isoform protein was unaltered as was the amount of its mRNA, but both α2 mRNA and protein expression were found to be reduced by about 50 %[32]. In a GP abdominal AC cardiac hypertrophy and HF model, α1 isoform mRNA and protein expression were unchanged at the hypertrophy stage[124]. Conversely, α2 isoform mRNA and protein expression increased at the hypertrophy stage, but then declined in HF compared with the hypertrophy stage[124].

A limited number of functional studies have been carried out. No significant changes in current and Na^+ extrusion rate were found in a HF rabbit model[116] and in a compensated hypertrophy dog model[125], but a decrease in Na^+/K^+ ATPase current was seen in a MI rat model[126]. Smaller Na^+/K^+ ATPase current, resulting mainly from a reduced current carried by the α2 isoform, was shown in a SERCA2 gene knockout mice HF model[127]. Reduced Na^+/K^+ ATPase current with unaltered pump protein expression was found in an AC cardiac hypertrophy mouse model[128]. However, it is difficult to directly correlate biochemical findings with Na^+/K^+ ATPase function because Western blotting methods cannot determine differences between functional and inactive Na^+/K^+ ATPase[89].

Furthermore, the function of the Na^+/K^+ ATPase may affected by phospholemman (PLM) protein expression or its phosphorylation status.

1.2.2.2.1.2 PLM

While the PLM regulation mechanism in HF is still not fully understood, hypophosphorylation of PLM was found in a mouse HF model and in human HF, resulting in inhibition of Na^+/K^+ ATPase and reduced Na^+/K^+ ATPase current with elevated $[Na^+]_i$ while the expression of Na^+/K^+ ATPase remained unaltered[128,129]. Expression of PLM was reduced together with higher fraction of phosphorylated PLM and reduced Na^+/K^+ ATPase expression in human HF and a rabbit HF model[123]. In this study the authors concluded that the reduced Na^+/K^+ ATPase expression in HF may be functionally offset by lower inhibition by PLM which resulted from reduced PLM expression and higher PLM phosphorylation.

1.2.2.2.2 Late Na^+ current

Persistent or late Na^+ current ($I_{Na,L}$) is a small component of I_{Na} that flows during the plateau of the action potential and contributes to prolongation of the APD[130]. It is caused either by a different form of Na^+ channel or the same $Na_v1.5$ form that inactivates with slower kinetics, or even reopens[4]. Although these channels carry a small inward Na^+ current (usually less than 1 % of the peak I_{Na}), this persists during the plateau phase so that the integral of the current is of similar value to the brief peak I_{Na}[131]. Importantly, the long persistence characteristic of $I_{Na,L}$ allows a substantial contribution of Na^+ influx throughout the action potential that is sufficient to prolong APD when $I_{Na,L}$ enhances.

$I_{Na,L}$ is found to be increased in several cardiac pathological conditions including ischaemia/reperfusion (I/R), myocardial infarction (MI), and HF[111,112,132-134]. The prolonged plateau of the action potential may allow more Ca^{2+} influx via L-type Ca^{2+} channels[111,135] because the longer time the E_m stays depolarised, the higher likelihood are the L-type Ca^{2+} channels to activate or reactivate, hence allowing more Ca^{2+} influx[136,137]. As discussed earlier in this chapter, the elevated $[Na^+]_i$ may cause more Ca^{2+} influx via NCX. Therefore, in a way, it could be inotropic. However, $I_{Na,L}$ was found to contribute to accumulation of $[Ca^{2+}]_i$, which could be arrhythmogenic[21,138], causing more pro-arrhythmic events in chronic HF[134,139].

Coppini and coworkers[140] investigated electromechanical dysfunction of ventricular myocytes from hypertrophic cardiomyopathy (HCM) patients, and proposed that $I_{Na,L}$ may also play a major role in modulating CaMKII pathways, causing alterations in Ca^{2+} handling in those HCM patients. However, alternatively, CaMKII can phosphorylate Na^+ channel to regulate the magnitude, and other properties, including $I_{Na,L}$ inactivation and recovery from inactivation[141]. Some potential CaMKII

phosphorylation site has been reported in the $Na_v1.5$ DI-DII linker, Ser-571[142,143]. Alterations in Ca^{2+} regulation can be partially reversed by inhibiting the $I_{Na,L}$ using ranolazine, which eliminates $[Na^+]_i$ overload and thus may shorten the APD and reduce enhanced reverse-mode NCX which contributes to intracellular Ca^{2+} overload. Ranolazine is a selective $I_{Na,L}$ inhibitor although it was found to have inhibition effect on other currents, including $I_{Ca,L}$ (IC_{50}=296 μM) and I_{kr} (IC_{50}=11.5 μM)[144].

1.2.2.3 Na^+ and mitochondrial function

The potential aggravating effects of increased $[Na^+]_i$ are not limited to sarcolemmal ion movements. O'Rourke and others have demonstrated that such increases affect mitochondrial function[145,146]. Increases and decreases in myocyte cytoplasmic Ca^{2+} are mirrored in changes of mitochondrial matrix Ca^{2+} ($[Ca^{2+}]_m$). Increases in $[Ca^{2+}]_m$ activate dehydrogenases and phosphorylation enzymes and match cell respiratory capacity and oxidative phosphorylation to energy requirements on a beat-to-beat basis. Mitochondrial Ca^{2+} homeostasis is a balance of Ca^{2+} influx through the mitochondrial uniporter and efflux through the mitochondrial NCX. An increase in cytoplasmic (extramitochondrial) $[Na^+]$ causes a decrease in $[Ca^{2+}]_m$ and reduces oxidative phosphorylation during periods of increased work. Energy production is limited, with net oxidation of NADPH and increases in intracellular reactive oxygen species that contribute to cell damage[145-148]. In an animal model of HF, inhibiting the mitochondrial NCX preserved cardiac function, slowed the hypertrophic remodelling and halted the increase in mortality from sudden cardiac death[149]. It is also important to note that ACE inhibitors, drugs with established benefit in the treatment of HF[150], stimulate the Na^+/K^+ ATPase by an unknown mechanism[151] and lower $[Na^+]_i$.

1.2.3 T-tubule remodelling

Maron *et al* identified irregularly shaped or dilated T-tubules in hypertrophied cells and loss of T-tubules in degenerating cells from human hypertrophied cardiomyocytes[152]. Ion channels, transporters and signalling molecules at T-tubules are reported to be either reduced or redistributed elsewhere to non-T-tubule sarcolemma. For example, the remodelling of T-tubule organisation alters the spatial relationship between L-VDCCs and RyRs, leading to decreased E-C coupling efficacy and increased dyssynchrony of SR Ca^{2+} release. Generally, there are four common characteristics of T-tubule alterations: (1) loss of T-tubules; (2) disorganisation of T-tubule network; (3) a decrease in transverse elements and an increase in longitudinal elements; and (4) T-tubule dilation[61]. The T-tubule system undergoes progressive deterioration from compensated hypertrophy to advanced HF. In other words, remodelling of T-tubule may be an early event driving cardiac hypertrophy towards failure. Furthermore, T-tubule integrity highly correlates with cardiac ejection fraction[61,153]. While Junctophilin-2 (JP2), BIN1, caveolin-3, telethonin (Tcap) have been implicated in formation or

remodelling of T-tubules[61,154-156], the roles of these proteins in cardiac T-tubule development and pathogenesis are not fully understood and remain to be determined (Fig. 1-5).

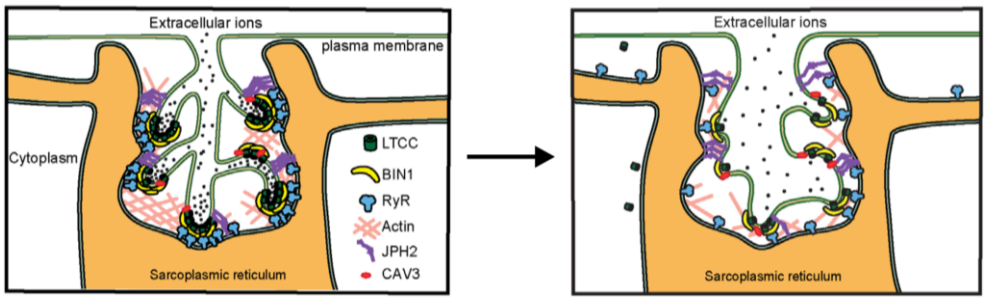

Figure 1-5. T-tubule remodelling.

Remodelling of T-tubule may be associated with reduction of JP2, BIN1 or caveolin-3 (Fu et al, 2017).

1.3 Sex differences in HF

1.3.1 Clinical manifestation between sexes

Sex disparities appear in clinical data describing (a) the progression of cardiac hypertrophy towards HF, (b) outcomes after MI, and (c) outcomes after valve replacement[157,158]. In HF particularly, differences in clinical course, aetiology and function of the left ventricle between men and women have been described. Data from the Framingham heart study show that the age-adjusted incidence of HF is higher in men compared with women, as is the prevalence at the ages of 40 - 59 and 60 - 79 years (1.9 % versus 0.8 % and 9.0 % versus 5.4 %, respectively)[159]. However, the prevalence of HF is similar in both sexes over the age of 80 years (11.5 % versus 11.8 %)[159]. In studies including the Euro Heart Failure Survey systolic HF was found predominantly in men, whereas more women presented with HF with preserved ejection fraction[160-163]. Furthermore, women tended to have HF with preserved left ventricular function almost twice as often as that of men[161]. The distribution of risk factors for HF differs between sexes and these may play a part in producing different outcomes. Men with HF have more coronary artery disease and dilated cardiomyopathy, whereas in women, hypertension, diabetes and valvular heart diseases are the most prevalent risk factors[164-166]. Women appear to have better survival than men, but the reasons are not entirely clear[167-170]. Women were also less likely to be admitted to cardiology wards, or have an assessment of left ventricular function[167]. The Framingham study showed that the prognosis in women is significantly better than in men after the onset of HF[171]. In advanced HF, females still have a mortality advantage[172]. It remains a challenge for all clinicians to ensure suitable treatment for men and women with HF. Therefore, it is important that clinicians are aware of the differences between sexes while managing

men and women with HF. Male and female patients respond to HF treatment with variations; therefore, sex based treatments are gaining attention[157,165,173,174].

1.3.2 Ovarian hormones and cardiovascular disease

The mechanisms behind sex differences during the progression towards HF are still not fully understood. Some evidence suggests that oestrogen is linked to cardiovascular protection in premenopausal women[175-178]. The incidence of cardiovascular disease, including HF, increases dramatically after menopause[158,179]. Postmenopausal women are much more vulnerable to arrhythmia-related sudden cardiac death compared with premenopausal women[180,181]. Premenopausal women with ventricular premature beats (VPBs) which mostly originate from the right ventricle outflow tract (RVOT), showed a decrease in beat frequency near the period of ovulation when serum oestradiol reaches its peak[182]. Furthermore, postmenopausal women who have idiopathic outflow tract ventricular arrhythmia had lower serum oestradiol levels than postmenopausal women without such arrhythmia, and the occurrence of ventricular arrhythmia events was lower in women with oestrogen replacement[183].

Studies have shown dysregulation of cellular Ca^{2+} handling following ovariectomy (OVx), which is rescued by oestrogen supplementation[184-186]. An ovariectomised rat model showed increases in susceptibility to adrenaline-induced arrhythmias compared with gonad-intact female animals[187]. The above evidence suggests a cardioprotective role of oestrogen while deprivation of female sex hormones may be linked to arrhythmogenesis.

There are studies that have investigated the effects of ovarian hormones on cardiac contractility. Two OVx rats studies showed an increase in contractility in the OVx groups after 3 - 6 weeks of steroid withdrawal[188,189]. Conversely, contractions were reported to be decreased in OVx rat myocytes 9 - 10 weeks after OVx[190,191]. These latter effects of OVx on cardiac contractile force were reversed by 17β-oestradiol supplementation. The conflicting results may be explained by the different time frames of ovarian hormones deprivation.

While clinical findings and animal studies suggest ovarian hormones may play a role in reducing the incidence of cardiovascular events and may provide some of the protective effects[175-178], hormone replacement therapy (HRT) showed no cardiovascular benefit[192]. These conflicting results have led to a timing hypothesis that the start time of hormone therapy may influence the cardiovascular outcome[193]. Pathways, including calcium handling, nitric oxide synthases (NOS), regulation of collagen and oestrogen/oestrogen receptor-beta axis may be involved in the oestrogen-related

protective effect (Fig. 1-6)[176,179,194-198]. The details of the mechanisms are still undergoing investigation. While the wealth of evidence suggests some cardioprotective effect of oestrogen, conversely, oestrogen may provide a pro-arrhythmic substrate in some conditions. In acquired LQTS, drug-induced QT prolongation is more pronounced and the risk for polymorphic ventricular tachycardia is higher when oestradiol serum levels are high during the oestrous cycle [199]. This observation is strengthened by the fact that HRT may have detrimental effects on cardiovascular function[175,192].

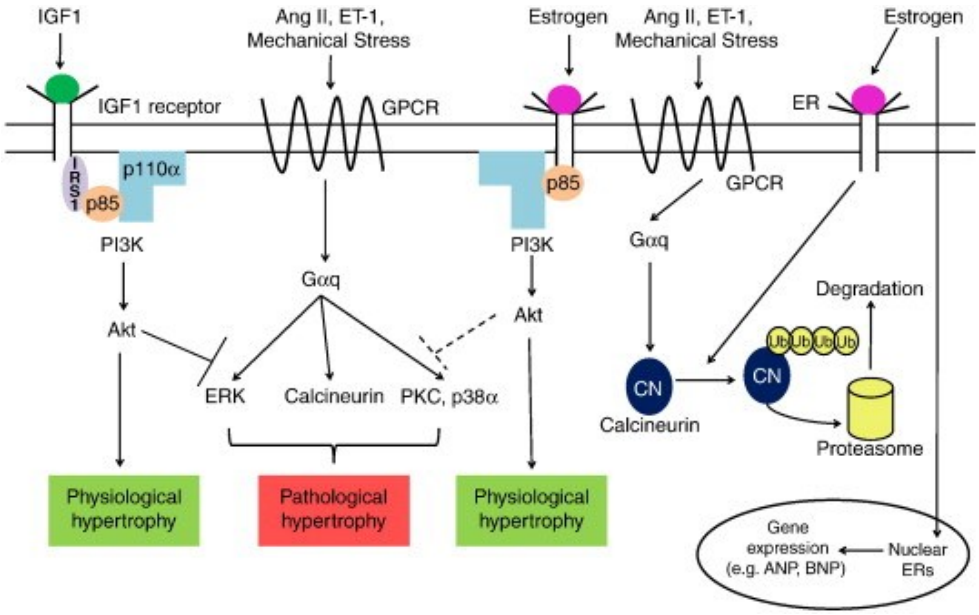

Figure 1-6. Oestrogen-mediated cardiac hypertrophy signalling pathway.

Non-genomic pathway: Oestrogen binds to ER which activates the PI3K-Akt pathway. This induces physiological hypertrophy and attenuates pathological signalling cascades that include activation of ERK, CN, PKC and P38α. Oestrogen is able to induce ubiquitination of CN which is then degraded by the proteasome. Genomic pathway: ERs enter the cell nucleus to alter gene expression and regulate cardiac hypertrophic responses (Ang II: Angiotensin II, ANP: Atrial Natriuretic Peptide, BNP: B-type Natriuretic Peptide, CN: Calcineurin, ER: Oestrogen Receptor, ERK: Extracellular Regulated Kinase, ET-1: Endothelin-1, GPCR: G Protein-Coupled Receptor, IGF1: Insulin-like Growth Factor 1, IRS1: Insulin Receptor Substrate 1, PI3K: Phosphoinositide 3-Kinase, PKC: Protein Kinase C, Ub: Ubiquitin) (Bernardo et al, 2010).

1.3.3 Differences in myocardial remodelling in HF between the sexes

Women are better protected against the development of cardiac hypertrophy than men. Animal studies showed that males respond to pressure-overload with an increased degree of hypertrophy compared with females[194]. In general, women develop a more concentric form of left ventricular hypertrophy than men and present smaller ventricular diameters and less ventricular dilatation[162,200-204]. Rodent animal models have shown that male and female hearts may adapt differently in response to cardiac stress (Fig. 1-7)[205]. In rats with ascending AC, an earlier transition to left ventricular dilation and depressed systolic function occurred in males compared with females[206]. FKBP12.6, an intracellular receptor for the immunosuppressant drug FK506, can bind and stabilise the RyR2 channel. One transgenic mouse study showed that disruption of the FKBP12.6 gene in mice results in cardiac hypertrophy in male mice, but not in females, despite the fact that male and female knockout mice display similar dysregulation of Ca^{2+}. The protection from developing cardiac hypertrophy was abolished by treating the female with tamoxifen, an oestrogen receptor antagonist. The female mice given tamoxifen then developed cardiac hypertrophy like the males[195]. OVx augments pressure overload-induced hypertrophy associated with changes in Akt and NOS signalling pathways in female pressure-overload ovariectomised rats[207], also strengthening the evidence that female sex hormones attenuate the development of cardiac hypertrophy. Further, a transgenic study using oestrogen receptor β (ER β) knock-out mice showed that cardiac hypertrophy and fibrosis was more severe in male wild types (WT) following AC than in female WT AC. This difference was abolished in ER β gene knockout mice. ER β knockout mice with AC showed more hypertrophied cardiomyocytes in both sexes compared with their WT AC groups[203]. The authors concluded that in females the ER β may play a role in attenuating the development of fibrosis and apoptosis, thus slowing the progression to HF[203].

Gene expression analysis shows that genes can be regulated in a sex-specific manner. In a pressure-overload mouse model, modulation of gene expression occurred early on after the pressure-overload operation despite changes in cardiac morphology and function occurring at a later time point[208]. Female hearts responded to pressure-overload with a better adaptation in cardiac energy metabolism. Genes encoding for mitochondrial function and fatty acid oxidation were less down-regulated in female hearts, while a relative up-regulation in matrix remodelling and ribosomal genes in males was reported[208].

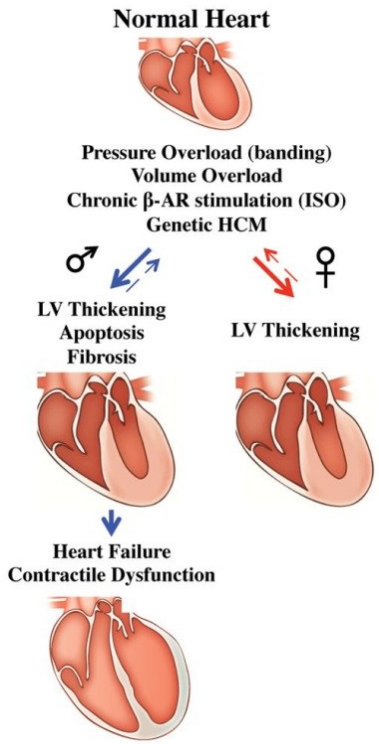

Figure 1-7. Myocardial remodelling in rodent between sexes.

Male and female rodent hearts may adapt differently in response to overload stress or drug stimuli. While left ventricles of both sexes increase in size in response to increases in metabolic demand, male hearts are more likely to develop fibrosis, apoptosis and progress towards HF (Blenck et al, 2016).

1.3.4 Sex-dependent Ca^{2+} regulation in hypertrophy and HF

Sex differences exist in the changes in Ca^{2+} regulation and E-C coupling in response to cardiovascular disease (CVD). A transgenic mouse study showed that overexpression of NCX increased I/R injury in male mice but not in females, suggesting that females may be less prone to injury when Ca^{2+} regulation is perturbed[209]. In pig hearts there were no differences in basal I_{NCX} and β-adrenergic responsiveness between males and females. However, in failing pig hearts there was increased I_{NCX} and reduced β-adrenergic responsiveness in the male HF group compared with the female group[210]. Thus, the increased NCX activity could impair contractile function by depleting SR Ca^{2+} content and promote unstable repolarisation with EADs/DADs in male. On the contrary, smaller NCX current and the preserved β-adrenergic regulation in female might contribute to the better survival in females with HF.

Following AC in the rat, the SERCA mRNA level was reduced in the male but not in the female hypertrophied heart[206]. While the NCX mRNA level increased in both male and female left ventricle

similarly in an AC mice model, oestrogen treatment restored ejection fraction and improved cardiac haemodynamics in both male and female mice[211]. SERCA mRNA expression was significantly down-regulated in the HF mice and partially restored by oestradiol treatment[211]. Thus oestrogen may have influence on the expression of SERCA.

Modulation of the SERCA regulatory protein, PLB has been reported in many CVD animal models. I/R-induced phosphorylation of PLB is proposed to be a protective mechanism[212]. Cross *et al* showed that PLB ablation increased ischaemic injury in both sexes, however females were less susceptible compared with male hearts, an effect that was reported to be NOS-mediated[213]. Male mice with overexpression of PLB developed ventricular hypertrophy and showed high mortality at 15 months, but females did not show these phenotypes at this age[214]. Reduction in Ser-16 PLB phosphorylation is one major factor determining the reduced SERCA2a activity in HF[97,215]. In a human HF model, cardiac myocytes from both male and female patients show significantly reduced SERCA protein while the PLB and calsequestrin levels were not altered. However, a reduction in phosphorylation of Ser-16 at PLB occurred only in male hearts when compared with their control groups[216].

In a human cardiac hypertrophy and HF study[217], there were comparable changes in Ca^{2+} cycling properties, including diastolic Ca^{2+} levels, Ca^{2+} transient amplitudes and SR Ca^{2+} load in hypertrophic hearts between sexes. Spark frequency and spark-mediated SR leak was also not different. In HF, while both sexes showed increased spark frequency and spark-mediated SR Ca^{2+} leak compared with hypertrophic heart groups, males showed more pronounced spark frequency and spark-mediated SR leak compared with females[217]. Thus sex differences may also play a role in regulation of RyR2 channel open probability.

In conclusion, this chapter has highlighted the changes that occur to proteins involved with cardiac E-C coupling and ionic regulation in response to pathological stimuli. Some of these changes may be sex-dependent and there may be a modulatory role of oestrogen in Ca^{2+} and Na^{+} regulation.

1.4 Hypothesis

The central hypothesis of the work detailed in this thesis is that there are sex differences in electrophysiology and Na^+ and Ca^{2+} homeostasis in the progression from cardiac hypertrophy to HF. It is proposed that, in the failing heart, males experience greater alterations to their intracellular Ca^{2+} handling and Na^+ regulation than that of females, causing more compromised cardiac function. It is hypothesised that oestrogen provides protective effects against dysregulated Ca^{2+} and Na^+ during the progression towards HF in female. In addition, it is hypothesised that long-term deprivation of female sex hormones provides a pro-arrhythmic substrate by causing dysregulation of Ca^{2+} handling.

1.4.1 Main aims

(1) To investigate if sex differences exist in the cardiac responses to AC and are associated with differential dysfunction of cellular Ca^{2+} handling mechanisms.
(2) To investigate if oestrogen is associated with modulation of $Ca^{2+}$and Na^+ regulation and provides a cardioprotective effect.
(3) To investigate if long-term deprivation of female sex hormones causes dysregulation of Ca^{2+} and Na^+, which may provide pro-arrhythmic substrates.

1.4.1.1 Aims

(1) To assess the changes in physical characteristics and cardiac function in the progression towards HF in AC GPs model.
(2) To assess the changes in APD in response to pressure-overload.
(3) To evaluate changes in cellular Ca^{2+} handling properties including Ca^{2+} transient, SR Ca^{2+} content and $I_{Ca,L}$ in the progression to HF.
(4) To determine the spontaneous Ca^{2+} spark frequency, morphology and spark-mediated SR Ca^{2+} leak in sham and HF groups.
(5) To assess the changes in Na^+ regulation including Na^+/K^+ ATPase expression, current and function and $I_{Na,L}$ at the stages of cardiac hypertrophy and HF.
(6) To assess the differences between sexes in the physical characteristics of the heart, the function of the heart and intracellular Ca^{2+} and Na^+ regulation in response to AC.
(7) To assess if long-term deprivation of ovarian hormones alters Ca^{2+} regulation in ventricular myocytes and leads to more arrhythmogenic events.
(8) To assess if long-term deprivation of ovarian hormones alters Ca^{2+} and Na^+ regulation in AC GPs.
(9) To test if oestrogen supplementation confers cardiac protection and modulates Ca^{2+} handling and Na^+ regulation in ovariectomised GPs.

2 Methods

General methods used throughout the project are described in the following sections. Any variation in techniques or protocols for specific experiments will be detailed in the relevant chapter.

2.1 Animals

All animal studies were carried out with the approval of the Home Office, United Kingdom and in accordance with the United Kingdom Home Office Guide on the Operation of the Animals (Scientific Procedures) Act 1986 under assurance number A5634-01.

Dunkin-Hartley GPs were used as the experimental animal model. In many relevant physiological aspects, GPs display similar features to the human. The relative amounts of trans-sarcolemmal Ca^{2+} influx and SR Ca^{2+} release in their cardiac myocytes, and the roles of Ca^{2+} uptake and efflux proteins (SERCA and NCX) are almost identical to that of human, in contrast to the corresponding fluxes in rat or mouse which are far removed from the human situation because of their very "high gain" EC coupling system[1]. Most ionic currents shaping the ventricular action potential of the GP are similar to human and very dissimilar to rat or mouse[218,219]. In terms of sex hormone balance and steroidogenesis, again the GP is similar to the human[220,221]. Throughout the study, the animals were housed at 21 ± 1 °C in a controlled lighting environment (12 h light-dark cycles).

2.1.1 Ascending AC animal model

Male or female Dunkin-Hartley GPs weighing 350 - 450 g underwent surgical procedures. Animals were randomly selected to have an AC or sham operation. The AC model is characterized by an initial phase of compensated hypertrophy that is followed by a transition to HF, mimicking human pressure overload-induced HF in a number of aspects[222,223]. Any study of HF requires reliable and relevant animal models to examine the chronic changes in myocardial structure and function taking place and to follow their progression toward HF. AC is a well-established surgical technique for induction of LV chronic pressure-overload and hypertrophy with transition to failure in rodents[224]. Furthermore, the AC GP model also has similarities to human HF with respect to the changes in calcium cycling, E-C coupling and myocardial function. HF induced by AC takes place slowly over 150 days, and so models a gradual and more chronic disease process[222].

2.1.1.1 Anaesthesia and medication

Animals were given premedication of atropine sulphate (0.05 mg/kg sc; Atrocare, Animalcare Limited) to reduce saliva secretions followed by prophylactic antibiotic (enrofloxacin, 5 mg/kg sc; Baytril, Bayer), analgesic (carprofen, 4 mg/kg sc; Rimadyl, Pfizer) and narcotic analgesic (buprenorphine, 0.05 mg/kg sc; Vetergesic, Alstoe Ltd) (Fig. 2-1. A). Animals were anaesthetised with

2 - 4 % isoflurane (Isoflo, Abbott)/ 95 % oxygen mix inhalation (Fig. 2-1. D). Lidocaine spray (Xylocaine 10 %, AstraZeneca) (Fig. 2-1. A) was applied to the oral cavity prior to endotracheal intubation. Intubation was accomplished with 14 G x 64 mm intravenous catheters (Surflo® I.V. Catheters, Terumo, UK) (Fig. 2-1. C), and anaesthesia was maintained using isoflurane inhalation, via the catheter, through a Zoovent Mini ventilator (Triumph Technical Services, Milton Keynes, UK) at 70 ml/kg and 70 cycles/min (Fig. 2-1. B). Peripheral oxygen saturation and pulse rate were monitored with a pulse-oxymeter (SurgiVet, Smiths Medical). A heating pad was used to prevent hypothermia (Fig. 2-1. B). Before incision, a local anaesthetic (Bupivacaine, 2mg/kg sc; Macaine Polyamp, AstraZeneca) was injected around the incision site.

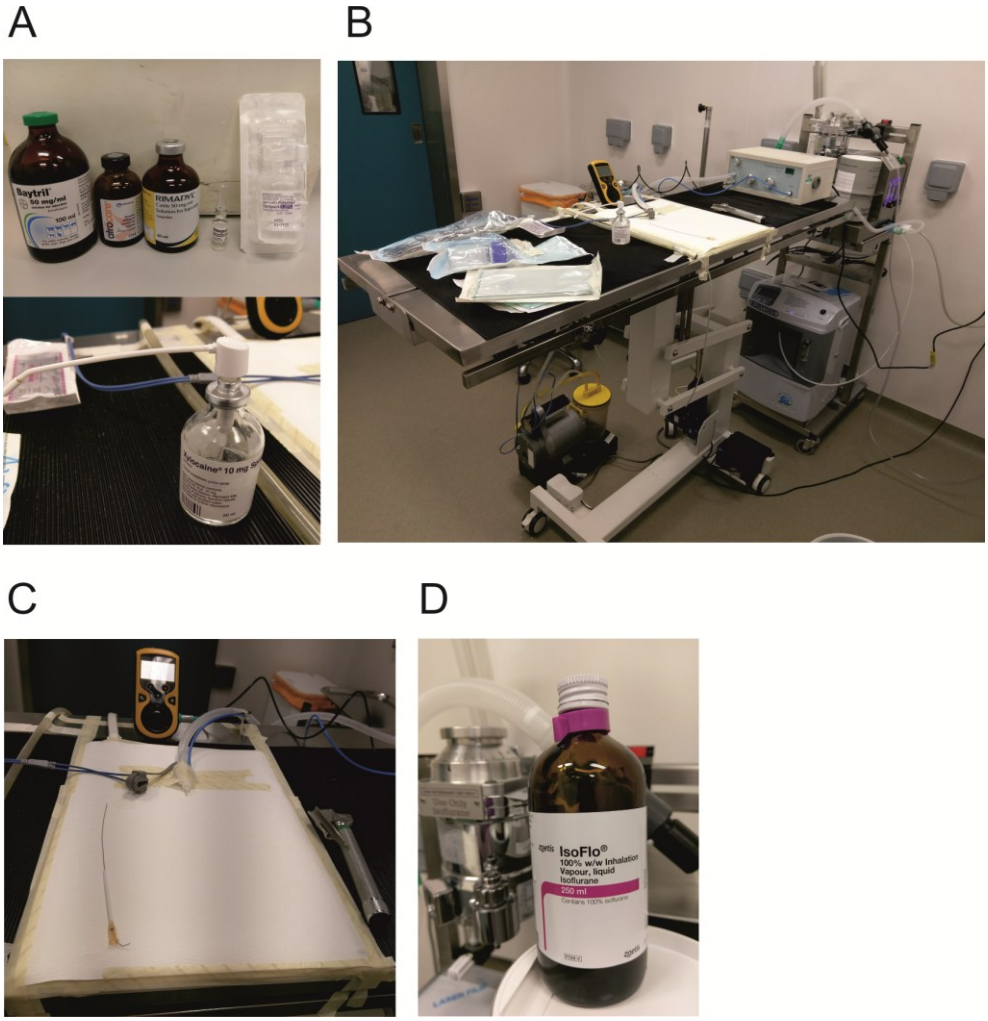

Figure 2-1. Medication and surgical equipment

A: Premedications (above), lidocaine spray (below) and Isoflurane with anaesthesia machine (D). B: Surgical platform with equipment including anaesthesia setup, ventilator, pulse oximeter, oxygenator, suction system, instrument and drapes. C: A 14 G x 64 mm intravenous catheter with a guiding wire for intubation and a paediatric laryngoscope for trachea access.

2.1.1.2 Surgical procedures

Animals were put in a right-lateral supine position with retraction of the left forelimb towards the head to allow access to the left chest wall. Fur was shaved and skin sterilized with povidone-iodine (Videne Alcoholic Tincture, Adams). Sterilized drapes were used to cover the animal and only the operative area was exposed (Fig. 2-2. A). Surgical instruments were sterilised using an autoclave prior to operation. Thoracotomy was performed via a 5 cm skin incision on the left chest wall. Muscles above the ribs were separated and the left chest was opened through the second intercostal space. The pericardium was opened and the thymus tissues were dissected to identify and isolate the ascending aorta. The aorta was constricted by a 2 mm ID polytetrafluoroethylene (PTFE) ring just below the first branch of aortic arch (Fig. 2-2. B). A 20 G intravenous catheter was placed as a chest drainage tube and the intercostal incision was closed by 3-0 Vicryl sutures. The muscle and skin were subsequently sutured layer by layer with 3-0 Vicryl and 4-0 Nylon sutures, respectively. Isoflurane was discontinued when the suturing was completed. Residual air was drained out via the chest tube to recover the collapsed lung. After recovery of muscle tone and spontaneous breathing, the endotracheal tube was removed. Animals were then transferred to a recovery chamber heated to 32 °C and oxygen was delivered around the nose of the animal via a face mask. After recovery from anaesthetics, it was returned to a cage for post-operative observation and care. The total operation time was around 50 ± 10 min. Sham operations were performed with the same procedure without constriction of the ascending aorta.

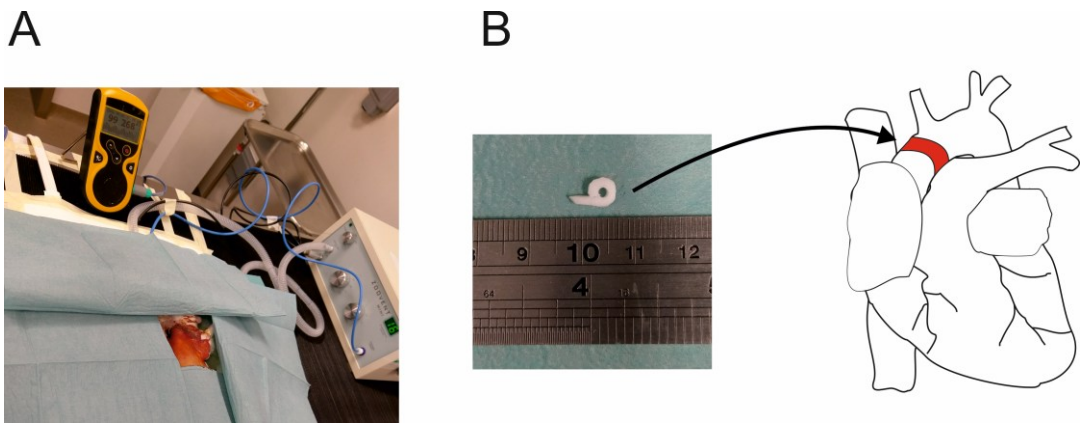

Figure 2-2. Operative area and aortic PTFE clip.

A: The anaesthetized animal was covered with drapes and only sterile operative area was exposed. B: The ''tau'' shape self-designed PTFE clip was 2 mm ID that contained a tail to facilitate aorta looping.

2.1.1.3 Post-operative care

Post-operation, the GPs were allowed water and a standard casein-based diet *ad libitum*. Wooden tongue depressors were introduced for the animals to chew, preventing them from biting their wound sutures that was a usual occurrence. Carprofen (15 mg in 300 mL water) was given orally for 3 days to maintain post-operative analgesia. The surgical wound was checked daily for the first 3 days after the operation. The primary healing of the wound was usually complete within 7 - 10 days after the operation. If required, re-suturing was performed under the project license 30/3288 if sutures became dislodged. On occasion, needle aspiration was carried out for subcutaneous hematoma or fluid accumulation. Antibiotic treatment was given on the advice of the veterinary surgeon if wound infection had occurred. GPs were sacrificed for experiments approximately 60 or 150 days after the operation or when a humane endpoint was reached. Humane endpoints are when animals developed severely compromised cardiopulmonary function with symptoms including dyspnoea and cyanosis, or uncontrolled wound infection causing severe pain and distress.

2.1.1.4 Complications

Overall, 110 operations, including 67 sham and 43 AC operations were performed. The surgical mortality rate for AC surgery was 16.2 %. Complications are detailed in Table 2-1. The animals with wound dehiscence all underwent wound re-suturing and wound hematomas subsided after needle aspiration. Fatal complication rate of males and females AC operation was no difference.

	Sham (%)			AC (%)		
Fatal complications	**M**	**F**	**T**	**M**	**F**	**T**
Anaesthetic cause or ventilation issues	2	1	3	0	2.3	2.3
Intra-operative bleeding	0	0	0	2.3	0	2.3
Acute heart failure	0	0	0	4.7	6.9	11.6
Lung injury	1.5	0	1.5	0	0	0
Intubation trauma	1.5	0	1.5	0	0	0
Total Fatal complication	**5**	**1**	**6**	**7**	**9.2**	**16.2**
Minor complications						
Wound dehiscence	2	1	3	2.3	0	2.3
Hematoma formation	1.5	1.5	3	2.3	2.3	4.7
Total minor complications	**3.5**	**2.5**	**6**	**4.7**	**2.3**	**7**

M: Male, F: Female, T: Total.

Table 2-1. Complications of AC and sham surgery.

2.1.1.5 The challenge of AC surgery and technical refinements

Dr Hung-Yen Ke, a previous Ph.D student in our research group, mainly performed surgery on male GPs revealed that the occurrence of acute HF was reduced to < 15 % by using small GPs with body weight 350-450g. The smallest size of Portex non-cuffed endotracheal tube (ID 2.0 mm, OD 3.0 mm) was however too large for smaller female GPs. A 14 G x 64 mm intravenous catheter was successfully used fitting all GPs well, and causing no ventilation problems during anaesthesia. On occasion, GPs bit the endotracheal tube when recovering from anaesthesia before extubation. No serious complications were noted when the catheters were removed from the GPs.

2.1.2 Bilateral ovariectomised GPs

The GP is polyoestrus all year round with a 16-day ovarian cycle and a full luteal phase, similar to women[225]. The serum levels of ovarian hormones were markedly reduced after OVx[226]. For these reasons, it is suggested that the GP is an appropriate species in which to examine the influence of ovarian hormones on ionic regulation in E-C coupling[225,227].

2.1.2.1 Anaesthesia and medication

Animals were given premedication of atropine sulphate followed by prophylactic antibiotic as described in section 2.1.1.1. Animals were anaesthetised with a 2 - 4 % isoflurane / 95 % oxygen mix delivered with a rodent mask (Rodent Mask Delivery System, Vet-Tech Solutions Limited, UK) (Fig. 2-3). Peri-operative monitoring and post-operative medication were as described in section 2.1.1.1 and 2.1.1.3.

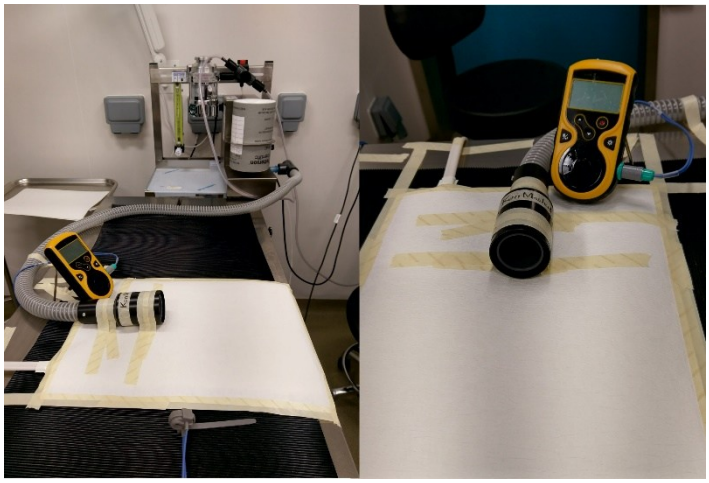

Figure 2-3. GP mask delivery system.

2.1.2.2 Surgical procedure

Ovaries were removed through bilateral flank incisions under sterile surgical conditions[228]. Animals were put in a prone position. Fur on the back was shaved and skin was sterilized with povidone-iodine. The point of reference for incision of the skin was the flank region 1.5 cm from the line of the last cartilaginous rib and 1.5 cm from the line of the lateral vertebral processes. The incision line

bisects the angle formed by these two lines, with a craniocaudal and dorsoventral direction. The subcutaneous tissue was bluntly dissected until the external oblique abdominal muscle was exposed. The muscular walls including the external oblique abdominal muscle, the internal and the transverse laminar abdominal muscles were bluntly dissected with scissors, until the abdominal cavity was entered. The ovary and the proximal tract of the uterine horn were exposed with gentle traction of the exposed fat. Ligation of the ovarian artery was performed and ovary was dissected free from the surrounding fat tissue. The proximal end of the uterine horn was then repositioned into the abdominal cavity. The muscular walls were sutured in one layer. The skin was sutured and the surgical approach was then repeated on the contralateral flank. A sham operation was performed by exposing the ovaries without removal.

2.1.2.3 Post-operative care

Post-surgery, the GPs were provided with water and a casein-based, soy-free diet to minimize the uptake of phytoestrogens *ad libitum*. The principle of wound care and post-operative analgesics usage were as described in section 2.1.1.3. GPs dorsal skin was thicker, tougher with higher tension than ventral skin. In the case of wound dehiscence, the wound was treated with hydrogel (INTRASITE Gel, Smith & Nephew, UK) to allow secondary wound healing instead of re-suturing. Operated GPs were housed up to 150 days before use.

2.1.3 AC GPs combined with bilateral OVx

To address the question whether females lose their protection against CVD after menopause, animals with OVx combined with AC surgery were needed. GPs initially underwent an OVx operation followed by AC surgery, detailed in section 2.1.1.2, separated by a 5 - 7 days recovery period. Post-operative care was performed as described in section 2.1.1.3.

2.1.3.1 Complications

In total 18 GPs underwent OVx combined with AC surgery. There were 3 cases of fatal complication, including 2 acute HF and 1 intra-operative lung injury, giving a mortality rate of 16.6 %. No minor complications were noted.

2.1.4 17β-oestradiol pellet implantation

Pellets (60-day release) containing 1 mg 17β-oestradiol (E2) (Innovative Research of America) were implanted subcutaneously in the back region of selected OVx animals 90 days post-OVx surgery. The anaesthesia procedure was analogous to the OVx surgery detailed in section 2.1.2.1. Animals were put in a prone position. Skin on the upper back was shaved and sterilized with povidone-iodine. Subcutaneous dissection in the caudal direction was done via a small skin incision to create a space for the pellet. After implantation, the skin wound was closed with 4-0 nylon sutures. Post-operative

care was as section 2.1.2.3. In total, 21 GPs, including 14 OVx and 7 OVx+AC GPs, underwent oestradiol pellet implantation. The first 2 GPs received the pellets using 10 G trocar (Innovative Research of American). The blind skin penetration of the trocar caused marked subcutaneous hematoma with subsequent infection in the 2 GPs. An open method was preferred for the remaining 19 GPs, reporting no wound complications. 3 of the 19 GPs developed a decrease in activity and appetite with oedema on the ventral side 10 - 14 days after implantation. These 3 GPs recovered without complications after one week. The suspected reaction was from pellet-related acute inflammation or infection.

2.2 *In vivo* Echocardiography study

M-mode echocardiography was performed by using an HP Sonos 5500 echo machine with S-12 paediatric probe. The depth was set at 2 cm for small young GPs or 3 cm for large old GPs. For AC or sham operated animals, echo scans were carried out pre-operatively and post-operatively at 60 days and 150 days to longitudinally assess the cardiac function during the progression from hypertrophy to HF after AC surgery. Echo studies were performed on OVx animals pre-operatively and 150 days after OVx. The echo scans were performed on unanaesthetised GPs to avoid anaesthetic effects on heart function. The left ventricular internal diameters in diastole (LVIDd) and systole (LVIDs) were measured to calculate fractional shortening (FS) (Fig. 2-4). FS = (LVIDd - LVIDs)/LVIDd. Images were recorded in VHS tape for off-line analysis.

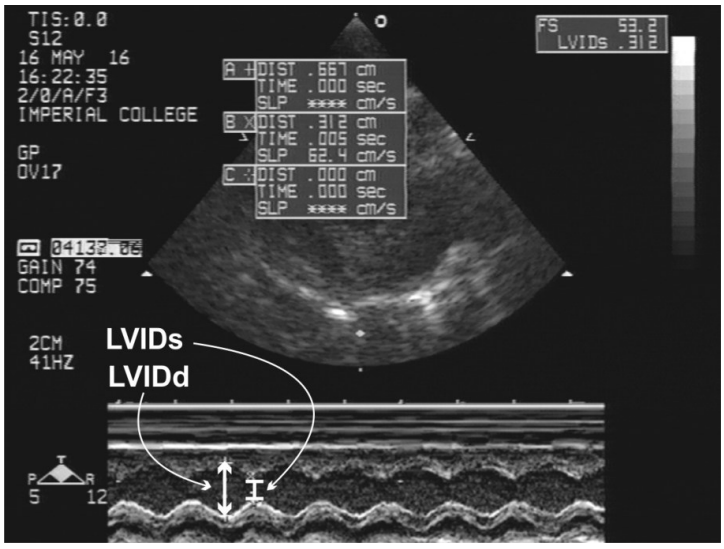

Figure 2-4. Image of M-mode echocardiography on a GP.

Echo scans were performed on an unanaesthetised GP. M-mode echocardiography allows measuring left ventricular LVIDd and LVIDs (see above image) which are used to calculated FS.

2.3 Isolation of GP cardiac myocytes

2.3.1 Cardiomyocytes isolation protocol

Cardiac myocytes were enzymatically-dissociated by using a collagenase/protease blend enzyme (Liberase TL 5 mg, Roche) and a Langendorff perfusion system with a constant-flow roller pump (Fig. 2-5. A) as previously described[229]. Firstly, the GP heart was removed under non-recovery anaesthesia or by a schedule 1 method (when reaching a humane end point). The heart and lungs were removed together and were immediately placed in ice-cold Krebs-Henseleit (KH) solution, containing heparin (10 U/ml) to prevent blood clotting. The heart was trimmed free from adherent tissues and the aorta was tied to a 12 G Luer lock cannula which was then connected to a Langendorff setup (Fig. 2-5. B). The heart was surrounded by a heated jacket, to maintain temperature at 37 °C, and retrogradely perfused with a pre-oxygenated KH solution for 1 - 2 min at a steady flow of 6 - 8 mL/min/g. The perfusate was switched to low Ca^{2+} solution (LC) for 4 - 5 min before adding Liberase TL enzyme (5 mg in 50 ml enzyme solution (ES)) for 6 - 10 min. The heart was then removed from the cannula that supplied the retrograde perfusion, and the left ventricle was chopped into 2 - 4 mm size tissues. The tissues were transferred to a small jar containing the same ES, shaken gently and oxygenated. The content of the jar was filtered through a piece of nylon mesh (opening size: 300 μm) and the residual, undigested tissues returned to the jar for further digestion. This cycle was repeated every 3 min until the digestion was complete. The flow-through from each filtering cycle was centrifuged at low speed (400 rpm) for 1 min. The resulting cell pellet was re-suspended in fresh ES in the absence of Liberase TL enzyme. Finally, myocytes were stored in Dulbecco's modified Eagle's medium solution (DMEM, containing 1 g/L D-glucose, 0.584 g/L L-Glutamine, 25 mM HEPES, 0.11 g/L pyruvate and 1.8 mM Ca^{2+}, Gibco BRL, Life Technologies) at 20 - 22 °C room temperature (RT) and were used within 6 to 8 h.

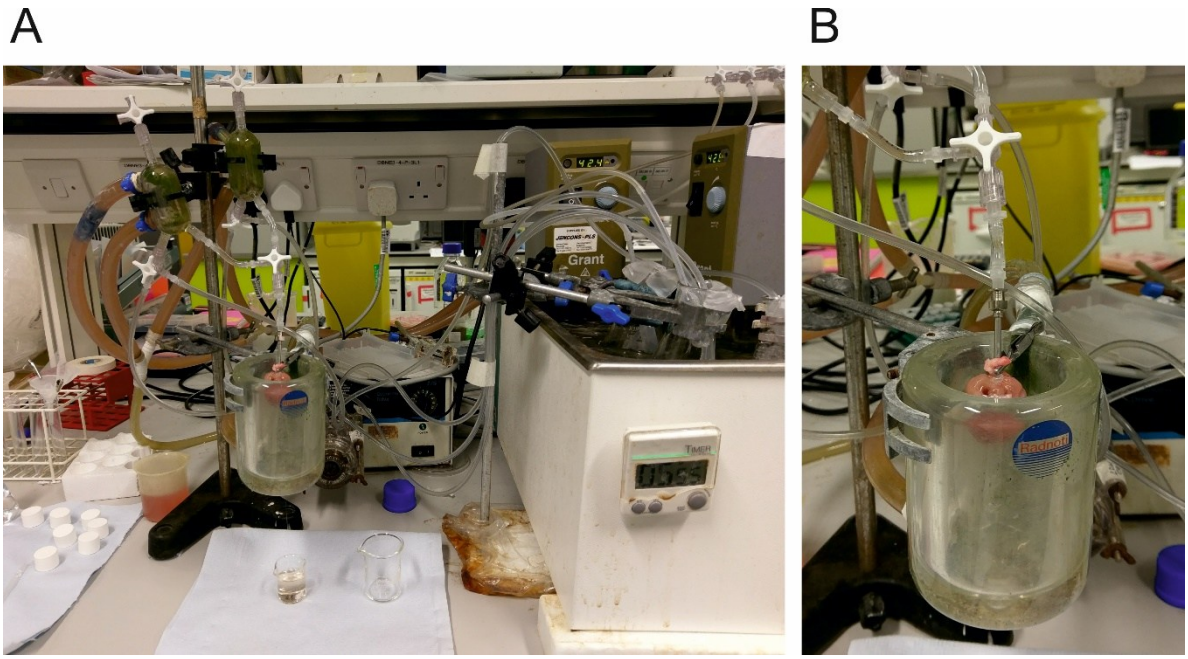

Figure 2-5. Langendorff perfusion system (A) and a cannulated heart (B).

Solutions, oxygenated and kept in a warm bath, were pumped to a bubble trap container before reaching the heart. In order to perfuse the heart at 37 °C, the temperature of the warm bath was set to 42 °C to overcome heat loss from the uninsulated tubing.

2.4 Cellular electrophysiological measurements

Action potential, NCX inward current and $I_{Ca,L}$ were recorded by using a switch-clamping system with high resistance microelectrodes to minimise cell dialysis so preserving the intracellular milieu[230,231]. Sharp microelectrodes with resistances of 20 - 40 MΩ were made by a microelectrode puller (DMZ universal electrode puller, Zeitz-Instruments, Germany). Na^+/K^+ ATPase and late Na^+ current ($I_{Na,L}$) were measured by using the whole-cell patch clamp technique to improve cytoplasmic ionic control. Whole-cell patch was performed by using the conventional method of applying gentle, negative pressure[232] to encourage formation of a high resistance (giga-ohm) seal between glass pipette and cell membrane. The resistances of the patch-pipettes were 4 - 7 MΩ. Glass capillaries for sharp electrodes and patch pipettes had thick walls with an internal glass filament and diameters of 1.5 mm OD and 0.86 mm ID (Borosilicate glass capillaries, GC150F-15, Harvard Apparatus, USA). Experiments were carried out at 37 °C. Techniques involved in action potential recording, assessment of SR Ca^{2+} content and Ca^{2+} transients recording from Fluo-4 AM loaded cells have been well described and are currently in use in the laboratory[233-235]. Refinements to these techniques are detailed below.

2.4.1 Setup for electrophysiological measurement

A low profile open diamond recording chamber (RC-26GLP, Warner Instruments) was mounted on the stage of an inverted Nikon microscope. A 40x oil immersion objective was used. A superfusate switching system (solenoids) was used to allow fast switching between solutions. Microelectrodes were attached to a HS-2A x0.1LU headstage which was connected to Axoclamp 2B amplifier (Molecular Devices, Sunnyvale, CA, USA). The required signals (transmembrane voltage and current) were recorded with Axoclamp-2B amplifier in conjunction with Digidata 1440A and Clampex 10.3 acquisition and analysis software (MDS Analytical Technologies).

2.4.2 Measurement of action potential

Cells were loaded into a chamber using a pipette following the application of 2 µl mouse laminin (1 mg/ml, Gibco, Life technologies) to the base, allowing cells to adhere to the coverslip. Cells were superfused with NT solution. In current clamp mode, action potentials were elicited with 3 ms current pulses (typically 1.5 - 2.5 nA) applied at a rate of 0.5 Hz or 1 Hz (Fig. 2-6). After reaching steady-state, normally around 20 times current pulses, 10 action potentials were recorded for signal averaging. APDs were expressed as the time to 10 % and 90 % repolarisation (APD_{10} and APD_{90}, respectively).

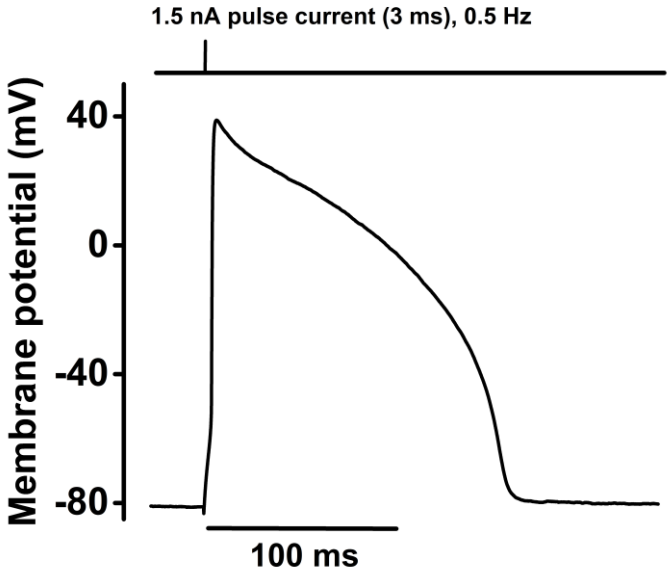

Figure 2-6. Typical action potential recording.

A typical action potential from an isolated GP left ventricular cardiac myocyte elicited by applying a 1.5 nA positive pulse of current through the recording electrode.

2.4.3 Cell capacitance

Membrane test, a built-in system in Clampex 10.3, was used to measure cell capacitance. Cells were superfused with NT solution. In voltage clamp mode, the membrane test was used to assess the integral of the current changes (two capicitative spikes) in response to short period voltage steps of 10 mV for 20 ms at 100 Hz from a holding potential of -75 mV. Ionic currents obtained from cells were normalised by corresponding cell capacitance.

2.4.4 Assessment of SR Ca^{2+} content

Sarcoplasmic reticulum (SR) Ca^{2+} content was assessed by integrating the inward NCX current induced by fast application of 10 mM caffeine to voltage-clamped cells as previously described (Fig. 2-7)[236]. Firstly, cells were voltage-clamped at -80 mV with NT superfusion. Prior to caffeine application, the cells were subjected to a SR Ca^{2+} loading protocol consisting of a train of action potential clamp at 1 Hz for 20 s. After the loading train, stimulation was stopped and the superfusate was rapidly changed to NT solution containing 10 mM caffeine. The rapid and continuous application of caffeine activates and maintains RyR openings, leading to a sustained release of SR Ca^{2+}. The released Ca^{2+} is predominately removed from the cell by the NCX. Only a little amount of the released Ca^{2+} (less than 2 %) is removed by slower Ca^{2+} transporter including PMCA and mitochondria Ca^{2+} uniporter, which is negligible in this setting[28,237]. Therefore, SR Ca^{2+} content can be calculated by integrating the inward NCX current [Integral of inward NCX current (pC) / Faraday constant (-96.485) / Mean cell volume (cell capacitance/5) x accessible volume (1.125)].

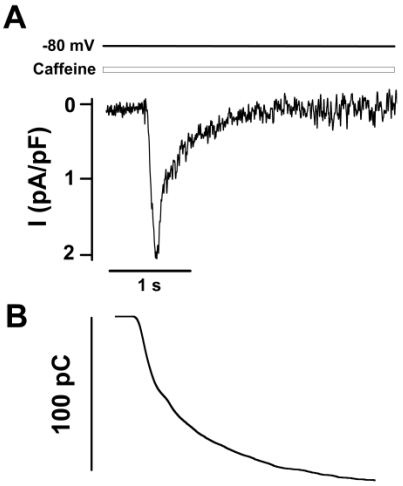

Figure 2-7. Typical recording of caffeine-induced inward NCX current and the corresponding current integral trace.

Inward NCX current was elicited by rapid application of 10 mM caffeine when voltage-clamped at -80 mV (A). The SR Ca^{2+} content was calculated by integrating the inward current (B).

2.4.5 Measurement of $I_{Ca,L}$

$I_{Ca,L}$ was recorded in discontinuous single electrode voltage clamp mode (gain 0.5 - 1.5 nA/mV and switching rate 4 - 6 kHz) in the presence and absence of 200 µM cadmium. $I_{Ca\,L}$ was evoked from a holding potential of -40 mV by 200 ms steps from -45 to +55 mV in 5 mV increments (Fig. 2-8). Steady-state inactivation of $I_{Ca,L}$ was assessed with double pulse protocols in which conditioning pulses of 200 ms duration and ranging from -45 to +55 mV were followed by a 5 ms step to -40 and a 200 ms step to +5 mV (Fig. 2-8. A). $I_{Ca,L}$ was determined by subtracting the trace in the presence of cadmium (Fig. 2-8. B) from the original trace at each voltage (Fig. 2-8. C). The current-voltage relationship (I-V) was drawn from the subtracted $I_{Ca,L}$ traces.

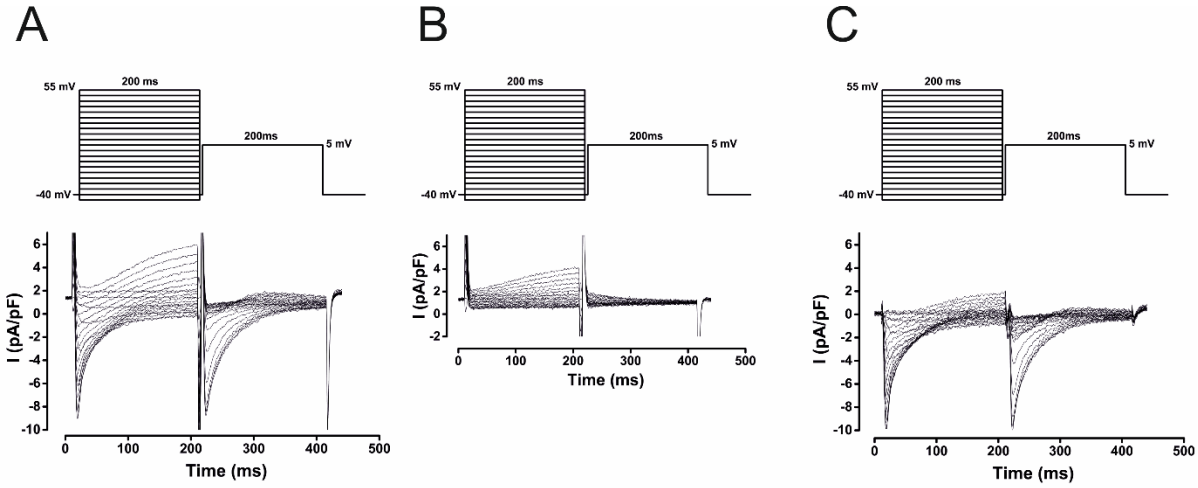

Figure 2-8. $I_{Ca,L}$ recordings with the corresponding voltage steps protocol.

$I_{Ca,L}$, or cadmium-sensitivity current (C) was obtained by subtracting the traces in the presence of 200 µM cadmium (B) from the original traces (A).

2.4.6 Measurement of Na^+/K^+ ATPase current and function.

Na^+/K^+ ATPase currents were measured using a modification of described methods (Fig. 2-9)[53]. Cells were voltage-clamped at -40 mV throughout the experiment to inactivate Na^+ channels. The pipette solution (see section 2.11) contained high Na^+ concentration (30 mM NaCl) to activate maximally the Na^+/K^+ ATPase. K^+ currents were blocked by a Cs^+-based pipette solution. The inward currents from the NCX and L-type Ca^{2+} channel were inhibited by using a Ca^{2+} free Tyrode's solution with the addition of 2 mM Ba^{2+} and 5 mM Ni^{2+} (see section 2.11). Following whole-cell configuration, the superfusate with 6 mM K^+ was changed to one that was K^+ free. The resulting current change is referred to as Na^+/K^+ ATPase current. During the K^+-free period, $[Na^+]_i$ is expected to gradually increase. After 2 min the Na^+/K^+ ATPase was reactivated by adding back 6 mM K^+. The reactivated

Na^+/K^+ ATPase starts to pump out the intracellular Na^+ that accumulated during the K^+ free period resulting in an outward current that reaches a peak then decays as the extrusion process proceeds. The rate of decline in the Na^+/K^+ ATPase-mediated outward current indicates the Na^+ extrusion rate which was used to assess the function of Na^+/K^+ ATPase.

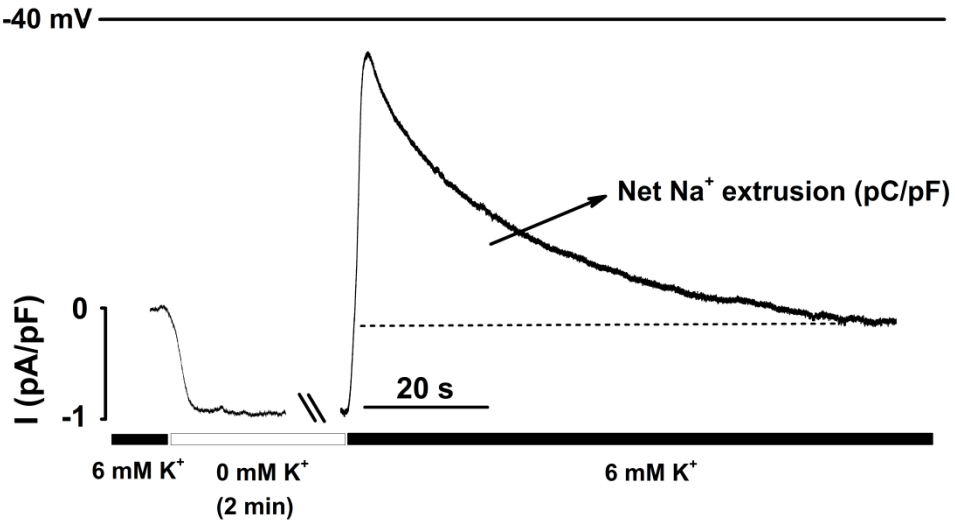

Figure 2-9. Protocol of Na^+/K^+ ATPase current and function measurement.

The cell was voltage-clamped at -40 mV. The superfusate was switched to 0 K^+ for 2 min. The resulting current change was referred to as Na^+/K^+ ATPase current. $[Na^+]_i$ started to build up during the 2 min. The superfusate was switched back to 6 mM K^+ to reactivate Na^+/K^+ ATPase. The outward current resulted from Na^+ extrusion by Na^+/K^+ ATPase, and the rate at which the current declined to steady-state indicates the Na^+ extrusion rate which was used to assess the function of Na^+/K^+ ATPase.

2.4.7 Measurement of $I_{Na,L}$

The protocol was a modification of a previously described method (Fig. 2-10)[4,238]. $I_{Na,L}$ was recorded at RT (20 - 22 °C). Cells were firstly held at -120 mV as almost 100 % of voltage-gated Na^+ channels would be available from this potential[239-241]. Pipette and external solutions were Cs^+-based to block K^+ current. Cells were subjected to a depolarising step to -20 mV for 2 s from a holding potential of -120 mV (at a rate of 2 Hz) to induce Na^+ current (Fig 2-10). This sequence was subsequently repeated following superfusion of 10 μM ranolazine for 3 min. $I_{Na,L}$ was obtained by subtracting the trace in the presence of ranolazine from the original trace. The amplitude of $I_{Na,L}$ was determined from the averaged current measured between 210 and 220 ms after the depolarising step to -20 mV. This time interval was chosen to avoid contribution of the transient (early) Na^+ current which is reported to be completely inactivated within 200 ms[113].

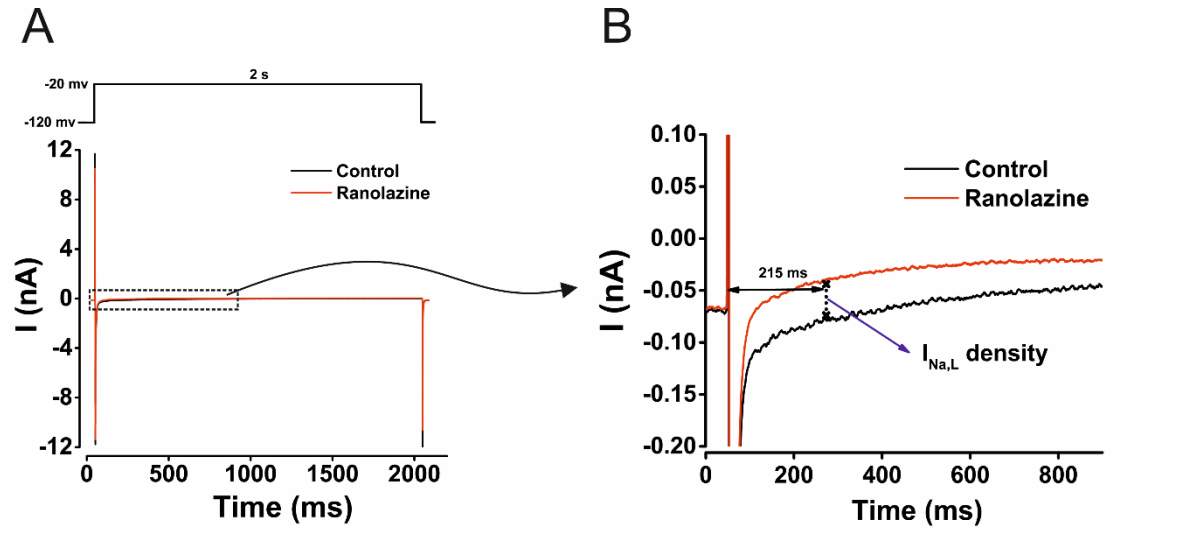

Figure 2-10. Representative $I_{Na,L}$ recording.

A: Cell was firstly voltage-clamped at -120 mV, following a depolarisation step to -20 mV to elicit Na^+ current. B: $I_{Na,L}$ density was measured by subtracting the two traces which were recorded in the presence and absence of 10 μM ranolazine 215 ms after the -20 mV depolarising step.

2.5 Intracellular Ca^{2+} monitoring

Cells were loaded with Ca^{2+}-sensitive fluorescent dye Fluo-4 AM (Invitrogen, Life Technologies Ltd). The Fluo-4 is a single wavelength calcium indicator with maximum excitation wavelength at around 490 nm and emission at 520 nm[232]. The emission intensity represents the level of bound Ca^{2+}. Fluo-4 is an analogue of Fluo-3 with minor structural modification which results in increased quantal efficiency and consequently higher signal levels for detection. Due to its single wavelength excitation and emission characteristics, it is difficult to use Fluo-4 for quantitative studies. Therefore, relative, qualitative assessments of intracellular Ca^{2+} changes using Fluo-4 were expressed as F/F_0, where the fluorescence intensity F was normalised to the diastolic baseline fluorescence intensity F_0.

2.5.1 Ca^{2+} transient and relaxation contribution

2.5.1.1 Epifluoresence microscope system

A Nikon inverted microscope was equipped with a xenon arc lamp as an epifluorescence illuminator. Neutral density filters were used to adjust the intensity of the light to avoid oversaturated signals. The 485 nm excitation filter and the 520 nm emission filter together with a dichroic mirror were fitted in Nikon DM-510 filter cube. Fluorescence output was detected using a photomultiplier tube (PMT). The PMT current was converted by a current/voltage convertor and this output was digitised with a Digidata 1440A data acquisition system and visualised using Clampex 10.3 software.

2.5.1.2 Ca^{2+} dye loading

A stock solution of 1 mM Fluo-4 AM was made by resuspending 45.6 µL dimethyl sulphoxide (DMSO) with a vial containing 50 µg Fluo-4 AM. 16 µL 10 % Pluronic F-127 (Invitrogen) in water was added to a 1 ml cell suspension to achieve a final concentration of 0.16 %. Pluronic F-127 is a non-ionic detergent that has been reported to facilitate the solubilisation of water-insoluble dyes, such as Fluo-4 and Fura-2, in physiological medium. To make a final Fluo-4 concentration of 10 µM in cell incubation medium, 10 µL of the stock Fluo-4 AM was added in 1 ml cell incubation medium. The cells were incubated with the dye at RT for 25 min on a rocking platform. Thereafter the cell suspension was centrifuged at low speed (400 rpm) for 1 min replacing the supernatant with DMEM. The cells were further incubated at RT for 30 min to allow for de-esterification of the intracellular Ca^{2+} indicator leaving free Fluo-4 inside the cell. The dye-loaded cells were used to monitor Ca^{2+} transients for up to 2 h. It was important to use a second loading of cells following the initial 2 h batch to avoid Fluo-4 leakage, maintaining a high signal-to-noise ratio.

2.5.1.3 Measurements of the Ca^{2+} transient

A fast exchange open diamond recording chamber (RC24N, Warner Instruments) with platinum field electrode placed on each site of the chamber enabled field stimulation via a bipolar stimulator. Cells were superfused at 37 °C with NT solution. Ca^{2+} transients were assessed during steady-state external field stimulation at 0.5 Hz as previously described[242]. Ca^{2+} transient amplitudes were measured as peak Ca^{2+} transient fluorescence normalised to basal diastolic Ca^{2+} fluorescence (F/F_0). To assess the relaxation contribution from NCX, SERCA and other slow components (including the sarcolemma Ca^{2+} ATPase and mitochondria Ca^{2+} uniport), a standard single exponential equation was used to fit the decay trace of a steady-state Ca^{2+} transient to obtain a tau value (time constant) which represented the combined contributions of NCX, SERCA and other slow components to Ca^{2+} extrusion from the cytoplasm (τ_1) (Fig. 2-11. A). Cells were then subjected to an exposure of 10 mM caffeine in NT rapidly applied to induce a transient. The decay phase of this caffeine-induced transient represented the contribution of NCX and slow components (τ_2) (Fig. 2-11. B). Removal of the caffeine and external field stimulation at 0.5 Hz ensured the cell returned to the steady-state. Caffeine was rapidly applied a second time but in $0Na^{+}$-$0Ca^{2+}$ solution to elicit another caffeine-induced Ca^{2} transient (Fig. 2-11. C). In this case, NCX was blocked by the $0Na^{+}$-$0Ca^{2+}$ solution, therefore the decay tau of the second caffeine-induced transient represented the contribution of the slow components (τ_3) to Ca^{2+} efflux The rate constant of the Ca^{2+} transient decay (R) was calculated as $1/\tau_1$. The rate constant of NCX (R_{NCX}) was $1/\tau_2 - 1/\tau_3$. The rate constant of slow component (R_S) was $1/\tau_3$. The rate constant of SERCA (R_{SERCA}) was calculated as $R-R_{NCX}-R_S$, which is equal to $1/\tau_1 - 1/\tau_2$. SR Ca^{2+} Fractional release (x/y) was calculated using the steady-state Ca^{2+}

transient amplitude (x) and caffeine-induced Ca^{2+} transient amplitude (y) under the assumption that there is no change in cytosolic buffering power or buffering capacity between groups.

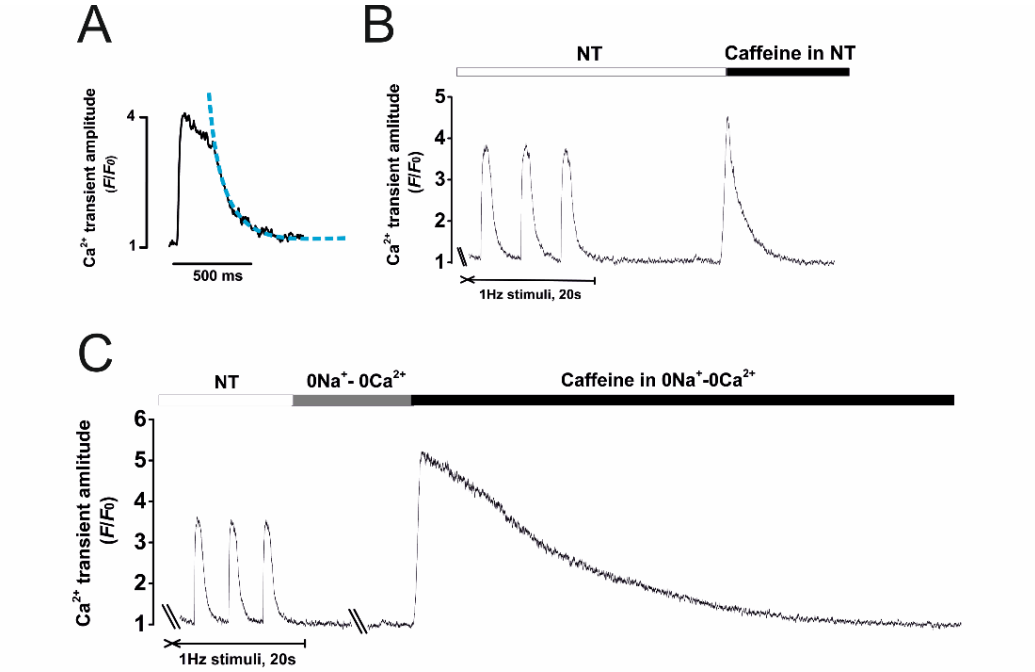

Figure 2-11. Protocol for Ca^{2+} transient assessment.

A: Decay phase of Ca^{2+} transient was fitted to a standard single exponential equation to obtain a tau value (time constant). B: A caffeine-induced Ca^{2+} transient was elicited after a SR Ca^{2+} loading protocol (1 Hz stimulation for 20 s). The decay of the transient was used to assess the relative contribution of NCX and other slow components. The short delay for the caffeine application was due to the manual control of the solution and the speed of the caffeine. Cells were all treated in the same way, and the potential SR Ca^{2+} leak during the short period of delay was negligible. C: After a SR Ca^{2+} loading protocol, cells were superfused with $0Na^{+}$-$0Ca^{2+}$ solution for 20 s to block NCX, followed by exposure to caffeine (in $0Na^{+}$-$0Ca^{2+}$). This last protocol allowed the contribution of the slow components to be calculated.

2.5.2 Imaging Ca^{2+} sparks and waves using line-scanning confocal microscopy

2.5.2.1 Experimental set-up for Ca^{2+} sparks and waves measurements

An inverted Nikon Eclipse TE-300 microscope with a "Bio-Rad Radiance 2000" confocal attachment was used as line-scanning microscope. A Nikon 40x oil immersion objective was used. Lasersharp 2000 (Bio-Rad, UK) software was used to operate the confocal microscope in line-scanning mode. A drop of cell suspension was loaded onto the chamber's coverslip following the application of 2 µl

mouse laminin to the base, allowing cells to adhere to the coverslip. Standard superfusate was NT solution with or without pharmacological agents detailed in the specific chapters. All experiments were conducted at 37 °C with the dye-loaded cells protected from light to avoid photobleaching of the Ca^{2+} probe.

2.5.2.2 Protocol for Ca^{2+} sparks and waves acquisition

Cells were loaded with Fluo-4 AM as described in section 2.7.1.2. Cells were initially stimulated at 0.5 Hz for 2 min to allow for steady state SR Ca^{2+} loading and contraction. Confocal settings for recording Ca^{2+} sparks and waves were as follows and not changed: laser power of 10 %, iris of 3 mm (z-axis depth of 1.5 µm) and scan speed of 500 lps. Once in steady-state cells were stimulated at 2 Hz for 20 s followed by a 30 s period of quiescence to detect Ca^{2+} sparks and waves. During the quiescence period, 15000 lines were scanned. This scan was timed to include the last 2 or 3 Ca^{2+} transients of the stimulation train (Fig. 2-12. A).

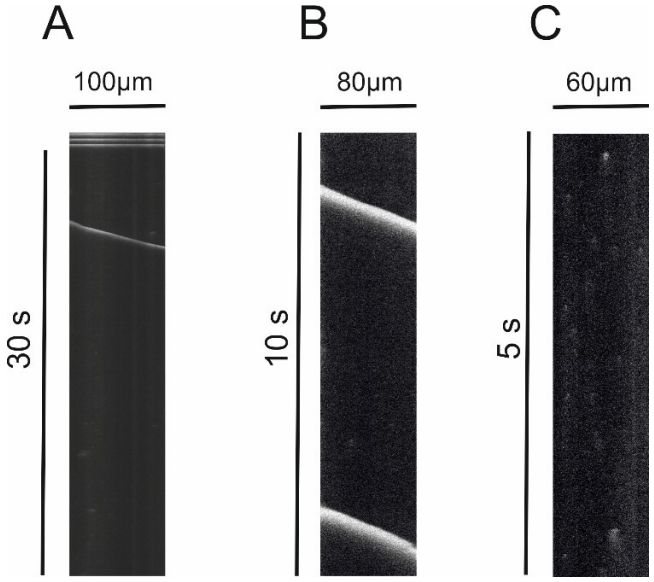

Figure 2-12. Representative line-scanning images of Ca^{2+} sparks and waves.

Ca^{2+} sparks and waves were measured during the quiescence 30 s following three Ca^{2+} transients (A). B, C: Typical traces of Ca^{2+} waves and sparks.

2.5.2.3 Data analysis

SparkMaster plugin in ImageJ (NIH, USA) was used to analyse Ca^{2+} sparks in the line scan image[243]. Detection criteria for Ca^{2+} sparks were set at 4.2 times the standard deviation above the mean background value instead of 3.8 to reduce false identification of Ca^{2+} sparks resulting from background noise. The SparkMaster plugin generated images of the line scans enabling the verification of automatically detected sparks. The Ca^{2+} spark parameters calculated by the plugin included frequency, amplitude, full width at half maximal amplitude (FWHM) and full duration at

half maximal amplitude (FDHM). Spark mass and SR leak were calculated using the formulae below[244]:

Spark mass = Amplitude x 1.206 x $FWHM^3$

Spark-mediated SR leak = Mass x Frequency

Ca^{2+} waves were analysed by using an ImageJ macro coded by Dr Markus Sikkel[242]. The parameters calculated included wave speed, frequency and amplitude. Wave-free survival analysis was performed by using Kaplan-Meier Estimates. Ca^{2+} spark morphological parameters including the amplitude, FWHM, FDHM and mass, and the spark-mediated SR leak data were log-transformed, resulting in normally distributed populations for statistical analysis. Ca^{2+} spark frequency data was skewed but contained zero value data, thus a Mann-Whitney Test (a nonparametric test), was used.

2.6 Composition of experimental solutions

All chemicals were purchased from Sigma-Aldrich. Composition (in mM):

Solutions for cardiac myocytes isolation:

Krebs-Henseleit (KH) solution

NaCl 119, KCl 4.7, $MgSO_4$ 0.94, $CaCl_2$ 1, KH_2PO_4 1.2, $NaHCO_3$ 25, Glucose 11.5; pH adjusted to 7.4 with 1M HCl

Low Ca^{2+} solution

NaCl 120, KCl 5, $MgSO_4$ 5, Na pyruvate 5, glucose 20, taurine 20, HEPES 10, NTA 5, $CaCl_2$ 35 µM (estimated final free [Ca^{2+}]: 12-15 µM); pH 6.96 adjusted with 1M NaOH

Enzyme solution

NaCl 120, KCl 5, $MgSO_4$ 5, Na pyruvate 5, glucose 20, taurine 20, HEPES 10, $CaCl_2$ 200 µM; pH 7.4 adjusted with 1M NaOH

Experimental external superfusate solutions:

NT solution

NaCl 140, KCl 6, glucose 10, N-2-hydroxyethylpiperazine-N'-2-ethanesulphoic acid (HEPES) 10, $MgCl_2$ 1, $CaCl_2$ 2; pH 7.4 adjusted with 1M NaOH

0Na^+-0Ca^{2+} solution

LiCl 140, KOH 6, glucose 10, HEPES 10, $MgCl_2$ 1, EGTA 1; pH 7.4 adjusted with 1M LiOH

External solution for Na^+/K^+ ATPase experiment

NaCl 140, KCl 6 (or 0 for inhibition of Na^+/K^+ ATPase), glucose 10, HEPES 10, $MgCl_2$ 1, $BaCl_2$ 2, $NiCl_2$ 5; pH 7.4 adjusted with 1M NaOH

External solution for $I_{Na,L}$ experiment

NaCl 137, CsCl 5.4, glucose 10, HEPES 10, $MgCl_2$ 2, $CaCl_2$ 1.8, Nitrendipine 0.002; pH 7.4 adjusted with 50 wt.% in water CsOH

Pipette filling solutions:

Sharp pipette filling solution

KCl 2M, EGTA 0.1, HEPES 5; pH 7.2 adjusted with 1M KOH

Patch pipette filling solution for Na^+/K^+ ATPase experiment

Cs-methanesulfonate 100, NaCl 30, CsCl 10, HEPES 10, EGTA 5, Mg-ATP 5, $MgCl_2$ 0.75; pH 7.2 adjusted with 50 wt.% in water CsOH

Patch pipette filling solution for $I_{Na,L}$ experiment

Cs-methanesulphonate 100, NaCl 10, CsCl 30, HEPES 10, EGTA 5, Mg-ATP 5, $MgCl_2$ 0.75; pH 7.2 adjusted with 50 wt.% in water CsOH

2.7 Statistical Analysis

Data were stored and processed using Microsoft Office Professional Plus 2010 (Microsoft Corporation, Redmond, WA, USA). Statistical analyses and figure construction were performed with OriginPro 9.1.0 (OriginLab Corporation, Northampton, MA, USA) and CorelDRAW ver. X5 (Corel Systems Corp., Ottawa, Canada). Statistical differences between means were calculated using Student's *t*-test, two-sample proportion test or a one-way ANOVA with a Fisher post-hoc test for more than two group comparison. Values are expressed as mean ± S.D., and where appropriate, n=number of cells from total number of hearts (n=cells/hearts). Statistical significance was denoted as not significant (n/s): $p>0.05$, *$p<0.05$, **$p<0.01$ and ***$p<0.001$.

3 LONGITUDINAL OBSERVATION OF CHANGES IN PHYSICAL CHARACTERISTICS DURING PROGRESSION OF PRESSURE-OVERLOAD RESPONSES IN GUINEA PIGS

3.1 Aims

- To assess the changes in physical characteristics and cardiac function in progression towards HF in a pressure-overload GP model of hypertrophy and HF.

3.2 Introduction

The development of cardiac hypertrophy is part of a complex series of responses to physiological or pathological stimuli[245]. Physical training and pregnancy are typical examples of physiological hypertrophy with changes in cardiac structure and function are reversible in contrast to pathological hypertrophy. Pathological hypertrophy occurs in hemodynamic stress (volume or pressure-overload) or ischemic heart disease, which is associated with structural changes such as fibrosis and cardiac dysfunction. In general, cardiac hypertrophy initially can be regarded as an adaptive compensation. However, if the pathological stimuli persists, the compensation may be inadequate and is likely to advance towards a decompensated condition with HF[246]. The transition from compensation to decompensation involves neurohumoral dysregulation and intra- and extra-cellular molecular signalling changes that are complex. Understanding the multifactorial mechanisms is important if we wish to intervene to prevent preclinical HF (AHA/ACC classification of Stage A and B HF) from progressing to HF[247].

In rodents, AC has been validated as a reproducible model to study the cardiac response to pressure-overload. The AC model is characterised by a first phase of compensated hypertrophy followed by a transition to HF, mimicking human pressure overload-induced HF[222]. In the GP the only studies of AC were those of the Sheridan group[223,248]. Much more *in vivo* characterisation of this model was needed and this part of the thesis describes such work.

3.3 Methods

The animal model, pressure-overload GPs, and echocardiography measurements were described in detail in chapter 2. Data and n numbers were a combination both male and female GPs (Males and females n number was shown in Chapter 6).

3.4 Results

3.4.1 Physical characteristics changes

Table 3-1 lists the changes in physical characteristics following sham or AC operation. There were no significant changes in body weight (BW) between the 60 days (D) and 150 D AC animals (60AC and 150AC, respectively) compared with their age-matched sham groups (60Sham and 150Sham, respectively). GPs had significantly heavier heart weight (HW) after 60 D and 150 D AC operations compared with age-matched sham operated GPs. Lung weight (LW) did not increase in 60AC operated animals compared with 60Sham, however LW significantly increased after 150AC. HW/BW ratio significantly increased in 60AC by 34 % and 150AC by 58 % compared with their age-matched sham 60Sham and 150Sham, respectively (Fig. 3-1. A). LW/BW ratio was unaltered between sham and AC group at 60 D, but showed a significant increase by 35 % at 150 D (Fig. 3-1. B). When comparing AC progression longitudinally, 150AC had 18 % higher HW/BW ratios and 19 % higher LW/BW ratios compared with the 60AC group (Fig. 3-1. A & B).

	Sham	AC	p value
Body weight (g)			
Pre-Op	408 ± 46	398 ± 43	n/s: p>0.05
60 days	726 ± 103	759 ± 145	n/s: p>0.05
150 days	882 ± 142	827 ± 90	n/s: p>0.05
Heart weight (g)			
60 days	2.32 ± 0.30	3.14 ± 0.68	***p<0.001
150 days	2.73 ± 0.44	4.07 ± 0.55	***p<0.001
Lung weight (g)			
60 days	3.19 ± 0.36	3.49 ± 0.68	n/s: p>0.05
150 days	3.7 ± 0.51	4.7 ± 0.93	***p<0.001

60Sham, n=23 (M=12, F=11); 60AC, n=21 (M=10, F=11); 150Sham, n=25 (M=10, F=15); 150AC, n=24 (M=11, F=13); n=GP numbers; Student's *t*-test.

Table 3-1. Changes in physical characteristics following sham or AC operation.

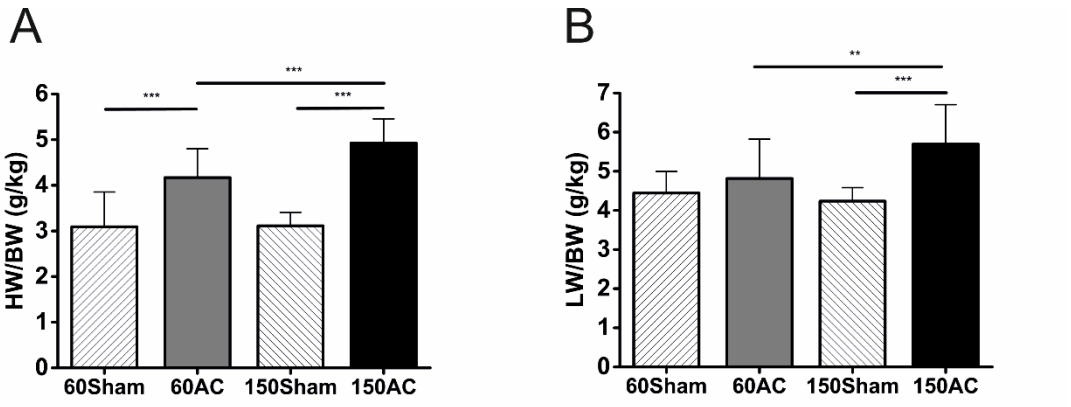

Figure 3-1. Comparing HW/BW and LW/BW ratios between sham and AC animals 60 D and 150 D post-operation.

*A: The HW/BW ratio at 60 D and 150 D was significantly increased in the AC group compared with the sham group. The 150AC group had higher HW/BW ratio compared with the 60AC group. B: The LW/BW ratio did not change between 60sham and 60AC groups. The ratio however was significantly increased in the 150AC group compared with their age-matched sham group. The 150 D AC operated animals had a higher LW/BW ratio compared with the 60AC group (60Sham, n=23; 60AC, n=21; 150Sham, n=25; 150AC, n=24; n=GP numbers; one-way ANOVA with a Fisher post-hoc test, **p<0.01, ***p<0.001).*

3.4.2 *In vivo* echocardiography for cardiac function study

Figure 3-2 depicts typical M-mode echocardiography from pre-op AC, 60AC and 150AC GPs. LVIDd and LVIDs progressively increased in the AC-operated animals from the time of pre-op to 60 D and the final end-point of 150 D. Pre-operative cardiac function, determined by LVIDs, LVIDs and FS, was similar between the animals selected for sham and AC groups (Fig. 3-2). At 60 D, the AC group had larger LVIDd by 10 % and LVIDs by 15 % compared with the sham group (Fig. 3-3. A & B). However, FS remained unchanged between AC with sham at this stage (Fig. 3-3. C). At 150 D, the AC GPs had significantly dilated LVIDd by 18 % and LVIDs by 71 % with markedly reduced FS by 40 % compared with sham-operated GPs (Fig. 3-4). Comparing the echocardiography changes during the progression of AC, LVIDd and LVIDs significantly increased post-operatively at 60 D, with marked dilatation at 150 D (Fig. 3-5. A & B). FS remained unchanged at AC 60 D but severely declined by 28 % at 150 D compared with Pre-op AC (Fig. 3-6).

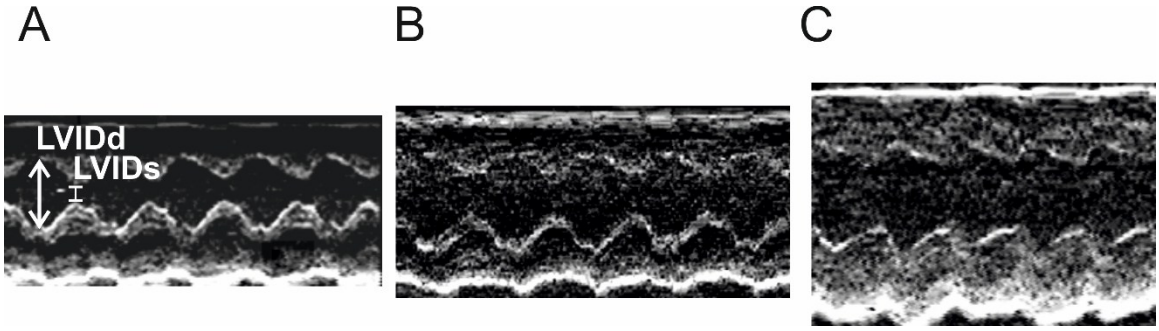

Figure 3-2. Typical M-mode echocardiography images from pre-op AC (A), 60AC (B) and 150AC (C) GPs.

Image A depicts the measurement of LVIDd and LVIDs. Both LVIDd and LVIDs increased progressively from the pre-operative measurements, to 60AC and 150AC.

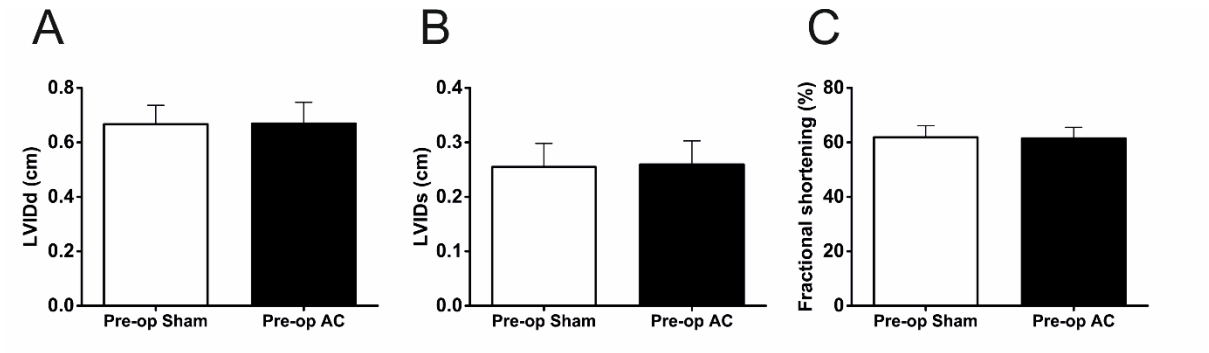

Figure 3-3. Pre-operation echocardiography study of sham and AC group.

The pre-operative echocardiography study indicated that the (A) LVIDd, (B) LVIDs and (C) FS showed no significant differences between sham and prospective AC group (Pre-op Sham, n=30; Pre-op AC n=29; n=GP numbers; Student's t-test).

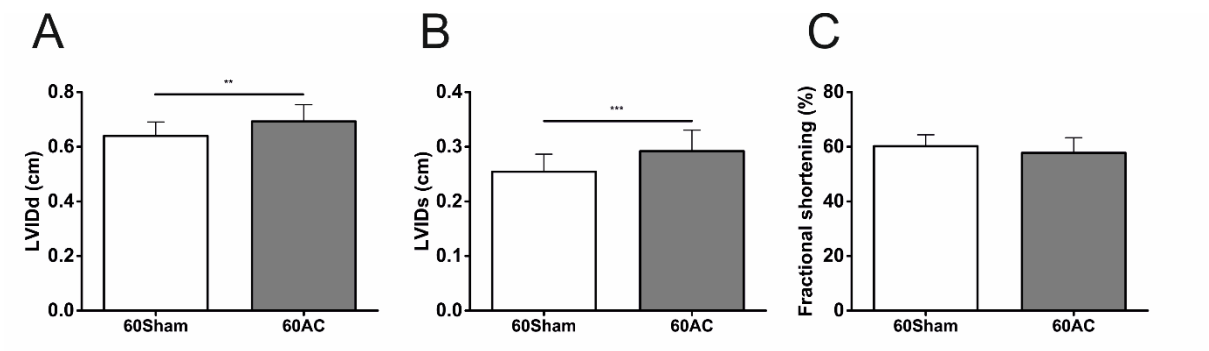

Figure 3-4. Echocardiography study of sham and AC group 60 D post-operation.

*Both (A) LVIDd and (B) LVIDs were significantly larger in 60AC compared with the 60Sham group. C: FS remained unchanged between 60Sham and 60AC (60Sham, n=24; 60AC, n=23; n= GP numbers; Student's t-test, **p<0.01, ***p<0.001).*

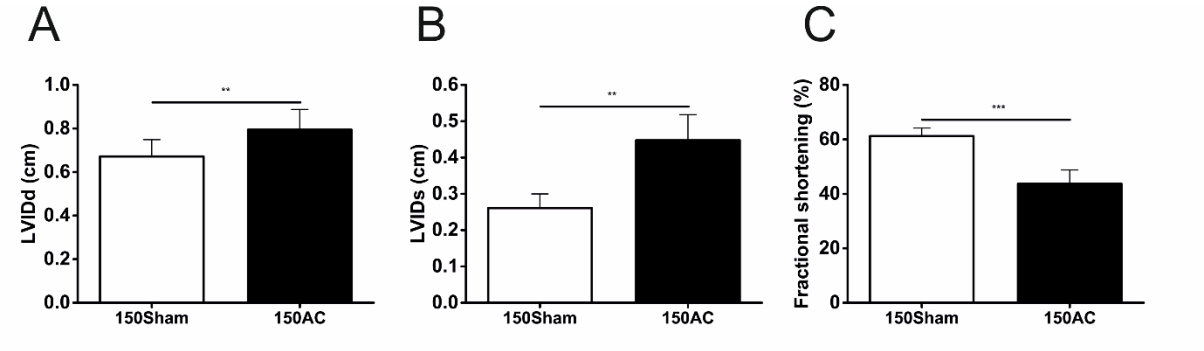

Figure 3-5. Echocardiography study of sham and AC group 150 D post-operation.

*A & B: The 150AC GPs had larger LVIDd and LVIDs compared with the 150Sham. C: 150AC GPs showed significantly decreased FS compared with those in the 150Sham group (150Sham, n=25; 150AC, n=20; n= GP numbers; Student's t-test, **p<0.01, ***p<0.001).*

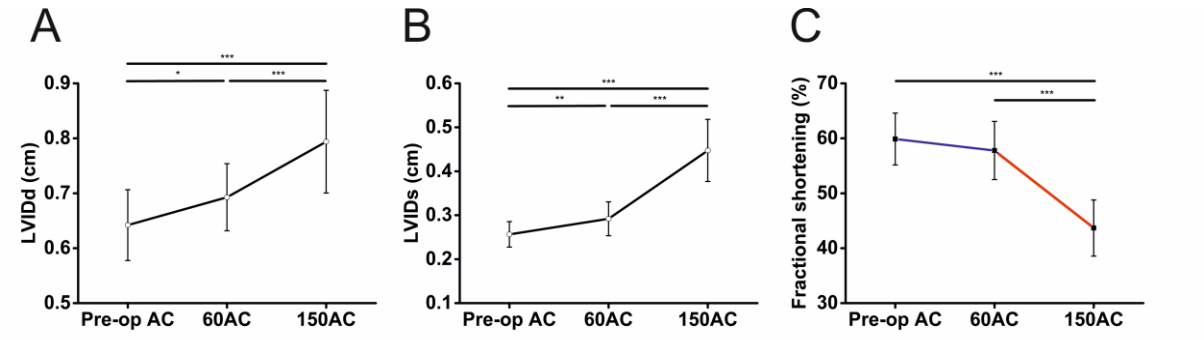

Figure 3-6. Serial echocardiography study of AC group.

*A, B: LVIDd and LVIDs showed a significant increase at 60AC with a further marked increase at 150AC. C: FS remained unchanged at 60AC compared with the Pre-op values but markedly decreased in 150AC (Pre-op AC, n=29; 60AC, n=23; 150AC, n=20; n= GP numbers; one-way ANOVA with a Fisher post-hoc test, *p<0.05, **p<0.01, ***p<0.001).*

3.5 Discussion

The purpose of this chapter was to assess the changes in the animal physical characteristics and their cardiac function in the progression from cardiac hypertrophy to HF induced by pressure-overload AC.

GP AC model is a well-established model for the investigation of pressure overload-induced cardiac hypertrophy and HF. Kinsbury *et al* showed chronic ascending AC (149 ± 6 days) resulted in significant increases in HW/BW and LW/BW ratio with reduced cardiac output and increased levels of plasma atrial natriuretic peptide in GPs[223]. Gray *et al* reported GP hearts started to develop cardiac hypertrophy after ascending AC 60 days[114]. Naqvi *et al* used relative small GPs (BW 200 -300 g) and showed cardiac hypertrophy developed after ascending AC around 80 days[249]. The timeline of

AC progression varies among species. While mice subjected to transverse AC presented hypertrophy as early as 7 days and decompensated HF at 4 weeks, rats need 7 - 8 weeks to develop cardiac hypertrophy and 18 - 20 weeks for decompensated HF[224,250].

Here we used the parameters of HW, LW, HW/BW, and LW/BW ratios to indicate the physiological changes occurring during the progression alongside echocardiographic assessments of cardiac function at the proposed compensated hypertrophy stage (60 D after AC) and decompensated HF (150 D after AC). We not only made comparison between age-matched sham and AC-operated groups but also investigated the changes in AC operated GPs from 60 D to 150 D.

There were significant increases in HW and HW/BW ratio following 60 D and 150 D AC operated animals compared with the age-matched sham-operated groups. The LW and LW/BW ratio remained unchanged between the 60 D sham and AC-operated animals however both significantly increased in the 150 D AC group. In pressure-overload HF, poor LV function causes blood retention in the LV chamber which not only leads to LV chamber dilatation, but also retrogradely results in pulmonary congestion[251]. We suggest that cardiac hypertrophy develops without congestion of the lungs at the 60 D stage, with 150 D AC animals developing cardiac hypertrophy combined with congestion of the lungs. The GPs had a tendency to lose weight after AC surgery but the trend was not statistically significant. LVIDd and LVIDs were significantly larger in AC animals compared with the sham group but FS was unaltered at 60 D. Although the morphology of the heart changed following AC, heart function was maintained. At 150 D post-AC operation, significant LV chamber dilatation was observed with a drastic decrease in FS. This is compatible with an observation that the AC operated GPs started to show poor appetite and lethargy when around 150 D after the operation.

According to the American Heart Association, human cardiac systolic function is quantitatively classified as 4 classifications, which are normal, mild, moderate and severe dysfunction according to ejection fraction (50 - 70, 40 - 49, 30 - 39, and < 30 %, respectively). The New York Heart Association (NYHA) Functional Classification classifies HF in human into class I - IV based on the activity and symptom of the patients. With correlation to human, AC operated GPs at 60D could be classified as normal or mild dysfunction of ejection fraction and a function class I - II. 150D AC group may be classified as moderate or severe dysfunction with function class III - IV. Human pressure-overload cardiac hypertrophy and HF has several clinical entities including essential hypertension, aortic stenosis, subvalvular aortic stenosis, and coarctation of the aorta. 13 % of patients with chronic hypertension induced LV hypertrophy progressed to systolic dysfunction during a 3-year of follow-

up[69]. Patients with aortic stenosis showed a long compensated period. However, once the symptoms of angina, syncope or HF develop, survival drops with an average survival of only 2 years after HF symptom onset[252].

It was confirmed that our GP pressure-overload animal model showed a transitional progression from cardiac hypertrophy to HF following AC surgery. We recognise that at 60 D post AC surgery, GPs adapt to the pressure-overload and enter into a compensatory stage. After this, FS declines almost by half illustrating the failure of compensatory mechanisms and decompensation occurring at 150 D.

3.6 Conclusions

Based on the findings mentioned above, the progression from hypertrophy to HF in the aortic constricted GPs is similar to the progression of pressure-overload cardiac disease in human although on a different time-scale. While compensated cardiac hypertrophy with maintained FS was shown at 60 D after AC operated GPs, animals showed LV dilatation, congested lungs and deteriorated cardiac function at 150 D after AC, which represents the HF stage. We suggest the pressure-overload GP model is suitable for longitudinal study for the progression from cardiac hypertrophy to HF.

4 CHANGES IN ACTION POTENTIAL DURATION AND Ca^{2+} REGULATION DURING THE PROGRESSION TOWARDS HEART FAILURE

4.1 Aims

- To assess the changes in APD in response to pressure-overload cardiac hypertrophy and HF in cardiac myocytes.
- To evaluate changes in Ca^{2+} transient, SR Ca^{2+} content and $I_{Ca,L}$ in the progression to HF
- To determine the spontaneous Ca^{2+} spark frequency, morphology and spark-mediated SR leak in sham and HF groups.

4.2 Introduction

Dysregulation of Ca^{2+} handling occurs in cardiac hypertrophy and HF, which alters E-C coupling, leading to contractile dysfunction[72]. Cardiac hypertrophy is initially viewed as an adaptive process or a transitional zone, maintaining strength of contraction and cardiac output to meet the need of the body. At some time point, the hypertrophy response becomes inadequate and the heart enters a decompensated stage, signalling the progression towards HF. The underlying mechanisms switching from an initial compensated period to a decompensated stage are however still to be determined. Here the measurements of APD, $I_{Ca,L}$, SR Ca^{2+} content, Ca^{2+} transient and spontaneous Ca^{2+} sparks were performed to elucidate the changes in calcium handling during the progression of hypertrophy towards HF.

4.3 Methods

4.3.1 Myocytes isolation and electrophysiology measurement

Experiments were performed on single cardiac myocytes isolated from sham or AC operated GPs from either sexes at 60 D or 150 D according to the methods described in section 2.3.1 (Males and females n number was shown in Chapter 6). Techniques and protocols for electrophysiology measurements including APD, $I_{Ca,L}$, Ca^{2+} transient, SR Ca^{2+} content and spontaneous Ca^{2+} sparks were detailed in sections 2.4 and 2.5.

4.3.2 Decay phase of peak $I_{Ca,L}$

To investigate the inactivation of the peak $I_{Ca,L}$, the decay phase of peak $I_{Ca,L}$ was fitted in a standard double exponential equation to obtain a fast and a slow time constants- tau 1 and tau 2. The inactivation phase of peak $I_{Ca,L}$ may have fast phase in the beginning followed by a slow phase. Single

exponential equation, which only gives one time constant, cannot fit the decay curve well in some cases but double exponential equation is able to fit the curves in these cases, which may be more representative to the decay phase of peak $I_{Ca,L}$ (Fig. 4-1).

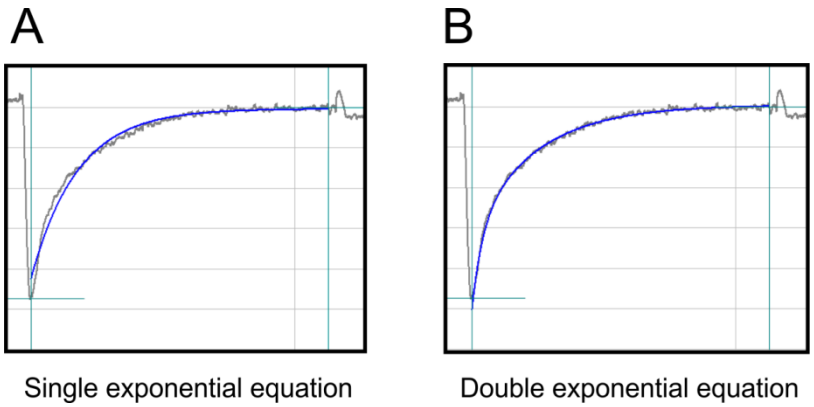

Figure 4-1. Comparison of single and double exponential equation fitness of peak $I_{Ca,L}$.

Blue lines indicated the fit-in curves generated from fitting the decay phase of the peak $I_{Ca,L}$ in single (A), which tau=55.2ms, and double (B) exponential equation, which tau1=7.2 ms, tau2=40.5ms.

4.3.3 Relaxation contribution for Ca^{2+} transient decay phase

The measurement of Ca^{2+} transient decay rate constant, rate constant of SERCA, NCX and other slower transporters (PMCA and mitochondria Ca^{2+} uniporter) were detailed in section 2.5.1.3. SERCA, NCX and other slower transporters are the three major contributors for the decay of Ca^{2+} transient, therefore the Ca^{2+} transient decay rate constant is the sum of the rate constant of SERCA, NCX and other slower transporters[28]. The definition of relaxation contribution is the ratio of rate constant of a certain contributor to Ca^{2+} transient decay rate constant[28].

4.3.4 Analysis of Ca^{2+} sparks

Ca^{2+} sparks morphological parameters including the amplitudes, FWHM, FDHM and mass, and the spark-mediated SR leak data were log-transformed, resulting in normally distributed populations for statistical analysis. Ca^{2+} spark frequency data were skewed but contained zero value data, thus a Mann-Whitney test (a nonparametric test) was used.

4.4 Results

4.4.1 APD

Figure 4-2 shows representative action potential recordings from sham and AC groups at their 60 D (60Sham and 60AC, respectively) and 150 D periods (150Sham and 150AC). Figure 4-3 illustrates a comparison of APD_{90} between sham and AC groups. There was no significant change in APD_{90} between 60Sham and 150Sham, however APD_{90} was significantly prolonged in 60AC by 24 % compared with 60Sham. The APD_{90} in the 150AC group was significantly 29 % longer compared with 150Sham and was also longer by 7 % compared with the 60AC group.

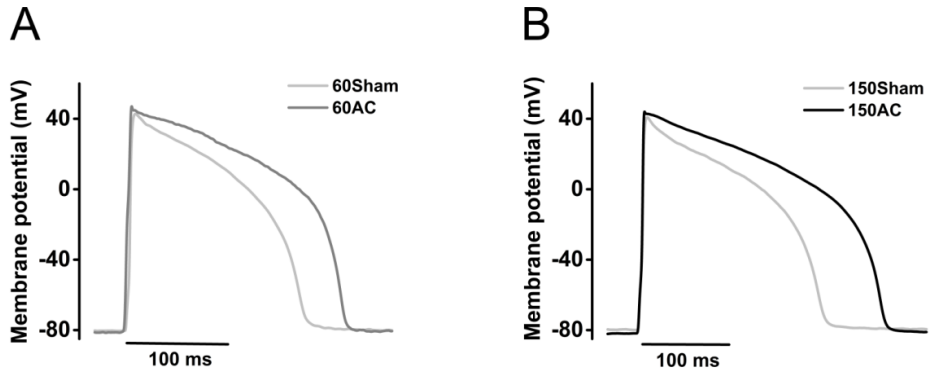

Figure 4-2. Typical traces of action potentials from sham and AC groups at 60 D and 150 D post-operatively.

APD_{90} was prolonged in the AC groups compared with sham at both 60 D (A) and 150 D (B) following the AC operation.

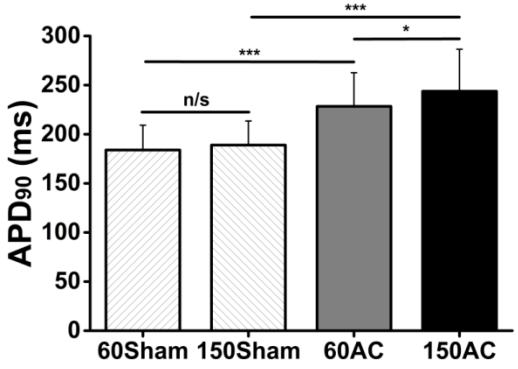

Figure 4-3. APD_{90} in sham and AC groups.

*Action potential duration was significantly prolonged in 60AC and 150AC compared with their age-matched sham-operated groups. 150AC had longer APD_{90} compared with 60AC (60Sham, n=67/8; 150Sham, n=87/10; 60AC, n=50/6; 150AC, n=70/6; one-way ANOVA with a Fisher post-hoc test, n/s: p>0.05, *p<0.05, ***p<0.001).*

4.4.2 Cell capacitance

Mean cell capacitances of 60Sham, 150Sham, 60AC and 150AC were 167.0 ± 48.3, 174.9 ± 42.1, 211.2 ± 60.5, and 262.4 ± 65.0 pF, respectively (60Sham, n=164; 150Sham, n=96; 60AC, n=154; 150AC, n=97). There was no difference between mean cell capacitance of 60Sham and 150Sham. Mean cell capacitance of 60AC was larger than 60Sham (***p<0.001). Mean cell capacitance of 150AC was larger than 150Sham (***p<0.001). 150AC has larger cell capacitance compared with 60AC (***p<0.001). One-way ANOVA with a Fisher post-hoc test was used.

4.4.3 $I_{Ca,L}$

There was no change in peak $I_{Ca,L}$ between 60Sham and 150Sham (Fig. 4-4. A). The 60AC and 150 AC had similar peak $I_{Ca,L}$ compared with 60Sham and 150Sham, respectively (Fig. 4-4. B & C). There was no significant difference in peak $I_{Ca,L}$ between 60AC and 150AC (Fig. 4-4. D). Time constants: tau 1 and tau 2 remained unchanged between 60Sham and 60AC (Fig. 4-5. B & C), however the tau values were significantly longer in 150AC compared with the 150Sham and 60AC groups.

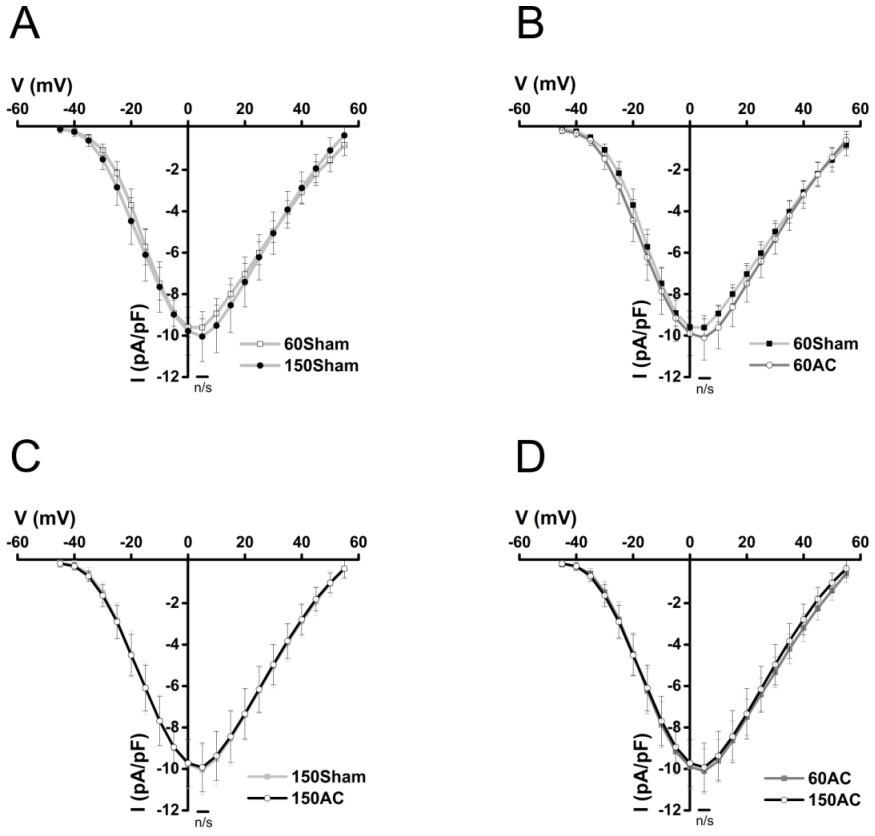

Figure 4-4. I-V relationship of L-type Ca^{2+} channel in sham and AC groups.

A: Maximum peak $I_{Ca,L}$ at 5 mV remained unchanged between 60Sham and 150Sham. B: 60AC had similar peak $I_{Ca,L}$ compared with age-matched sham group. C: 150Sham and 150AC had similar peak $I_{Ca,L}$. D: There was no change in peak $I_{Ca,L}$ between 60AC and 150AC (60Sham, n=29/4; 150Sham, n=64/8; 60AC, n=36/6; 150AC, n=39/6; Student's t-test, n/s: p>0.05).

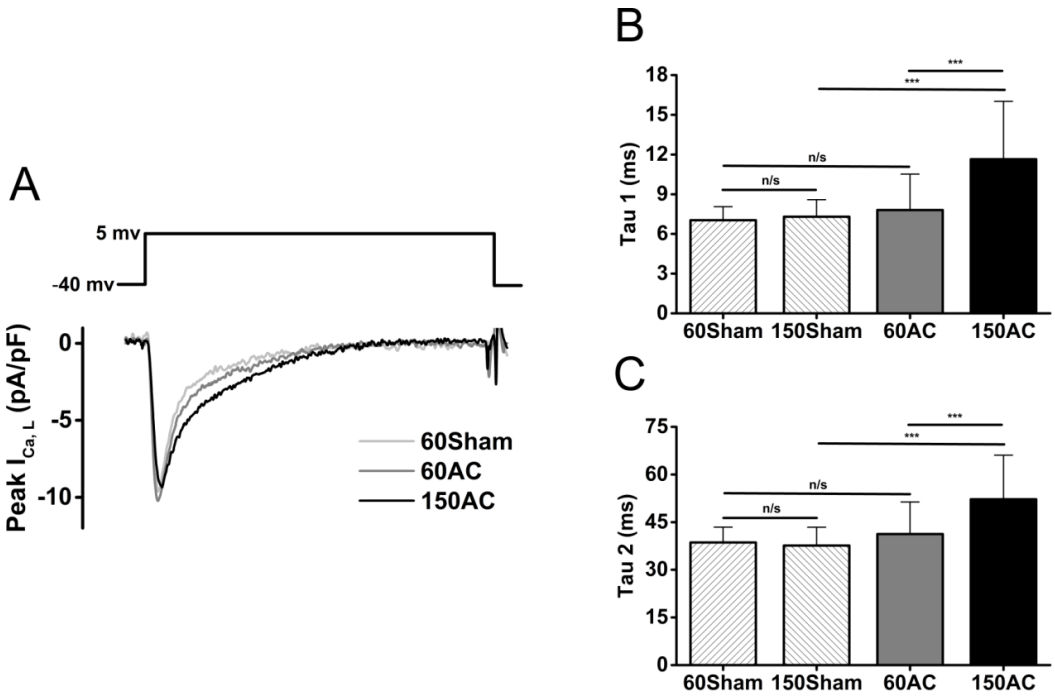

Figure 4-5. Typical peak $I_{Ca,L}$ in 60Sham, 60AC and 150AC, and the corresponding decay tau.

*B & C: The decay phase of peak $I_{Ca,L}$ was fitted in a standard double exponential equation to obtain time constants: tau 1 and tau 2. 150AC had a longer tau 1 and tau 2 compared with the 150Sham and 60AC. Tau 1 and tau 2 remained unchanged between 60Sham and 60AC (60Sham, n=29/4; 150Sham, n=64/8; 60AC, n=36/6; 150AC, n=39/6; one-way ANOVA with a Fisher post-hoc test, n/s: p>0.05, ***p<0.001).*

4.4.4 Ca^{2+} transient

4.4.4.1 Ca^{2+} transient amplitudes, time to peak, decay 50 % and 90 % time

Figure 4-6 (A) depicts typical traces of Ca^{2+} transients from 60Sham, 60AC and 150AC cells. Cells from 60AC had 11 % larger Ca^{2+} transient amplitudes compared with 60Sham (Fig. 4-6. B). Ca^{2+} transient amplitudes were significantly reduced in 150AC by 34 % compared with 150Sham (Fig. 4-6. B). Time to peak (TTP) of Ca^{2+} transient was 18 % longer in 60AC compared with 60Sham (Fig. 4-7. A). TTP was considerably longer in 150AC by 88 % compared with 150Sham (Fig. 4-7. A). The peak to 50 % decay time (R_{50}) was unaltered between 60Sham and 60AC but was 15 % longer in 150AC than in 150Sham (Fig. 4-7. B). From the peak to 90 % decay time (R_{90}) was 9 % and 33 % prolonged in 60AC and 150AC compared with 60Sham and 150Sham, respectively (Fig. 4-7. C). The 150AC group had 53 % and 23 % longer TTP and R_{90} respectively compared with that in 60AC, but the R_{50} remained unchanged between 60AC and 150AC (Fig. 4-7. A, B & C).

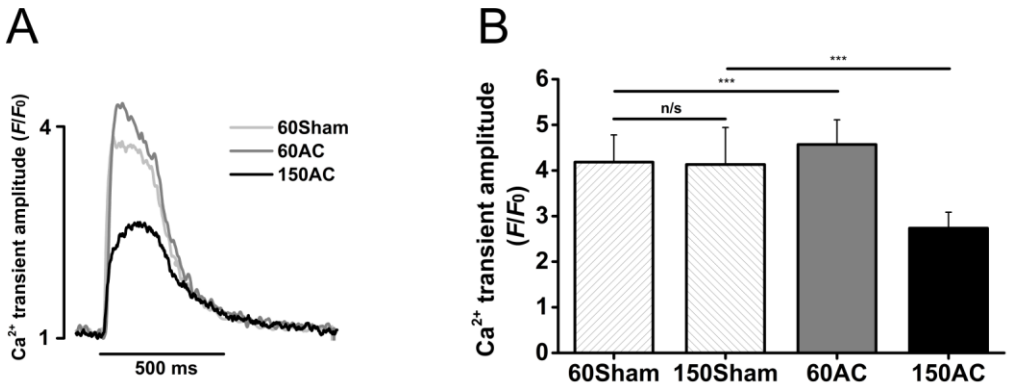

Figure 4-6. Ca^{2+} transients in 60Sham, 60AC and 150AC.

*A: Typical traces of Ca^{2+} transients in 60Sham, 60AC and 150AC. B: Ca^{2+} transient amplitudes in sham and AC group. B: Ca^{2+} transient amplitudes were 11 % greater in 60AC compared with 60Sham but significantly reduced in 150AC compared with 60AC and 150Sham by 40 % and 34 %, respectively (60Sham, n=55/5; 150Sham, n=81/6; 60AC, n=56/5; 150AC, n=84/6; one-way ANOVA with a Fisher post-hoc test, n/s: p>0.05, ***p<0.001).*

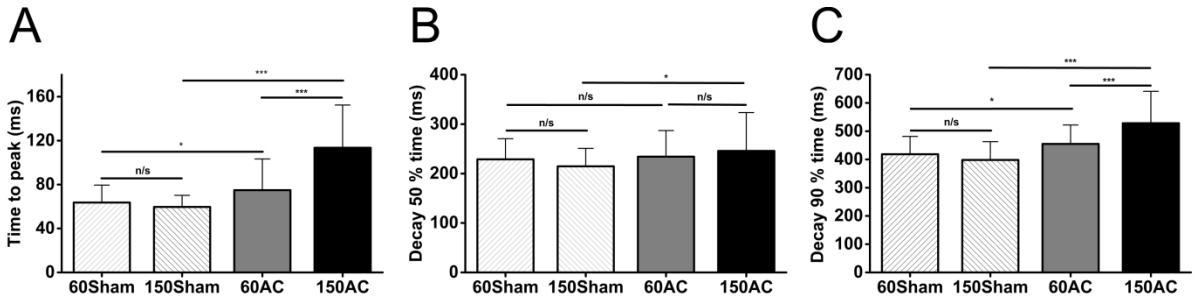

Figure 4-7. Ca^{2+} transient TTP, R_{50} and R_{90} in sham- and AC-operated GPs.

*A: 150AC had 88 % and 53 % longer TTP compared with 150Sham and 60AC, respectively. 60AC had 18 % longer TTP than 60Sham. B & C: 150AC and a prolonged R_{50} and R_{90} compared with 150Sham. While the R_{50} remained unchanged between 60Sham and 60AC, 60AC had 9 % longer R_{90} compared with 60Sham (60Sham, n=55/5; 150Sham, n=54/4; 60AC, n=46/5; 150AC, n=75/6; one-way ANOVA with a Fisher post-hoc test, n/s: p>0.05, *p<0.05, ***p<0.001).*

4.4.4.2 Ca^{2+} transient decay rate constant and relaxation contribution

The Ca^{2+} transient decay rate constant was 33 % slower in 150AC compared with 150Sham (Fig. 4-8), however the rates were similar between 60Sham and 60AC groups. Rate constant of 150AC was 34 % smaller compared with 60AC (Fig. 4-8). The rate constants of SERCA, NCX and other slower transporters remained unchanged between 60Sham and 60AC (Fig. 4-9. A). Also the relaxation contribution showed no differences between 60Sham and 60AC (Fig. 4-9. B). 150AC showed significant 11 % and 16 % increases in rate constant of NCX and other slower transporters respectively and a 51 % decrease in the rate constant of SERCA compared with those in 150Sham (Fig. 4-9. C). Again 150AC had a 28 % decrease in the contribution relaxation from SERCA and 63 % and 70 % increases in relaxation contribution from NCX and other components, respectively (Fig. 4-9. D). Compared with 60AC, 150AC had a 51 % reduced rate constant of SERCA function and 10 % increased rate constant of NCX function (Fig. 4-9. E). 150AC had 28 % decrease in relaxation contribution from SERCA and 64 % increase in relaxation contribution from NCX compared with 60AC (Fig. 4-9. F). Fractional SR Ca^{2+} release was 11 % larger in 60AC than in 60Sham, and this change was also seen in 150AC compared with 150Sham cells by 33 % increase (Fig. 4-10). 150AC had 17 % higher fractional SR Ca^{2+} release compared with 60AC (Fig. 4-10).

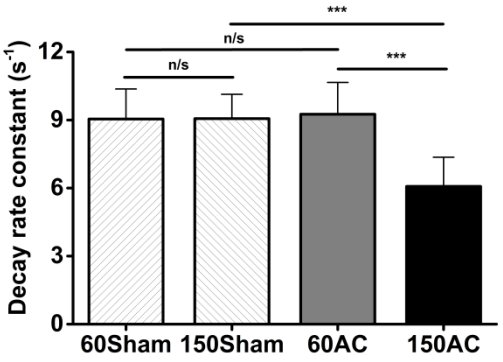

Figure 4-8. Decay rate constant in sham and AC groups.

*150AC had marked reduction in transient decay rate constant compared with 60AC and 150Sham by 34 % and 33 % respectively. 60Sham and 60AC had similar decay rate constants (60Sham, n=55/5; 150Sham, n=54/4; 60AC, n=46/5; 150AC, n=75/6; one-way ANOVA with a Fisher post-hoc test, n/s: p>0.05, ***p<0.001).*

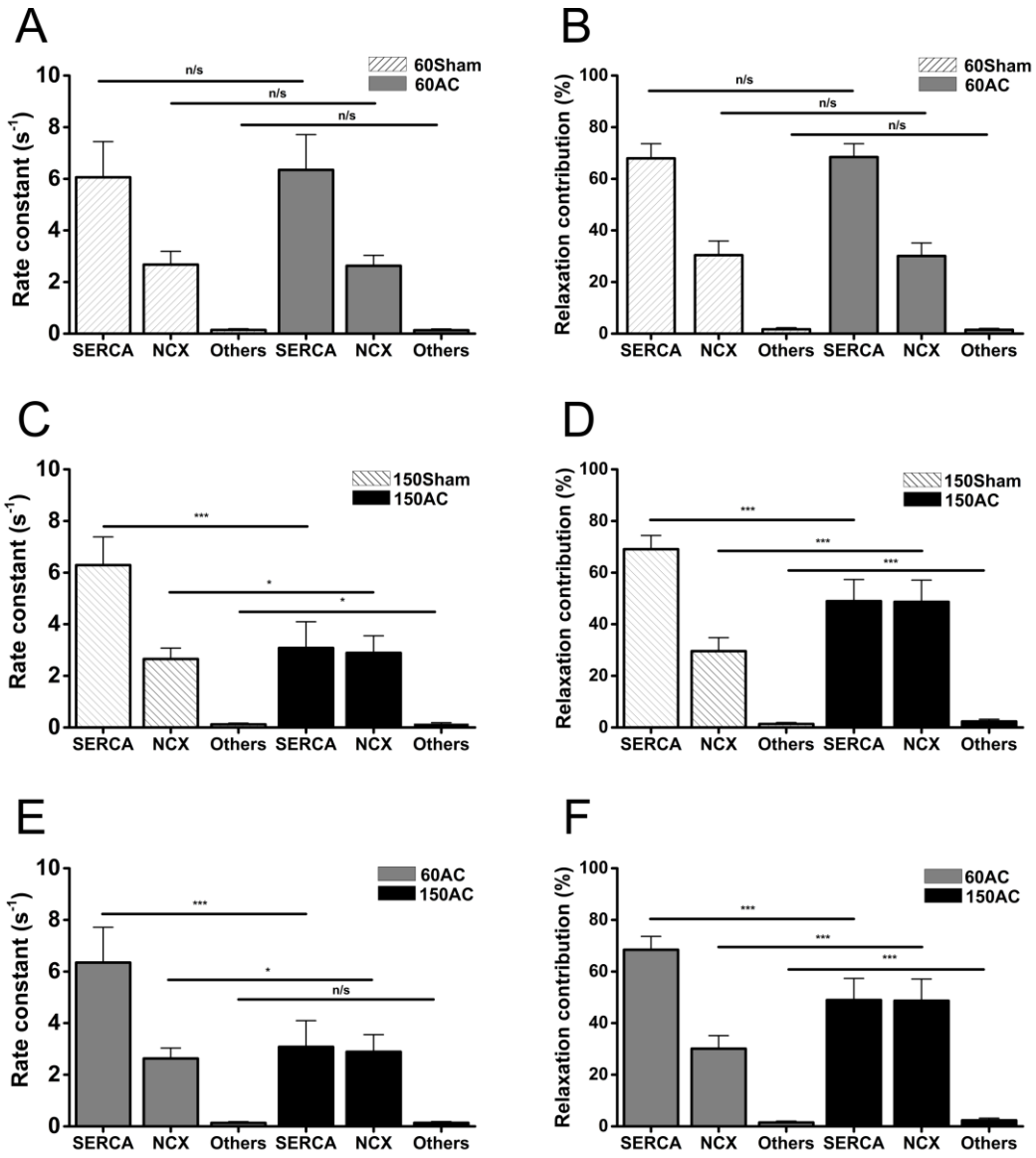

Figure 4-9. Relaxation contribution in sham and AC groups.

*A & B: 60Sham and 60AC had similar rate constant of SERCA, NCX and other slower transporters and the corresponding relaxation contributions. C & D: 150AC had 51 % reduced rate constant of SERCA and 11 % increased rate constant of NCX with 28 % decrease in relaxation contribution from SERCA and 63 % increase in contribution from NCX when compared with 150Sham. E & F: Compared with 60AC, 150AC had 51 % reduced rate constant of SERCA and 10 % increased rate constant of NCX with 28 % decrease in relaxation contribution from SERCA and 64 % increase in contribution from NCX (60Sham, n=55/5; 150Sham, n=54/4; 60AC, n=46/5; 150AC, n=75/6; one-way ANOVA with a Fisher post-hoc test, n/s: p>0.05, *p<0.05, ***p<0.001).*

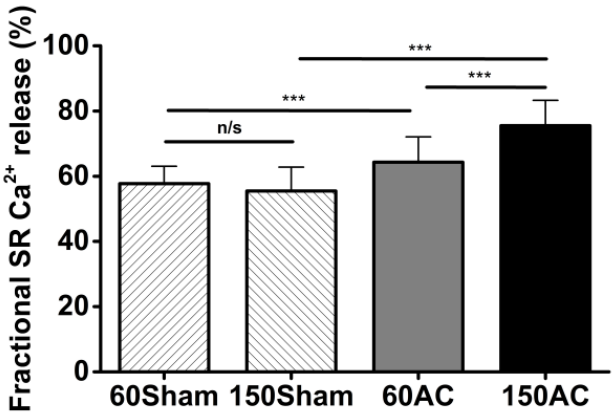

Figure 4-10. Fractional SR Ca^{2+} release in sham and AC groups.

*150AC had 33 % and 17 % greater fractional SR Ca^{2+} release compared with 150Sham and 60AC respectively. 60AC showed 11 % increased fractional SR Ca^{2+} release compared with 60Sham (60Sham, n=42/5; 150Sham, n=68/6; 60AC, n=54/6; 150AC, n=64/6, one-way ANOVA with a Fisher post-hoc test, n/s: p>0.05, ***p<0.001).*

4.4.5 SR Ca^{2+} content

While the SR Ca^{2+} content, calculated by integrating the caffeine-evoked NCX inward current, was greater in 60AC compared with 60Sham by 10 %, it showed marked reduction by 46 % in the 150AC group compared with 150Sham and 60AC (Fig. 4-11).

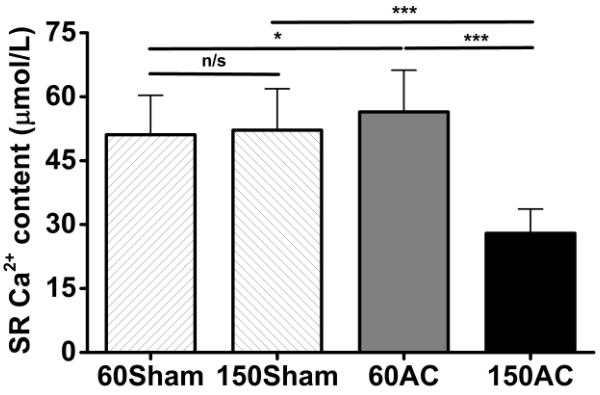

Figure 4-11. SR Ca^{2+} content in sham and AC groups.

*60AC cells had significant greater SR Ca^{2+} contents compared with 60Sham. 150AC showed a marked reduction in SR Ca^{2+} content compared with 150Sham and 60AC. (60Sham, n=25/6; 150Sham, n=50/5; 60AC, n=35/4; 150AC, n=61/7; one-way ANOVA with a Fisher post-hoc test, n/s: p>0.05, *p<0.05, ***p<0.001)*

4.4.6 Spontaneous Ca^{2+} sparks and spark-mediated SR leak

Spontaneous Ca^{2+} spark frequency was significantly higher in 150AC compared with 150Sham (Fig. 4-12. A). Spark amplitudes (F/F_0) were unaltered between 150Sham and 150AC (Fig. 4-12. B). 150AC had longer FWHM and FDHM compared with 150Sham (Fig. 4-12. C & D). 150AC also had larger spark mass compared with 150Sham (Fig. 4-12. E). Spark-mediated SR leak (Leak= Mass x Frequency) was significantly greater in 150AC compared with 150Sham (Fig. 4-12. F).

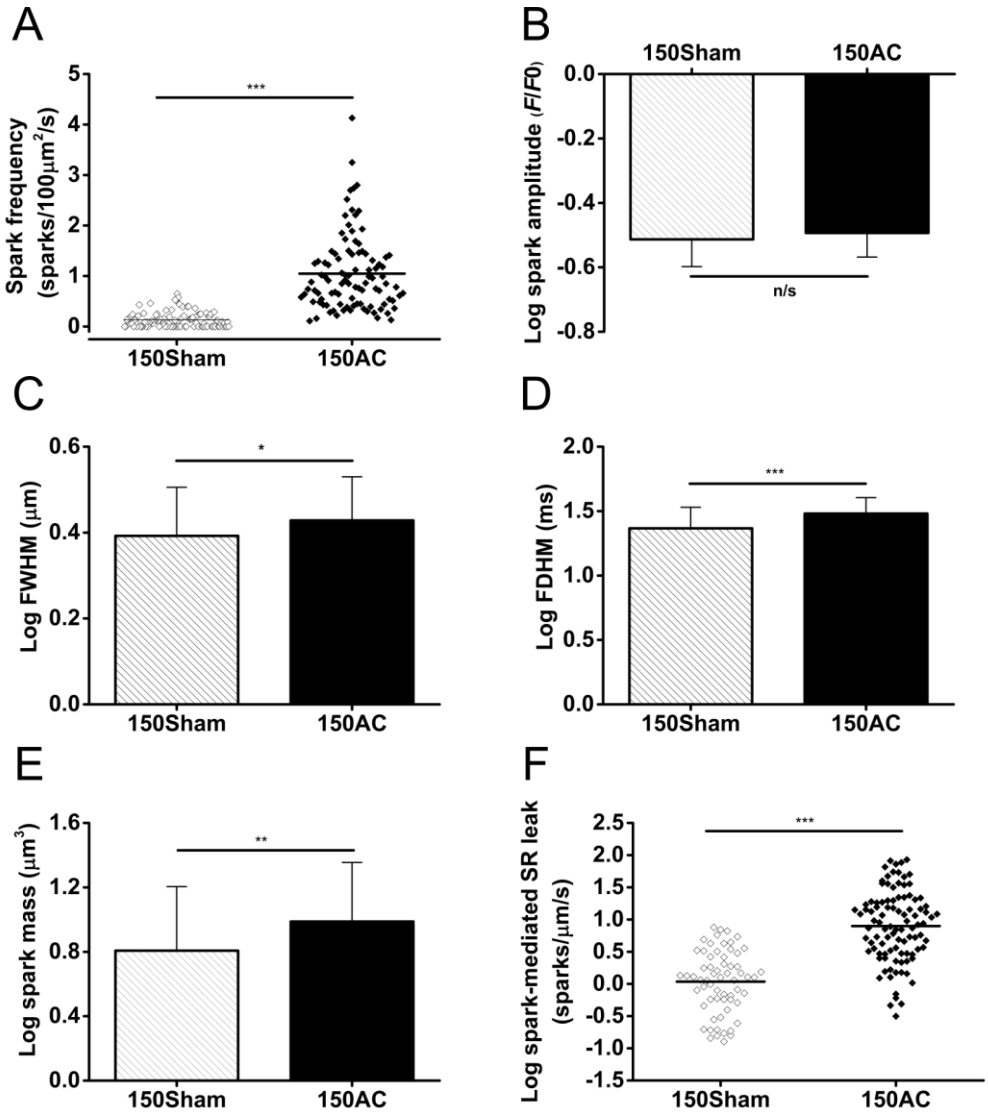

Figure 4-12. Spontaneous Ca^{2+} sparks and spark-mediated SR leak.

*A: Ca^{2+} spark frequency in 150AC was significantly higher compared with 150Sham. B: Ca^{2+} spark amplitudes were unchanged between 150AC and 150Sham. C & D: Spark morphology including FWHM and FDHM was longer in 150AC compared with 150Sham. E: 150AC had a significantly larger spark mass than 150Sham. F: Spark-mediated SR leak was greater in 150AC than in 150Sham (150Sham, n=63/8; 150AC, n=98/7; Student's t-test, n/s: p>0.05, *p<0.05, **p<0.01, ***p<0.001).*

4.5 Discussion

This chapter detailed the changes in cellular APD and Ca^{2+} regulation that occurred following pressure-overload cardiac hypertrophy and HF. Prolongation of APD and dysregulation of Ca^{2+} handling were involved in the compensated stage of cardiac hypertrophy and decompensated HF.

4.5.1 Prolongation of APD

The action potential initiates EC coupling and is determined by the complex interaction of a number of ion channels and transporters[253]. A prolongation of the APD may therefore reflect an alteration of Ca^{2+} regulation and contraction[82]. Increases in inward currents, such as $I_{Ca,L}$, $I_{Na,L}$ and I_{NCX}, promote the prolongation of APD. On the contrary, a reduction in outward currents, including I_{to} and I_{K1}, will also contribute to the prolongation of APD[79], and such modulation of the action potential has been reported to alter Ca^{2+} regulation and E-C coupling[254]. Our data reveals that action potential in 60AC is prolonged, implying that there may be an increases in inward currents to overcome or compensate for the stress from AC, which in turns leads to prolongation of APD. Decreased density of outward K^+ currents, such as I_{to} and I_{K1} play an important role in the prolongation of APD in cardiac hypertrophy and HF[82,255]. Reduced I_{to} also results in reduced phase 1 early repolarisation, thus may decrease the driving force for Ca^{2+} influx. However, the reduced I_{to} may have relative small effect on APD in our case because unlike mice and rat[255], GPs ventricular myocytes have smaller I_{to}[256]. Decreases in I_{K1} may contribute to action potential prolongation, but it would be mainly in the very late phase of final repolarisation. While reduced I_{K1} may take part in the prolongation in our GP model, there was a report showed unchanged I_{K1} in a AC GP model[257]. Increased $I_{Na,L}$ has been shown to contribute to prolongation of APD[4]. Our data showed increased $I_{Na,L}$ at both cardiac hypertrophy and HF stages, which may lead to the prolongation of APD. $I_{Na,L}$ will be discussed in chapter 5.

SR Ca^{2+} content was found higher in 60AC which may support that there was an increased Ca^{2+} influx. We then investigated $I_{Ca,L}$ in 60AC and found there was no change in peak $I_{Ca,L}$ in 60AC. Therefore, the increased Ca^{2+} influx may not be a result of increased Ca^{2+} influx from L-type Ca^{2+} channel. We suspect there could be an elevated $[Na^+]_i$ to influence NCX operation, allowing more Ca^{2+} influx or less Ca^{2+} extrusion via NCX[31]. Although a reverse-mode of NCX causes outward current, an elevated Na^+ influx may overwhelm the effect and then result in prolongation of action potential. In later chapter, we will discuss the role of Na^+/K^+ ATPase, which is primarily responsible for the regulation $[Na^+]_i$ and $I_{Na,L}$, who could be an contributor to elevated $[Na^+]_i$.

Further prolongation of APD_{90} was noted at 150AC compared with 60AC, but FS was markedly reduced at 150AC. The decompensation status may have resulted from alteration of other

mechanisms, including reduced SERCA function, decreased SR Ca^{2+} content, lower Na^+/K^+ ATPase, and up-regulated NCX function[83]. We found SR Ca^{2+} content was markedly reduced in 150AC. The rate constant of SERCA was considerably reduced, which will discuss in later section. The relaxation contribution of NCX significantly increased in 150AC. Therefore there may be more Ca^{2+} extrusion via NCX, causing depletion of SR Ca^{2+} content and also more inward current. Na^+ influx may still continue to increase for the purpose of inotropic effect. Altogether contributes to the prolongation of APD in 150AC. But overall, the Ca^{2+} transient and SR Ca^{2+} content decreased, leading to a systolic dysfunction in 150AC.

4.5.2 Changes in Ca^{2+} regulation

4.5.2.1 $I_{Ca,L}$

Ca^{2+} handling, involving Ca^{2+} influx into the cell, intracellular Ca^{2+} release and uptake and Ca^{2+} efflux from the cell is altered in cardiac hypertrophy and HF. During the action potential, Ca^{2+} influx through L-type Ca^{2+} channels not only triggers Ca^{2+} release from the SR to initiate contraction but also contributes to the shape of the AP. We found the peak $I_{Ca,L}$ remained unchanged in 60AC group when the stage is suggested to be compensated hypertrophy. Naqvi *et al* also reported unaltered peak $I_{Ca,L}$ in hypertrophied myocytes from a AC rabbit model[258]. The unaltered $I_{Ca,L}$ may not be the primary reason for the increases in SR Ca^{2+} content and Ca^{2+} transient amplitude in the 60AC group. Again, there could be an elevated $[Na^+]_i$ to cause more Ca^{2+} influx from reverse-operated NCX. While many reported an unchanged $I_{Ca,L}$ density in HF model, some studies have shown increased $I_{Ca,L}$ in the early stage of cardiac hypertrophy[85].

Our data showed the peak $I_{Ca,L}$ still remained unchanged at 150AC compared with sham group. However, the time constants: tau1 and tau 2 for the decay phase of peak $I_{Ca,L}$ were longer in 150AC, implying that the inactivation kinetics may be altered at the HF stage. Slower inactivation of L-type Ca^{2+} channel may allow longer time for Ca^{2+} to stay in the cell, which could provide more available Ca^{2+} for myofilament. While there were reports showing decreased peak $I_{Ca,L}$ in human HF[259], most studies agree that peak $I_{Ca,L}$ density is unaltered in cardiac hypertrophy and HF but the kinetics of the channel have been shown to be altered[68,85]. A slowing of the Ca^{2+} dependent inactivation (CDI) has been observed in HF model[260,261]. The maintained $I_{Ca,L}$ together with a slowing of its inactivation in 150AC could be seen as a mechanism to increase the amount of Ca^{2+} influx to overcome the shortage of SR Ca^{2+} content in HF. The mechanisms of CDI are not yet fully understood, however several structures seem to be associated with CDI, including $Ca_v\beta$ and the N-terminus of $Ca_v1.2$, involved in slow inactivation[19,262]. The Ca^{2+}/calmodulin-dependent protein kinase II (CaMKII)-

mediated phosphorylation may also modulate the kinetics of L-type Ca^{2+} channel when specific sites of the channel are phosphorylated[263].

4.5.2.2 SR Ca^{2+} content and Ca^{2+} transient

The data above showed that both Ca^{2+} transient amplitudes and SR Ca^{2+} content were greater in the 60AC group, and in chapter 3 it was reported that FS was unchanged at the same stage of pathology. The enhanced SR Ca^{2+} loading may allow compensation so that FS remains unchanged in the setting of increased afterload by AC. Increased Ca^{2+} influx via L-type Ca^{2+} channel and increased function of SERCA were found to contribute to the increase in SR Ca^{2+} content as well as Ca^{2+} transient amplitudes[85,264]. But we showed that the peak $I_{Ca,L}$ was unchanged in 60AC. The rate constant and relaxation contribution of SERCA remained unchanged in 60AC. The increased SR Ca^{2+} content may be a result of increased Ca^{2+} influx or decreased efflux from NCX in response to an elevated $[Na^+]_i$[33,89,265].

Although we showed the function of SERCA remained unchanged in 60AC group, some studies reported a decrease in expression of SERCA in human and animal models of cardiac hypertrophy and failure[93,97,99,266]. However in the early stage of the cardiac hypertrophy, the expression of SERCA may remain unchanged or was slightly decreased[92,95]. The unaltered function of SERCA could be due to changes in expression and/or its phosphorylation status. For example, the SERCA function is inhibited by un-phosphorylated phospholamban (PLB)[267]. The PKA and CaMKII have been shown to phosphorylate PLB selectively at Ser-16 or Pro-17, resulting in release of inhibition of SERCA function[267].

150AC had significantly reduced Ca^{2+} transient amplitudes, prolonged TTP, R_{50}, R_{90}, slower decay rate constant, higher fractional SR Ca^{2+} release and decreased SR Ca^{2+} content. The prolonged Ca^{2+} transient decay time suggested longer Ca^{2+} removal from the cytoplasm by impaired Ca^{2+} efflux and/or uptake mechanisms. The rate constant of SERCA was markedly reduced at 150AC. The impaired Ca^{2+} uptake mechanism of SERCA may cause a reduction in SR Ca^{2+} content. The expression of SERCA has been shown to decrease in cardiac hypertrophy and HF[93,95,98]. 150AC also showed an increase in rate constant of NCX, implying an up-regulation of NCX function to remove excess intracellular Ca^{2+}. However, the up-regulated NCX could further contribute to the depletion of SR Ca^{2+} content[87,268]. In addition to Ca^{2+} regulation, the NCX function is also regulated by intracellular Na^+ which is primarily controlled by Na^+/K^+ ATPase. The role of Na^+/K^+ ATPase and Na^+ regulation will be discussed in chapter 5.

4.5.2.2.1 Spontaneous Ca^{2+} sparks

The depletion of SR Ca^{2+} content may not only result from a decrease function of SERCA and up-regulated NCX but increased open probability of RyR2 to cause Ca^{2+} leak from the SR[107,269]. Our results showed 150AC cells had higher spontaneous Ca^{2+} spark frequencies although the amplitudes of the sparks were unchanged. Spark-mediated SR leak was in greater in 150AC cells compared with 150Sham cells. Therefore, basal diastolic SR Ca^{2+} leak may also contribute to the depletion of SR Ca^{2+} content in the 150AC group. The present data is in agreement with studies in animal HF model and human HF which show an increased diastolic SR Ca^{2+} leak was associated with depletion of SR Ca^{2+} content[110,269,270]. Hyperphosphorylation of RyR2 by CaMKII has been shown to increase diastolic SR Ca^{2+} leak[110,271,272]. In human HF, CaMKII-dependent hyperphosphorylation of RyR2 at Ser-2815 may be the key factor evoking RyR2 dysfunction[273]. In addition, a chronic hyperadrenergic state in HF has been suggested to induce RyR2 hyperphosphorylation at Ser-2809 by PKA, which causes detachment of the RyR2-stabilising protein FKBP12.6 from the RyR2 complexes and also uncouples adjacent RyR2 complexes, can lead to instability of RyR2 gating and an increase in Ca^{2+} spark frequency in HF[40]. Increased SR Ca^{2+} leak may also increase diastolic $[Ca^{2+}]_i$, contributing to diastolic dysfunction, and could be arrhythmogenesis[107]. Increased SR Ca^{2+} leak may favour Ca^{2+} waves formation, which can drive inward NCX (forward-mode) current, eliciting EADs and DADs, respectively[274,275].

4.6 Conclusions

During the AC progression, prolongation of APD was noted at the stage of compensation to pressure-overload stress. Peak $I_{Ca,L}$ remained unaltered at this stage. During the compensation period, increased SR Ca^{2+} content and Ca^{2+} transient were found, which may result from reverse-mode operated NCX in response to elevated $[Na^+]_i$, which help to maintain contractile force. However, with progression to decompensated HF, further prolonged APD was noted, suggesting there were more increased inward current or more decreased outward current, which may in turn recruit more Ca^{2+} into cells to maintain contractile force. Peak $I_{Ca,L}$ still remained unaltered but with slower inactivation kinetics at HF stage, which may also suggest more Ca^{2+} influx are in demand. But the SR Ca^{2+} content and Ca^{2+} transient amplitude were markedly reduced as a result of decreased Ca^{2+} uptake from SERCA and up-regulated function of NCX which caused detrimental amount of Ca^{2+} efflux during Ca^{2+} transient decay. Increased basal diastolic SR Ca^{2+} leak in HF also played a role in depletion of SR Ca^{2+} content and may not only contribute to increased $[Ca^{2+}]_i$, resulting in diastolic dysfunction, but may also be arrhythmogenic.

5 CHANGES IN Na^+/K^+ ATPase and $I_{Na,L}$ DURING THE PROGRESSION FROM CARDIAC HYPERTROPHY TO HEART FAILURE

5.1 Aims

- To assess the changes in function and expression of the Na^+/K^+ ATPase at the stages of cardiac hypertrophy and HF.
- To assess the effect of Na^+/K^+ ATPase inhibition on the Ca^{2+} transient and SR Ca^{2+} content by using a cardiac glycoside, strophanthidin.
- To assess the changes in $I_{Na,L}$ at the cardiac hypertrophy and HF stages.

5.2 Introduction

Na^+/K^+ ATPase maintains the $[Na^+]_i$ by transporting 3 Na^+ ions out and 2 K^+ ions into the cell, while consuming one ATP. The activity of Na^+/K^+ ATPase influences the level of $[Na^+]_i$ which in turn affects the way that the NCX operates, therefore regulating Ca^{2+} handling. Reduced activity of the Na^+/K^+ ATPase increases $[Na^+]_i$ causing more Ca^{2+} influx (and less Ca^{2+} extrusion) by promoting more reverse-mode NCX activity during the cardiac cycle, resulting in an inotropic effect[72]. While it is widely known that blockade of the pump with therapeutic agents increases muscle contractility, there is less information on how the Ca^{2+} transient and SR Ca^{2+} load are affected by smaller reductions in Na^+/K^+ ATPase current, as observed in early HF.

It is also unclear if the expression of Na^+/K^+ ATPase isoforms change in the progression towards HF. While α1 isoform mRNA and protein expression are unaltered in some rat HF models[124], there are studies that report reduced protein expression of Na^+/K^+ ATPase in rabbit, rat and human HF[90,123,276]. Swift *et al* reported reduced protein expression of Na^+/K^+ ATPase α1 and α2 together with decreased pump current in their rat HF model[276]. Schwinger showed reduced expression of Na^+/K^+ ATPase α1, α3 and β1 with decreased pump activity and ouabain binding sites in human HF myocardium[90]. Bossuyt *et al* also showed reduced expression of Na^+/K^+ ATPase α1 and α3 with decreased Na^+/K^+ ATPase activity in rabbit HF model[123]. However, reduced Na^+/K^+ ATPase current with unaltered pump protein expression was found in a cardiac hypertrophy mouse model[128] suggesting that the changes occurring to Na^+/K^+ ATPase function may involve associated regulatory proteins, the most likely candidate being PLM, the ϒ subunit of the Na^+/K^+ ATPase and a substrate for protein kinases A and C[29,32,123]. These studies also indicate that care is needed when attempting to directly correlate molecular biology findings with Na^+/K^+ ATPase function.

While lower activity of Na^+/K^+ ATPase could explain increased $[Na^+]_i$ in HF, there is also evidence suggesting that there is a substantial Na^+ contribution from late sodium current ($I_{Na,L}$) , a very slowly inactivating I_{Na} component[4,238]. However, very little is known about changes in $I_{Na,L}$ in the progression from pressure-induced hypertrophy to HF. In this chapter, GPs with AC were used to investigate Na^+/K^+ ATPase current, function and expression at the cardiac hypertrophy and HF stages. We also investigate whether inhibition of Na^+/K^+ ATPase influences Ca^{2+} handling, resulting in an inotropic effect. Finally, $I_{Na,L}$ was measured during the progression from cardiac hypertrophy and HF.

5.3 Methods

5.3.1 Cell isolation

Experiments were performed on single cardiac myocytes isolated from male and female sham or AC operated GPs 60 (60Sham and 60AC, respectively) or 150 days following banding (150Sham and 150AC, respectively) according to the methods as described in section 2.3.1 (Males and females n number was shown in Chapter 6).

5.3.2 Measurement of Na^+/K^+ ATPase current and reactivation

Techniques and protocol for the measurements of Na^+/K^+ ATPase current and reactivation are detailed in section 2.4.6.

5.3.3 Effect of Na^+/K^+ ATPase inhibition on Ca^{2+} transients and SR Ca^{2+} contents

Methods for measurements of Ca^{2+} transient and SR Ca^{2+} content (the integral of caffeine-induced inward NCX current) were detailed in section 2.4 and 2.4, accordingly. Strophanthidin (10 µM) was used to inhibit the Na^+/K^+ ATPase. At this concentration it produced about 50 % inhibition of the Na^+/K^+ ATPase current (Fig. 5-3. A). Ca^{2+} transients and SR Ca^{2+} content were measured in the absence or in the presence of 10 µM strophanthidin after 2 min exposure. Using a cardiac glycoside to partially block pump current at a dose which replicates 50 % reduction in pump current, approximately the same amount of inhibition measured in HF, was hypothesised to increase diastolic Ca^{2+}, Ca^{2+} transient amplitude and SR Ca^{2+} content in cardiomyocytes. This set of experiments was designed as a Cardiovascular Sciences BSc project and performed by the student Harishanan Surendra under Dr. MacLeod and my supervision.

5.3.4 Immunocytochemistry and confocal microscopy imaging of Na^+/K^+ ATPase isoform α1

5.3.4.1 Protocol

Materials and solutions are listed in Table 5-1. The surface of glass-bottomed Petri dishes was covered with a thin layer of mouse laminin onto which isolated left ventricular cardiomyocytes suspended in DMEM were placed. The dishes were incubated at 37 °C for 30 min allowing cells to attach securely onto the surface of the well. After incubation, phosphate buffer saline (PBS) was added circumferentially to each dish and which was gently tilted to wash away excess and unattached cells. 150 µl of mouse anti-Na^+/K^+ ATPase α1 antibody solution (1.5 µl antibody in 150 µl PBS and 150 µl blocking buffer) or 150 µl of rabbit anti-Na^+/K^+ ATPase α2 antibody solution (2 µl antibody in 150 µl PBS and 150 µl blocking buffer) was pipetted onto the cells and the dishes incubated overnight at 4 °C. The dishes were gently washed twice with 2 ml PBS, and 400 µl of anti-mouse antibody solution or anti-rabbit antibody solution (1 µl antibody in 200 µl PBS and 200 µl blocking buffer) was added into the α1 or α2 antibody dish accordingly and incubated for 3 h. After a second wash step, five drops of Vectashield + DAPI were added to each dish. Great care was taken to minimise the loss and drying of myocytes. The Petri dishes were covered with foil to protect them from light. Image acquisition was carried out with a Zeiss LSM780 confocal microscope. Confocal images were processed using Zen© software (Carl Zeiss Microscopy GmbH, 2011). Reports suggest that the α1 isoform of the Na^+/K^+ ATPase is uniformly distributed between surface sarcolemma and the T-tubules, while the α2 isoform is more concentrated in T-tubules and therefore in the central area of the cells[48,49]. To account for this potential variable distribution, two regions of interest were identified for every cell studied. ImageJ software (NIH, USA) was used to define fixed regions of interest (3 x 20 μm^2 placed over the sarcolemma region (largely assessing the α1 isoform) and 10 x 20 μm^2 placed in the central region of the cell (largely assessing α2). The average fluorescence density for each ROI was measured and normalised to sham group to obtain relative expression of fluorescence density.

Petri dish	35 mm, with a 14 mm inner well and no.0 cover glass (MatTek)
PBS	1 tablet in 200 ml water (Fisher Chemical)
Blocking solution	2 - 4 % bovine serum albumin (BSA) in PBS with goat serum (2 - 3 %)
Primary antibodies	mouse anti-Na^+/K^+ ATPase α1 monoclonal antibody (Life Technologies) rabbit anti-Na^+/K^+ ATPase α2 polyclonal antibody (EMD Millipore)
Secondary antibodies	Alexa Fluor® 488 goat anti-mouse IgG for α1 (Invitrogen) Alexa Fluor® 488 goat anti-rabbit IgG for α2 (Invitrogen)
Nuclear and chromosome dye	Vectashield® mounting medium for fluorescence with 4',6-diamidino-2-phenylindole (DAPI, Vector Laboratories)

Table 5-1. Materials and solutions for immunocytochemistry.

5.3.5 Western blot of Na^+/K^+ ATPase isoform α1 and PLM.

Western blotting was used to assess the protein expression of Na^+/K^+ ATPase isoform α1, and the regulatory protein PLM and its phosphorylated form (phosphorylated PLM-Ser^{68}) in sham and HF. I am grateful to Miss Alice Francis for help with most parts of the Western blot work.

5.3.5.1 Protein extraction

Following the Langendorff cell isolation, left ventricular myocytes were re-suspended in cell lysis buffer (composition listed in Table 5-2) and homogenised by sonication. The lysate was centrifuged for 1 min at 10000 rpm, at 4°C. The supernatant was aliquoted and stored at -80°C until required.

Component	Volume (µl)
Cell lysis buffer (10X, Cell Signaling Technology, USA)	100
Phenylmethanesulfonyl Fluoride (PMSF, 200 mM, Cell Signaling Technology, USA)	5
Phosphatase inhibitor cocktail 2 (Sigma-Aldrich, UK)	10
Phosphatase inhibitor cocktail 3 (Sigma-Aldrich, UK)	10
Sodium dodecyl sulphate (SDS, 10 %, Sigma-Aldrich, UK)	100
Dithiothreitol (DTT, 1 M, Sigma-Aldrich, UK)	1
Protease inhibitor cocktail (Sigma-Aldrich, UK)	10
dH_2O	764

Table 5-2. Components of cell lysis buffer.

5.3.5.2 Protein quantification

Proteins were quantified using a Pierce BCA Protein Assay Kit (Thermo Scientific) according to the manufacturer's instructions. Concentrations of known bovine serum albumin (BSA) standards from 25, 125, 250, 500, 750, 1000, 1500 to 2000 µg/ml were used to construct a standard curve (Table 5-3). Samples were measured by optical density (O.D.) at 562 nm using a microplate reader. Standards and samples were added in duplicate to the microplate and the corresponding O.D. values were averaged. Sample protein concentrations were obtained from the standard curve corresponding to the mean O.D. of the samples.

Vial	Volume of Diluent (µL)	Volume and Source of BSA (µL)	Final BSA Concentration (µg/ml)
A	0	300 of Stock	2000
B	125	375 of Stock	1500
C	325	325 of Stock	1000
D	175	175 of vial B dilution	750
E	325	325 of vial C dilution	500
F	325	325 of vial E dilution	250
G	400	325 of vial F dilution	125
H	400	100 of vial G dilution	25
I	400	0 (blank control)	0

Table 5-3. BSA standards preparation.

5.3.5.3 SDS-PAGE Gels

The Bio-Rad mini gel system with 1.5 mm glass plates was used to make SDS-PAGE gels. Different percentage gels were used for specific proteins of interest; 8 % gels for Na^+/K^+ ATPase α1 and 12 % gels for PLM and phosphorylated PLM-Ser[68]. The gel solutions were made using the components as listed in Table 5-4. The resolving solution was poured between the glass plates and isopropanol was layered on top to seal the resolving gel. The gels were left to set for 25 min. Subsequently, the isopropanol was removed from the plates which were then gently rinsed with water and dried using filter paper. The stacking buffer was then poured above the resolving buffer. A 1.5 mm 15-well "comb" was then quickly inserted, ensuring that there were no air bubbles in the gel. Gels were kept at RT for 30 min before use or stored in wet tissue paper for up to 2 weeks in the fridge.

Gel (%)	8 %	10 %	12 %		4 %
Resolving buffer (ml)				**Stacking buffer (ml)**	
Bis-Tris buffer (4x)	2	2	2	Bis-Tris buffer (4x)	0.5
MBG water	4.359	3.959	3.559	MBG water	1.278
40 % acrylamide	1.6	2	2.4	40 % acrylamide	0.2
10 % APS (µl)	32	32	32	10 % APS (µl)	16
TEMED (µl)	8.6	8.6	8.6	TEMED (µl)	6.2
Total	8	8	8		2

Table 5-4. SDS-PAGE Gels preparations.

5.3.5.4 Na^+/K^+ ATPase α1 Western blotting

8 % SDS PAGE gels were used for Na^+/K^+ ATPase α1 Western blotting. They were loaded with 10 µg sample protein and electrophoresis started by applying 80 - 100 V for 15 min then increasing the voltage to 130 V for 45 min or until the protein sample had migrated to the bottom of the gel. The separated proteins were transferred to a PVDF membrane using the Trans-Blot Turbo Transfer System according to the manufacturer's instructions (BioRad). The PVDF membrane containing the transferred proteins was placed in TBST for 5 min then "blocked" with BioRad blocking grade buffer overnight in a cold room (4 °C) to prevent non-specific binding of the detection antibodies during the subsequent steps following transfer. The membrane was incubated with either Na^+/K^+ ATPase α1 primary antibody (Life Technologies) at 1:2000 dilution or GAPDH primary antibody (Santa Cruz) at 1:5000 dilution for 1 h at RT. The membrane was washed four times for 5 min each time with TBST. The membrane was then incubated with secondary antibody (anti-mouse IgG-HRP, Cell Signaling Technology) against both primary antibodies at 1:2000 dilution for 1 h at RT. The membrane was subsequently washed again, 4 x 5 min with TBST. The membrane containing the HRP-conjugated antibody bound to the target protein was visualised by Clarity Western ECL Substrate (BioRad) and captured by BioImager and GeneSnap software.

5.3.5.5 PLM Western blotting

A 12 % SDS PAGE gel was used for PLM western blotting. Samples were electrophoresed at 80 - 100 V for 15 min then at 110 V for 55 min. Western blotting was performed as described in section 5.3.3.4 but using the PLM primary antibody (Badrilla) at 1:1000 dilution and the GAPDH primary antibody (Santa Cruz) at 1:10,000 dilution. Following the subsequent blocking and wash steps the secondary antibody (anti-rabbit IgG-HRP, Cell Signaling Technology) or GAPDH secondary antibody (anti-mouse IgG-HRP, Cell Signaling Technology)) was applied at 1:2000 dilution for 1 h at RT. The membrane was washed and developed as described in Na^+/K^+ ATPase α1 Western blotting methods.

5.3.5.6 Phosphorylated PLM-Ser^{68} Western blotting

The Western blotting protocol for phosphorylated PLM-Ser^{68} was performed as described in section 5.3.4.5 except that the primary antibody used was phosphorylated PLM-Ser^{68} primary antibody (Thermo Fisher) at 1:1000 dilution, GAPDH primary antibody (Santa Cruz) at 1:10,000 dilution and the secondary antibody was rabbit anti-sheep IgG-HRT (Thermo Fischer) at 1:2000 dilution.

5.3.6 $I_{Na,L}$

The techniques used and the voltage clamp protocol for measurement of $I_{Na,L}$ were detailed in section 2.4.7. The amplitude of $I_{Na,L}$ was determined from the averaged current measured between 210 and 220 ms after the depolarising step to -20 mV. This time interval was chosen to avoid contribution of the transient (early) Na^+ current which is reported to be completely inactivated within 200 ms[113]. To test the contribution of $I_{Na,L}$ to the APD, action potentials were measured in the absence or in the presence of 10 µM ranolazine, a selective $I_{Na,L}$ inhibitor[134,140]. The decay phase of $I_{Na,L}$ was best fitted by a standard single exponential function to obtain its time constant. Na^+ influx produced by the $I_{Na,L}$ was calculated by integrating the Na^+ inward current from the time measuring the amplitude of $I_{Na,L}$ to the end of the 2 s voltage step to -20 mV.

5.4 Results

5.4.1 Na^+/K^+ ATPase current

The Na^+/K^+ ATPase current in the 60AC group was significantly reduced by an average of 33 % compared with the 60Sham group (Fig. 5-1. B). By 150 days the Na^+/K^+ ATPase current had decreased by an average of 49 % (150AC group compared with 150Sham) (Fig. 5-1. B).

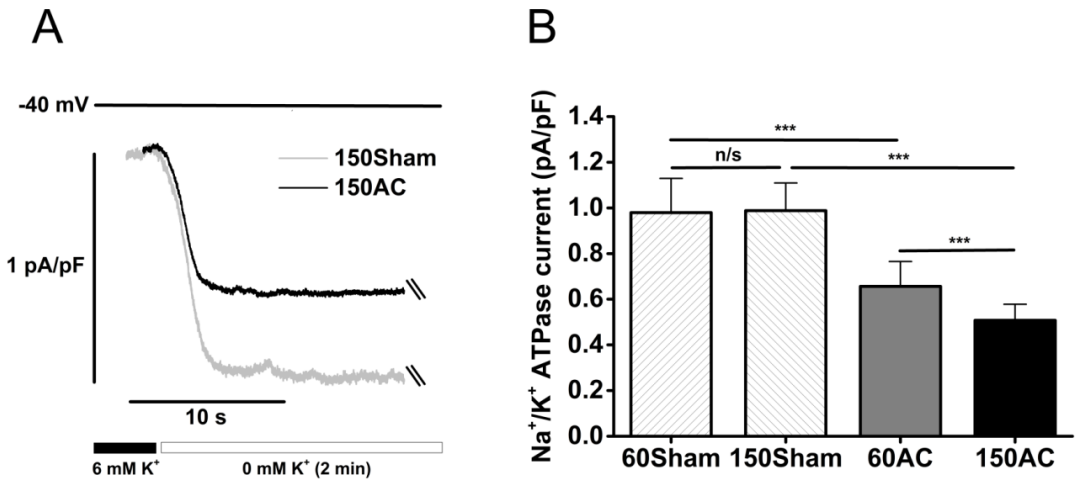

Figure 5-1. Na^+/K^+ ATPase current in sham and AC groups.

*A: Typical traces of steady-state Na^+/K^+ ATPase currents superimposed to allow comparison between 150Sham and 150AC groups. Na^+/K^+ ATPase current was measured as the current difference which resulted from switching superfusate with 6 mM K^+ to 0 mM K^+. Cells were then superfused in a K^+-free solution for 2 min before reactivating the Na^+/K^+ ATPase using 6 mM K^+ solution. B: Both 60AC and 150AC showed significantly reduced Na^+/K^+ ATPase current by, on average, 33 % and 49 %, respectively compared with their age-matched sham groups (60Sham, 39/4; 150Sham, 39/4; 60AC, n=47/4; 150AC, n=46/6; one-way ANOVA with a Fisher post-hoc test, n/s: p>0.05, ***p<0.001).*

5.4.2 Reactivation of Na^+/K^+ ATPase

The decay phase following a re-addition of K^+ to the superfusate represents the decrease in $[Na^+]_i$ that occurs on pump reactivation and therefore indicates net Na^+ extrusion. The amount of Na^+ pumped from the cells was therefore calculated as the integral of the current to the point where it had reached a steady-state (Fig. 5-2. A). The steady-state phase is assumed to start when equilibrium is reached i.e. when passive Na^+ influx is balanced by the pump current. The Na^+ extrusion rate was significantly decreased in the 60AC group by an average of 34 % and in the 150AC group by an average of 54 % compared with 60Sham and 150Sham groups, respectively. The 150AC group had a significantly lower Na^+ extrusion rate compared with 60AC (Fig. 5-2. B).

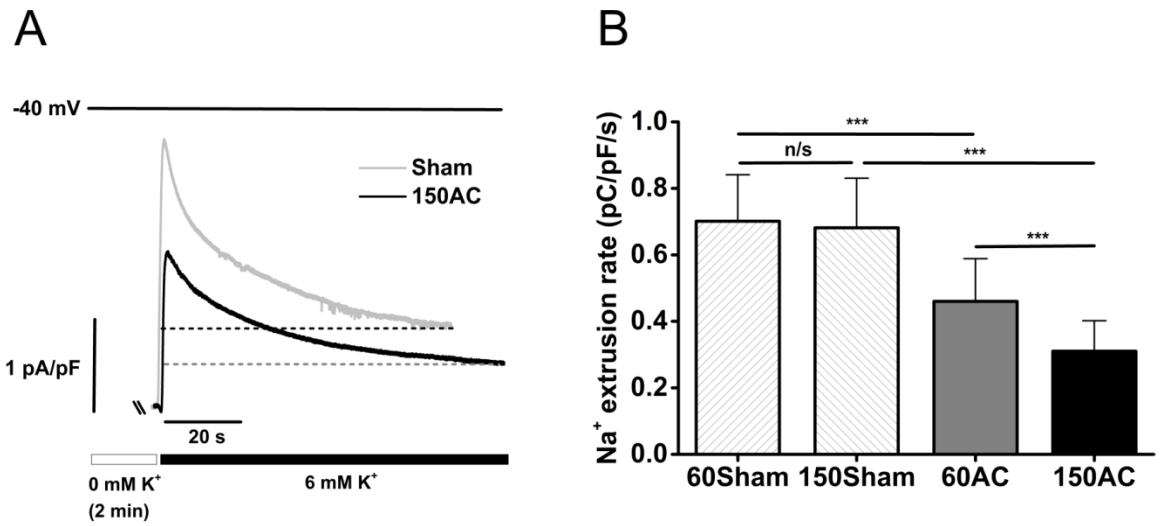

Figure 5-2. Na^+ extrusion by reactivation of Na^+/K^+ ATPase.

*A: When the Na^+/K^+ ATPase was inhibited by superfusion of the cells in K^+-free solution the $[Na^+]_i$ is expected to gradually increase. After 2 min the superfusate was switched to 6 mM K^+ to reactivate the Na^+/K^+ ATPase. The reactivation of the Na^+/K^+ ATPase is responsible for extruding the accumulated Na^+ from the cell, resulting in an outward current. The rate of the Na^+ extrusion was used to assess the function of the Na^+/K^+ ATPase. B: 60AC and 150AC had significantly reduced Na^+ extrusion rates compared with their age-matched sham groups. (60Sham, 28/4; 150Sham, 29/4; 60AC, n=34/4; 150AC, n=35/6; one-way ANOVA with a Fisher post-hoc test, n/s: p>0.05, ***p<0.001).*

5.4.3 Effect of strophanthidin on Ca^{2+} regulation in normal GP cardiac myocytes.

It has been shown in the above experiments that pump function decreases during the progression towards HF. It was also shown in an earlier chapter that after 60 days of AC, cardiac hypertrophy developed with an increase in Ca^{2+} transients and SR Ca^{2+} content. The experiments detailed in this section were done to test if partial inhibition of the Na^+/K^+ ATPase to a similar extent as noted in the 60 day AC group but in physiologically uncompromised cells, indeed results in comparable increases in Ca^{2+} transients and SR Ca^{2+} content to those observed at the 60 day stage. The function of the Na^+/K^+ ATPase determined by assessing steady-state current in male Sham myocytes was inhibited by an average of 46 % (N = 8/3) in the presence of 10 µM strophanthidin (Fig. 5-3. A). After 2 min exposure of strophanthidin, SR Ca^{2+} content (the integral of caffeine-induced inward NCX current) increased by an average of 36 % in strophanthidin-treated cells compared with control cells (Fig. 5-3. B). These cells on average had a 12 % larger Ca^{2+} transient amplitude a mean 18 % increase in

caffeine-induced Ca^{2+} transient amplitudes and a mean 13 % increase in diastolic Ca^{2+} fluorescence in the presence of 10 µM strophanthidin compared with control cells (Fig. 5-3. C, D & E).

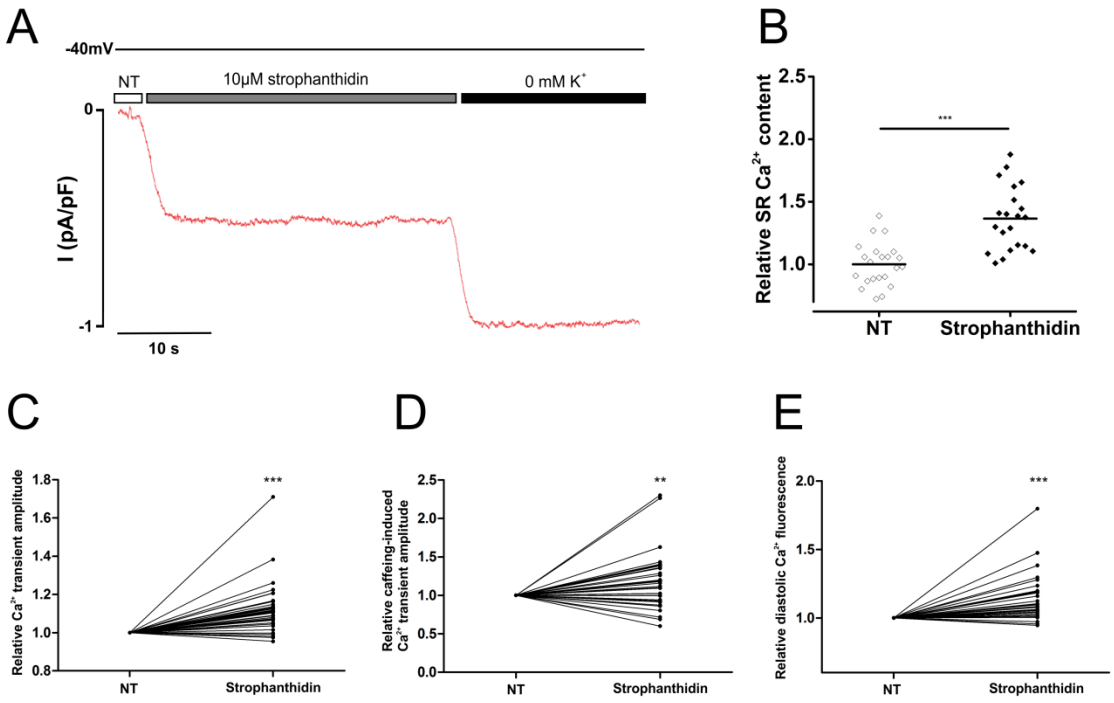

Figure 5-3. Effect of strophanthidin on Ca^{2+} handling in GP cardiomyocytes.

*A: 10 µM strophanthidin inhibited Na^{+}/K^{+} ATPase current by 46.2 ± 6.6 % (n=8/3). B: SR Ca^{2+} content increased by 36 % in the presence of strophanthidin compared with control cells (Control cell, n=23/4; strophanthidin treated cell, n=22/4). C, D & E: Strophanthidin-treated cells showed mean increases of 12 % in Ca^{2+} transient amplitudes, 18 % in caffeine-induced Ca^{2+} transient amplitudes, and 13 % in diastolic fluorescence compared with control cells (n=38/4, Student's t-test, **p<0.01, ***p<0.001) (Data were obtained by Mr Hari Surendran, a BSc project student).*

5.4.4 Protein expression of Na^+/K^+ ATPase isoform α1

The protein expression of the Na^+/K^+ ATPase isoform α1 was normalised to GAPDH, a well-described "housekeeping" gene product. The inherent assumption in using GAPDH is that its expression remains constant in the cells under investigation (see Fig 5-4. A). This assumption has not been tested in our animal model. The 60AC group had a significant decrease in relative protein expression of α1 by an average of 69 % compared with the age-matched sham group (Fig 5-4. B). In addition, the 150AC group also had a significant reduction in relative protein expression of α1 by an average of 55 % compared with 150Sham (Fig 5-4. C).

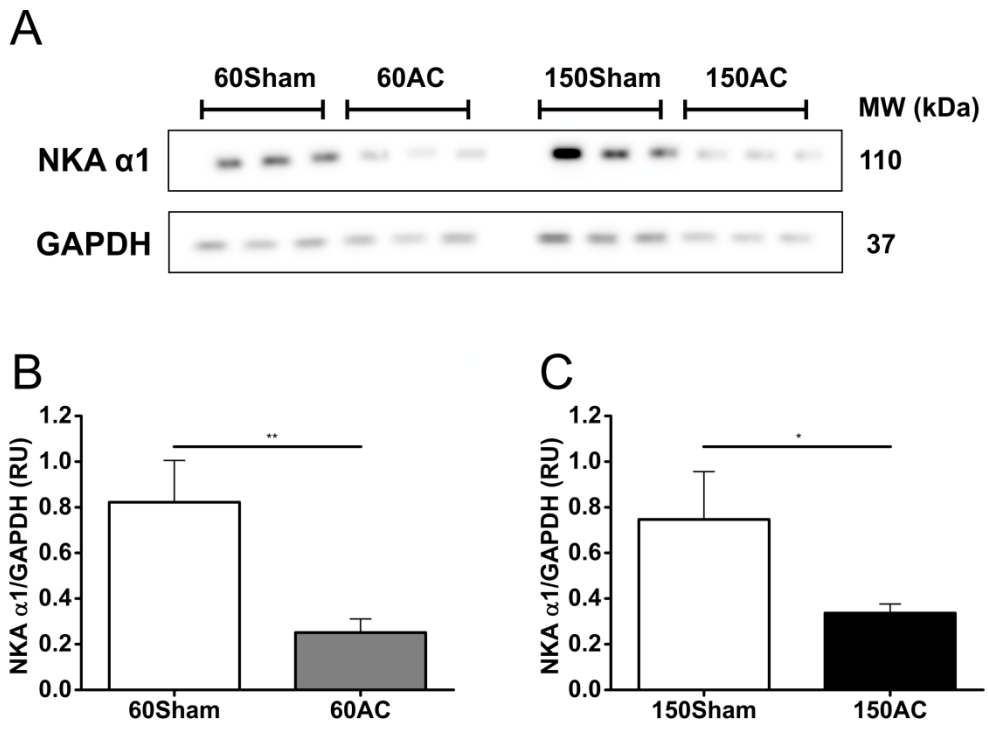

Figure 5-4. Western blot of Na^+/K^+ ATPase isoform α1 in sham and AC groups.

*Relative protein expression of α1 was significantly reduced in 60AC and 150AC compared with their age-matched groups by 69 % and 55 %, respectively (NKA=Na^+/K^+ ATPase; 60Sham, n=3; 60AC, n=3; 150Sham, n=3; 150AC, n=3; n=heart numbers; Student's t-test, *p<0.05, **p<0.01)*

5.4.5 Protein expression of PLM and phosphorylated PLM-Ser^{68}

The protein expression of PLM was also normalised to GAPDH (Fig. 5-5. A). There was no difference in relative PLM protein expression between 60Sham and 60AC, and also between 150Sham and 150AC (Fig. 5-5. B & C). Furthermore, the protein expression of phosphorylated PLM-Ser^{68} was also similar between 60Sham and 60AC, and between 150Sham and 150AC (Fig. 5-6. B & C).

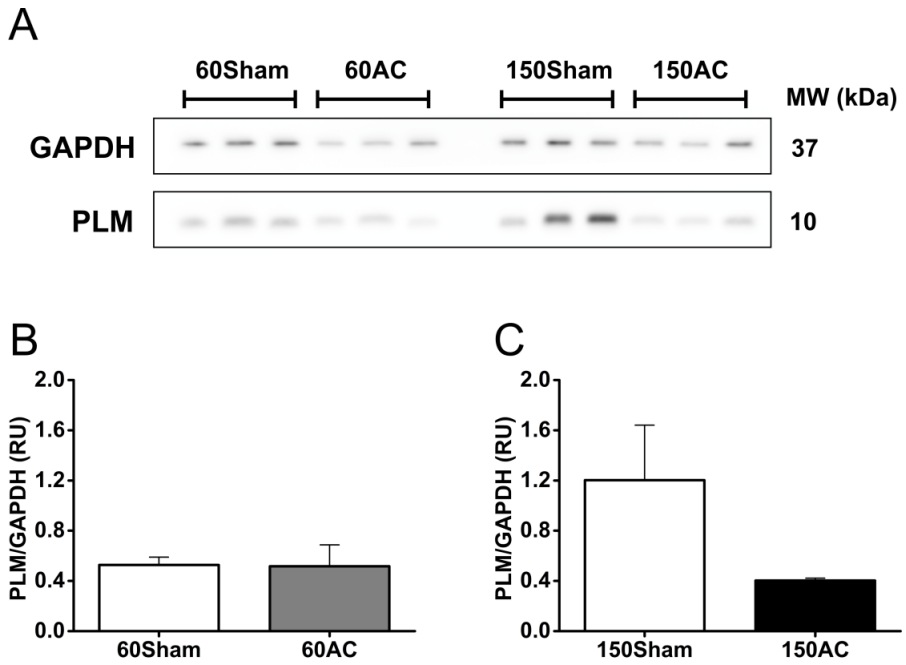

Figure 5-5. Western blot of PLM in sham and AC groups.

PLM protein expression was unaltered between 60Sham and 60AC, and also between 150Sham and 150AC (60Sham, n=3; 60AC, n=3; 150Sham, n=3; 150AC, n=3; n=heart numbers; Student's t-test).

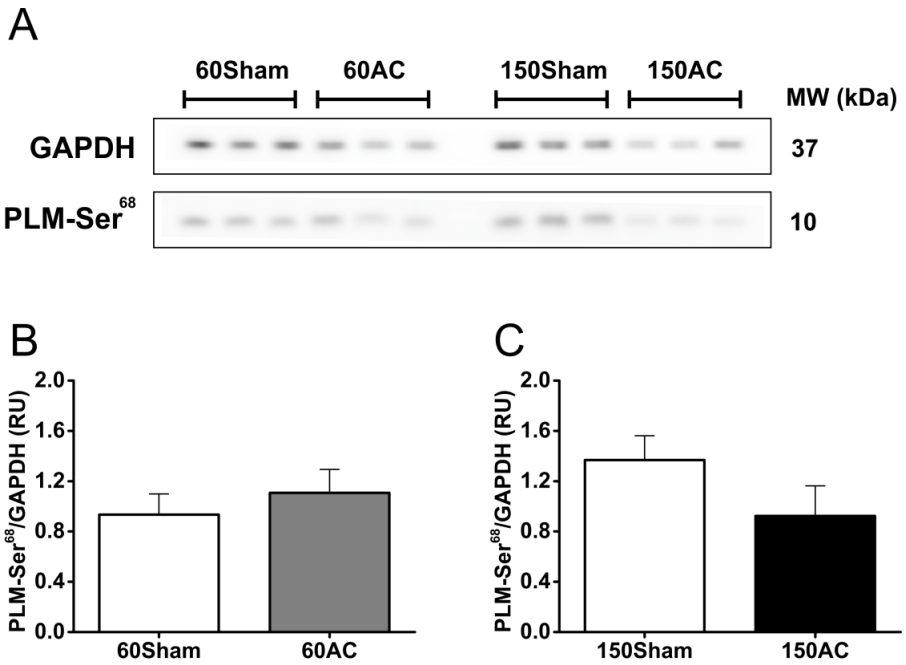

Figure 5-6. Western blot of phosphorylated PLM-Ser^{68} in sham and AC groups.

Phosphorylated PLM-Ser^{68} protein expression was unchanged between 60Sham and 60AC, and also between 150Sham and 150AC (60Sham, n=3; 60AC, n=3; 150Sham, n=3; 150AC, n=3; n=heart numbers; Student's t-test).

5.4.6 Immunofluorescence staining of Na^+/K^+ ATPase α1 isoform

Figure 5-7 shows typical staining patterns from α1 and α2 labelling of the cells isolated from 150 day sham-operated controls and 150 day AC hearts. The 150AC group had an average 48 % reduction in relative fluorescence intensity of Na^+/K^+ ATPase α1 in the sarcolemma region compared with 150Sham (Fig. 5-7. A & B). The 150AC also had a decrease in fluorescence intensity of Na^+/K^+ ATPase α2 in the central region by an average of 75 % compared with 150Sham (Fig. 5-7. C & D).

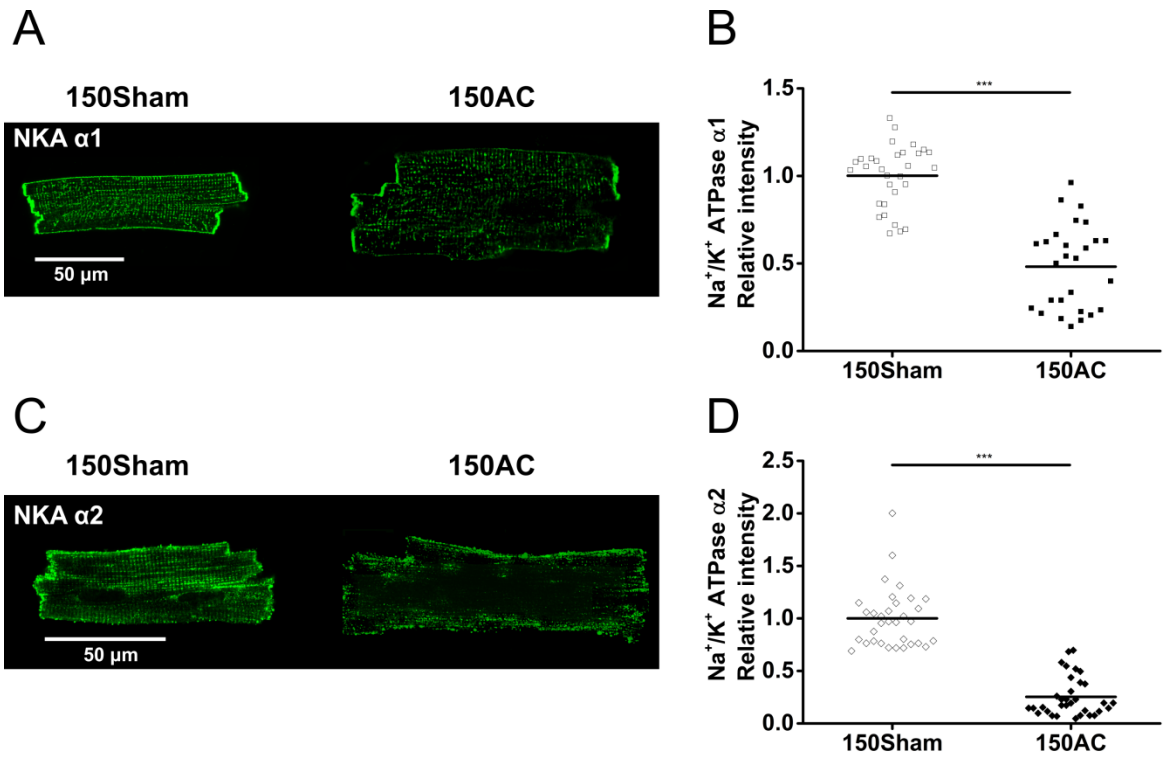

Figure 5-7. Immunostaining of Na^+/K^+ ATPase α1 and α2 in sham and AC groups.

*A & B: The fluorescence intensity of Na^+/K^+ ATPase α1 in the sarcolemma was significantly reduced in 150AC compared with 150Sham (NKA=Na^+/K^+ ATPase; 150Sham, n=31/3; 150AC, n=27/3; Student's t-test, ***p<0.001). C & D: The fluorescence intensity of Na^+/K^+ ATPase α2 in the central region declined by an average of 75 % in 150AC compared with 150Sham (NKA=Na^+/K^+ ATPase; 150Sham, n=33/4; 150AC, n=33/4; Student's t-test, ***p<0.001).*

5.4.7 $I_{Na,L}$ and APD

Although very small in comparison to the main Na^+ current that produces the AP upstroke, the late Na^+ current's persistence ensures it contributes to the plateau phase potential, morphology and duration and to Na^+ influx. Following treatment with 10 µM ranolazine, a selective $I_{Na,L}$ inhibitor[133], cells from the 150AC group on average had a 16.5 % shortening of APD_{90} in comparison with sham cells (Fig 5-8. B).

The 60AC group had a 77 % mean increase in $I_{Na,L}$ and $I_{Na,L}$-mediated Na^+ influx was on average 70 % greater compared with the age-matched sham group (Fig. 5-9. B & C). The tau for the decay phase of $I_{Na,L}$ was unaltered between 60Sham and 60AC (Fig. 5-9. D). Cell isolated from 150AC had 100 % greater $I_{Na,L}$ and 123 % greater $I_{Na,L}$-mediated Na^+ influx compared with cells isolated from the 150Sham group (Fig. 5-9. B & C). The time constant was on average 21 % longer in this group compared with age-matched sham group (Fig. 5-9. D). The $I_{Na,L}$ and the corresponding Na^+ influx was significantly larger with longer decay tau in the 150AC group compared with the 60AC group (Fig. 5-9. B, C & D).

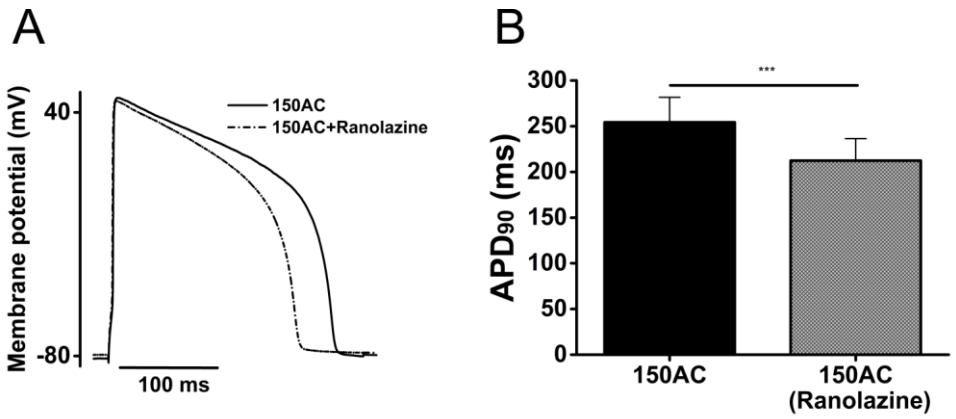

Figure 5-8. Ranolazine shortened APD_{90} in the 150AC group.

*A: APD was shortened in the presence of 10 µM ranolazine in a cardiac myocyte from 150AC group. B: APD_{90} in cardiac myocytes from 150AC group was significantly shortened by 16.5 % in the presence of 10 µM ranolazine (A & B) (150AC, n=6/23; Student's t-test, ***p<0.001).*

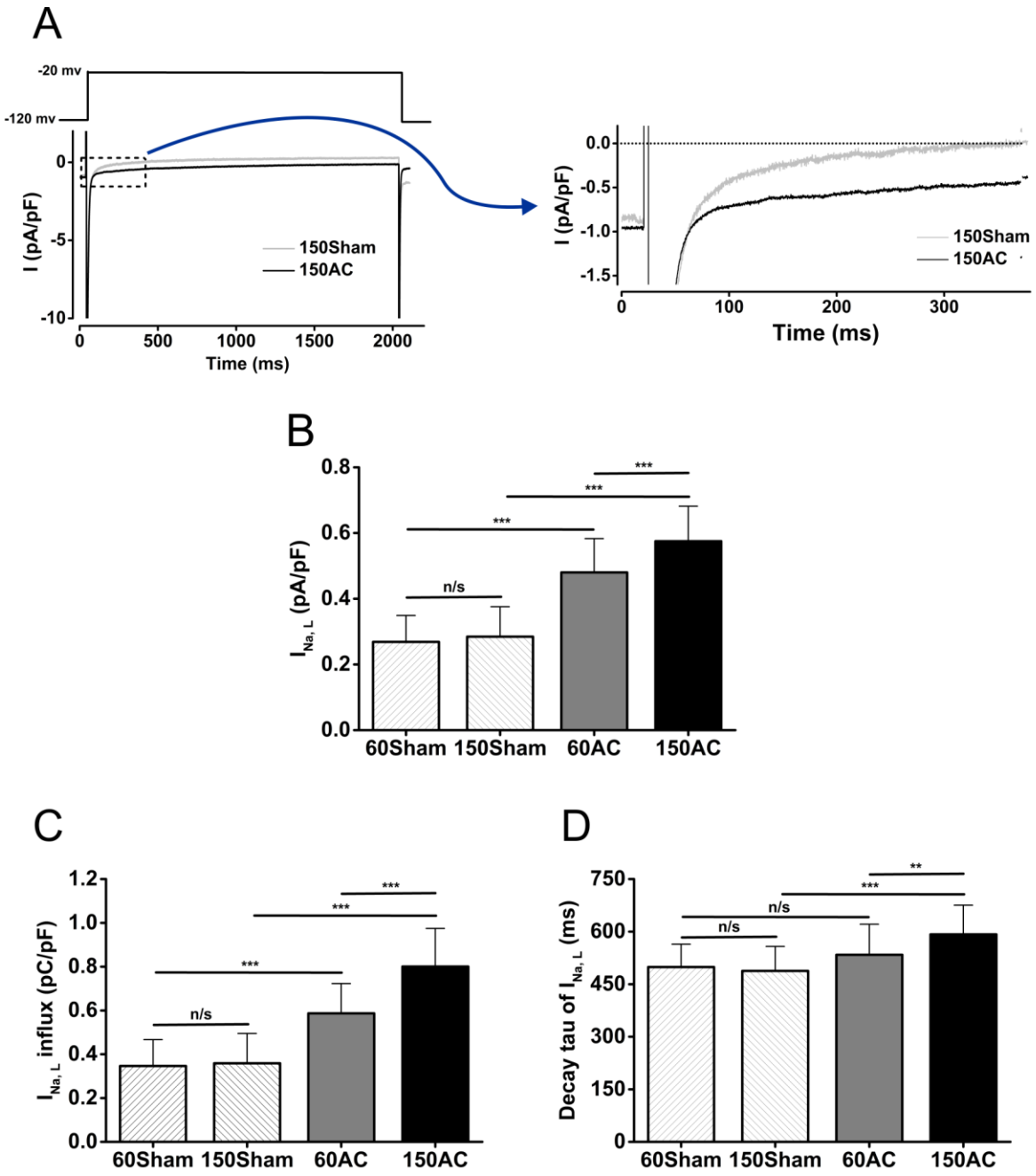

Figure 5-9. $I_{Na,L}$ and the corresponding Na^+ influx and decay time constant.

*A: Typical $I_{Na,L}$ traces in 150Sham and 150AC. B, C & D: Mean data show that 60AC had larger $I_{Na,L}$ and greater Na^+ influx from $I_{Na,L}$ compared with 60Sham. The time constant for the decay phase of $I_{Na,L}$ was unchanged between 60Sham and 60AC. Mean data also show that the 150AC group had markedly enhanced $I_{Na,L}$, greater Na^+ influx from $I_{Na,L}$ and a 21 % longer tau compared with 150Sham (60Sham, n=42/8; 150Sham, n=54/6; 60AC, n=33/5; 150AC, n=42/6; one-way ANOVA with a Fisher post-hoc test, n/s: p>0.05, **p<0.01, ***p<0.001).*

5.5 Discussion

In this chapter, we longitudinally investigated the changes in Na^+/K^+ ATPase function and $I_{Na,L}$ during the cardiac hypertrophy and HF stages following AC surgery. To complement the functional studies, protein expression of the Na^+/K^+ ATPase α1 isoform and PLM was also investigated. In addition, we partially inhibited the Na^+/K^+ ATPase current to approximately the same extent as that noted in HF, but in healthy cells, to establish conditions intended to mimic the decrease in function of the Na^+/K^+ ATPase observed in HF progression. This was to clarify whether such an inhibition influences Ca^{2+} handling and generates the proposed inotropic effects. Our results indicate that changes in Na^+/K^+ ATPase and $I_{Na,L}$ current and function occur early during HF progression. The decrease in function occurs in parallel with reduced expression of α1 at both the cardiac hypertrophy and HF stages. It is proposed that the changes in Na^+/K^+ ATPase function result in an initial inotropic effect that may be viewed as a compensatory mechanism at the cardiac hypertrophy stage.

5.5.1 Na^+/K^+ ATPase in cardiac hypertrophy and HF

There have been some studies that have assessed protein expression of the Na^+/K^+ ATPase isoforms in cardiac hypertrophy and HF, but the findings have been variable and only a handful of studies have conducted Na^+/K^+ ATPase current or other measurements of its function in pathological conditions[32,116,126]. α1 protein and mRNA expression was unaltered, but both α2 mRNA and protein expression were found to be reduced by 50 % in a rat HF model[6]. While mRNA expression of Na^+/K^+ ATPase α1, α2, and α3 was reported to be unaltered in failing human myocardium[122], protein expression of Na^+/K^+ ATPase was reduced in another human HF study[90].

Boguslavskyi *et al*, reported a reduced Na^+/K^+ ATPase current, elevated $[Na^+]_i$ with unaltered protein expression in an AC cardiac hypertrophy mouse model[128]. Verdonck *et al*, reported the $[Na^+]_i$ dependence of Na^+/K^+ ATPase current in atrioventricular block-induced hypertrophied myocytes shifted to the right indicating a decreased sensitivity of pump current for $[Na^+]_i$. Therefore, with the same patch-pipette Na^+ concentration, the hypertrophied cells had decreased pump current[125]. In addition, the same group reported increased subsarcolemmal $[Na^+]_i$ in hypertrophied myocytes, which may have resulted from increases in Na^+ influx, and the decreased sensitivity of pump current for Na^+. Semb *et al*, also reported a decrease in Na^+/K^+ ATPase current and function with unaltered total Na^+/K^+ ATPase protein expression although the group noted isoform shifts from α2 to α3 in their MI rat model[126].

In our GP AC model, we have observed that the pump current and function declined early in the hypertrophy stage (with further reduction progressing to HF) and this reduction in Na^+/K^+ ATPase function was accompanied with decreased α1 protein expression (at both the cardiac hypertrophy and HF stages). The Western blot data were supported by the α1 and α2 immunofluorescence intensity measurements that showed significant reduction at the HF stage. Therefore in this study there is a decrease in function of the pump in the working cell that is substantiated both by protein determinations from tissue preparations and immunocytochemical evidence from fixed cells that each indicate a loss of the α1 isoform.

It is tempting to directly correlate the biochemical findings with the functional observations. However, there are a number of other aspects that must be reviewed before arriving at that conclusion. The Western blot technique does not distinguish between cytosolic and sarcolemmal Na^+/K^+ ATPase proteins nor between functional and inactive Na^+/K^+ ATPase[89]. Furthermore, PLM plays a regulatory role in the modulation of Na^+/K^+ ATPase function and this may change in HF[29,129]. While unphosphorylated PLM produces a tonic inhibition on the Na^+/K^+ ATPase, phosphorylated PLM relieves this inhibition and stimulates Na^+/K^+ ATPase activity. Expression and phosphorylation of PLM was reduced together with reduced Na^+/K^+ ATPase expression in a human HF and rabbit HF model[123]. The authors concluded that the reduction in Na^+/K^+ ATPase expression in HF may be functionally offset by the lower inhibition exerted by PLM that resulted from its reduced expression and greater phosphorylation. However, hypophosphorylation of PLM has also been reported in a mouse HF model and in humans, resulting in inhibition of Na^+/K^+ ATPase while the expression of the Na^+/K^+ ATPase itself remained unchanged[128,129]. Our data showed an unaltered expression of PLM and phosphorylated PLM at Ser-68 between the AC and Sham groups suggesting PLM may not be involved in the decline in function in this model.

The distribution of α1 has been reported to be either evenly distributed between sarcolemma and T-tubule or more localised on sarcolemma[48], and the α2 isoform has been reported to be mainly localised in the T-tubule[48,49]. Our immunostaining images showed decreased α1 intensity in the sarcolemma region and reduced α2 intensity in the central T-tubule region in failing myocytes compared with sham myocytes, which supports our suggestion that the pump current and protein are decreased in HF. Decreased expression of α1 and α2 in these regions may alter the regulation of nearby NCX. Both α1 and α2 have been reported to be physically co-localised with NCX, regulating the function of nearby NCX[51,277,278]. However, overexpression of Na^+/K^+ ATPase α2 was shown to significantly decrease the muscle dysfunction occurring in cardiac hypertrophy by improving Ca^{2+}

regulation in a transgenic AC mouse model[279]. The overexpressed α2 not only had a greater affinity for Na^+, which led to more efficient Na^+ extrusion but resulted in a faster removal of intracellular Ca^{2+} by influencing the function of the co-localised NCX. Furthermore, Swift *et al,* reported that inhibition of α2 produced a relatively small reduction in pump current but significantly increased cell contraction with unchanged $[Na^+]_i$[280]. The group concluded that the α2 isoform may regulate co-localised NCX by altering local subsarcolemmal $[Na^+]$.

5.5.2 Na^+/K^+ ATPase and Ca^{2+} regulation in cardiac hypertrophy and HF

$[Na^+]_i$ is linked to the regulation of Ca^{2+} by influencing NCX-mediated Ca^{2+} flux[89]. Increased $[Na^+]_i$ is associated with cardiac hypertrophy and HF[89,114,116,117]. Therefore, the increased $[Na^+]_i$ in cardiac hypertrophy and HF alters the operation of NCX favouring reverse-mode that results in more Ca^{2+} influx and less Ca^{2+} efflux during each cardiac cycle, which may in turn increase SR Ca^{2+} content and be associated with inotropic effects. Pieske *et al*, reported that increased $[Na^+]_i$ in human failing cardiomyocytes enhanced Ca^{2+} influx via reverse-mode operated NCX, thus maintaining SR Ca^{2+} load and force development[117]. Studies have shown that decreased Na^+/K^+ ATPase function in HF[90] and decreased Na^+/K^+ ATPase current in cardiac hypertrophy[125] elevate $[Na^+]_i$.

However, it is not known if the increase in $[Na^+]_i$ at an early HF or hypertrophy stage produces inotropic effects to maintain cardiac function. Our data showed increased SR Ca^{2+} content and Ca^{2+} transients in healthy cells in the presence of strophanthidin with a dose producing about half inhibition of pump current. Hypokalemia-induced inhibition of Na^+/K^+ ATPase also reported increased Ca^{2+} transient amplitude and SR Ca^{2+} load[33]. The reverse-mode operated NCX may result from an increased subsarcolemmal $[Na^+]_i$ rather than an increased bulk cytoplasmic $[Na^+]_i$, however Gray *et al*, reported an increase in "bulk" cytosolic $[Na^+]_i$ of 4 - 5 mM in hypertrophied cardiomyocytes from AC GP[114] , a figure in agreement with Verdonck *et al*, who reported a 5 mM increase in $[Na^+]_i$ in their cardiac hypertrophied dog model[32]. We suggest that the decline in Na^+/K^+ ATPase current occurs early in HF progression in our AC GP and this, coupled with the increase in late Na^+ current, increases $[Na^+]_i$ that then influences NCX to operate in reverse-mode, subsequently allowing more Ca^{2+} influx. As a result, the myocytes from 60AC had increased SR Ca^{2+} content and Ca^{2+} transient amplitudes, which maintained adequate cardiac function at compensated cardiac hypertrophy stage. Wide scatter in responses of Ca^{2+} handling to strophanthidin could be due to different cell isolation quality on different and also the cell toxicity of strophanthidin, causing the variation of Ca^{2+} handling properties.

In this chapter, we showed a further reduction in Na^+/K^+ ATPase function and current in the 150AC failing heart, which is proposed to further elevate $[Na^+]_i$. However, Pieske *et al*, reported that increasing $[Na^+]_i$ further in HF myocytes was not able to extend SR Ca^{2+} load and improve force development[117]. Therefore, elevated $[Na^+]_i$ may not be able to produce a compensatory inotropic effect when $[Na^+]_i$ increases beyond a certain level. In addition, NCX may operate differently during the progression of pressure-overload. In failing hearts, NCX accounts for more Ca^{2+} removal in response to reduced SERCA Ca^{2+} uptake function in HF, resulting in further depletion of SR Ca^{2+} content. In chapter 4, we described other factors including reduced SERCA function and increased SR Ca^{2+} leak from RyR2, associated with depletion of SR Ca^{2+} content. Therefore, the compensatory effect from elevated $[Na^+]_i$ may perhaps be surpassed by the dysregulation of Ca^{2+} handling in HF.

5.5.3 $I_{Na,L}$ in in cardiac hypertrophy and HF

The amplitude of $I_{Na,L}$ is relatively small but contributes substantially to $[Na^+]_i$ when enhanced due to its slow inactivation characteristics. Due to the prolonged nature of $I_{Na,L}$ during the plateau of the action potential, it can contribute to the prolongation of APD[130]. $I_{Na,L}$ has been reported to be increased in several cardiac pathological conditions, including I/R, MI and HF[111,112,132-134], and was suggested to lead to intracellular Na^+ overload. As $I_{Na,L}$ generates Na^+ influx and thereby an inward current throughout the AP, it is expected to contribute to the prolongation of APD, which increases the susceptibility to EAD development[281]. In addition, Na^+ cycling is tightly connected with Ca^{2+} handling, due to Na^+ modulation of the operational direction of NCX. The net result can be an elevated diastolic Ca^{2+} concentration[139]. Abnormal diastolic intracellular Ca^{2+} accumulation, in turn, not only worsens contractility but could be arrhythmogenic[72,134].

While most studies mainly focused on the effect of $I_{Na,L}$ on HF stage, little is known regarding the role of $I_{Na,L}$ at the hypertrophy stage. In an AC mouse model, cardiac hypertrophy with preserved systolic function developed after one week[238], however both APD and $I_{Na,L}$ remained unchanged up until the development of HF five weeks later when the myocytes had prolonged APD and enhanced $I_{Na,L}$[238]. However, our data revealed that there is increased $I_{Na,L}$ earlier at the cardiac hypertrophy stage. Although the decay rate of the $I_{Na,L}$ remained unchanged, the calculated Na^+ influx was increased compared with sham. Therefore, the increased $I_{Na,L}$ may significantly contribute to the $[Na^+]_i$ and also contribute to the prolonged APD also noted at the cardiac hypertrophy stage. Interestingly, an increased $I_{Na,L}$ with prolonged APD was reported in a rabbit cardiac hypertrophy model[282]. The group showed that the endocardium had a larger $I_{Na,L}$, causing differential APD between the endocardium and epicardium, suggesting that the increased $I_{Na,L}$ resulted in an amplified transmural dispersion of repolarisation, capable of initiating EADs and ventricular arrhythmias[282].

Alterations in Ca^{2+} regulation can be partially reversed by inhibiting the $I_{Na,L}$ with ranolazine. This eliminates $[Na^+]_i$ overload and thus shortens APD and reduces NCX reverse-mode. Ranolazine has been shown to improve Ca^{2+} regulation and decrease pro-arrhythmic events by indirectly reducing diastolic Ca^{2+} overload and $[Ca^{2+}]_i$ accumulation[134,140,238]. The APD shortening effect of ranolazine was confirmed in our failing myocytes, and also indicated that $I_{Na,L}$ contributes towards the prolongation of APD in the HF GP model. However, ranolazine was found to have inhibition effect on I_{kr}[144] in therapeutic dose range, which may prolong the APD in normal cardiomyocytes. In AC myocytes, ranolazine supressed the enhanced $I_{Na,L}$, thus shortening APD, which effect surpassed the I_{kr} block-produced APD prolongation by the same drug.

While enhanced $I_{Na,L}$ and decreased Na^+/K^+ ATPase function may together elevate $[Na^+]_i$ and lead to more Ca^{2+} influx from NCX, producing an inotropic effect, it is still unclear how they interact with one another as both are $[Na^+]_i$ contributors. Hoyer *et al*, reported that ouabain, a cardiac glycoside, enhanced $I_{Na,L}$ in cardiomyocytes from GPs[283]. The enhanced $I_{Na,L}$ was abolished by application of a CaMKII inhibitor. Sapia *et al*, reported that cardiac glycosides increased both $[Na^+]_i$ and $[Ca^{2+}]_i$, and activated CaMKII[284]. Therefore, increased $I_{Na,L}$ may result from enhanced activity of CaMKII that is activated during the exposure of the Na^+/K^+ ATPase inhibitor, ouabain. Thus, the increased $I_{Na,L}$ at the cardiac hypertrophy stage in our AC GP model may be attributed to the decline in Na^+/K^+ ATPase function, purporting to activate CaMKII, in turn, enhancing $I_{Na,L}$. Increased activity of CaMKII has also been reported in HF models, causing detrimental effects on Ca^{2+} handling by phosphorylating various target proteins and channels[40,110,269,272,273]. CaMKII is able to phosphorylate $Na_v1.5$ to regulate the magnitude, and other properties, including $I_{Na,L}$ inactivation and its recovery from inactivation[141]. Some potential CaMKII phosphorylation sites have been identified, such as Ser571 in the $Na_v1.5$ DI-DII linker[142,143]. Thus, further enhancing $I_{Na,L}$ with slower decay rate in HF may result from the phosphorylation of Na^+ channel by the activated CaMKII in HF.

5.6 Conclusions

Reduced Na^+/K^+ ATPase function occurs early in the progression of HF starting at the cardiac hypertrophy stage and continues to decline to the HF stage. The proposed accumulation of $[Na^+]_i$ causes more Ca^{2+} influx via NCX resulting in increased SR Ca^{2+} content and Ca^{2+} transient amplitudes, maintaining cardiac function at hypertrophy stage. The decline in Na^+/K^+ ATPase function is associated with a decrease in protein expression of Na^+/K^+ ATPase while the PLM/phosphorylated PLM remained unchanged. Similar to the trend in Na^+/K^+ ATPase function, enhanced $I_{Na,L}$ was found early at cardiac hypertrophy stage and continued to increase to the HF stage, contributing to APD prolongation. The interaction between declined Na^+/K^+ ATPase function and enhanced $I_{Na,L}$ and their mechanisms during HF progression is not clear, requiring further in depth investigation.

6 REVEALING SEX DISPARITIES IN Na^+ AND Ca^{2+} REGULATION DURING THE PROGRESSION FROM CARDIAC HYPERTROPHY TO HEART FAILURE

6.1 Aims

- To assess the differences between sexes in the physical characteristics of the heart and its function in the progression to HF in the AC pressure-overload GP model.
- To investigate the differential changes in cellular Ca^{2+} handling between the sexes in response to pressure-overload.
- To evaluate the differential changes in Na^+/K^+ ATPase and $I_{Na,L}$ function between the sexes in the progression to HF.

6.2 Introduction

Clinically, there appear to be different effects between the sexes on the progression towards HF[177]. Females have better cardiac function and survival in the face of cardiovascular disease (CVD) compared with men, leading to the suggestion that females might be "better protected" against the development of cardiac hypertrophy and failure[163,171,285]. However, this advantage is lost in postmenopausal women compared with age-matched men[167,286]. Premenopausal women have lower incidence of sudden cardiac death, which could be related to the delayed onset of coronary artery disease and a reduced risk of malignant ventricular arrhythmias. However, postmenopausal women seem to lose this protection[287]. Females exhibit a marked increase in the incidence of LV hypertrophy after menopause, when the prevalence of hypertension increases[288]. Sex disparities are also observed in cellular electrophysiology. In normal physiological circumstances sex differences in E-C coupling and electrophysiology appear to exist, but there have been an insufficient number of studies comparing these aspects in both sexes with some of the findings being inconsistent[289-292]. In pathophysiological conditions, a pressure-overload rat model showed differential SERCA mRNA levels in hypertrophied hearts between genders[206]. An AC mouse model also reported a more efficient metabolic regulation in female hearts in the early response to pressure-overload[208].

The work detailed in this chapter aims to assess if sex differences exist in the progression from cardiac hypertrophy to HF and if these variations are associated with differential dysfunction of Ca^{2+} handling, Na^+ regulation and E-C coupling. In chapter 7, it will be illustrated that long-term deprivation of ovarian oestrogen alters Ca^{2+} handling mechanisms in ventricular myocytes and predisposes them to more arrhythmia. The work in chapter 8 melds these two lines of thought and

assesses if oestrogen confers cardiac protection and modulates Ca^{2+} handling in the pressure-overload GP model. This work will help clarify the pathophysiology of HF between the sexes that may allow more novel and specific therapeutic approaches in the future.

6.3 Methods

6.3.1 AC pressure-overload GP model and *in vivo* echocardiography study

The AC pressure-overload GP model was detailed in section 2.1.1, and echocardiography measurements were described in section 2.2. Weights of male and female guinea pigs at the time of operation were 405 ± 53 g and 392 ± 33 g, respectively (males, n=21; females, n=24; $p>0.05$).

6.3.2 Myocyte isolation and electrophysiological measurements

Experiments were performed on single cardiac myocytes isolated from sham or AC-operated GPs at 60 D or 150 D according to the methods described in section 2.3.1. Sham or AC-operated male (M) and female (F) GPs at 60 D and 150 D were categorised as M-60Sham, M-60AC, F-60Sham, F-60AC, and M-150Sham, M-150AC, F-150Sham and F-150AC, respectively. Techniques and protocols for electrophysiology measurements including APD, $I_{Ca,L}$, Na^+/K^+ ATPase current and reactivation and $I_{Na,L}$ are detailed in sections 2.4 and those for the measurement of Ca^{2+} transient, SR Ca^{2+} content and spontaneous Ca^{2+} sparks, are detailed in section 2.5.

6.4 Results

6.4.1 Changes in physical characteristics

Male and female BWs were unchanged in the 60AC group compared with 60Sham (Fig. 6-1. A & B). While M-150AC BWs decreased by 14 % compared with M-150Sham, female 150Sham and 150AC BWs were similar (Fig. 6-1. A & B). Male HW/BW ratios increased by 26 % and 61 % in 60AC and 150AC, respectively, compared with their age-matched sham groups. The HW/BW ratio in female GPs also increased by an average of 44 % and 50 % in their 60AC and 150 AC groups, respectively, compared with their age-matched sham groups (Fig. 6-1. C & D). Both sexes had further increased mean HW/BW ratios in 150AC compared with 60AC groups (Fig. 6-1. C & D). While LW/BW ratios remained unaltered between 60Sham and 60AC in males and females, the ratio significantly increased in 150AC compared with 150Sham groups in males by an average of 49 % and in females by an average of 27 % (Fig. 6-1 E & F). Males had a significantly higher LW/BW ratio 150 days after AC at 6.22 compared with 5.47 in females.

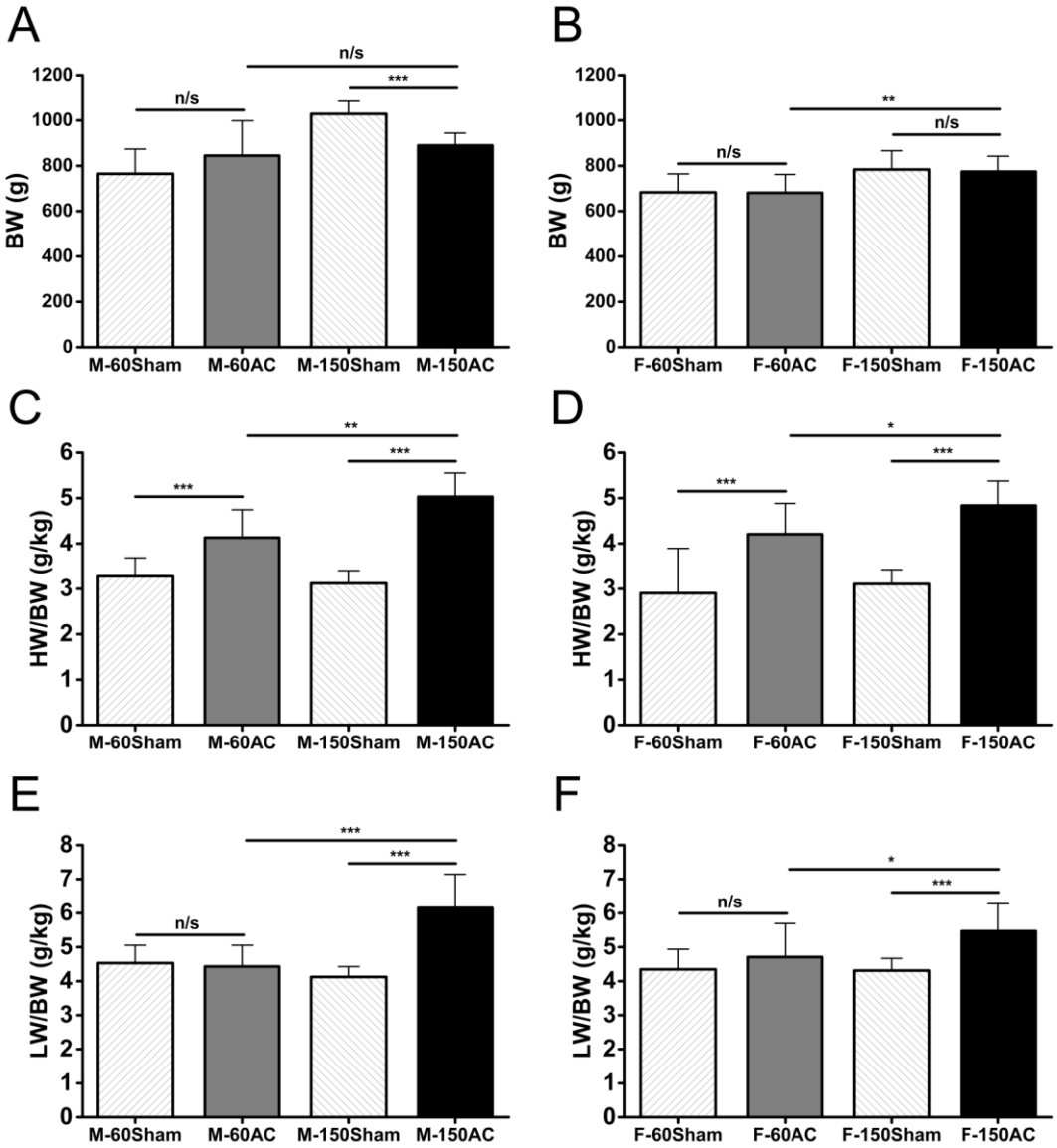

Figure 6-1. Changes in physical characteristics in sham and AC groups between sexes.

*A & B: Body weight changes in males (A) and females (B) at 60 and 150 days following sham or AC operations. C & D: HW/BW ratios in males (C) and females (D) at and 150 days following sham or AC operations. E & F: LW/BW ratios in males (E) and females (F) at 60 and 150 days following sham or AC operations. (M-60Sham, n=12; M-60AC, n=10; M-150Sham, n=10; M-150AC, n=11; F-60Sham, n=11; F-60AC, n=11; F-150Sham, n=15; F-150AC, n=13; n=GP numbers; one-way ANOVA with a Fisher post-hoc test, n/s: p>0.05, *p<0.05, **p<0.01, ***p<0.001).*

6.4.2 *In vivo* M-mode echocardiography

The LVIDd and LVIDs remained unchanged between Pre-operation (Pre-op) Sham, 60Sham and 150Sham groups in both males and females (Fig 6-2. A, B, D & E). FS was also unaltered in males and females between Pre-op Sham, 60Sham and 150Sham groups (Fig 6-2. C & F). Both sexes had similar LVIDd, LVIDs and FS in pre-op AC groups (Fig. 6-2. A, B & C). While LVIDd and LVIDs remained unchanged between male Pre-op and 60AC, females showed increased LVIDd and LVIDs by 10 and 15 %, respectively between Pre-op and 60AC (Fig. 6-3. A & B). LVIDd and LVIDs markedly increased in 150AC compared with Pre-op in both genders (Fig. 6-3. A & B). FS was unaltered in 60AC but was considerably reduced in 150AC by 35 % in males and 30 % in females compared with pre-op (Fig. 6-3. C). Males shows significantly more reduced FS in 150AC compared with females (Fig. 6-3. C).

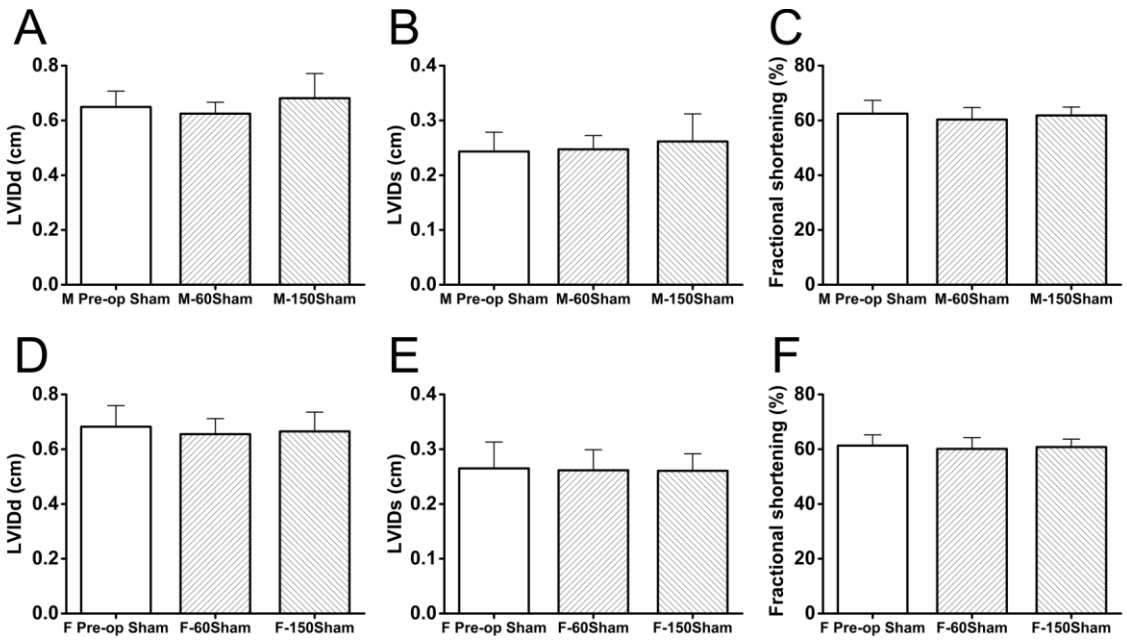

Figure 6-2. *In vivo* echocardiography study in Sham-operated GPs.

Panels A, B, and C: Male left ventricular dimensions at diastole (LVIDd), systole (LVIDs), and fractional shortening (FS), respectively. Panels D, E, and F: Female LVIDd, LVIDs and FS, respectively. (M Pre-op Sham, n=14; M-60Sham, n=12; M-150Sham, n=10; F Pre-op Sham, n=16; F-60Sham, n=12; F-150Sham, n=15; n=GP numbers; one-way ANOVA with a Fisher post-hoc test).

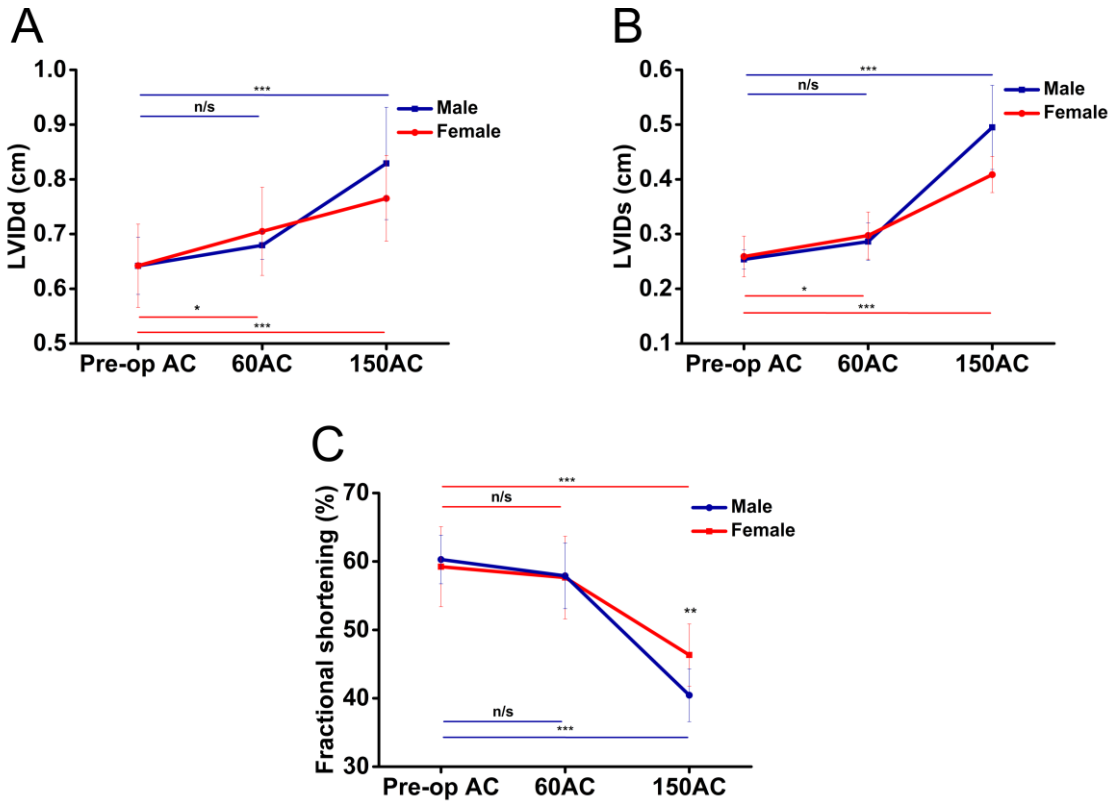

Figure 6-3. *In vivo* echocardiography comparing the longitudinal changes occurring in AC-operated GPs.

*A: LVIDd changes from Pre-op to 150 days in males (blue) and females (red). B: LVIDs changes from Pre-op to 150 days in males (blue) and females (red). C: FS changes from Pre-op to 150 days in males (blue) and females (red). (Male: Pre-op AC, n=14; 60AC, n=11; 150AC, n=9; Female: Pre-op AC, n=15; 60AC, n=12; 150AC, n=11; n=GP numbers; one-way ANOVA with a Fisher post-hoc test, n/s: p>0.05, *p<0.05, **p<0.01, ***p<0.001).*

6.4.3 APD

Females showed longer APD_{90} compared with males in both 60Sham groups by an average of 8 % and 150Sham groups by an average of 9 % (Fig. 6-4. B & C). APD_{90} was unchanged in both genders between 60Sham and 150Sham groups (Fig. 6-5. A & B). APD_{90} was markedly prolonged in 60AC by an average of 21 % in males and 18 % in females compared with their age-matched sham group (Fig. 6-5. A & B). APD_{90} was further significantly prolonged in 150AC groups by 32 % in males and 26 % females compared with their 150Sham groups (Fig. 6-5. A & B). The male and female 150AC groups had longer APD_{90} compared with the 60AC groups (Fig. 6-5. A & B).

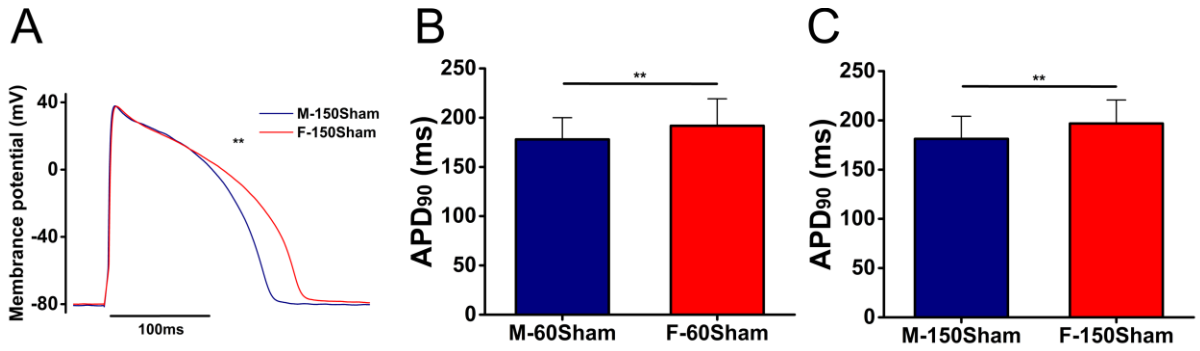

Figure 6-4. Comparing APD in sham-operated male and female GPs.

*A: Typical action potential traces from 150Sham male (blue trace) and female (red trace) cardiomyocytes. B: Mean data of male (blue) and female (red) APD_{90} in the 60Sham groups, C: Mean data of male (blue) and female (red) APD_{90} in the 150Sham groups (M-150Sham, n=44/5; F-150Sham, n=43/5; Student's t-test, **p<0.01).*

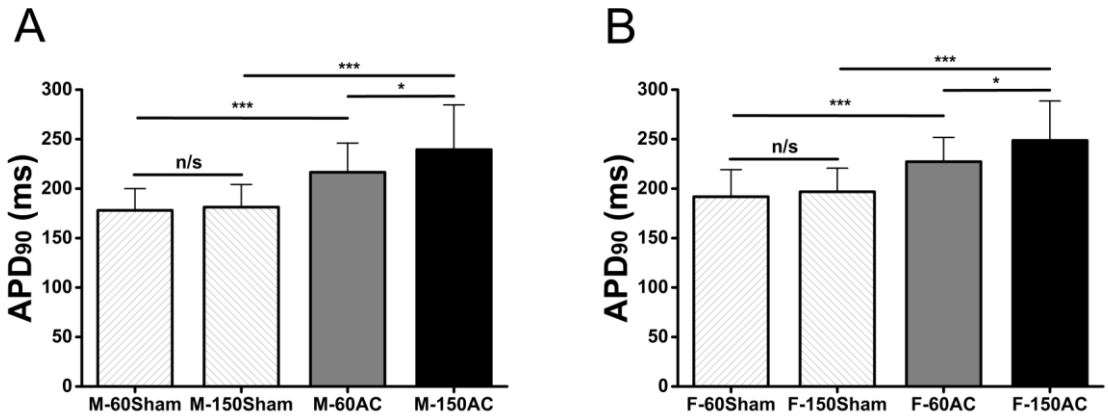

Figure 6-5. Assessing APD_{90} between sham and AC-operated male and female GPs.

*A & B: APD_{90} remained unchanged between 60Sham and 150Sham groups in males and females. Males and females showed prolonged APD_{90} in 60AC by 21 % and 18 %, respectively compared with their age-matched sham group. Both males and females showed further prolongation in APD_{90} in 150AC by 32 % and 26 % respectively, compared with their 150Sham groups (M-60Sham, n=38/4; M-150Sham, n=44/5; M-60AC, n=23/3; M-150AC, n=37/3; F-60Sham, n=29/4; F-150Sham, n=43/5; F-60AC, n=27/3; F-150AC, n=33/3; one-way ANOVA with a Fisher post-hoc test, n/s: p>0.05, *p<0.05, ***p<0.001).*

6.4.4 Cell capacitance

There was no sex difference between mean cell capacitances (M-60Sham=172.4 ± 52.1, F-60Sham=160.9 ± 43.1, p>0.05; M-150Sham=177.5 ± 42.7, F-150Sham=173.2 ± 41.9 pF, p>0.05; M-60Sham, n=73; F-60Sham, n=64; M-150Sham, n=82; F-150Sham, n=125). M-60AC had larger mean

cell capacitance compared with F-60AC (M-60AC=223.7 ± 53.8, F-60AC=199.8 ± 64.3 pF, **p<0.01; M-60AC, n=86; F-60AC, n=80). M-150AC also showed larger mean cell capacitance compared with F-150AC (M-150AC= 286.4 ± 66.7, F-150AC= 241.6 ± 56.0, ***p<0.001; M-150AC, n=93; F-150AC, n-107). One-way ANOVA with a Fisher post-hoc test was used.

6.4.5 Ca^{2+} regulation in cardiac hypertrophy and HF between sexes

We investigated some key indices of Ca^{2+} regulation, including $I_{Ca,L}$, Ca^{2+} transients, SR Ca^{2+} content and Ca^{2+} sparks to test the hypothesis that sex differences exist in Ca^{2+} regulation in cardiac hypertrophy and HF.

6.4.5.1 $I_{Ca,L}$

Males and females showed similar peak $I_{Ca,L}$ in both 60Sham and 150Sham groups (Fig. 6-6. A & B). There were no differences in peak $I_{Ca,L}$ between 60Sham and 60AC male groups nor between the 150Sham and 150AC male groups (Fig. 6-6. C & D). In female GPs, peak $I_{Ca,L}$ also remained unchanged at 60 and 150 days (Fig. 6-6. E & F).

The time constants tau 1 and tau 2 for the decay phase of the $I_{Ca,L}$ remained similar between 60Sham and 60AC in both males and females (Fig. 6-7). However, at 150 days the AC group had markedly prolonged tau 1 by 70 % and 48 % in males and females compared with 150Sham, respectively (Fig. 6-7. A & C). In addition, 150AC also had a significantly longer tau 2 compared with 150Sham by 45 % in males and 35 % in females (Fig. 6-7. B & D).

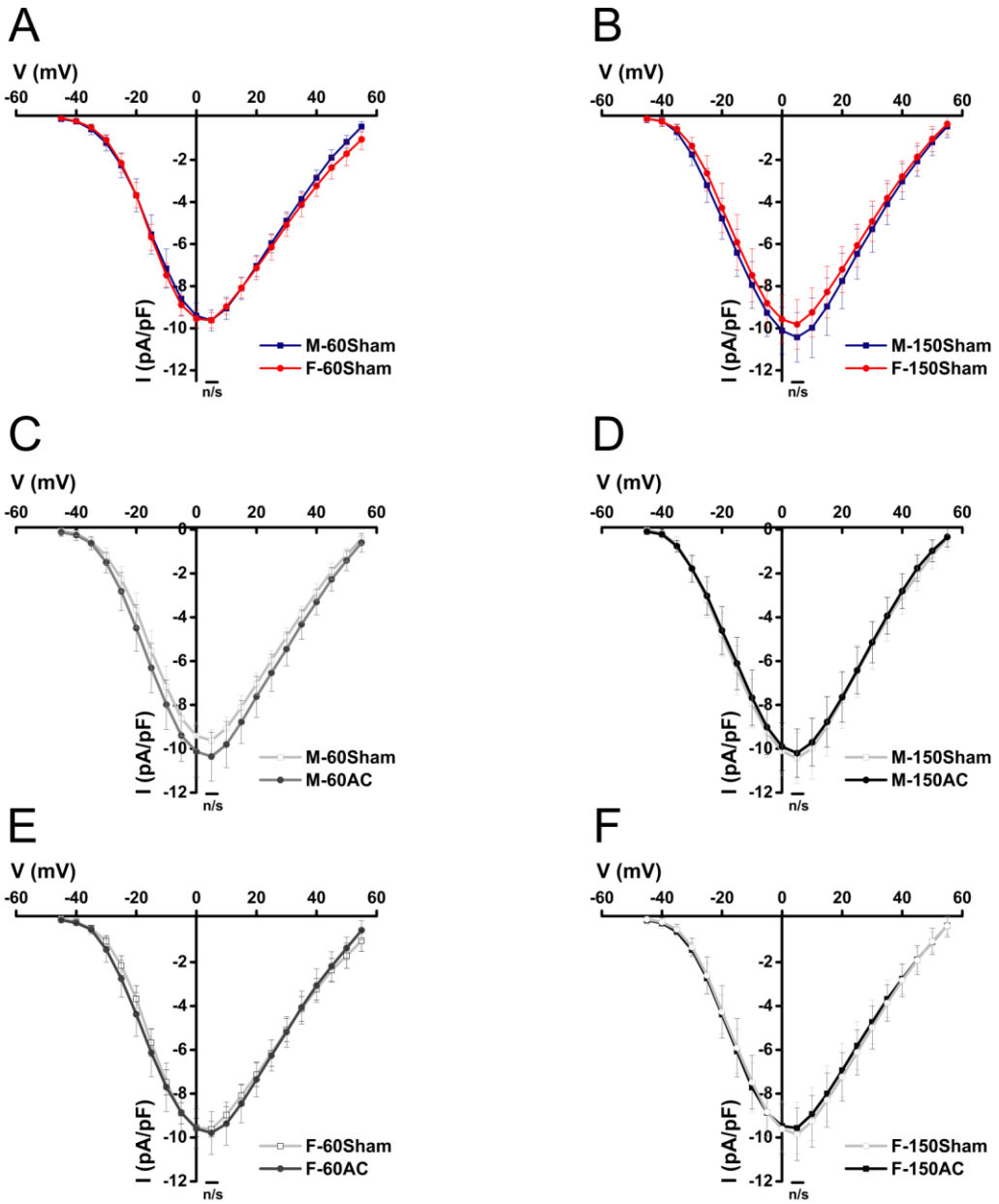

Figure 6-6. I-V relationship of L-type Ca^{2+} channel in sham or AC-operated male and female GPs.

A & B: Maximum peak $I_{Ca,L}$ at 5 mV was similar between male and female 60Sham and 150Sham groups. C & D: Maximum peak $I_{Ca,L}$ at 5 mV remained unchanged between male 60Sham and 60AC, and between 150Sham and 150AC. E & F: Female 60AC and 150AC had unaltered peak $I_{Ca,L}$ compared with 60Sham and 150Sham, respectively (M-60Sham, n=16/2; M-150Sham, n=24/3; M-60AC, n=20/3; M-150AC, n=22/3; F-60Sham, n=14/2; F-150Sham, n=40/5; F-60AC, n=16/3; F-150AC, n=17/3; Student's t-test, n/s: p>0.05).

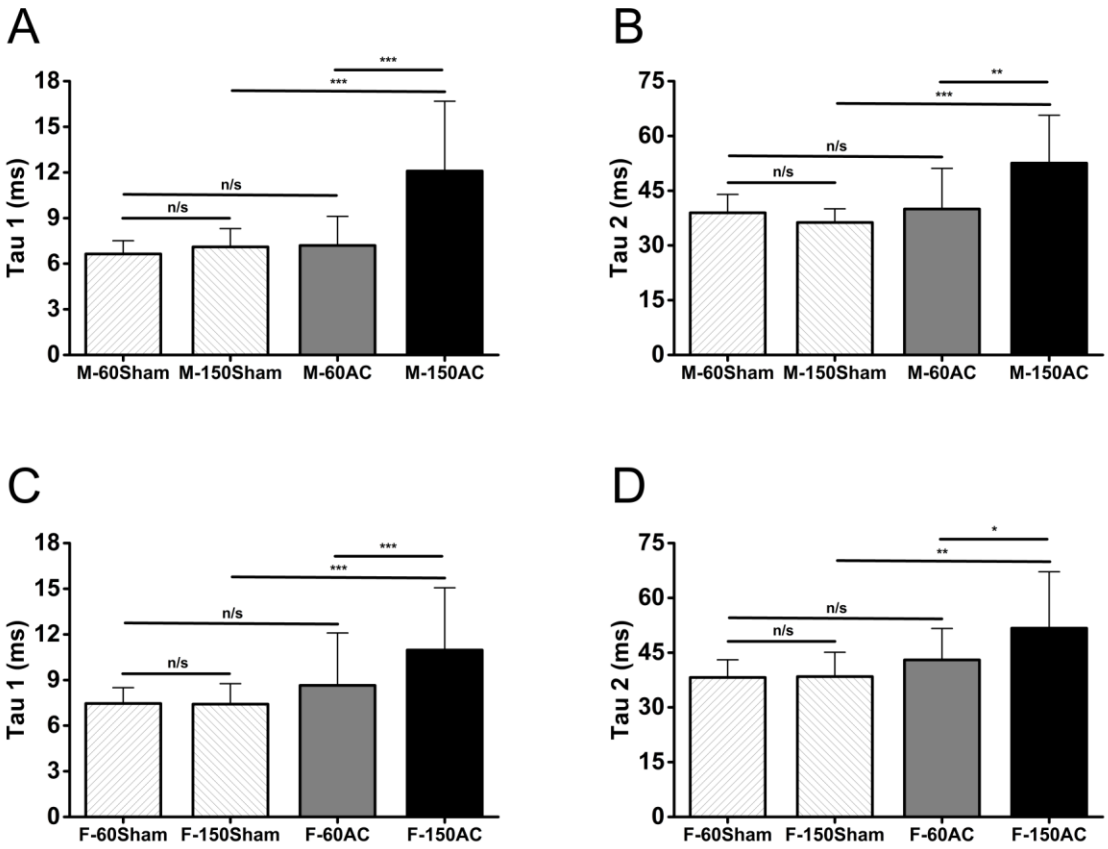

Figure 6-7. Time constants for decay phase of peak $I_{Ca,L}$ in sham- or AC-operated male and female GPs.

*A & B: The time constants tau 1 and tau 2 were obtained by fitting the decay phase of the $I_{Ca,L}$ with a double exponential equation. M-60AC showed unaltered tau 1 and tau 2 compared with M-60Sham. M-150AC had 70 % longer tau 1 and 45 % longer tau 2 compared with those in M-150Sham. C & D: F-60AC also showed unchanged tau 1 and tau 2 compared with F-60Sham. F-150AC showed prolonged tau 1 and tau 2, by 48 % and 35 %, respectively, compared with F-150Sham (M-60Sham, n=16/2; M-150Sham, n=24/3; M-60AC, n=20/3; M-150AC, n=22/3; F-60Sham, n=14/2; F-150Sham, n=40/5; F-60AC, n=16/3; F-150AC, n=17/3; one-way ANOVA with a Fisher post-hoc test, n/s: p>0.05, *p<0.05, **p<0.01, ***p<0.001).*

6.4.5.2 Ca^{2+} transient

Males had greater Ca^{2+} transient amplitudes compared with females in both 60Sham and 150Sham groups (Fig. 6-8. A & B). Male 60AC had increased Ca^{2+} transient amplitudes by an average of 10 % compared with M-60Sham (Fig. 6-8. C). Female 60AC had similar Ca^{2+} transient amplitudes compared with F-60Sham (Fig. 6-8. D). As the hearts progressed towards failure the Ca^{2+} transient amplitudes decreased in both males and females (by 38 % in M-150AC and by 30 % in F-150AC compared with M-150Sham and F-150Sham, respectively (Fig. 6-8. C & D)).

The rate constants for the decay of the Ca^{2+} transient were similar in the male and female sham myocytes (Fig. 6-9. A-D). Both male and female 60AC groups had unaltered Ca^{2+} transient decay rate constants compared with their 60Sham groups (Fig. 6-9. C & D). The decay rate constant was significantly slower in M-150AC by 39 % and F-150AC by 29 % compared with their age-matched sham groups, M-150Sham and F-150Sham, respectively (Fig. 6-9. C & D). M-150AC had a significantly slower mean decay rate constant, at 5.60 ± 0.83 s^{-1}, compared with the mean rate constant of the 150 day aortic-constricted females (F-150AC) of 6.37 ± 1.43 s^{-1} (values were expressed as mean ± S.D.; Student's *t*-test, $p<0.01$).

The rate constants derived for SERCA, NCX and other slower transporters (PMCA and mitochondria Ca^{2+} uniporter), indicated that their contributions to the decline in Ca^{2+} remained unchanged between M-60Sham and F-60Sham (Fig. 6-10. A & B), and this was also seen between M-150Sham and F-150Sham (Fig. 6-10. C & D). These transporter rate constants were also similar for both sexes in the 60AC groups compared with the age-matched sham groups, 60Sham (Fig. 6-11). The mean rate constant of SERCA function was reduced by a mean of 58 % in the M-150AC group compared with the M-150Sham group (Fig. 6-12. A). In contrast, the contribution from NCX increased by an average of 76 % in the M-150AC group compared with M-150Sham (Fig. 6-12. B). In females at the same experimental time point (F-150AC), the rate constant of SERCA function was reduced by 48 % compared with the equivalent sham group (F-150Sham) (Fig. 6-12. C) and NCX function increased by 56 % (Fig. 6-12. D). Compared with females, males had a slower mean rate constant of SERCA function at 150AC (2.65 ± 0.56 s^{-1} vs 3.23 ± 1.10 s^{-1}; values were expressed as mean ± S.D.; Student's *t*-test, $p<0.05$).

Males and females had similar fractional Ca^{2+} release between their 60Sham and 150Sham groups, (Fig. 6-13. A & B). However, the AC animals had increased fractional release. M-60AC showed a 10 % increase in fractional SR Ca^{2+} release compared with M-60Sham (Fig. 6-13. C) and, as the disease process progressed, this increased to 29 % (M-150AC had a 29 % increased fractional SR Ca^{2+} release compared with M-150Sham, Fig. 6-13. C). The fractional SR Ca^{2+} release increased by 15 % and 30 % in F-60AC and F-150AC respectively compared with F-60Sham and F-150Sham (Fig. 6-13. D).

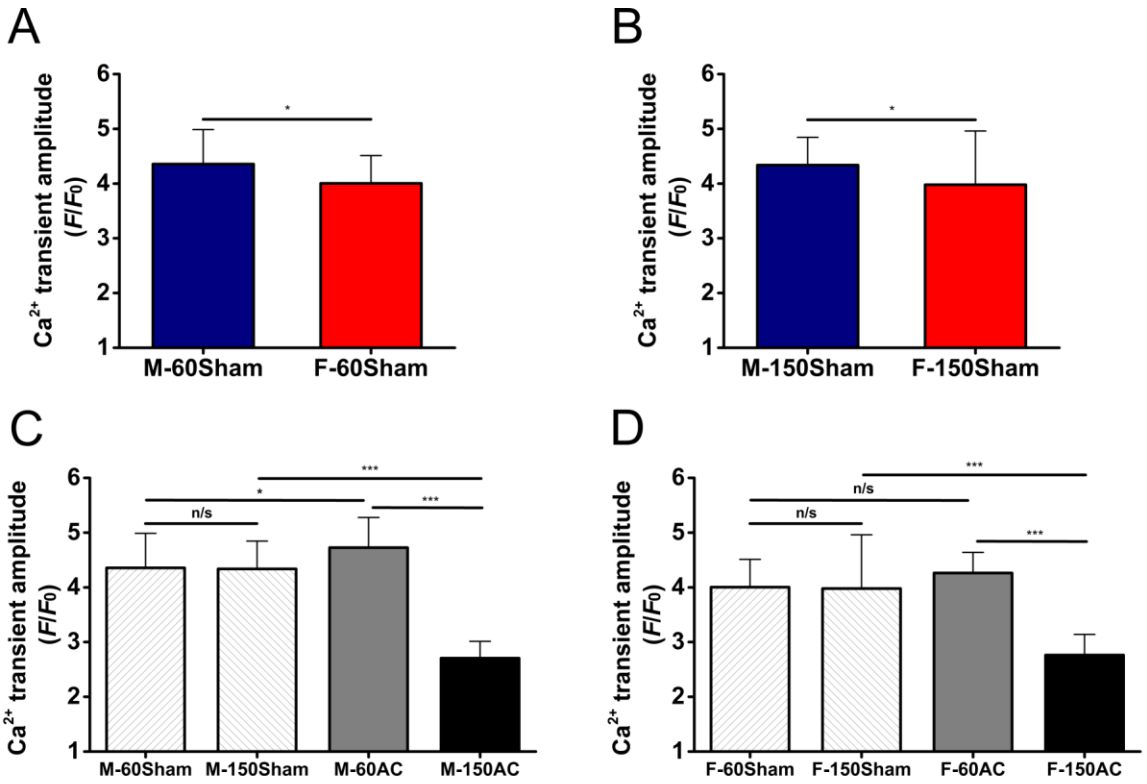

Figure 6-8. Ca^{2+} transient amplitudes in sham- or AC-operated male and female GPs.

*A & B: Males had larger Ca^{2+} transient amplitudes compared with females in their 60Sham and 150Sham groups. C & D: Ca^{2+} transient amplitudes were increased in M-60AC by 10 % but remained unaltered in F-60AC compared with M-60Sham and F-60Sham, respectively. However, Ca^{2+} transient amplitudes were considerably smaller by 38 % in M-150AC and in F-150AC by 30 % compared with their age-matched sham controls (M-60Sham, n=28/3; M-150Sham, n=37/3; M-60AC, n=37/3; M-150AC, n=37/3; F-60Sham, n=27/2; F-150Sham, n=44/3; F-60AC, n=19/2; F-150AC, n=47/3; Student's t-test or one-way ANOVA with a Fisher post-hoc test, n/s: p>0.05, *p<0.05, ***p<0.001).*

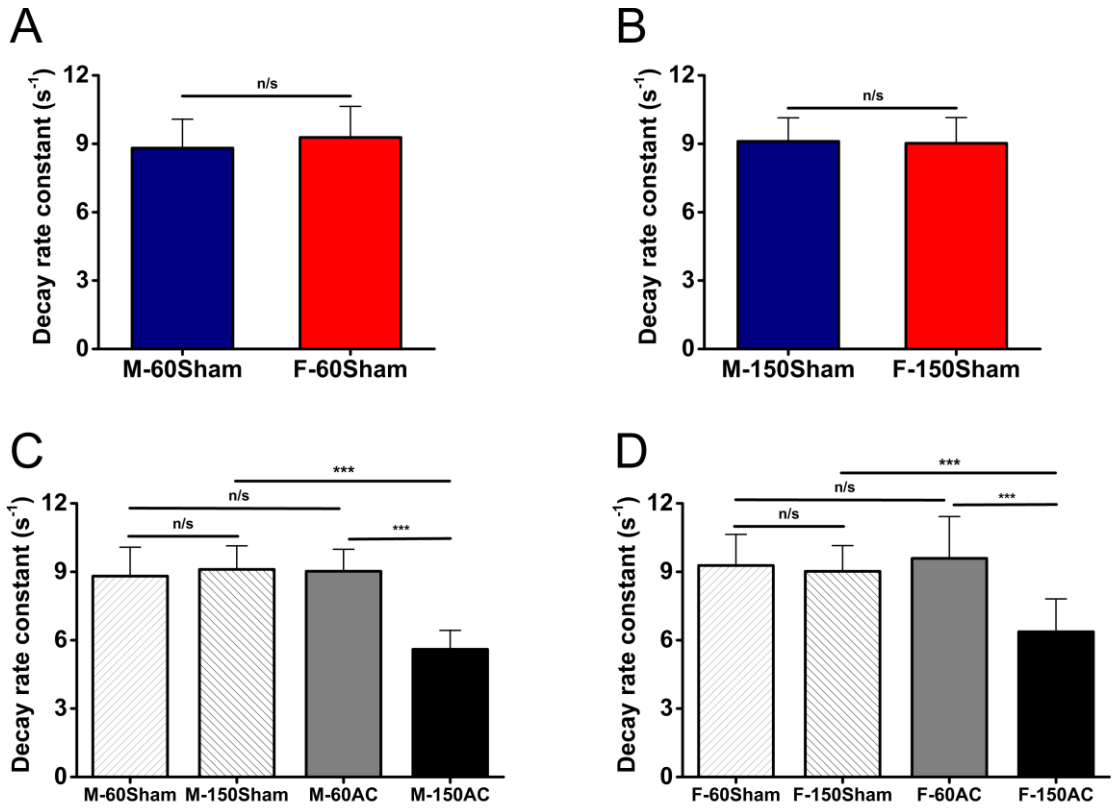

Figure 6-9. Rate constants for the decay of Ca^{2+} transient in sham and AC groups between sexes.

*A & B: Control males and females had similar rate constants for the decay of their Ca^{2+} transients. C & D: M-60AC and F-60AC had unaltered Ca^{2+} transient decay rates compared with M-60Sham and F-60Sham groups, respectively. However the decay rate constant was significantly reduced in M-150AC by 39 % and F-150AC by 29 % compared with their age-matched sham groups, M-150Sham and F-150Sham, respectively. Furthermore, M-150AC had significant slower decay rate constant, at 5.60 ± 0.83 s^{-1}, compared with F-150AC, at 6.37 ± 1.43 s^{-1} (M-60Sham, n=29/3; M-150Sham, n=30/2; M-60AC, n=27/2; M-150AC, n=26/2; F-60Sham, n=29/2; F-150Sham, n=27/2; F-60AC, n=19/2; F-150AC, n=41/2; Student's t-test or one-way ANOVA with a Fisher post-hoc test, n/s: p>0.05, ***p<0.001).*

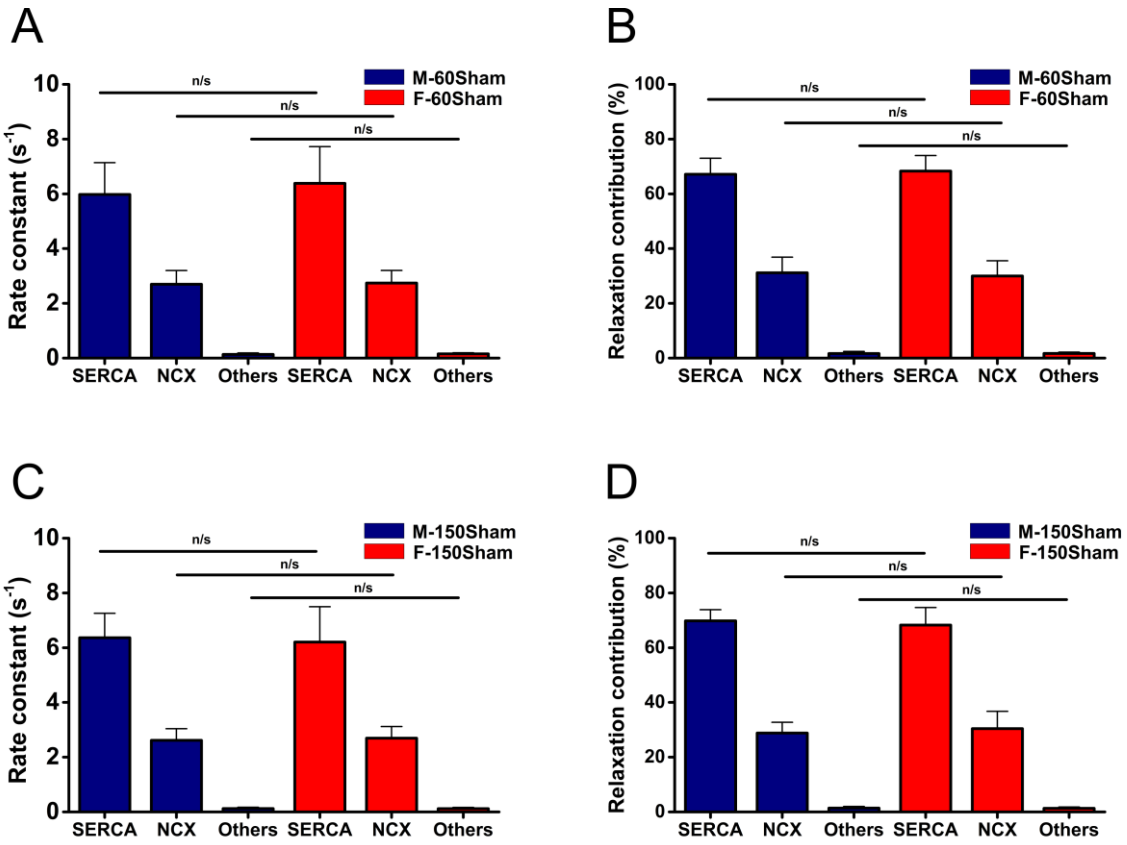

Figure 6-10. Rate constants and relaxation contribution of SERCA, NCX and other slower components in sham-operated male and female GPs.

The rate constants and the corresponding contributions to relaxation of SERCA, NCX and other slower transporters (PMCA and mitochondria Ca^{2+} uniporter) remained unchanged between M-60Sham and F-60Sham (A & B), and also between M-150Sham and F-150Sham (C & D) (M-60Sham, n=29/3; M-150Sham, n=30/2; F-60Sham, n=29/2; F-150Sham, n=27/2; one-way ANOVA with a Fisher post-hoc test, n/s: p>0.05).

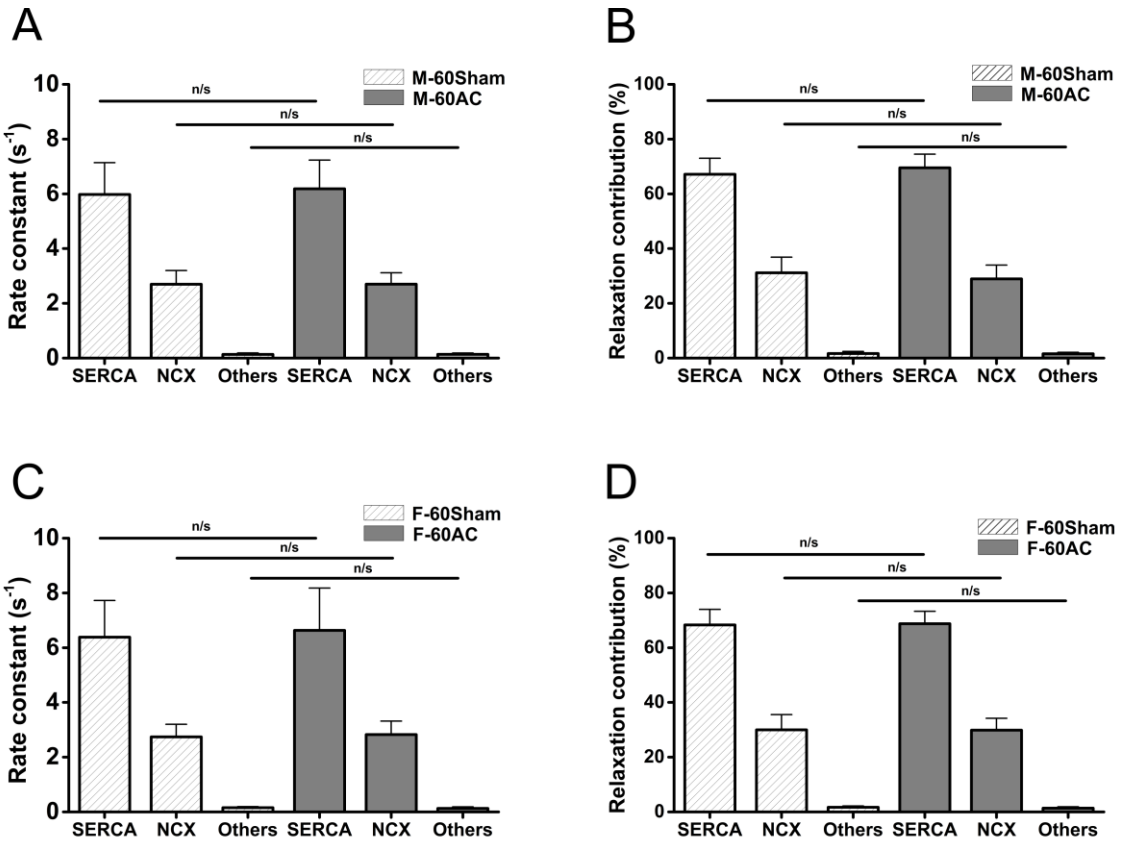

Figure 6-11. Rate constants and relaxation contribution of SERCA, NCX and other slower components in male and female 60Sham and 60AC GPs.

Both males and females showed unaltered rate constants of SERCA, NCX and other slower transporters and their relaxation contribution in 60AC compared with their age-matched 60Sham groups (M-60Sham, n=29/3; M-60AC, n=27/2; F-60Sham, n=29/2; F-60AC, n=19/2; one-way ANOVA with a Fisher post-hoc test, n/s: p>0.05).

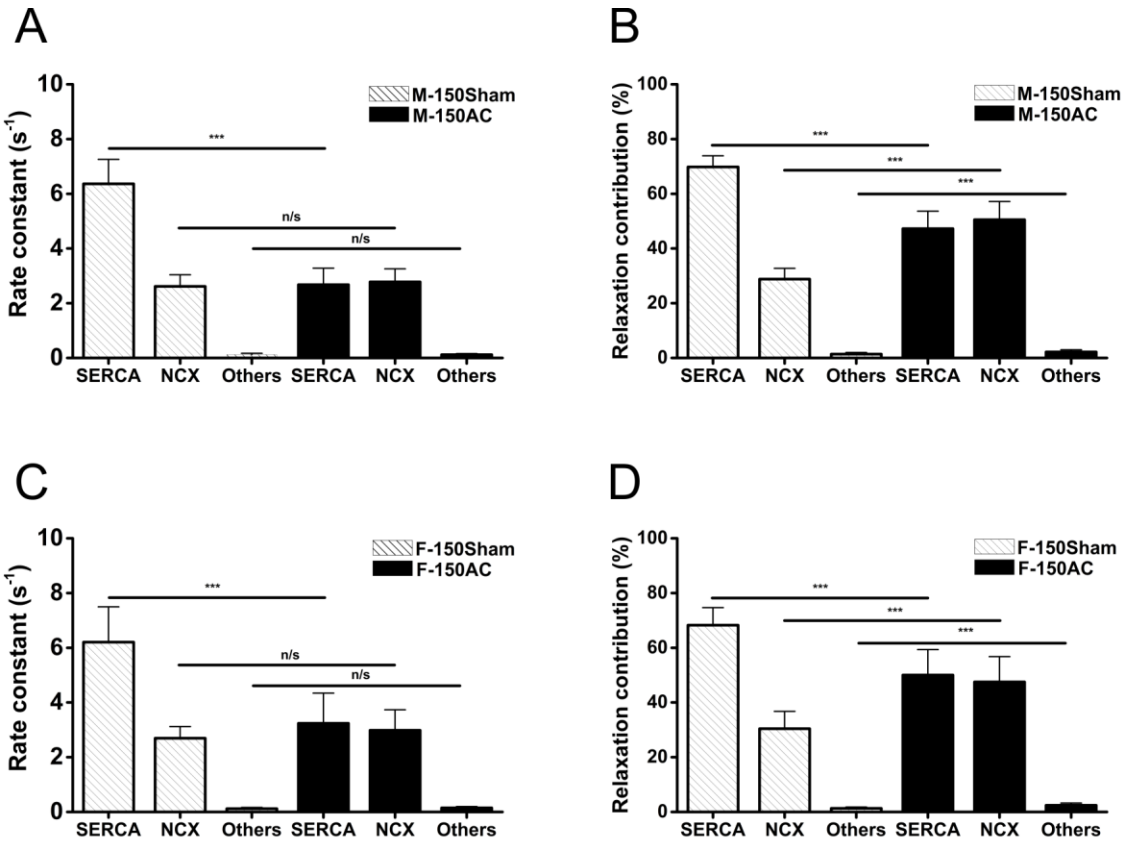

Figure 6-12. Rate constants and relaxation contribution of SERCA, NCX and other slower components in male/female 150Sham and 150AC.

*A & B: M-150AC had a slower SERCA rate constant by 58 % compared with M-150Sham. B: The relaxation contribution from SERCA decreased by 32 %, and relaxation contribution from NCX increased by 76 % in M-150AC compared with M-150Sham group. C: The rate constant of SERCA in F-150AC was reduced by 48 % compared with F-150Sham. D: While the relaxation contribution from SERCA decreased by 27 %, NCX increased by 56 % in F-150AC compared with F-150Sham. M-150AC had slower rate constant of SERCA, at 2.65 ± 0.56 s^{-1} compared with F-150AC, at 3.23 ± 1.10 s^{-1} ($p<0.05$) (A & C) (M-150Sham, n=30/2; M-150AC, n=26/2; F-150Sham, n=27/2; F-150AC, n=41/2; one-way ANOVA with a Fisher post-hoc test, n/s: $p>0.05$, ***$p<0.001$).*

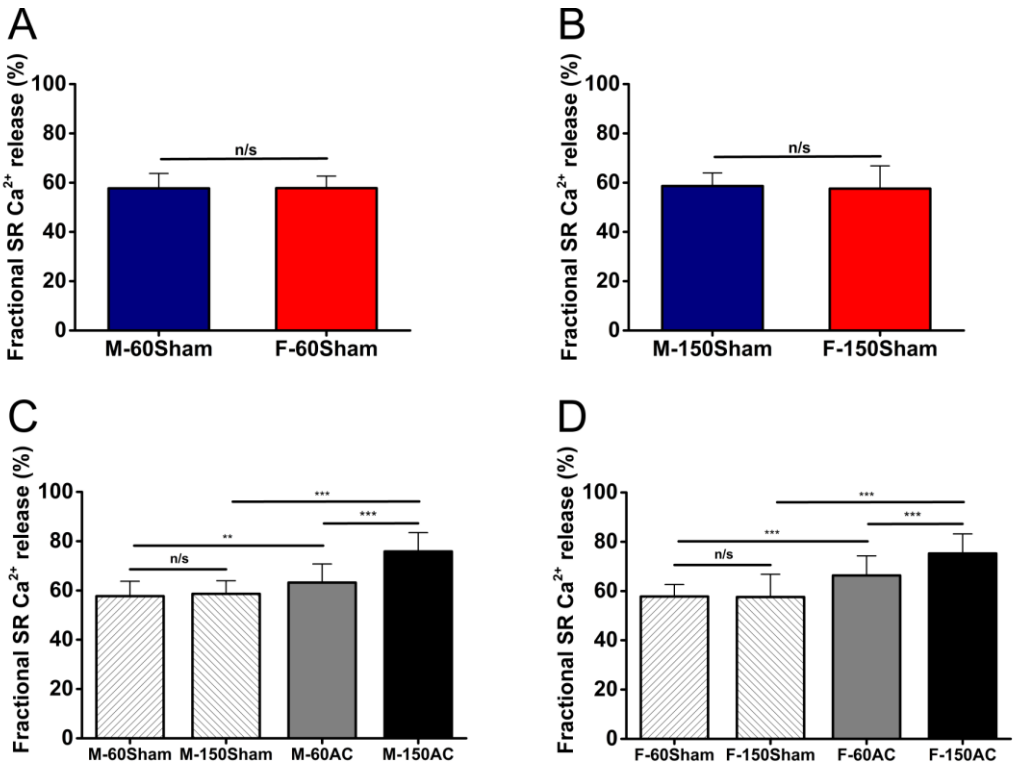

Figure 6-13. Fractional SR Ca^{2+} release in sham and AC groups between males and females.

*A & B: Fractional SR Ca^{2+} release remained unchanged between the male and female control groups at 60 and 150 days. C: Compared with M-60Sham, M-60AC showed a 10 % increase in fractional SR Ca^{2+} release. The fractional SR Ca^{2+} release increased by 29 % in M-150AC compared with M-150Sham. D: While F-60AC had a 15 % greater fractional SR Ca^{2+} release compared with F-60Sham, F-150AC had a 30 % greater fractional release compared with the age-matched F-150Sham (M-60Sham, n=18/3; M-150Sham, n=18/3; M-60AC, n=35/3; M-150AC, n=31/3; F-60Sham, n=24/3; F-150Sham, n=46/5; F-60AC, n=19/2; F-150AC, n=33/3; Student's t-test or one-way ANOVA with a Fisher post-hoc test, n/s: p>0.05, **p<0.01, ***p<0.001).*

6.4.5.3 SR Ca^{2+} content

Males and females had similar SR Ca^{2+} content between both the 60Sham and 150Sham groups (Fig. 6-14. A & B). The SR Ca^{2+} content was increased by an average of 11 % in M-60AC compared with M-60Sham. However the SR Ca^{2+} content was markedly reduced by an average of 53 % in the M-150AC group compared with M-150Sham (Fig. 6-14. C). There was no statistically significant difference between the F-60AC mean content compared with F-60Sham. F-150AC, however, had a considerable 41 % reduction in SR Ca^{2+} content compared with F-150Sham (Fig. 6-14. D). In the 150AC groups, males had significantly lower SR Ca^{2+} content by 19 % compared with females (Student's *t*-test, p<0.001).

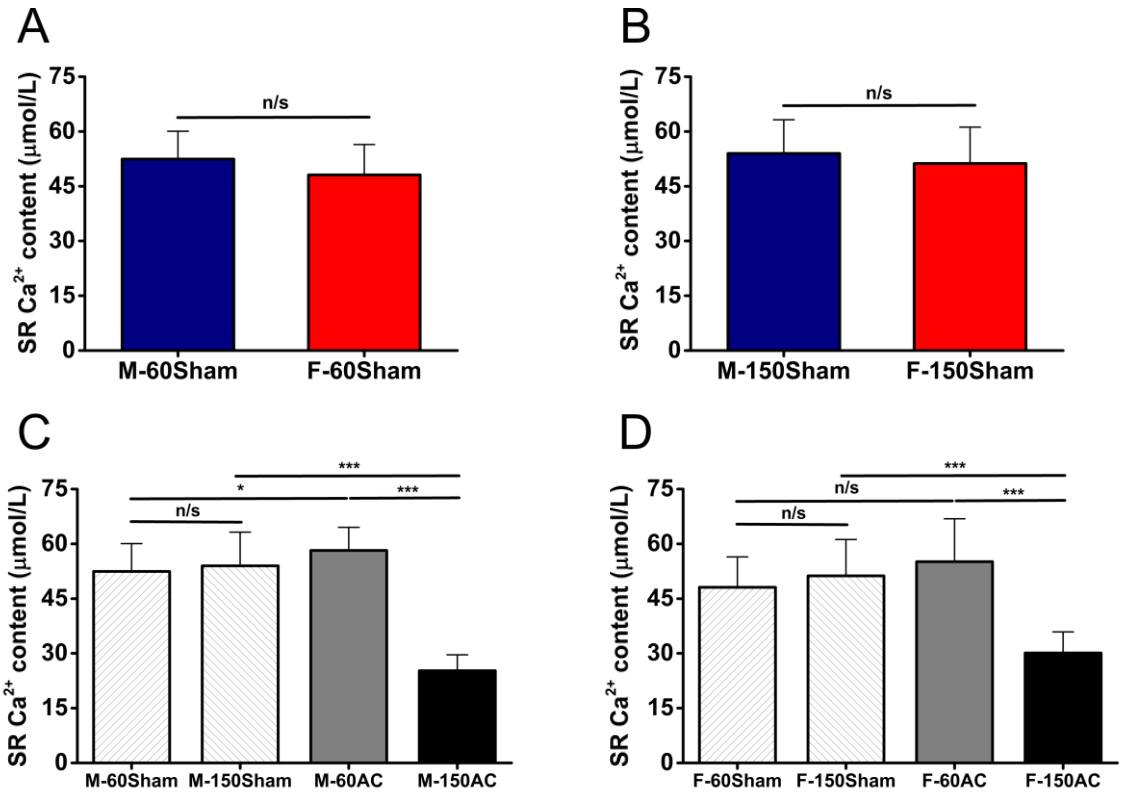

Figure 6-14. Comparing SR Ca^{2+} content between male and female sham and AC groups.

*A & B: Males (blue) and females (red) had similar SR Ca^{2+} content between both 60Sham and 150Sham groups. Panels C & D show the differences in SR Ca^{2+} content as HF develops over time and groups together males data (C) and female data (D) (M-60Sham, n=14/3; M-150Sham, n=17/2; M-60AC, n=15/2; M-150AC, n=27/3; F-60Sham, n=11/3; F-150Sham, n=33/3; F-60AC, n=20/2; F-150AC, n=34/4; Student's t-test or one-way ANOVA with a Fisher post-hoc test, n/s: p>0.05, *p<0.05, ***p<0.001).*

6.4.5.4 Spontaneous Ca^{2+} sparks and spark-mediated SR leak

The morphological parameters of Ca^{2+} sparks including the amplitudes and mass, and the spark-mediated SR leak data were log-transformed, resulting in normally distributed populations for a mean comparison test. Both males and females had higher spontaneous Ca^{2+} spark frequencies in their 150AC groups compared with the age-matched 150Sham groups. Male 150AC had higher average spark frequency compared with female 150AC. Spark amplitudes were not different (Fig. 6-15. A & B). M-150AC had a larger spark mass compared with M-150Sham (Fig. 6-15. C). Both sexes showed noticeable spark-mediated SR Ca^{2+} leak in their 150AC groups compared with their age-matched sham groups (Fig. 6-15. D).

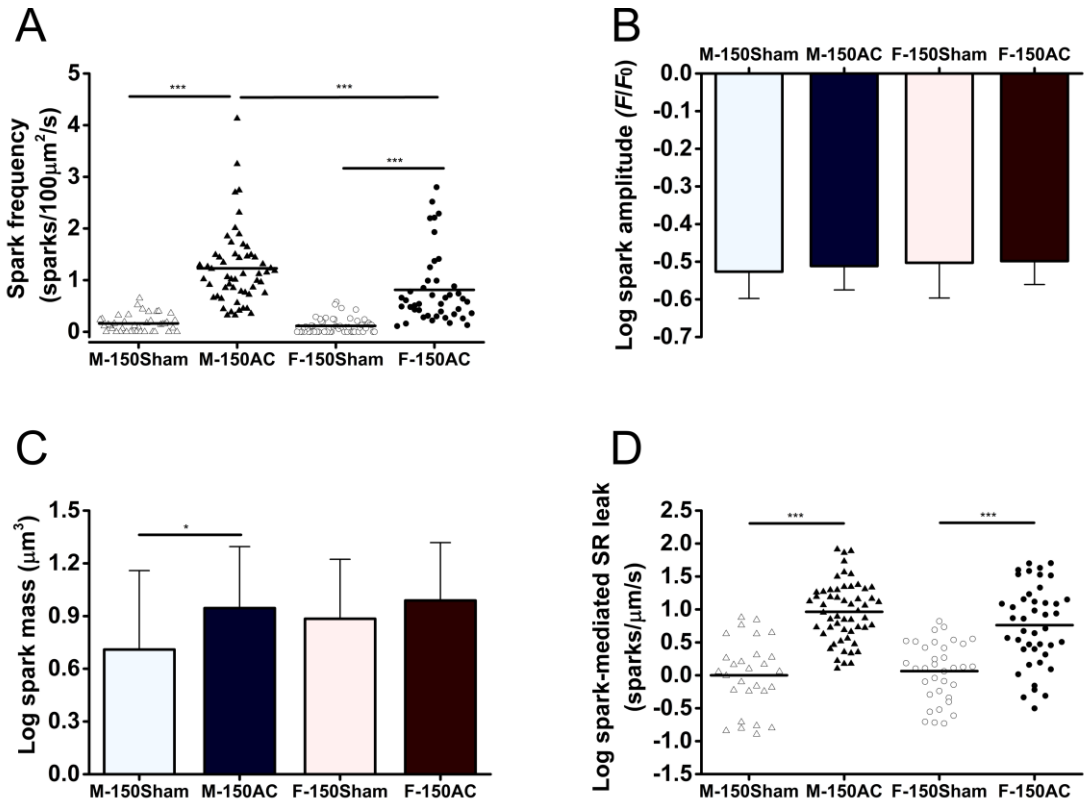

Figure 6-15. Spontaneous Ca^{2+} sparks and spark-mediated SR leak in sham- and AC operated male and female GPs.

*Panel A: Scatter graph of the spontaneous Ca^{2+} spark frequencies in males and females at 150 days following AC. Solid lines indicate means. Panel B: Log Ca^{2+} spark amplitudes in males and females at 150 days following AC. Panel C: Log Ca^{2+} spark mass in males and females at 150 days following AC and Panel D: Log spark-mediated SR leak in males and females at 150 days following AC (M-150Sham, n=41/3; M-150AC, n=55/4; F-150Sham, n=57/5; F-150AC, n=43/3; Mann-Whitney test for Ca^{2+} frequency, ***p<0.001; one-way ANOVA with a Fisher post-hoc test, n/s: p>0.05, *p<0.05, ***p<0.001).*

6.4.6 Na^+ regulation in cardiac hypertrophy and HF between genders

Changes to Na^+/K^+ ATPase current and function and $I_{Na,L}$ occurring in the progression to HF in males and females were measured to assess if there are sex-related differential changes in Na^+ regulation in cardiac hypertrophy and HF.

6.4.6.1 Na^+/K^+ ATPase

Both steady-state Na^+/K^+ ATPase currents and those produced following reactivation of the Na^+/K^+ ATPase were similar between male and female 60Sham and 150Sham groups (Fig. 6-16. A & B, C & D). M-60Sham and M-150Sham showed no difference in Na^+/K^+ ATPase current (Fig. 6-17. A). F-60Sham and F-150Sham also showed no difference in Na^+/K^+ ATPase current (Fig. 6-17. B). M-60AC showed a considerable decline in Na^+/K^+ ATPase current by an average of 43 % compared with the age-matched sham group (Fig. 6-17. A). M-150AC also had a marked average 51 % reduction in Na^+/K^+ ATPase current compared with M-150Sham (Fig. 6-17. A). The Na^+/K^+ ATPase current was reduced by an average of 22 % in female 60AC and by 45 % in F-150AC compared with their age-matched sham groups (Fig. 6-17. B). Males had smaller Na^+/K^+ ATPase current compared with females at 0.57 ± 0.07 pA/pF and 0.74 ± 0.06 pA/pF, respectively, at cardiac hypertrophy stage (Student's *t*-test, $p<0.001$). Males had a smaller mean steady-state Na^+/K^+ ATPase current, at 0.49 ± 0.05 pA/pF, compared with females, at 0.54 ± 0.08 pA/pF, at HF stage (Student's *t*-test, $p<0.05$).

The Na^+ extrusion rate was also reduced by 46 % and 57 % in M-60AC compared with M-60Sham and M-150AC compared with M-150Sham (Fig. 6-17. C). F-60AC and F-150AC had a 24 % and 51 % average decline in Na^+ extrusion rate compared with F-60Sham and F-150Sham, respectively (Fig. 6-17. C). Males had 33 % slower Na^+ extrusion rate compared with females at 60D AC stage (0.39 ± 0.11 to 0.52 ± 0.11 pC/pF/s, Student's *t*-test, $p<0.01$).

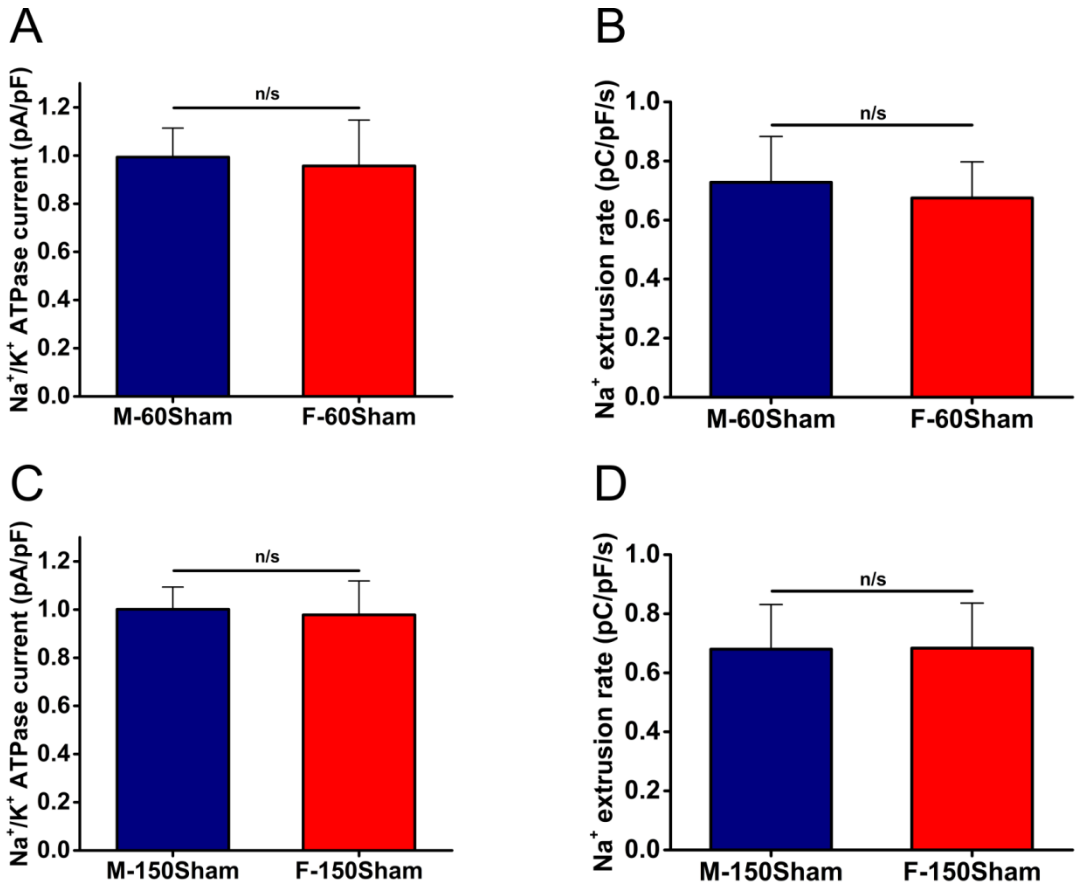

Figure 6-16. Na^+/K^+ ATPase current and reactivated Na^+/K^+ ATPase-mediated Na^+ extrusion rate in male and female sham-operated GPs.

A & B: Male and female 60Sham groups had similar Na^+/K^+ ATPase current and reactivated Na^+/K^+ ATPase-mediated Na^+ extrusion rate. C & D: No difference in Na^+/K^+ ATPase current and Na^+ extrusion rate were observed between M-150Sham and F-150Sham (M-60Sham, n=24/2; M-150Sham, n=17/2; F-60Sham, n=15/2; F-150Sham, n=22/2; Student's t-test, n/s: p>0.05).

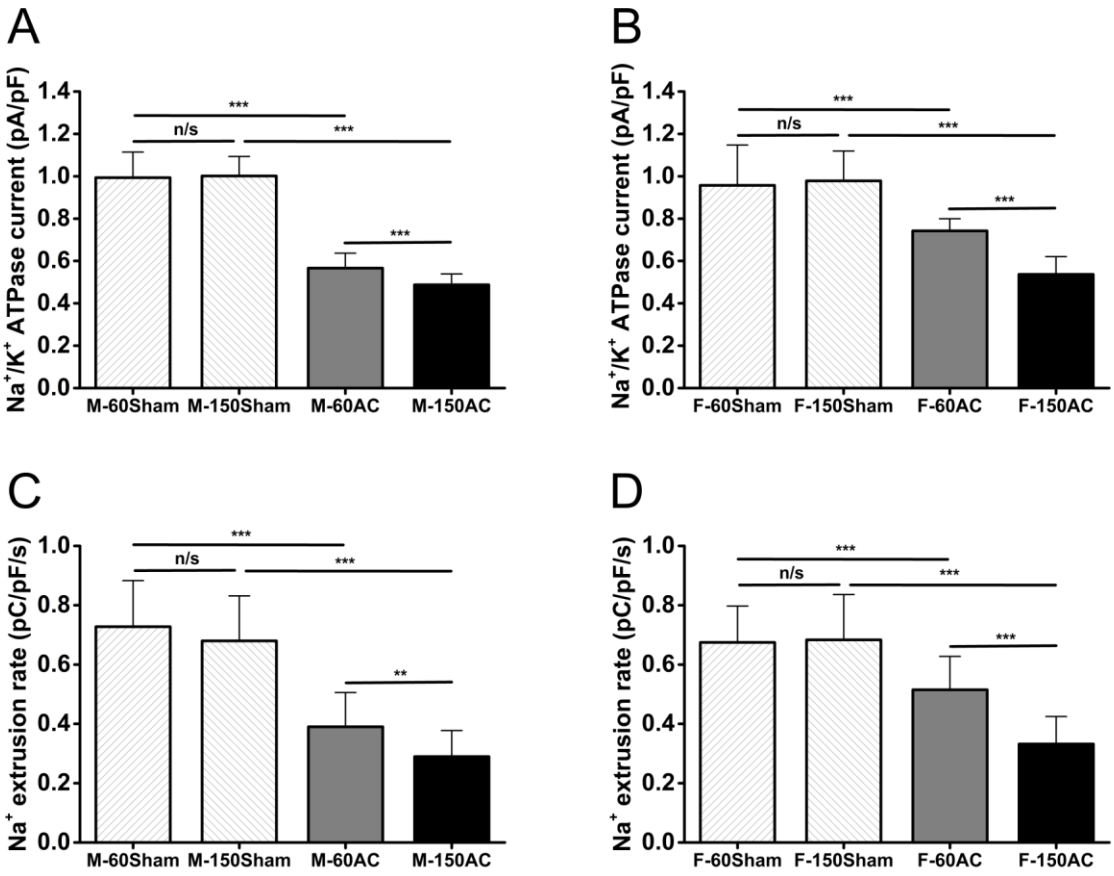

Figure 6-17. Na^+/K^+ ATPase current and reactivated Na^+/K^+ ATPase-mediated Na^+ extrusion rate in male and female sham- or AC operated GPs.

*A & B: Na^+/K^+ ATPase current was similar between M-60Sham and M-150Sham and also between F-60Sham and F-150Sham. Males had smaller Na^+/K^+ ATPase current compared with females at 60 D AC stage and also 150 D AC stage (Student's t-test, $p<0.001$ and $p<0.01$, respectively). C & D: The Na^+ extrusion rate was markedly reduced by 46 % in M-60AC and by 57 % in M-150AC compared with M-60Sham and M-150Sham. F-60AC and F-150AC showed a 24 % and 51 % decline in Na^+ extrusion rate compared with F-60Sham and F-150Sham, respectively. Male had slower Na^+ extrusion rate compared with female at 60D AC stage (Student's t-test, $p<0.01$) (M-60Sham, n=24/2; M-150Sham, n=17/2; M-60AC, n=23/2; M-150AC, n=27/3; F-60Sham, n=15/2; F-150Sham, n=22/2; F-60AC, n=24/2; F-150AC, n=19/3; one-way ANOVA with a Fisher post-hoc test, n/s: $p>0.05$, **$p<0.01$, ***$p<0.001$).*

6.4.6.2 $I_{Na,L}$

Male and female 60Sham groups had similar $I_{Na,L}$, the decay time constant (tau) of $I_{Na,L}$, and $I_{Na,L}$ related Na^+ influx (Fig. 6-18. A, B & C). M-150Sham and F-150Sham also had similar in $I_{Na,L}$, $I_{Na,L}$ related Na^+ influx and the decay time constant of $I_{Na,L}$ (Fig. 6-18. D, E & F).

$I_{Na,L}$ showed marked increases of 92 % in M-60AC and 122 % in M-150AC compared with their age-matched sham groups (Fig. 6-19. A). In females, $I_{Na,L}$ also significantly increased by 66 % in 60AC and by 88 % in 150AC compared with their age-matched sham groups (Fig. 6-19. B). $I_{Na,L}$-mediated Na^+ influx was considerably greater by 72 % in M-60AC and by 1.55 times in M-150AC compared with M-60Sham and M-150Sham, respectively (Fig. 6-19. C). The $I_{Na,L}$-mediated Na^+ influx also showed a significant increase by 67 % in F-60AC and by 1.05 folds in F-150AC compared with their age-matched sham groups (Fig. 6-19. D). While the decay tau remained unchanged between 60AC and 60Sham in both genders, the decay tau was 19 % longer in M-150AC and 23 % longer in F-150AC compared with M-150Sham and F-150Sham, respectively (Fig. 6-19 E & F).

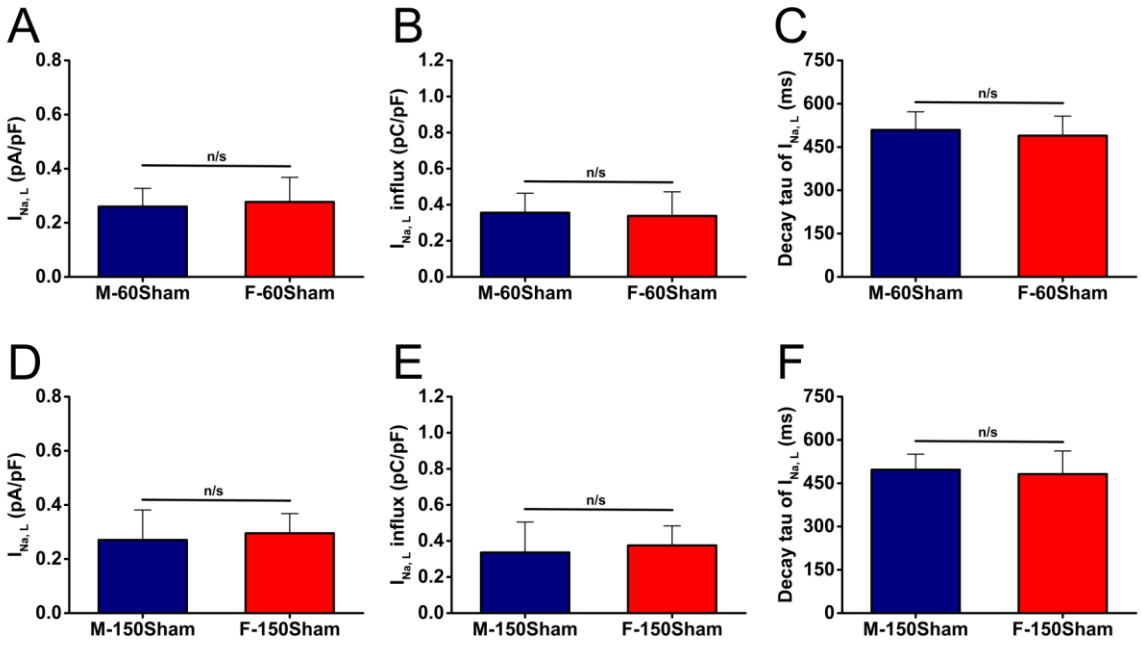

Figure 6-18. $I_{Na,L}$, corresponding Na^+ influx, and the time constant for decay phase in sham-operated male and female GPs.

$I_{Na,L}$, the corresponding Na^+ influx, and the decay time constant tau showed no difference between male and female 60Sham groups and between male and female 150Sham groups (M-60Sham, n=20/4; M-150Sham, n=23/3; F-60Sham, n=22/4; F-150Sham, n=31/3; Student's t-test, n/s: p>0.05).

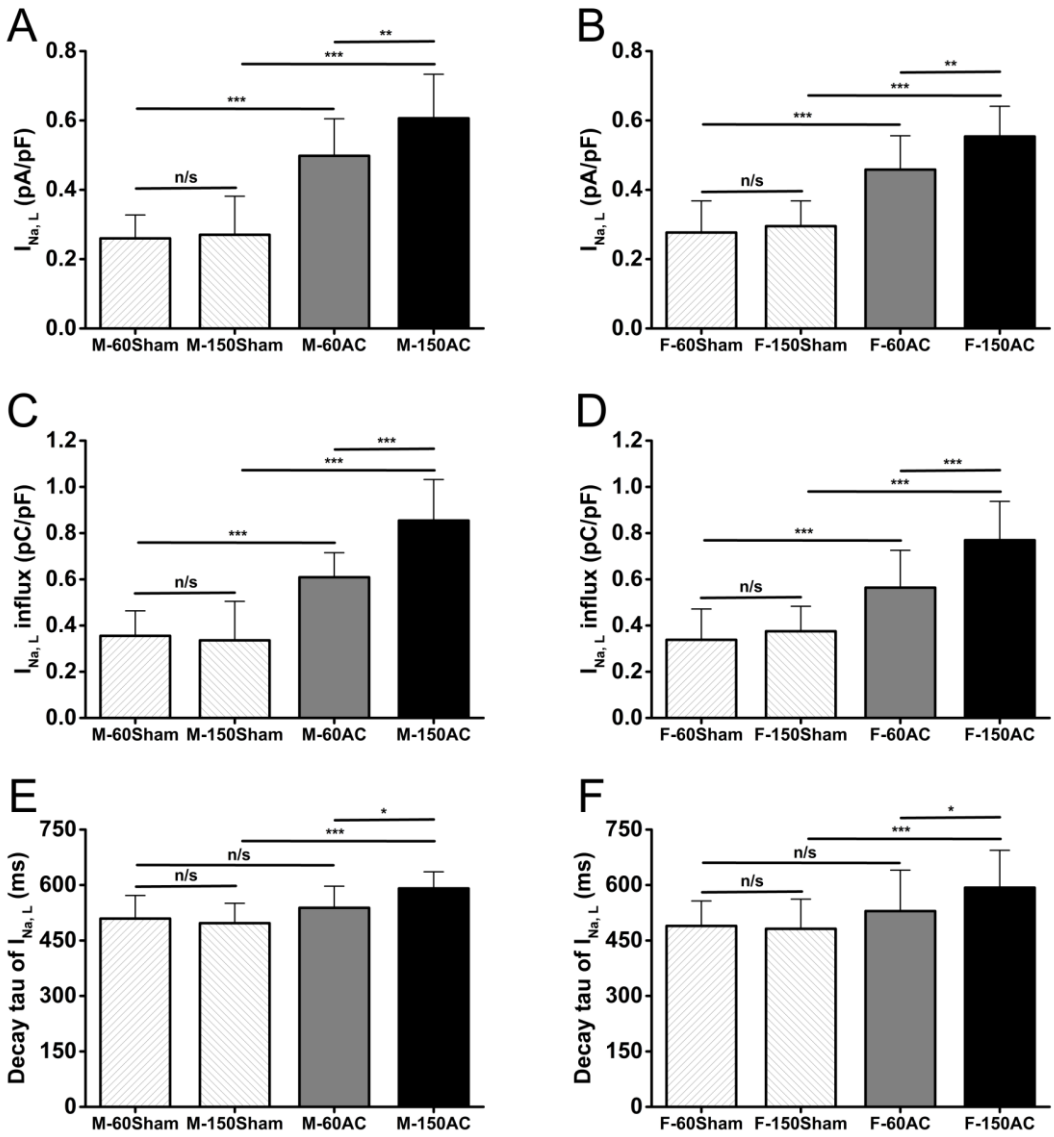

Figure 6-19. $I_{Na,L}$, the corresponding Na^+ influx, and the decay tau in sham- or AC-operated male and female GPs.

*A: $I_{Na,L}$ markedly increased by 92 % in M-60AC and by 1.22 times in M-150AC compared with their age-matched sham groups. B: $I_{Na,L}$ also significantly increased by 66 % in F-60AC and by 88 % in F-150AC compared with their age-matched sham groups. C: $I_{Na,L}$ associated Na^+ influx was considerably greater by 72 % in M-60AC and by 1.55 times in M-150AC compared with their age-matched sham groups. D: The $I_{Na,L}$ associated Na^+ influx was also significant greater by 67 % in F-60AC and by 1.05 times in F-150AC compared with their age-matched sham groups. E & F: The decay tau remained unaltered between 60AC and 60Sham in both sexes, but the decay tau was 19 % longer in M-150AC and 23 % longer in F-150AC compared with their age-matched sham groups, respectively (M-60Sham, n=20/4; M-150Sham, n=23/3; M-60AC, n=18/2; M-150AC, n=17/3; F-60Sham, n=22/4; F-150Sham, n=31/3; F-60AC, n=15/3; F-150AC, n=25/3; one-way ANOVA with a Fisher post-hoc test, n/s: p>0.05, *p<0.05, **p<0.01, ***p<0.001).*

6.5 Discussion

This chapter detailed differences to some physical characteristics and *in vivo* cardiac function of the heart occurring between males and females during the progression from cardiac hypertrophy to HF in a pressure-overload GP model. Differential changes in cellular Ca^{2+} handling (Ca^{2+} transient, $I_{Ca,L}$ and SR Ca^{2+} stores), and the important mechanisms involved in Na^+ regulation (Na^+/K^+ ATPase current and function, and $I_{Na,L}$) were also assessed. It is clear that males and females exhibit differential dysfunction of Ca^{2+} handling, Na^+ regulation and E-C coupling during the progression from cardiac hypertrophy to HF.

6.5.1 Changes in physical characteristics and cardiac function in AC progress between sexes.

Animal models showed male and female hearts may adapt differently in response to cardiac stress[205]. In a rat model of ascending AC, an earlier transition to left ventricular dilation and depressed systolic function was shown in males compared with females[206]. These data are also in line with clinical observations that females are more protected against cardiac hypertrophy and HF[179,293]. Our data (Fig. 6-20) showed both males and females produced cardiac hypertrophy and maintained adequate heart function 60 days following AC, a time period that we suggest is the stage of compensated cardiac hypertrophy. At the HF stage, the FS significantly declined alongside an increased HW/BW and LW/BW ratio in both genders, but males had more reduction of FS and higher LW/BW ratio compared with females. While male and female GPs had similar *in vivo* functional indices at the cardiac hypertrophy stage, males showed a more detrimental deterioration of function at the HF stage. Therefore, in terms of *in vivo* assessment, female GPs were more resistant to pressure-overload AC stress compared with males, which is in line with other studies[203,205,206].

In an ER β gene knock-out mice with AC, the wild type (WT) males showed more hypertrophy, cardiac fibrosis and heart failure signs than WT females[203]. This difference was abolished in ER β knockout mice, which suggested ER β may play a role in attenuating the development of fibrosis and apoptosis, resulting in slowing the progression to heart failure[203]. There are also reports that disruption of the FKBP12.6 gene results in similar dysregulation of Ca^{2+} in males and female, but only males developed hypertrophy. The protective effect was abolished by treatment of the females with tamoxifen, an oestrogen receptor antagonist, and this led to the females developing cardiac hypertrophy similar to the male[195]. These results support the present data suggesting the female GPs manage their responses to pressure-overload better than males and an obvious candidate for a role in the better management is oestrogen.

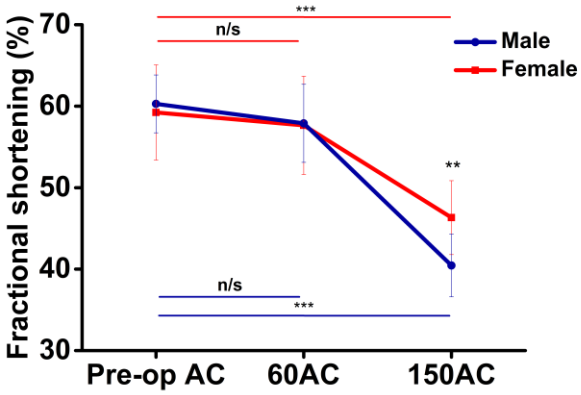

Figure 6-20. Changes in fractional shortening in AC progress between sexes.

Both sexes showed unchanged FS at 60AC. While both sex showed reduced FS at 150AC, male GPs showed more reduced FS compared with females (see Fig. 6-3. for more detail).

6.5.2 Sex differences in APD, Ca^{2+} handling and Na^{+} regulation in sham GPs.

Studies have shown that sex hormones profoundly influence the sex disparities in cardiac electrophysiology[175,177,178,185]. Our data showed female sham-operated 60 D and 150 D GPs had longer APD compared with males. Since males and females had similar peak $I_{Ca,L}$ and corresponding decay time constants, the APD prolongation in female could be due to a decline in the size of outward repolarising currents, such as I_{Kr}, I_{K1} or I_{to}. Similar to humans, APD in female rats and mice are longer compared with their male counterparts. However, mice and rats action potential do not present a plateau phase, and their ventricular cells repolarise rapidly without the delayed rectifiers, I_{Kr} and I_{Ks} observed in human cardiomyocytes[294].

The oestrus cycle has been shown to have an effect on APD. In a ovariectomised mice model, $I_{to,f}$ and I_{Kur} were lower in females at oestrus versus males[295]. With oestrogen treatment, ovariectomised mice showed decreased $I_{K,total}$[295]. Thus, I_K reduces in high oestrogenic conditions which were associated with prolongation of the APD. James *et al* found I_K tail current density was not significantly reduced in female GPs in oestrus day 0 when the serum oestradiol reaches its peak, and this did not contribute to the prolongation of APD in female[227]. Instead, they showed the oestrus cycle influences the density of $I_{Ca,L}$, which in turn affects the duration of action potential. However there is a conflicting report suggesting the oestrus cycle has no effect on $I_{Ca,L}$[296]. While Mason *et al* showed a longer APD in female GPs[290], Liew *et al* reported a similar APD between sexes using the same species. The discrepancy may result from different weight or age of animal and the timing in use. There was no difference in peak $I_{Ca,L}$ in our sham-operated GPs between sexes. Similar peak $I_{Ca,L}$

between sexes was also reported in a rat model[297]. Our GPs are not sacrificed according to their oestrus cycle so we cannot assess if peak $I_{Ca,L}$ is affected by the oestrus cycle.

Males had larger Ca^{2+} transient amplitudes compared with females, but in both sexes had similar Ca^{2+} transient decay rate constants, and the rate constants of SERCA, NCX and other slower components of the decline in Ca^{2+} that indicate the relative contributions of each mechanism were comparable. We showed similar density of $I_{Ca,L}$ and SR Ca^{2+} content between sexes. Therefore larger Ca^{2+} transient amplitudes in males may develop from other factors rather than a larger Ca^{2+} influx. Sex hormones may play a role in the differences. Farrell *et al* report a similar APD, density of $I_{Ca,L}$ but smaller Ca^{2+} transient in female mice compared with males[298]. Wasserstrom *et al* also reported smaller Ca^{2+} transient amplitudes in females in a rat whole heart model[292]. MacDonald *et al* showed oestrus cycle affects Ca^{2+} transient amplitudes in female mice. Larger Ca^{2+} transient amplitudes were shown in oestrus when the serum oestradiol was high in their mouse model.

Na^+/K^+ ATPase current and reactivated Na^+/K^+ ATPase mediated Na^+ extrusion rates were also similar between males and females. Therefore we suggest there is no gender difference in the basal function of the Na^+/K^+ ATPase. To the best of our knowledge, this is the first functional observation of Na^+/K^+ ATPase in cardiomyocytes between sexes. There is lack of studies of sex differences in Na^+/K^+ ATPase current and Na^+ extrusion function but there are experiments that indicate sex differences in the biochemical properties of the Na^+/K^+ ATPase. Vlkovicova *et al* report females had a similar K_m but fast V_{max} of Na^+/K^+ ATPase activation by substrate ATP compared with males, which used homogenates preparation from rat heart. Palacios *et al* report different Na^+/K^+ ATPase isoform abundance between sexes in aortic tissue[299].

6.5.3 Sex difference in Ca^{2+} handling and Na^+ regulation at cardiac hypertrophy and HF stages.

6.5.3.1 Cardiac hypertrophy stage

As mentioned in chapter 4, the prolongation of APD in cardiac hypertrophy and HF may be associated with elevated $[Na^+]_i$ or reduced K^+ outward current, such I_{K1} or I_{to}. We have discussed the longer baseline APD in female may be related to smaller outward K^+ current compared with male. Both sexes showed similar prolonged APD_{90} at the hypertrophy stage (Fig. 6-21), thus the degree of prolongation of APD in male surpassed the baseline difference, which implies males may have more increased inward currents or more reduced outward currents compared with females. I_{to} was reduced in hypertrophied myocytes from spontaneously hypertensive rats[300]. GPs have relatively smaller I_{to} which may affect APD to a limited extent. While reduced I_{K1} may contribute to the

prolonged APD in our GP model, unchanged I_{K1} was reported in hypertrophied myocytes from a AC GP model[257]. A decline in Na^+/K^+ ATPase function and an enhancement of $I_{Na,L}$, may contribute to an increase in $[Na^+]_i$ and a prolongation of APD at these stages of progression. We will discuss these two components in later section.

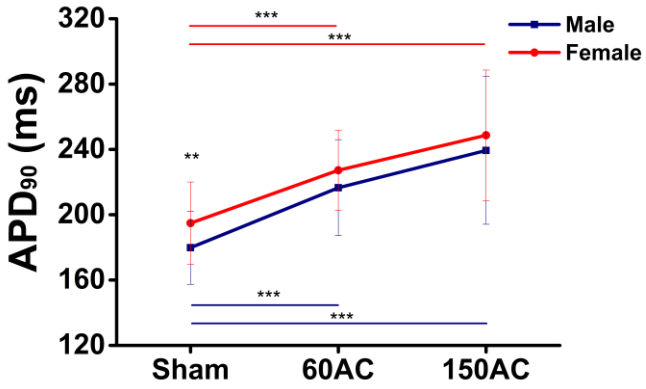

Figure 6-21. APD_{90} during AC progression between sexes.

While Females had longer APD_{90} in sham group, both sexes had similar prolonged APD_{90} (Sham=60Sham+150Sham; see Fig. 6-5 for more detail).

In chapter 4 we have shown unaltered peak $I_{Ca,L}$ and its inactivation kinetics at the hypertrophy stage. Most studies reported that peak $I_{Ca,L}$ density is unaltered in cardiac hypertrophy[68,85]. Here we further showed there was no difference in unaltered peak $I_{Ca,L}$ and its inactivation kinetics in cardiac hypertrophy between sexes. Males had increased Ca^{2+} transient amplitudes and SR Ca^{2+} content at this stage but in females these were unchanged (Fig. 6-22). In chapter 4 we pointed out that the decline in Na^+/K^+ ATPase current and function occurring at the cardiac hypertrophy stage could be regarded as a compensation mechanism that increases $[Na^+]_i$, which in turn, increases Ca^{2+} influx via NCX and loads the SR with more Ca^{2+} to produce an inotropic effect[90]. Males showed a larger decline Na^+/K^+ ATPase function compared with female at this stage (Fig. 6-24), which may imply males had more elevated $[Na^+]_i$ and in turn, this caused more Ca^{2+} influx via reverse-mode NCX, resulting in larger Ca^{2+} transients and greater SR Ca^{2+} contents. In an I/R mouse model, males showed a larger increase in $[Na^+]_i$ compared with females after an ischaemic insult, which suggests males may tend to accumulate more $[Na^+]_i$ in the face of cardiac stress compared with female[301].

We described in chapter 4 that the Ca^{2+} transient decay rate constant was unaltered at the hypertrophy stage. Both males and females had unaltered Ca^{2+} transient decay rates and unaltered SERCA and NCX functions (Fig. 6-23). Others have found that in the early stage of cardiac

hypertrophy, the expression of SERCA may remain unchanged or is slightly decreased[92,95]. Weinberg *et al* reported reduced mRNA expression of SERCA in male hypertrophied hearts which was not seen in females[206]. These authors also reported that both sexes showed increased mRNA expression of NCX but there was no difference between the sexes.

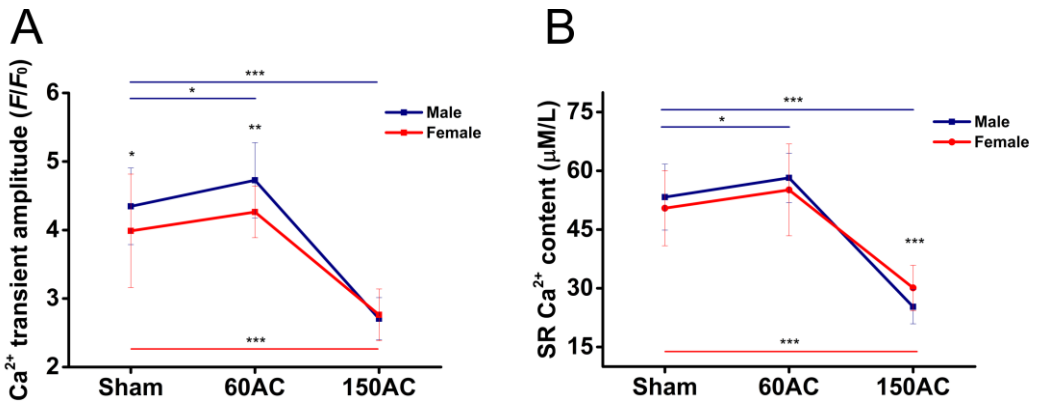

Figure 6-22. Ca^{2+} transient amplitude and SR Ca^{2+} content during AC progression between sexes.

Males showed increased Ca^{2+} transient and SR Ca^{2+} content at 60AC which was not observed in females. Both sexes had significantly declines in Ca^{2+} transient and SR Ca^{2+} content at 150AC, and males had less SR Ca^{2+} content at 150AC compared with females (Sham=60Sham+150Sham; see Fig. 6-13 & 6-14 for more detail).

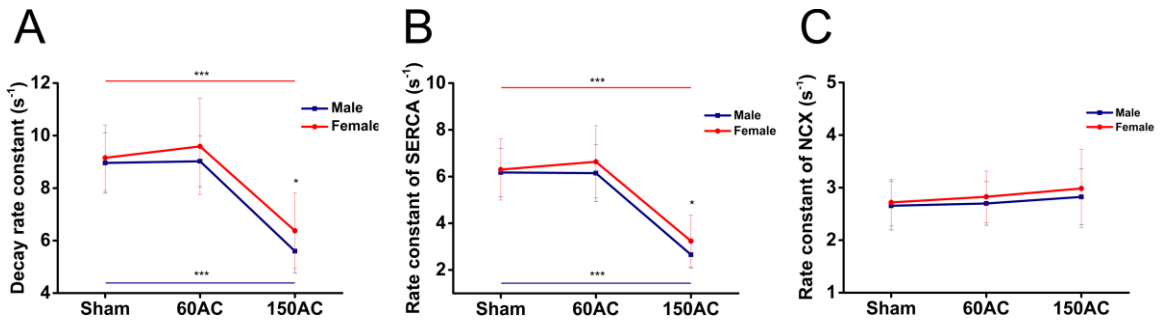

Figure 6-23. Ca^{2+} transient decay rate constant and rate constant of SERCA during AC progression between sexes.

Both sexes showed Ca^{2+} transient decay rate and rate constant of SERCA was unchanged at 60AC but significantly reduced at 150AC. Males had slower Ca^{2+} transient decay rate and rate constant of SERCA at 150AC compared with females. There was no significant difference in rate constant of NCX in Sham, 60AC and 150AC group between sexes (Sham=60Sham+150Sham; see Fig. 6-9, -10, -11 & -12 for more detail).

6.5.3.2 HF stage

APD_{90} was further prolonged in both sexes at the HF stage (Fig. 6-21). While reduced I_K may still be the possible contributor to the prolongation of APD in HF[257], here we reported markedly enhanced $I_{Na,L}$ at this stage in both sexes and this could contribute substantial Na^+ influx during action potential plateau, leading to prolongation of APD.

We reported unaltered peak $I_{Ca,L}$ with prolonged inactivation at the HF stage; an effect seen in both sexes and there was no gender difference. In chapter 4 it was reported that there were marked reductions in Ca^{2+} transient amplitudes and slower decay rates with slower rate constants of SERCA in HF. While both sexes had similar tendencies, males had a relatively slower Ca^{2+} transient decay rate constant and rate constant of SERCA compared with females at the HF stage (Fig. 6-23, A & B). The more reduced SERCA function in males may also help explain that males had relatively lower SR Ca^{2+} content at HF stage compared with females (Fig. 6-22. B).

One possible reason for these observations could be that males may have relatively lower mRNA or protein expression of SERCA. SERCA mRNA expression was shown to be reduced in male hypertrophic heart, which is not seen in females following aortic banding[206]. The differential dysfunction of SERCA between sexes may also result from differential phosphorylation of the SERCA regulatory protein, PLB. Reduction in PKA mediated Ser-16 PLB phosphorylation is regarded as one of the major factors determining the degree of reduced SERCA2a activity in HF[97,215]. A report studying human HF showed myocytes from patients of both sexes show significantly reduced SERCA protein with unaltered PLB and calsequestrin levels. However, the reduction in phosphorylation of Ser-16 in PLB was present only in male hearts and the phosphorylation levels in female were unaltered[216]. This may result in more inhibition of SERCA in males in HF. These studies provide evidence of sex differences in the expression of SERCA, its coding mRNA or in the modulation of PLB in cardiac hypertrophy and HF.

Both sexes showed increases in spark-mediated SR Ca^{2+} leak, but there was no difference in leak between males and females. However, the spark frequency was higher in male HF myocytes compared with females. In a human cardiac hypertrophic and HF study[217], there were comparable Ca^{2+} handling properties, including diastolic Ca^{2+} levels, Ca^{2+} transient amplitudes and SR Ca^{2+} content, and similar Ca^{2+} spark frequency and spark-mediated SR leak in hypertrophic heart between sexes. However, In HF, while both sexes showed increased spark frequency and spark-mediated SR leak compared with hypertrophic heart groups, males showed more pronounced spark frequency and spark-mediated SR leak compared with females[217]. Thus sex differences may also play a role in

the regulation of open probability of RyR2, which could be modulated by phosphorylation via kinases such as PKA and CalMKII[110,269]. Ma *et al* reported up-regulated expression of CaMKIIδ and phosphorylated CaMKII in the hearts from ovariectomised rats, which were restored to normal level by oestrogen replacement[196]. This provides evidence of a CaMKII suppression effect of oestrogen, which may modulate Ca^{2+} handling and provide cardioprotection[196].

6.5.3.3 Sex differences in Na^+/K^+ ATPase and $I_{Na,L}$ in cardiac hypertrophy and HF

One of the most striking changes taking place at the cardiac hypertrophy stage in both sexes was the decrease in steady-state Na^+/K^+ ATPase current and Na^+ extrusion rate. However, males had much greater decreases in both Na^+/K^+ ATPase current and Na^+ extrusion rate compared with females (Fig. 6-24). Males had more reduction in Na^+/K^+ ATPase current and function compared with females, and together with increased Ca^{2+} transient amplitudes and SR Ca^{2+} content, this may imply there may be more elevated $[Na^+]_i$ in males at this stage. Gender difference may exist in $[Na^+]_i$ accumulation in the face of CVD. Female mice showed less elevated $[Na^+]_i$ after ischaemic injury compared with males[301]. The difference in susceptibility to I/R injury appears to result from a difference in Na^+ influx. The authors indicated the sex difference in the $[Na^+]_i$ regulation may be mediated through a NO-dependent mechanism[301].

In both sexes, Na^+/K^+ ATPase currents and Na^+ extrusion function had further decreases in HF compared with that in the compensated stage with the Na^+/K^+ ATPase current more reduced in males compared with females. Sex differences have been shown in changes in Na^+/K^+ ATPase function and expression in response to pathological stimuli. A rat kidney ischaemic-reperfusion study reported that females had less reduction in mRNA and protein expression of the Na^+/K^+ ATPase α1 subunit and less reduction in the activity of the protein after ischaemic insult[302]. Vlkovicov *et al* showed that the Na^+/K^+ ATPase from SHR female hearts seems to be adapted better to hypertension because there is less reduction in enzyme activity when activated by ATP[303]. In addition, the group found that the Na^+/K^+ ATPase from female SHR hearts is able to increase its activity in the presence of increasing Na^+ concentration beyond the range where the Na^+/K^+ ATPase from males is already saturated[303].

Another contributor to Na^+ influx and $[Na^+]_i$ is the-$I_{Na,L}$ and this was enhanced in cardiac hypertrophy as highlighted in chapter 5. This increase is seen in both sexes (Fig. 6-25). Both males and females also showed further increases in $I_{Na,L}$ and $I_{Na,L}$ associated Na^+ influx at the HF stage. The decay time constant was also significantly increased in both sexes. Increased $I_{Na,L}$ has been shown in several

pathological conditions, including I/R, MI, and HF[111,112,132-134], and is a contributor to the increase in intracellular Na^+ and the prolongation of APD. There was no sex difference in the amplitude of the enhanced $I_{Na,L}$ and $I_{Na,L}$-mediated Na^+ influx at both the hypertrophy and HF stages. This may imply $I_{Na,L}$ contributes similar amounts of Na^+ to the cells of both sexes in all these types of cardiac pathology, but there is a lack of studies in the sex difference in $I_{Na,L}$ to compare with our data.

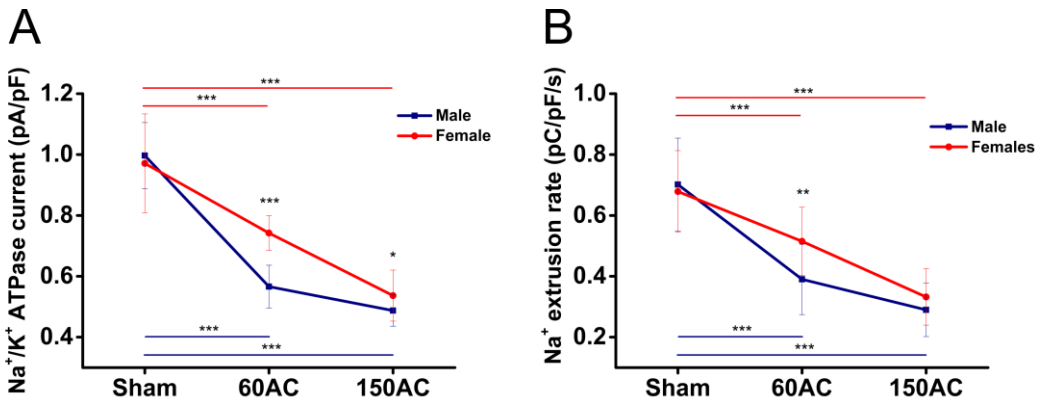

Figure 6-24. Na^+/K^+ ATPase current and Na^+ extrusion rate during AC progression between sexes.

While both sexes showed a continuous decline in Na^+/K^+ ATPase current and function during the progression towards HF, males showed a more marked reduction at 60AC compared with females (Sham=60Sham+150Sham; see Fig. 17 for more detail).

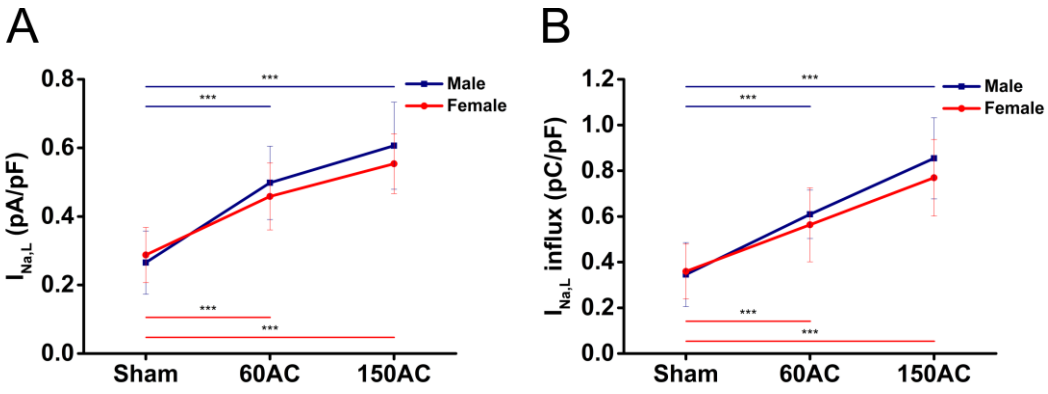

Figure 6-25. $I_{Na,L}$ and $I_{Na,L}$-mediated Na^+ influx during AC progression between sexes.

Both sexes showed continuously increased $I_{No,L}$ and the associated Na^+ influx with comparable amount of enhancement during AC progression (Sham=60Sham+150Sham; see Fig. 19 for more detail).

6.6 Conclusions

Sex differences exists in Ca^{2+} handling and Na^{+} regulation during the progression from cardiac hypertrophy to HF. Prolongation of the APD was observed at the cardiac hypertrophy and HF stages in both sexes. While both sexes maintained their cardiac FS at the hypertrophy stage, males showed more deterioration of cardiac function and more congested lungs at the later HF stage compared with females. Males had larger Ca^{2+} transient amplitudes and greater SR Ca^{2+} content at the cardiac hypertrophy stage, but afterwards had slower Ca^{2+} transient decay and more impaired Ca^{2+} uptake via SERCA with smaller SR Ca^{2+} content at the HF stage compared with females. While males had higher spontaneous Ca^{2+} spark frequency at HF, males and females has similar increased spark-mediated SR Ca^{2+} leak. Both sexes showed reductions in Na^{+}/K^{+} ATPase current and function at cardiac hypertrophy and HF, but males experienced more decline at the cardiac hypertrophy stage compared with females. $I_{Na,L}$ started to increase at the hypertrophy stage in both sexes with markedly increasing and prolonged decay kinetics at the HF stage in both sexes.

7 THE EFFECT OF OVARIECTOMY ON INTRACELLULAR Ca^{2+} REGULATION IN GUINEA PIG CARDIOMYOCYTES

7.1 Aims

- To assess if long-term deprivation of ovarian hormones in the GP alters intracellular Ca^{2+} regulation in ventricular myocytes and leads to more arrhythmogenic events.
- To assess if oestrogen supplementation to ovariectomised GPs reverses any alterations to cardiac Ca^{2+} handling and rescues pro-arrhythmic behaviour.

7.2 Introduction

Clinical observations show that premenopausal women have lower incidence of sudden cardiac death compared with men which could be related to reduced risk of malignant ventricular arrhythmias and delayed onset of coronary artery disease. However, postmenopausal women seem to lose this protection[202,287,304-306]. The risk of cardiovascular disease (CVD) is lower in premenopausal women than in age-matched men with CVD developing about 10 years later in females compared with males[307], but the risk increases noticeably in women after menopause[158,179]. Further, in animal models long-term deficiency of oestrogen was associated with cardiac contractile dysfunction[308,309], reduced myofilament force and increased Ca^{2+} sensitivity[310]. Postmenopausal women are more vulnerable to arrhythmia-related sudden cardiac death compared with premenopausal women[180,181]. Notably, premenopausal women with ventricular premature beats that mostly originate from the right ventricle outflow tract (RVOT) show decreased premature beat frequency around ovulation when serum oestradiol is at its peak[182].

While these clinical findings suggest ovarian hormones may provide some cardiovascular protection and reduce the incidence of pro-arrhythmic events[175-178], large studies examining hormone replacement therapy (HRT) showed no cardiovascular benefit[192]. These conflicting results led to the testing of a hypothesis which suggests that the timing of HRT is important and women receiving such therapy early after the menopause benefit from reduced risk of serious cardiovascular events[193]. However, the association between serum oestrogen levels and arrhythmias appears complex. For example, in acquired LQTS, drug-induced QT prolongation is more pronounced and the risk for polymorphic ventricular tachycardia is greater when oestradiol serum levels peak during the oestrous cycle, suggesting a pro-arrhythmic role for oestradiol[199]. Therefore further investigation is required to clarify the effect of ovarian hormones on cardiac function and elucidate underlying mechanisms. Furthermore, ineffective Ca^{2+} regulation is potentially arrhythmogenic and so a

deficiency of oestrogen could provide a pro-arrhythmic substrate. Indeed, an increase in susceptibility to epinephrine-induced arrhythmias (for example, premature ventricular contractions) was noted in ovariectomised rats compared with gonad-intact animals[187]. A clinical investigation also revealed that postmenopausal women who have idiopathic outflow tract ventricular arrhythmia had lower serum oestradiol levels than control postmenopausal women, and the occurrence of ventricular arrhythmia events was lower in women with oestrogen replacement[183]. In this chapter we identified which Ca^{2+} regulatory mechanisms are affected and investigated if oestrogen supplementation to ovariectomised GPs reverses any alterations to cardiac Ca^{2+} handling and rescues pro-arrhythmic behaviour.

7.3 Methods

7.3.1 Ovariectomised animal model

The OVx operation procedure was detailed in section 2.1.2.

7.3.2 17β-oestradiol pellet implantation

Implantation of oestradiol was described in section 2.1.4.

7.3.2.1 Serum oestradiol level

Blood samples were collected in serum separator tubes (Becton Dickinson, UK) and incubated at RT for 2 h before centrifugation at 3000 rpm for 15 min at 4°C. The serum supernatant was transferred to low-binding protein Eppendorf tubes and stored at -80°C until assayed. Levels of serum oestradiol were measured by quantitative sandwich enzyme-linked immunosorbent assay (ELISA) according to the manufacturer's instructions (MyBioSource, San Diego, USA). All standards and serum samples were added in duplicate to the reaction plate. Optical Density (O.D.) at 450 nm was obtained by using a microplate reader. O.D. values of the duplicate samples were averaged. The mean O.D. value of the blank control was subtracted from all other O.D. values. A standard curve was fitted using the standard data in logistic (5-PL) curve-fit (Fig. 7-1). The oestradiol level of samples was obtained from the standard curve corresponding to the mean absorbance of the samples. Data was collected from samples run in once reaction microplate.

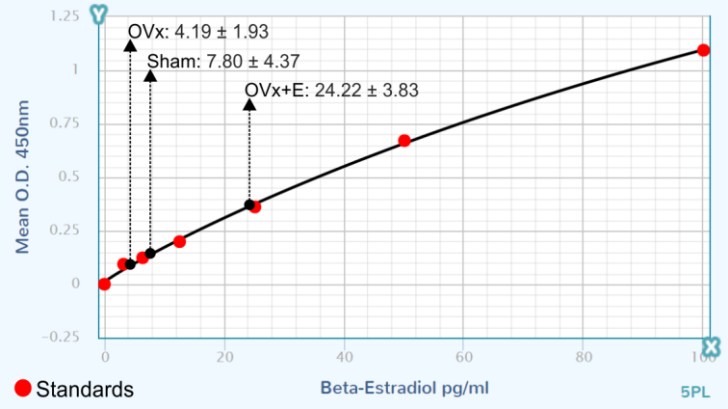

Figure 7-1. Standard curve of 17β-oestradiol against O.D. at 450 nm.

The oestradiol levels of samples from Sham, OVx and OVx+E were obtained from the standard curve corresponding to the mean absorbance of the samples accordingly.

7.3.3 Cardiac myocytes isolation and electrophysiological measurements

7.3.3.1 Cell isolation and electrophysiological measurements

Experiments were performed on single cardiac myocytes isolated from Sham, OVx, or OVx with oestradiol supplement (OVx+E) GPs according to the methods described in section 2.3.1. Techniques and protocols for electrophysiological and fluorescence measurements including action potential, $I_{Ca,L}$, SR Ca^{2+} content, Ca^{2+} transient, spontaneous Ca^{2+} sparks and waves were as detailed in section 2.4 and 2.5.

7.3.3.2 Voltage-dependent activation and steady-state inactivation of L-type Ca^{2+} channel

Voltage-dependent activation curves were constructed by plotting the value of the test voltage step against the corresponding normalised conductance (G/G_{max}). Conductance (G) was calculated by using the equation: $G = I/(V - V_{rev})$, where V is the test voltage step, I is the peak current at the test voltage and V_{rev} the reversal (or equilibrium) potential obtained by extrapolating the tail part of the I-V curve to its intersection with the voltage axis. Steady-state inactivation curves were constructed by plotting the current obtained from each test step (expressed as a percentage of maximal current (I/I_{max})) against the value of the initial activating voltage step. Voltage-dependent activation and steady-state inactivation curves were fitted with a Boltzmann equation ($y = 1/(1 + \exp[(x- V_{0.5})/ K])$). The probability of Ca^{2+} channels being open within the "window" range of voltages was calculated using the equation: $(1/\{1+\exp[(V_{0.5,\,activation}-V)/K_{activation}]\}x1)/(\{1+\exp[(V-V_{0.5,inactivation})/K_{inactivation}]\})$ described previously[311].

7.3.3.3 EADs and DADs induced by isoprenaline

To elicit early and delayed afterdepolarisations (EADs and DADs, respectively), cells were exposed to 50 nM isoprenaline (ISO) and paced at various frequencies (0.5, 1 and 2 Hz) for 30 s. The presence of EADs, appearing as transient repression of the repolarisation process and/or reversal of the membrane potential (reversal of *dV/dt*) during repolarisation, was confirmed by the reversal of the negative first derivative[312] of the membrane potential towards less negative or positive values, respectively. DADs were counted if their amplitudes were ≥ 5 mV.

7.3.3.4 mRNA expression of $Ca_v1.2$ and $Ca_v\beta2$

7.3.3.4.1 mRNA extraction

Total RNA from cells was extracted by using the RNeasy Mini Kit (Qiagen, UK) according to the manufacturer's instructions. Prior to RNA isolation, all surfaces were cleaned using Distel High Level Laboratory Disinfectant (Tristel Solutions Ltd, UK) to eliminate any potential RNase and DNA contaminants. The cell pellet suspended in the provided cell lysis buffer was homogenised using a sonicator before the extraction process. RNase-free water (40 µl) was used to elute the isolated RNA at the final stage of extraction. The concentration of isolated RNA was measured by using a NanoDrop™ 8000 Spectrophotometer (Thermo Fisher Scientific, MA, USA) before storing the RNA extraction in the -80 °C freezer.

7.3.3.4.2 Primer design

Primers were designed by using NCBI/Primer-Blast (http://www.ncbi.nlm.nih.gov/tools/primer-blast/). Target gene sequences were sourced from NCBI/Gene (https://www.ncbi.nlm.nih.gov/gene/). Designed primers (10 µM) were obtained from Invitrogen, UK. The primer sequences were as follows:

Target genes:

$Ca_v1.2$ (encoded by *CACNA1C*):

sense 5`-ACACTGCTGTGGACCTTCATC-3`,antisense 5`-TGCATACCAATCACGGCATA-3`.

$Ca_v\beta2$ (encoded by *CACNB2*):

sense 5`-CCAAGCCCAGTCAAACTAGAAAAC-3`, antisense 5`- CAAACTGGACGATGAATTTCCTCC-3`.

SERCA2a (encoded by *Atp2a2*):

sense 5`-GTAGCCAATGCAATTGTAGGTGT-3`,antisense 5`-GATACACTTTGCCCATTTCAGG-3`.

NCX1 (encoded by *Slc8a1*):

sense 5`-CTGGAAGTGATCATTGAGGAGTC-3`, antisense 5`-ACTGTTCTCTCCAGCTGTTGGTA-3`.

Housekeeping gene:

β-actin (encoded by *ACTB*):

sense 5`-ACTTTGCTGCGTTACACCCT-3`, antisense 5`-AATCAAAGTCCTCGGCCACA-3`.

7.3.3.4.3 qRT-PCR

Real-time RT-PCR was performed using the one-step QuantiTect SYBR Green PCR kit (Qiagen, UK) according to the manufacturer's instructions. RNA extraction was diluted to 3 ng/µl for assaying. A total 25 µl of reaction volume contained 30 ng of RNA and 0.5 µM of primer. Components in reaction were listed in Table 7-1. A 96-well reaction plate (Applied Biosystems) was used. Samples were added in duplicate to the reaction plate for data averaging. qRT-PCR cycles are detailed in Table 7-2. Cycle threshold (*C*t) values for target messenger RNA (mRNA) were normalised to the housekeeping gene coding β-actin (*ACTB*) and the relative gene expression in each sample was calculated using the $2^{-\Delta\Delta C_T}$ method[313].

Component	Volume (µl)	Final concentration
QuantiTect SYBR Green RT-PCR Master Mix	12.5	1 x
Primer (sense)	1.25	0.5 µM
Primer (anti-sense)	1.25	0.5 µM
QuantiTect reverse transcriptase Mix	0.25	-
RNA extraction	9.75	1.2 ng/µl
Total	25	-

Table 7-1. Components of RT-PCR reaction.

Step	Time	Temperature (°C)
Reverse transcription	30 min	50
PCR initial activation step	15 min	95
Denaturation	15 s	94
Annealing	30 s	60
Extension	30 s	72
Number of cycles	40	

Table 7-2. RT-PCR cycle.

7.3.4 Statistical analysis

Statistical methods were detailed in section 2.7. Kaplan-Meier estimates with Log Rank test was used to analyse Ca^{2+} wave-free survival interval.

7.4 Results

7.4.1 Physical characteristics of experimental animals

The serum oestrogen level decreased significantly in OVx GPs and increased when oestrogen was replaced (the OVx+E treatment group) (Table 7-3). Average body weight (BW) significantly increased by 10 % in the OVx group but the ratio of heart weight (HW) to body weight remained unchanged compared with Sham (Table 7-3). Both uterine weight and HW normalised to BW increased significantly in the OVx+E group (Table 7-3).

	n	BW (g)	UW (g)	HW (g)	UW/BW	HW/BW	Serum E2 (pg/mL)
Sham	9	784 ± 85	1.52 ± 0.47	2.38 ± 0.08	0.19 ± 0.05	0.31 ± 0.04	7.80 ± 4.37
OVx	10	870 ± 67*	0.37 ± 0.08***	2.66 ± 0.23***	0.04 ± 0.01***	0.31 ± 0.02	4.19 ± 1.93*
OVx+E	10	711 ± 57*	3.89 ± 0.60***	2.48 ± 0.13	0.55 ± 0.10***	0.35 ± 0.04*	24.22 ± 3.83***

Values expressed as means ± S.D.

n=number of animals; BW=Body weight, HW=Heart weight, UW=Uterine weight.

* p<0.05, ** p<0.01, and ***p<0.001 represent significant difference compared to Sham group.

Statistics calculated by one-way ANOVA with a Fisher post-hoc test.

Table 7-3. Physical characteristics of experimental animals.

7.4.2 *In vivo* M-mode echocardiography

OVx had 12 % larger LVIDd and 27 % larger LVIDs compared with Sham (Fig. 7-2. D & E). OVx+E had similar LVIDd but smaller LVIDs compared with OVx (Fig. 7-2. D & E). The FS decreased by 8 % in the OVx but remained unchanged in the OVx+E group compared with Sham (Fig. 7-2. F).

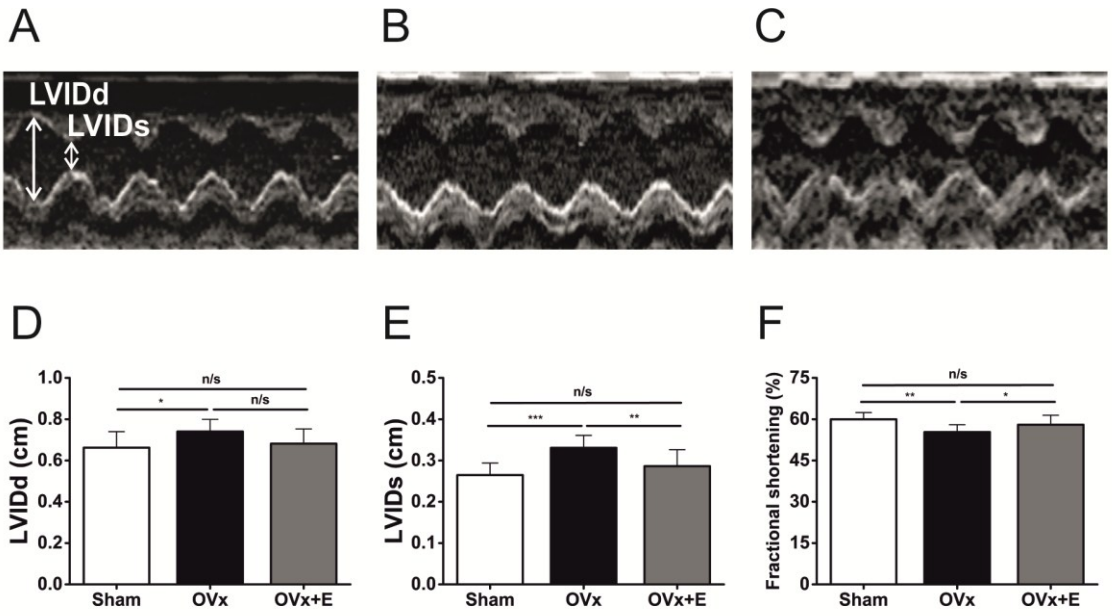

Figure 7-2. *In vivo* M-mode echocardiogram in Sham, OVx and OVx+E groups.

*Typical in vivo M-mode echocardiogram and LVIDd and LVIDs measurements from Sham (A), OVx (B) and OVx+E GPs (C). D, E & F: LVIDd and LVIDs were 12 % and 27 % larger in OVx animals in conjunction with an 8 % decrease in FS compared with Sham. LVIDd, LVIDs and FS were unaltered in OVx+E compared with Sham (Sham, n=9; OVx, n=10, OVx+E, n=10; n=GP numbers; one-way ANOVA with a Fisher post-hoc test, n/s: p>0.05, *p<0.05, **p<0.01, ***p<0.001).*

7.4.3 Ca^{2+} transient

7.4.3.1 Ca^{2+} transient amplitudes, time to peak, decay 50 % and 90 % time

Ca^{2+} transient amplitudes were 20 % larger in the OVx group than in Sham (Fig. 7-3. B). Myocytes isolated from the OVx+E group had similar Ca^{2+} transient amplitudes compared with myocytes isolated from the Sham group (Fig. 7-3. B). The time to peak (TTP) of the Ca^{2+} transients remained unchanged between Sham, OVx and OVx+E groups (Fig. 7-4. A). OVx+E had 20 % and 24 % longer 50 % decay time (R_{50}) than Sham and OVx groups, respectively (Fig. 7-4. B). OVx+E also had 17 % and 28 % longer 90 % decay time (R_{90}) than Sham and OVx groups respectively (Fig. 7-4. C). OVx had 9 % shorter R_{90} than Sham (Fig. 7-4. C).

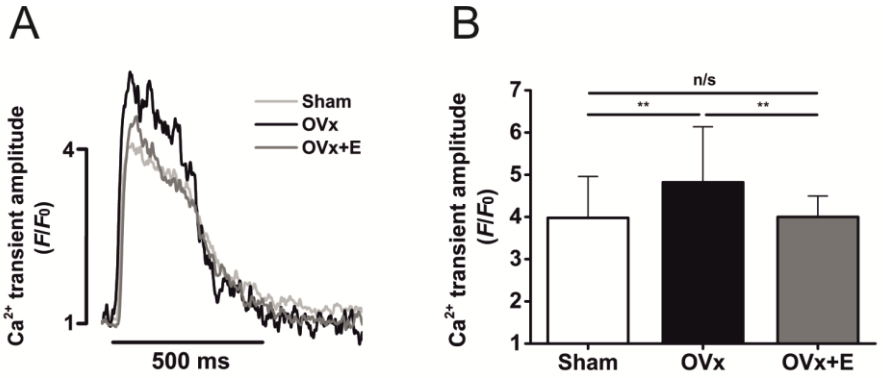

Figure 7-3. Ca^{2+} transients in Sham, OVx and OVx+E groups.

*A: Typical Ca^{2+} transients in Sham, OVx and OVx+E group. B: OVx had larger Ca^{2+} transient amplitude than Sham and OVx+E. Sham and OVx+E had similar Ca^{2+} transient amplitudes (Sham, n=44/4; OVx, n=55/4; OVx+E, n=40/3; one-way ANOVA with a Fisher post-hoc test, n/s: p>0.05, **p<0.01).*

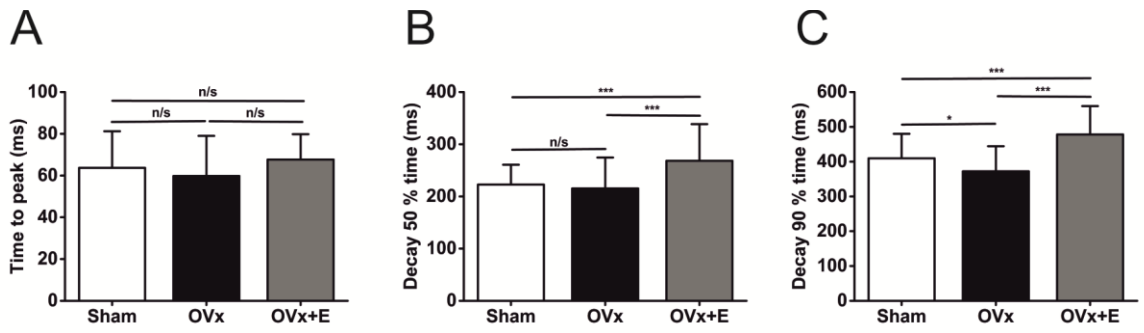

Figure 7-4. Ca^{2+} transient TTP, R_{50} and R_{90} in Sham, OVx and OVx+E groups.

*A: Ca^{2+} transient TTP was unaltered between Sham, OVx and OVx+E. B &C: OVx+E had longer R_{50} and R_{90} compared with Sham and OVx. C: OVx had shorter R_{90} compared with Sham amplitudes (Sham, n=44/4; OVx, n=55/4; OVx+E, n=40/3; one-way ANOVA with a Fisher post-hoc test, n/s: p>0.05, *p<0.05, ***p<0.001).*

7.4.3.2 Ca^{2+} transient decay rate constant

Cells isolated from OVx GPs had 7 % and 11 % faster Ca^{2+} transient decay rate constants compared with Sham and OVx+E, respectively (Fig. 7-5). Cells from Sham and OVx+E had similar decay rate constants. The rate constant of SERCA and the corresponding percentage contribution to relaxation made by the protein remained unchanged between Sham, OVx and OVx+E cells (Fig. 7-6. A & B). Compared with Sham, OVx had a 20 % greater rate constant of NCX and the corresponding percentage contribution to relaxation of NCX was increased by 65 % (Fig. 7-6. C & D). Compared with OVx+E, OVx had faster rate constant of NCX by 27 % and increased relaxation contribution from NCX by 64 % (Fig. 7-6. C & D). The rate constant of the other slower components, including PMCA and mitochondria uniporter, and their corresponding contribution to relaxation showed no difference between Sham, OVx and OVx+E (Fig. 7-6. E & F).

OVx had 13 % higher fractional SR Ca^{2+} release compared with Sham (Fig. 7-7). OVx had 37 % reduced relative mRNA expression of SERCA2a compared with Sham which was partially restored by 30 % in OVx+E. The relative mRNA expression of NCX remained unaltered between Sham, OVx and OVx+E (Fig. 7-8).

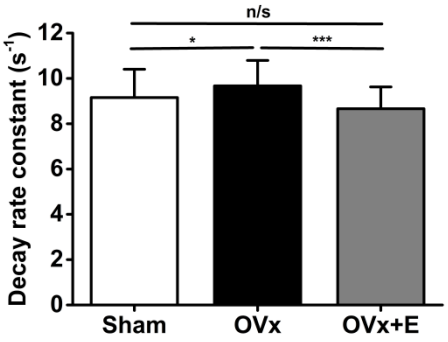

Figure 7-5. Ca^{2+} transient decay rate constant in Sham, OVx and OVx+E groups.

*OVx group had 7 % and 11 % quicker decay rate constant compared with Sham and OVx+E groups, respectively (Sham, n=56/3; OVx, n=38/3; OVx+E, n=33/3; one-way ANOVA with a Fisher post-hoc test, n/s: p>0.05, *p<0.05, ***p<0.001).*

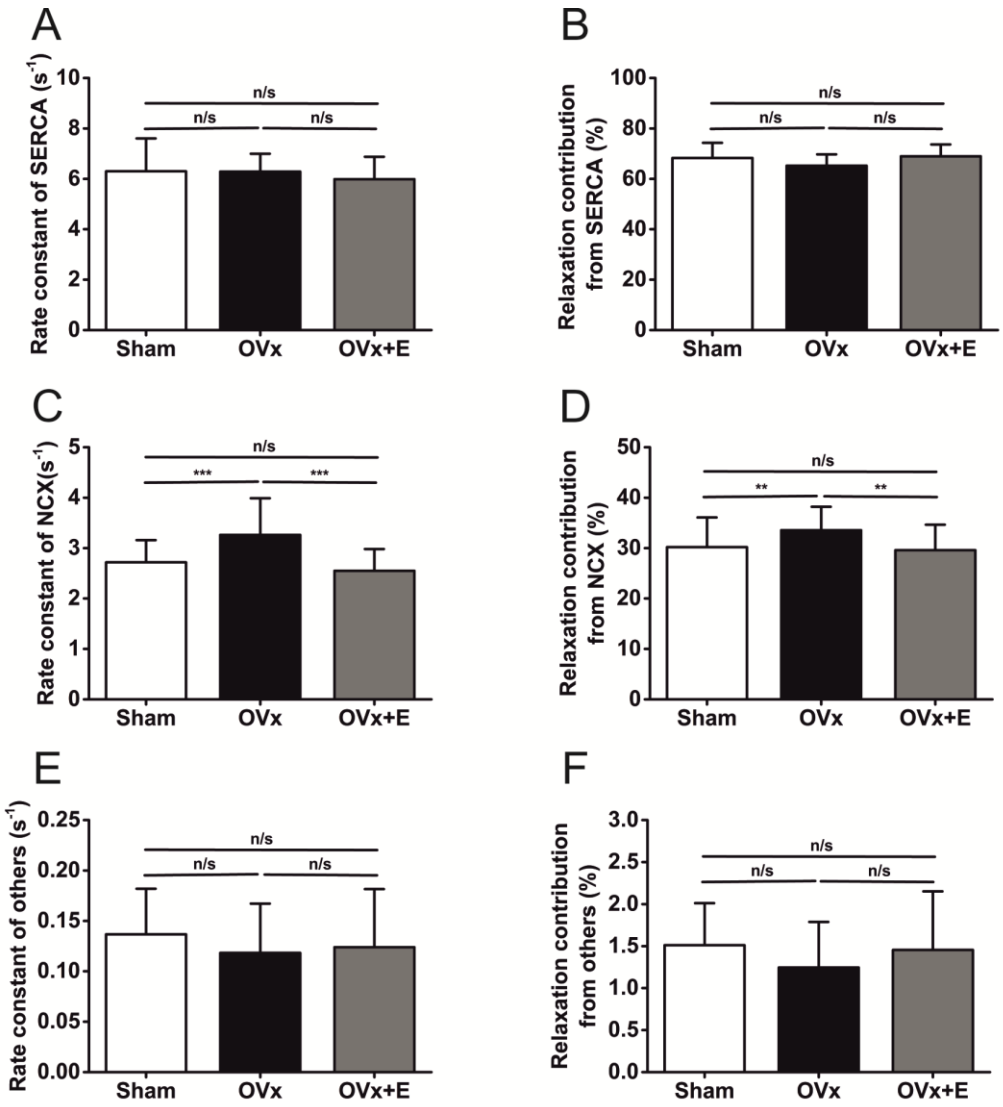

Figure 7-6. Rate constant and relaxation distribution of SERCA, NCX and other slower transporters in Sham, OVx and OVx+E groups.

*A, B, E & F: The rate constants of SERCA and other slower components and their corresponding contributions to relaxation remained unchanged between Sham, OVx and OVx+E groups. C & D: OVx had 20 % and 27 % greater rate constant of NCX and 65 % and 64 % increased relaxation contribution from NCX compared with those in Sham and OVx+E groups, respectively (Sham, n=56/3; OVx, n=38/3; OVx+E, n=33/3; one-way ANOVA with a Fisher post-hoc test, n/s: p>0.05, **p<0.01, ***p<0.001).*

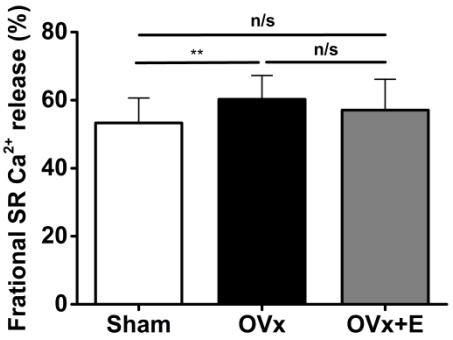

Figure 7-7. Fractional SR Ca^{2+} release in Sham, OVx and OVx+E groups.

*OVx had 13 % higher fractional SR Ca^{2+} release compared with Sham although there was no difference compared with OVx+E (Sham, n=34/4, OVx, n=48/4; OVx+E, n=40/3; one-way ANOVA with a Fisher post-hoc test, n/s: p>0.05, **p<0.01).*

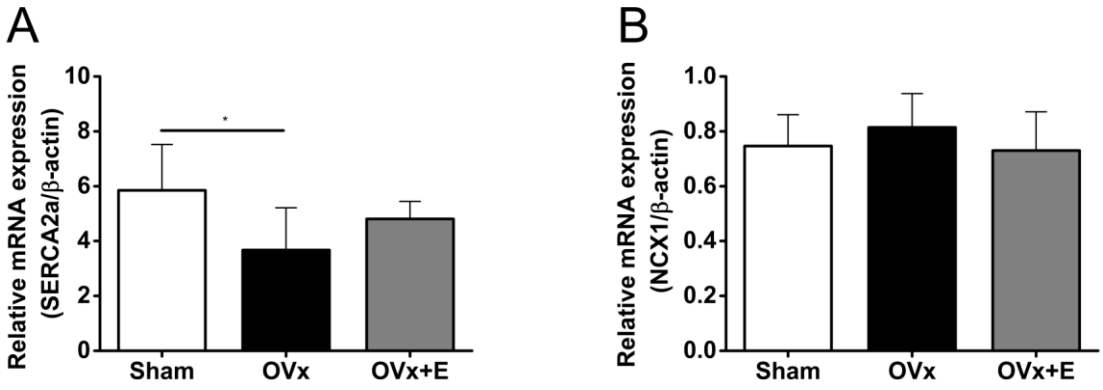

Figure 7-8. Relative mRNA expression of SERCA2a and NCX1 in Sham, OVx and OVx+E.

*OVx had 37 % reduced relative mRNA expression of SERCA2a compared with Sham which was partially restored by 30 % in OVx+E. The relative mRNA expression of NCX remained unaltered between Sham, OVx and OVx +E (Sham, n=6; OVx, n=6; OVx+E, n=6; n=GP numbers; one-way ANOVA with a Fisher post-hoc test, *p<0.05).*

7.4.4 Cell capacitance

There was no difference in cell capacitances between Sham, OVx and OVx+E groups (Sham=173.2 ± 41.9, OVx=169.5 ± 48.9, OVx+E=182.4 ± 43.1 pF, p>0.05; Sham, n=125; OVx, n=81; OVx+E, n=70; one-way ANOVA with a Fisher post-hoc test).

7.4.5 SR Ca^{2+} content

The SR Ca^{2+} content, obtained by integrating the caffeine-evoked inward NCX current (Fig. 7-9. A), was on average 20 % greater in the OVx group compared with the Sham group (Fig. 7-9. B). SR Ca^{2+} content was unaltered between cells isolated from Sham and OVx+E groups (Fig. 7-9. B).

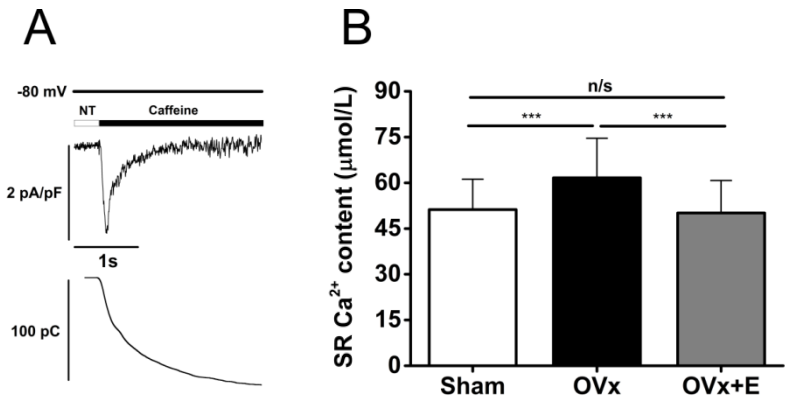

Figure 7-9. SR Ca^{2+} content in Sham, OVx and OVx+E groups.

*A: Typical trace of caffeine-induced NCX inward current and the current integrating trace to measure SR Ca^{2+} content. B: SR Ca^{2+} content was significantly higher in OVx myocytes compared with Sham and OVx+E myocytes (Sham, n=33/3; OVx, n=34/3; OVx+E, n=33/5; one-way ANOVA with a Fisher post-hoc test, n/s: p>0.05, ***p<0.001).*

7.4.6 Ca^{2+} sparks and waves

Since SR Ca^{2+} content was greater in the OVx group, we examined Ca^{2+} spark frequencies to assess if there were any changes in spontaneous Ca^{2+} release. In addition, we assessed if these cells had an increased tendency to produce Ca^{2+} waves or more Ca^{2+} sparks when provoked by an exposure of 0.5 µM isoprenaline (ISO challenge). Spark frequencies were higher in the OVx group compared with Sham (Fig. 7-10. B). In the presence of 0.5 µM ISO, myocytes showed more sparks, and the frequencies at which they occurred remained higher in cells from the OVx group (Fig. 7-10. B).

Spark amplitudes and mass were also larger in OVx myocytes with or without ISO (Fig. 7-11). In conjunction with Ca^{2+} sparks, wave frequencies were higher in the OVx group compared with Sham (Fig. 7-12. B). In the presence of 0.5 µM ISO, myocytes showed more waves and the frequencies at which they occurred remained higher in the OVx group (Fig. 7-12. B). Spark and wave frequencies significantly decreased in myocytes from animals supplemented with oestrogen compared with the OVx group, and wave-free survival times were longer in Sham and OVx+E in the absence or presence of ISO compared with OVx (Fig. 7-12. C & D).

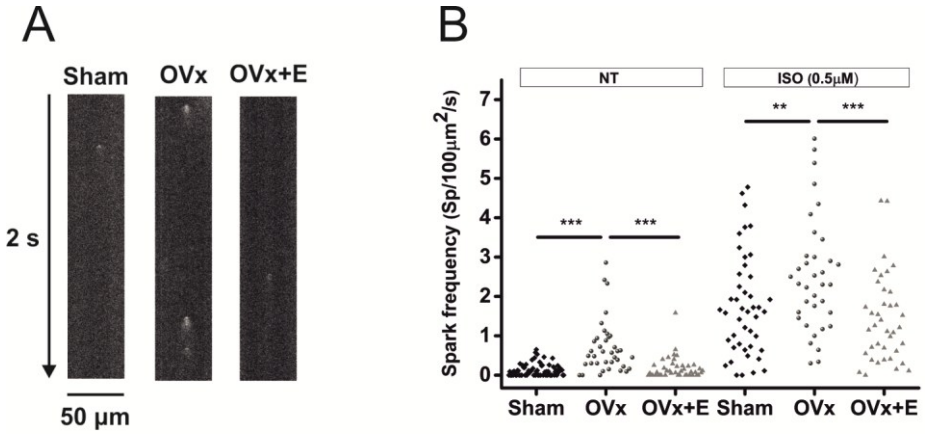

Figure 7-10. Spontaneous Ca^{2+}spark frequency with or without ISO challenge in Sham, OVx and OVx+E groups.

*A: The detection of Ca2+ sparks in Sham, OVx and OVx+E Fluo-4 loaded-myocytes using confocal line-scanning microscope to detect Ca^{2+} sparks in a Sham, OVx and OVx+E myocyte. B: Spark frequency was higher in OVx compared with Sham and OVx+E in the presence and absence of ISO (Sham, n=55/5; OVx, n=36/3, OVx+E, n=40/4; one-way ANOVA with a Fisher post-hoc test, **p<0.01, ***p<0.001).*

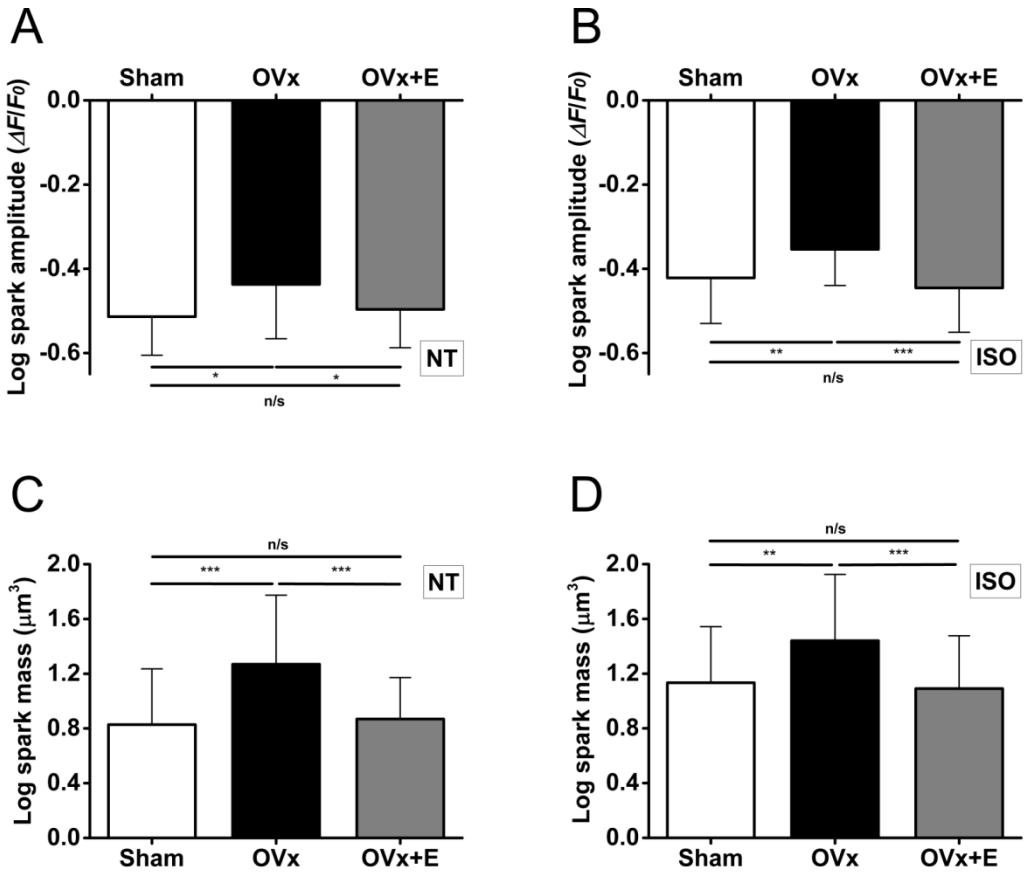

Figure 7-11. Ca^{2+} spark amplitudes and mass with or without the presence of ISO in Sham, OVx and OVx+E groups.

*A & B: Spark amplitudes were larger in OVx than in Sham and OVx+E with and without the presence of ISO. C & D: OVx myocytes had a larger spark mass compared with Sham and OVx+E with and without ISO treatment (Sham, n=55/5; OVx, n=36/3, OVx+E, n=40/4; one-way ANOVA with a Fisher post-hoc test, n/s: p>0.05, *p<0.05, **p<0.01, ***p<0.001).*

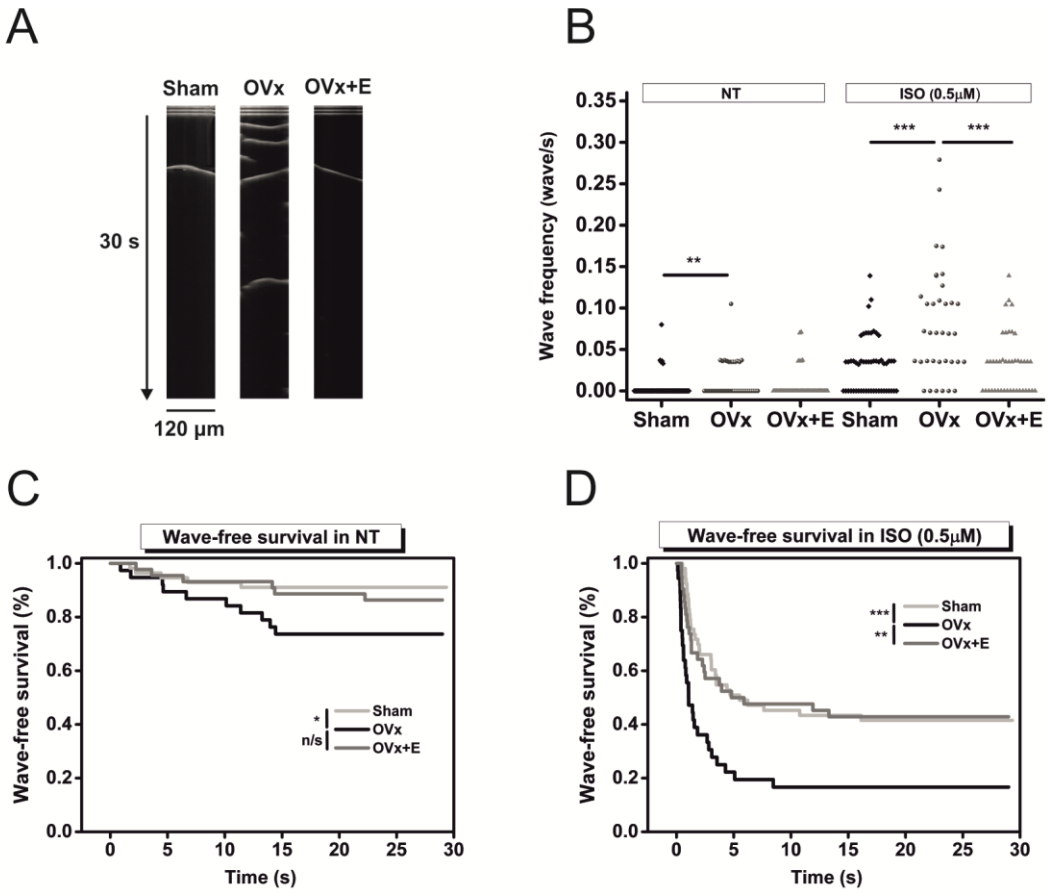

Figure 7-12. Ca^{2+} wave frequency and wave-free survival in Sham, OVx and OVx+E.

*A: Typical traces of Ca^{2+} waves recorded in Sham, OVx and OVx+E myocytes. B: Wave frequency was higher in OVx compared to Sham and OVx+E with and without the presence of ISO. C & D: Wave-free survival was longer in Sham compared with OVx myocytes in NT and following ISO challenge. Wave-free survival was significantly longer in OVx+E compared with OVx myocytes only in the presence of ISO (Sham, n=61/5; OVx=38/3; OVx+E=40/4; one-way ANOVA with a Fisher post-hoc test, n/s: p>0.05, *p<0.05, ***p<0.001).*

7.4.7 L-type Ca^{2+} channel

7.4.7.1 $I_{Ca,L}$ amplitude and gating

This assessment of Ca^{2+} regulation indicated that there were changes in intracellular Ca^{2+} handling following long-term absence of oestrogen. It was therefore necessary to measure L-type Ca^{2+} current to assess if changes in Ca^{2+} influx occurred following OVx. The peak $I_{Ca,L}$ was 16 % larger in OVx compared with Sham and OVx+E (Fig. 7-13. B), and the amount of Ca^{2+} influx calculated during the 200 ms activating clamp step was also 33 % larger in OVx myocytes compared with Sham and OVx+E myocytes (Fig. 7-13. D).

The steady-state inactivation of the L-type Ca^{2+} current shifted to more positive potentials in OVx myocytes ($V_{1/2,\ inactivation}$ shift: 3.0 mV, $P<0.001$) (Fig. 7-14. A). Channel gating, determined by the L-type Ca^{2+} current inactivation shift, was unaltered in OVx+E compared with Sham myocytes (Fig. 7-14. A & B). In Sham myocytes, the peak probability of Ca^{2+} channel being open was 0.07 ± 0.05 at -15 mV while in OVx cells, this reached 0.15 ± 0.05 at -10 mV, and subsequently decreased in the OVx+E group to 0.06 ± 0.02 at -10 mV (Fig. 7-14. C).

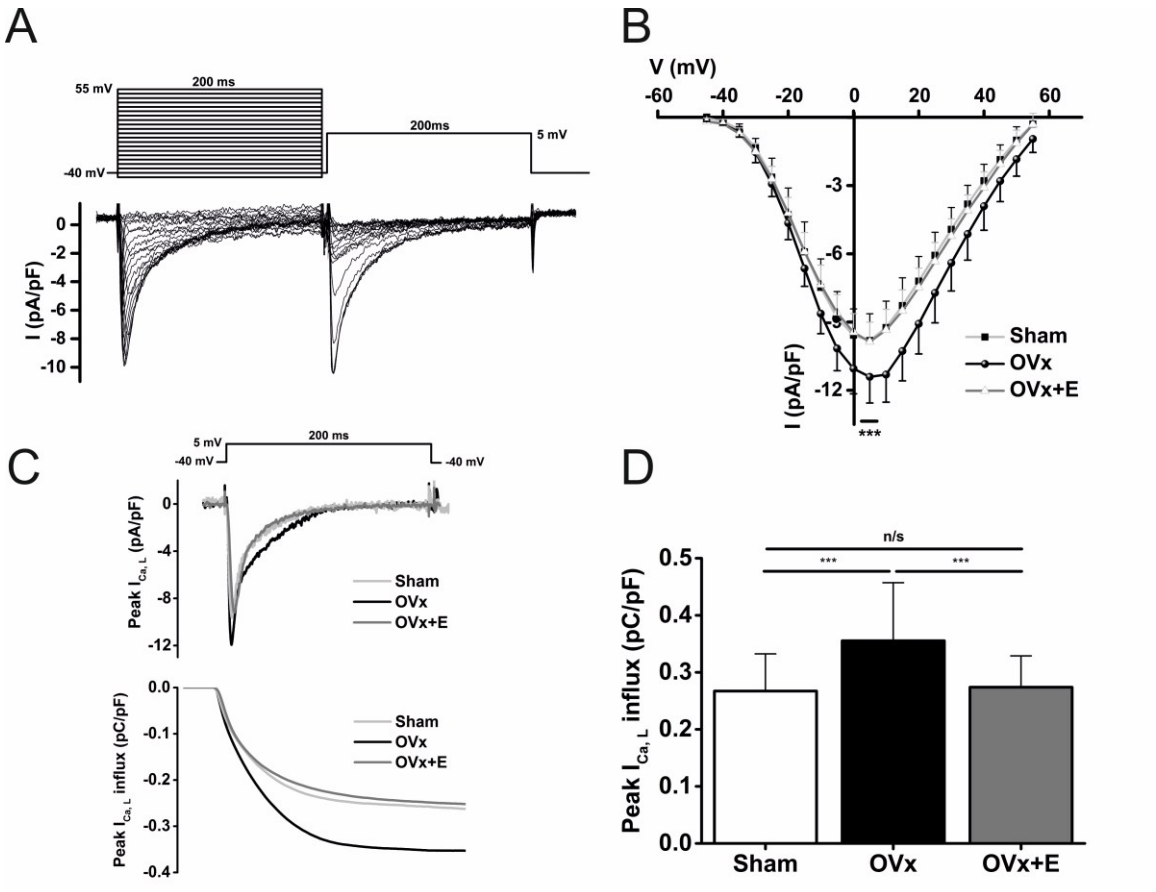

Figure 7-13. $I_{Ca,L}$ I-V relationship and Ca^{2+} influx of peak $I_{Ca,L}$.

*A: Typical traces of $I_{Ca,L}$ (cadmium-sensitive currents) and the corresponding voltage steps. B: I-V relationship of L-type Ca^{2+} channel of Sham, OVx and OVx+E myocytes. Maximum peak $I_{Ca,L}$ at 5 mV was larger in OVx myocytes compared with Sham and OVx+E. C: Representative figures of peak $I_{Ca,L}$ (top) and Ca^{2+} influx (bottom) in Sham, OVx and OVx+E myocytes. D: Ca^{2+} influx was larger in OVx myocytes compared with Sham and OVx+E myocytes (Sham, n=40/5; OVx, n=44/5; OVx+E, n=37/7; one-way ANOVA with a Fisher post-hoc test, n/s: p<0.05, ***p<0.001).*

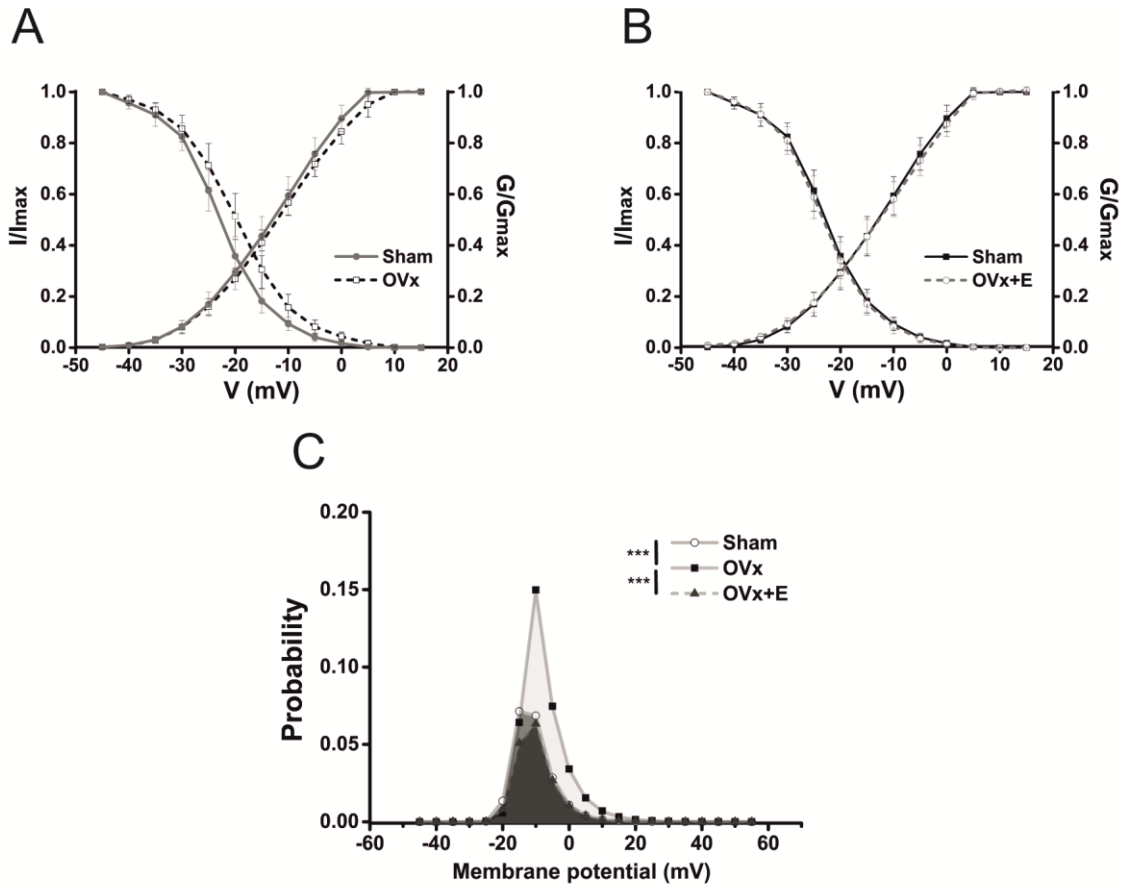

Figure 7-14. Activation and inactivation curve of L-type Ca^{2+} channel and the calculated window current from Sham, OVx and OVx+E myocytes.

*A & B: L-type Ca^{2+} channel gating shifted to more positive E_m in OVx myocytes compared with Sham ($V_{1/2,\ inactivation}$ shift: 3.0 mV, P<0.001). Channel gating was unaltered in OVx+E compared with Sham myocytes. C: The probability of having channel open within the "window" range of voltages in Sham myocytes peaked at -15 mV with a mean peak probability value of 0.07 ± 0.05, but the probability increased to 0.15 ± 0.05 at -10 mV in OVx cells (p<0.001). In OVx+E cells the mean peak probability value was 0.06 ± 0.02 at -10 mV that was similar to Sham (Sham, n=40/5; OVx, n=46/6, OVx+E, n=37/7; one-way ANOVA with a Fisher post-hoc test, ***p<0.001).*

7.4.7.1 Effect of H-89 on L-type Ca^{2+} channel current and gating

In the presence of 5 µM H-89, a PKA inhibitor, peak $I_{Ca,L}$ was reduced by 63 % and 59 % with peak values at -3.7 ± 0.8 and -4.8 ± 1.3 pA/pF (Student's *t*-test, p<0.01) in Sham and OVx groups, respectively (Fig. 7-15 A & B). Peak $I_{Ca,L}$ decreased by 65 % at peak value of -3.4 ± 0.6 pA/pF in OVx+E group in the presence of H-89 (Fig. 7-15. C). OVx still had greater peak $I_{Ca,L}$ in the presence of H-89 compared with Sham and OVx+E (Student's *t*-test, p<0.01 and p<0.001, respectively).

Following the addition of 5 µM H-89, in OVx myocytes the gating of L-type Ca^{2+} channel shifted toward more negative E_m ($V_{1/2,\ inactivation}$ shift: 3.9 mV, *P*<0.001) (Fig. 7-16. A). The channel gating again shifted to more negative E_m in Sham and OVx+E myocytes with H-89 treatment ($V_{1/2,\ inactivation}$ shift, Sham=1.7 mV, p<0.01; OVx+E=2.8 mV, p<0.001) (Fig. 7-16. B & C).

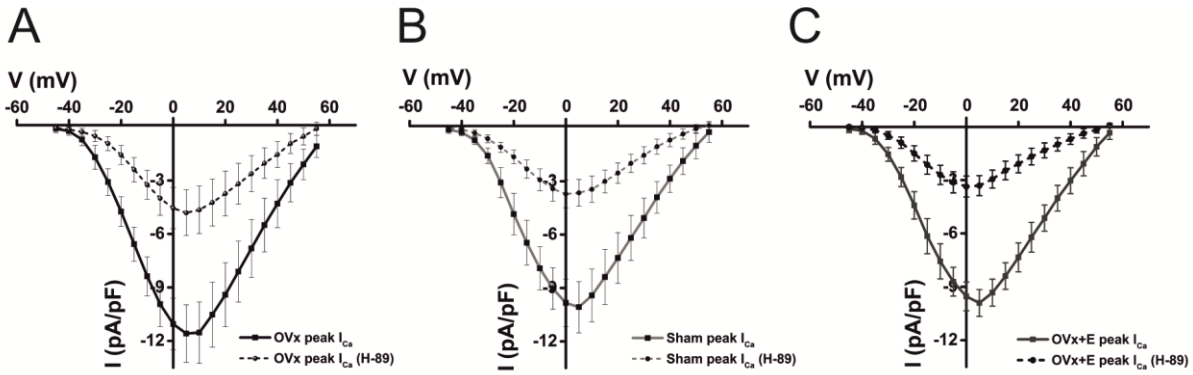

Figure 7-15. The effect of H-89 on maximum peak $I_{Ca,L}$ in Sham, OVx and OVx+E groups.

A & B: Maximum peak $I_{Ca,L}$ at 5 mV was reduced by 63 % and 59 % with peak values at -3.7 ± 0.8 and -4.8 ± 1.3 pA/pF with 5 µM H-89 treatment in Sham and OVx groups, respectively. C: OVx+E showed a decrease in peak $I_{Ca,L}$ decreased by 65 % with peak value at -3.4 ± 0.6 pA/pF in the presence of H-89. OVx still had larger peak $I_{Ca,L}$ in the presence of H-89 compared with Sham and OVx+E (Student's t-test, p<0.01 and p<0.001, respectively) (Sham, n=16/3; OVx, n=21/4; OVx+E, n=14/3).

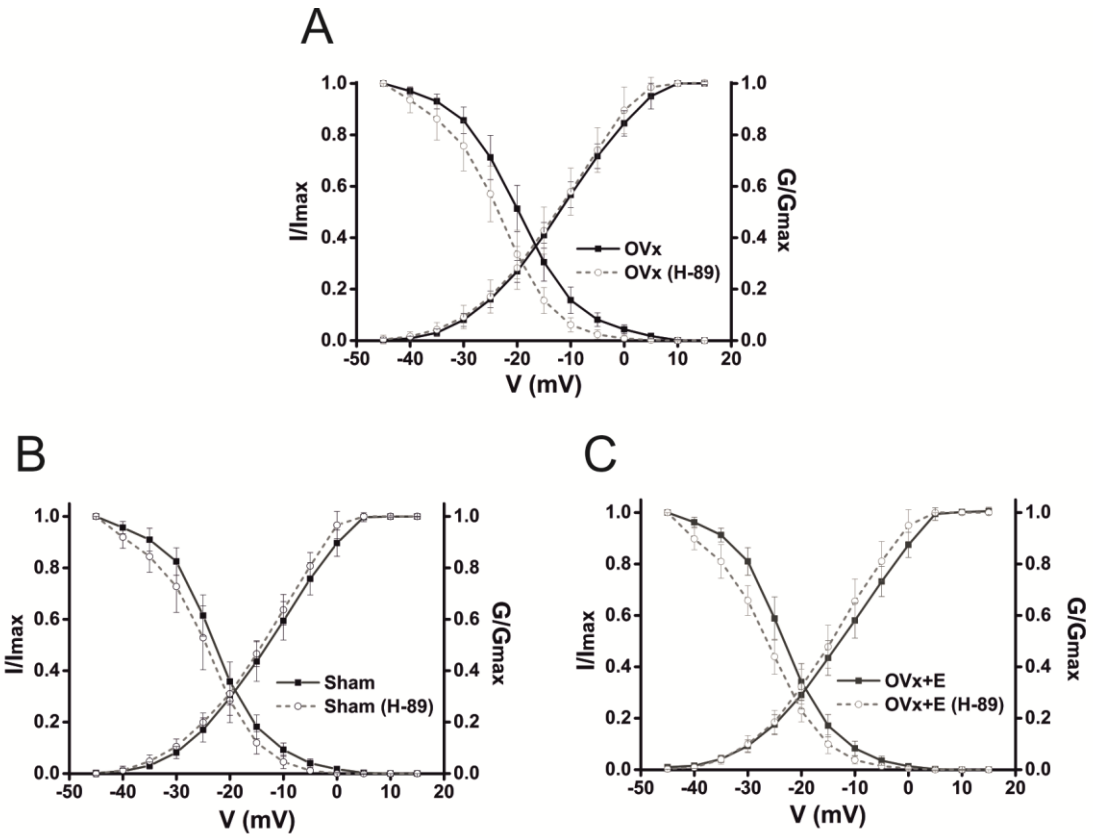

Figure 7-16. The effect of H-89 on the gating of L-type Ca^{2+} in Sham, OVx and OVx+E groups.

A: In OVx myocytes, the gating of L-type Ca^{2+} channel shifted toward more negative E_m following the addition of 5 µM H-89 ($V_{1/2,\ inactivation}$ shift: 3.9 mV in OVx, P<0.001; 1.7 mV in Sham, p<0.01; 2.8 mV in OVx+E, p<0.001; Student's t-test) (Sham, n=15/3; OVx, n=15/4, OVx+E, n=14/3).

7.4.7.2 L-type Ca^{2+} channel α_{1c} and β_2 subunit relative mRNA expression

A qRT-PCR was performed to measure relative mRNA expression levels of key subunits of the L-type Ca^{2+} channel to determine whether augmented OVx $I_{Ca,L}$ was a consequence of altered gene expression of α_{1c} or β_2 subunits. The relative mRNA expression of these subunits was unaltered between Sham, OVx and OVx+E groups (Fig. 7-17).

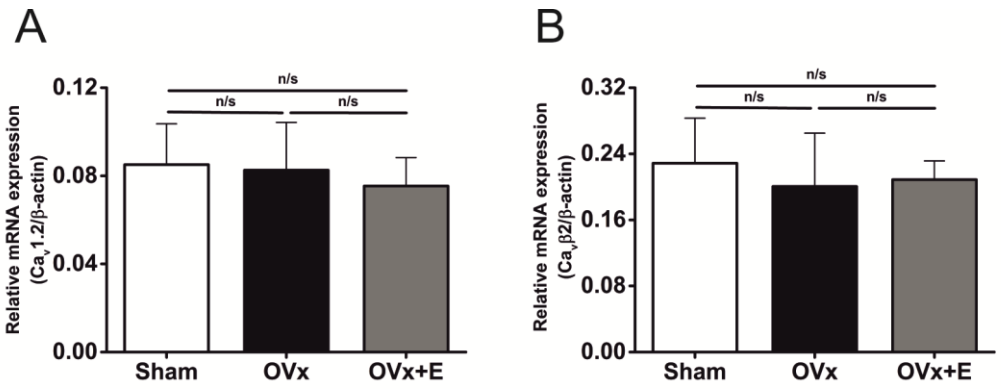

Figure 7-17. Quantifying the relative $Ca_v1.2$ and $Ca_v\beta2$ mRNA expression following OVx.

A: Relative $Ca_v1.2$ mRNA expression (normalised to β-action mRNA) was unaltered between Sham, OVx an OVx+E myocytes. B: The relative $Ca_v\beta2$ mRNA expression (normalised to β-actin mRNA) did not change following OVx and OVx+E compared with Sham (Sham, n=7; OVx, n=7; OVx+E, n=6; n=GP numbers; one-way ANOVA with a Fisher post-hoc test, n/s: p>0.05).

7.4.8 EADs and DADs induced by ISO

The rightward shift in Ca^{2+} current inactivation, increasing the window current, may favour more inward current flow that could encourage the generation of arrhythmic events following OVx. To assess pro-arrhythmic susceptibility following long-term deprivation of oestrogen, the frequency of EADs or DADs following an ISO challenge was determined. Firstly, we measured action potentials in cells isolated from each group (Fig. 7-18. A). APD_{90} remained unchanged between Sham, OVx and OVx+E groups (Fig. 7-18. B), however APD_{10} was 1.3 times longer in cells isolated from the OVx group compared with Sham and OVx+E groups (Fig. 7-18. C). This may indicate more inward current flow early in the action potential supporting the Ca^{2+} current measurements.

EADs or DADs were elicited by pacing cells at 0.5, 1 or 2 Hz frequency for 30 s in the presence of 50 nM ISO (Fig. 7-19). Myocytes from the OVx group showed 68 % and 38 % higher frequency of EADs compared with Sham and OVx+E, respectively (Fig. 7-10. A) and, in addition, a higher percentage of OVx cells showed DADs when stimulated at 0.5 and 1 Hz compared with Sham and OVx+E (Fig. 7-20. B & C). OVx myocytes also had higher percentage of cells showing DAD-induced triggered extra beats during 0.5 Hz and 1 Hz stimulation compared with Sham and OVx+E cells (Fig. 7-20. D & E)

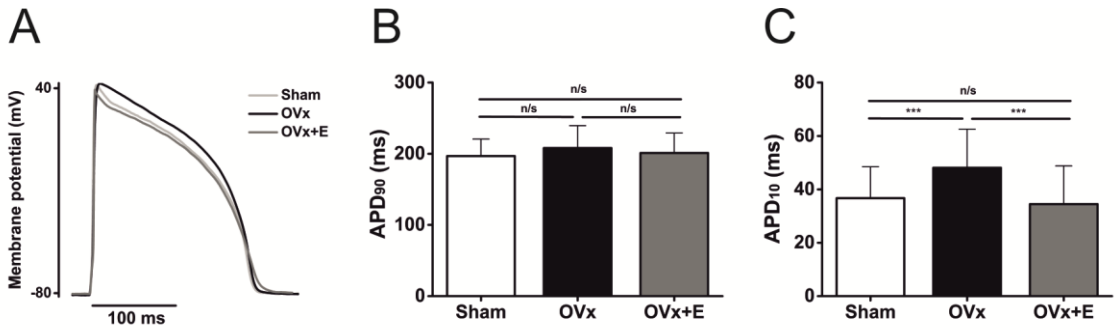

Figure 7-18. Assessing the long-term absence of oestrogen on APD.

*A: Representative figures of cardiac action potentials from ventricular myocytes. B: APD_{90} remained unchanged between Sham, OVx and OVx+E. C: APD_{10} was longer in OVx compared to Sham and OVx+E, however no differences in APD_{10} were observed between Sham and OVx+E (Sham, n=43/7; OVx, n=44/7; OVx+E, n=51/6; one-way ANOVA with a Fisher post-hoc test, n/s: p>0.05, ***p<0.001).*

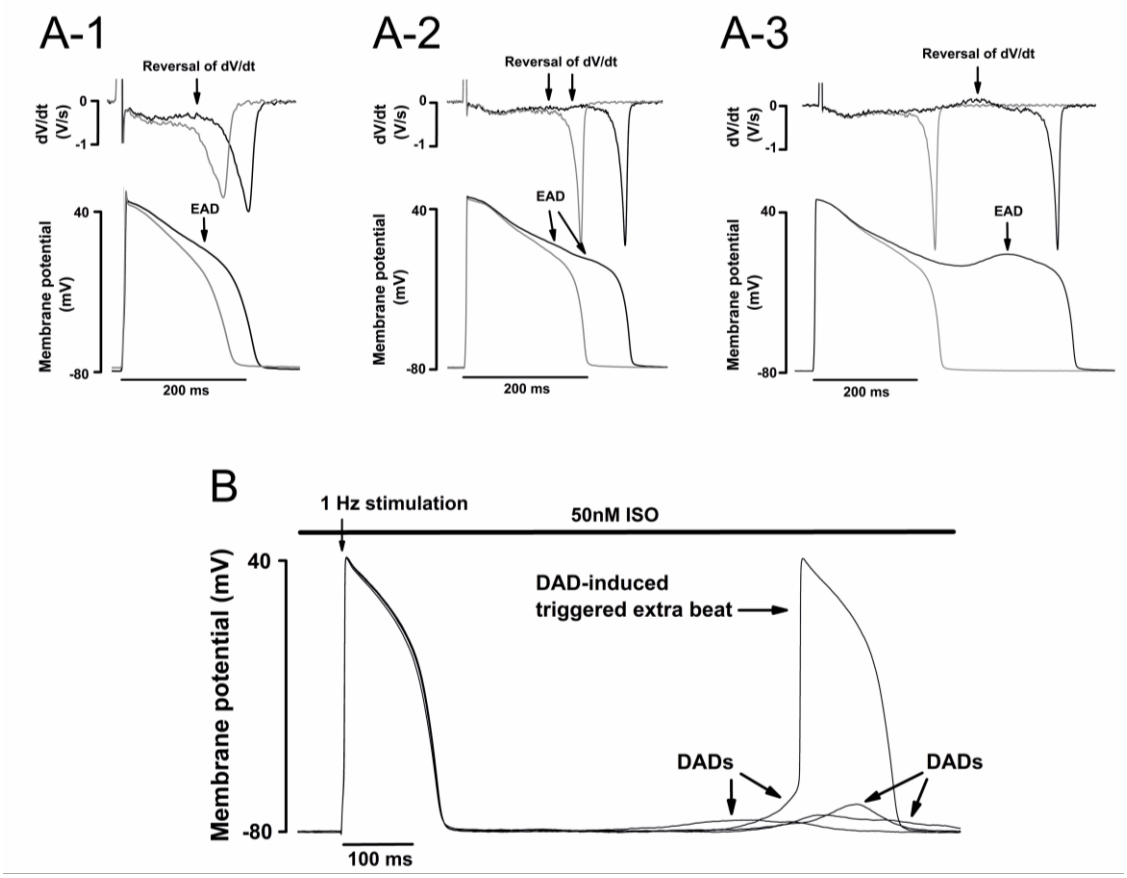

Figure 7-19. Representative quantification of EADs and DADs following ISO challenge.

A1-3: Typical traces of EAD formation in action potentials with short (A1), normal (A2) and long duration (A3) and the corresponding first derivative (dV/dt) traces from OVx myocytes at 2 Hz stimulation in 50 nM ISO. B: DAD formation and DAD-induced triggered extrasystole representations from a OVx myocyte following 1 Hz stimulation in 50 nM ISO.

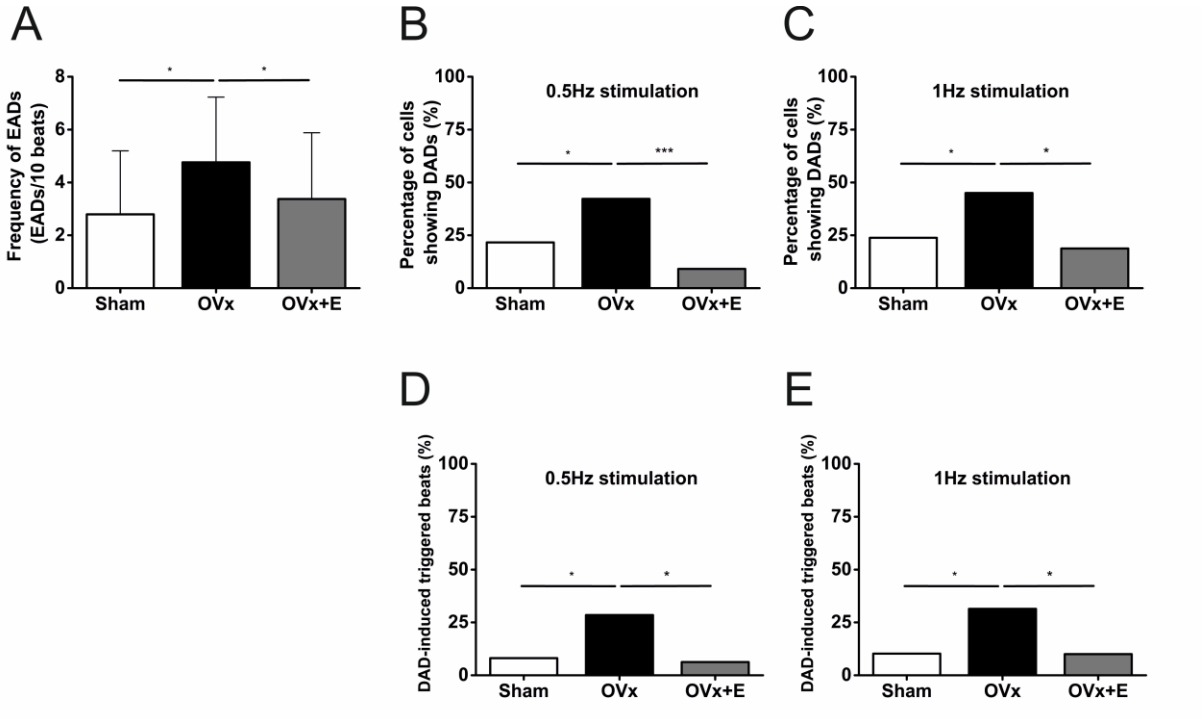

Figure 7-20. Assessing putative arrhythmogenic events following long-term absence of oestrogen.

*A: OVx myocytes had higher frequency of EADs per 10 beats compared to Sham and OVx+E myocytes following 50 nM ISO challenge at 2 Hz stimulation (Sham, n=39/5; OVx, n=30/4; OVx+E=30/5; one-way ANOVA with a Fisher post-hoc test, *p<0.05). B: A higher percentage of cells were observed with DADs from OVx when treated with 50 nM ISO at 0.5 Hz stimulation compared to Sham and OVx+E (Sham, n=37/5; OVx, n=45/4; OVx+E=33/5; one-way ANOVA with a Fisher post-hoc test, *p<0.05, ***p<0.001). C: At 1 Hz stimulation, the percentage of myocytes showing DADs remained higher from OVx compared to Sham and OVx+E groups (Sham, n=42/5; OVx, n=40/4; OVx+E=32/5; one-way ANOVA with a Fisher post-hoc test, *p<0.05). D & E: OVx myocytes showed higher percentage of cells showing DAD-induced triggered extrasystoles at both 0.5 Hz and 1 Hz stimulation compared with Sham and OVx+E (At 0.5 Hz, Sham, n=37/5; OVx, n=45/4; OVx+E=33/5; one-way ANOVA with a Fisher post-hoc test, *p<0.05) (At 1 Hz, Sham, n=42/5; OVx, n=40/4; OVx+E=32/5; one-way ANOVA with a Fisher post-hoc test, *p<0.05).*

7.5 Discussion

This chapter addressed the hypothesis that long-term deficiency of ovarian hormones alters intracellular Ca^{2+} regulation in a way that may predispose cardiac myocytes to more potentially arrhythmogenic events. Alongside testing this central hypothesis, we assessed whether 17β-oestradiol supplementation could reverse any changes to intracellular Ca^{2+} handling, thus preventing pro-arrhythmic behaviour. L-type Ca^{2+} current was measured to determine if it could be responsible for the increases in cellular Ca^{2+} content. We found the peak $I_{Ca,L}$ and the corresponding Ca^{2+} influx were larger in OVx myocytes. Furthermore, we observed that current inactivation shifted to more positive voltages and the probability of Ca^{2+} channels being open within the "window" voltage range was greater in OVx myocytes. Both parameters favour the generation of arrhythmic events[314,315]. Following ISO challenge, OVx myocytes had higher frequencies of EADs and a greater percentage of these showed DADs. Significantly fewer pro-arrhythmic events were observed in myocytes isolated from OVx GPs with 17β-oestradiol supplementation.

7.5.1 Ca^{2+} transient and SR Ca^{2+} load

OVx myocytes had greater SR Ca^{2+} content and larger Ca^{2+} transient amplitudes supporting a previous report[186]. We also found OVx myocytes had larger peak $I_{Ca,L}$ and corresponding Ca^{2+} influx. We suggest the greater SR Ca^{2+} content may result from the loading effect of the larger Ca^{2+} influx. Not only is the size of SR Ca^{2+} release proportional to the size of the Ca^{2+} current[68], but also increased Ca^{2+} influx loads the SR with more Ca^{2+} that augments subsequent fractional SR Ca^{2+} release[80,316]. The Ca^{2+} transient decay rate constant was significantly greater in OVx compared with Sham and OVx+E. While the rate constant of SERCA remained unchanged between Sham, OVx and OVx+E, the rate constant of NCX significantly increased in OVx compared Sham and OVx+E, leading to a faster Ca^{2+} transient decay in the OVx group. The rate constant representing SERCA function remained unaltered following OVx implying unchanged Ca^{2+} uptake into the SR. The mRNA expression of SERCA was reduced in OVx and was partially restored in OVx+E. While the findings was in line with other report[185], the expression and regulation of SERCA seems to vary among studies[184,317,318].

The up-regulated forward-mode NCX may help to facilitate Ca^{2+} efflux from the cell in response to increased Ca^{2+} influx after OVx. However this could potentially depolarise the membrane potential and causes arrhythmic events such as EADs[312]. The mRNA expression of NCX remained unchanged in our OVx group. However, up-regulated NCX function was also found in an ovariectomised rat model, which was reported to be associated with NCX phosphorylation by upregulated PKA[184]. Therefore we suggest the up-regulated function of NCX in OVx may result from the phosphorylation of NCX.

7.5.2 Ca^{2+} sparks and waves

These data showed significant increases in the frequency of Ca^{2+} sparks and waves following OVx. Spark amplitudes and mass were also larger in OVx myocytes. All these indices are indicative of an enhanced SR Ca^{2+} load[41] which is thought to alter ryanodine receptor Ca^{2+} sensitivity at luminal regulatory sites[38] or directly at the store-sensing gate in ryanodine receptor[39], and increase single channel current amplitude that governs cluster behaviour[319]. These changes increase the probability of Ca^{2+} waves formation and propagation that are considered to be pro-arrhythmic[320]. These will induce sufficient Ca^{2+}-dependent inward current, particularly forward-mode NCX current, to cause depolarisation of the cardiac cell membrane producing spontaneously triggered beats under certain conditions[36]. Therefore OVx myocytes may have increased tendency to develop arrhythmias, which could help explain the finding that OVx increased the susceptibility to ischaemia-induced arrhythmias [305] and the increased incidence of arrhythmias in post-menopausal women[287].

In addition, we investigated the cells responses to β-adrenergic stimulation (ISO challenge). Cells from Sham, OVx and OVx+E all produced significantly more sparks and waves when treated with ISO. OVx myocytes again showed higher frequencies of sparks and waves compared with Sham. On the contrary, OVx+E myocytes shared similar responses to ISO challenge as Sham myocytes. Therefore, OVx myocytes were more sensitive to adrenergic stimulation which elicited significantly more SR Ca^{2} release events. Oestradiol supplementation suppressed these potentially adverse effects.

7.5.3 Ca^{2+} current

Evidence suggests that the activity of L-type Ca^{2+} channels increased following OVx and these changes are reversed by oestrogen supplementation[321-323]. The changes appear to take place without alterations to the relative amounts of gene expression for L-type Ca^{2+} channel subunits α1c and β2. This was a similar finding to the levels of mRNA coding for L-type Ca^{2+} channel α-subunits in smooth muscle cells of coronary arteries following oestrogen withdrawal[323]. Therefore, we suggest the increased $I_{Ca,L}$ may result from the change in phosphorylation status of the channel. The increased Ca^{2+} influx via peak $I_{Ca,L}$ may also help provide evidence that increased SR Ca^{2+} content resulted from increased $I_{Ca,L}$ in the OVx group.

7.5.4 L-type Ca^{2+} channel gating and phosphorylation

These results showed a shift toward positive E_m in L-type Ca^{2+} channel inactivation in OVx myocytes. It was also noted that the positive shift was abolished by H-89 in OVx myocytes. The L-type Ca^{2+} channel inactivation shifted towards negative E_m with H-89 treatment in Sham and OVx+E groups. The activity of c-AMP dependent PKA was shown to increase in an ovariectomised rat model[321].

Phosphorylation of $Ca_v1.2$ via PKA shifts channel gating toward more negative membrane potentials[16]. However, in contrast to PKA-mediated phosphorylation of the L-type Ca^{2+} channel, phosphorylation of inner sarcolemma surface by basal kinases would be expected to shift channel gating to more positive E_m[324]. This modulation can be reversed towards more negative voltages if the phosphorylation is blocked by H-89[325]. Therefore the positive E_m channel gating shift in OVx may not result purely from PKA-mediated phosphorylation. We suspect it could be due to higher activity of basal or other forms of kinases which phosphorylate L-type Ca^{2+}channel or inner sarcolemma surface[324] following OVx. It is possible H-89 inhibits protein kinases (basal kinases, not necessarily PKA) that produce this kind of membrane phosphorylation at the inner surface proteins or amino acids terminal ends, such as Ser and Thr.

In fact, the phosphorylation of L-type Ca^{2+} channel via kinases other than PKA could shift the channel gating to more positive E_m. CaMKII, for instance may positively shift the steady-state inactivation by phosphorylating $Ca_v1.2$ at specific sites, such as Ser-1512 and Ser-1570[263,326]. There is also evidence showing CaMKIIδ and phosphorylated CaMKII were up-regulated in the hearts from ovariectomised rats[196]. Our OVx group showed dysregulation of Ca^{2+} handling such as increased $I_{Ca,L}$ and a larger Ca^{2+} transient, which could activate CaMKII, will have feedback effects on L-type Ca^{2+} channel function. However, it is still unclear how long-term deficiency of oestrogen may influence the phosphorylation of the L-type Ca^{2+} channel to change its gating characteristics, therefore further investigated is needed.

Basal peak $I_{Ca,L}$ was higher in OVx compared with Sham and OVx+E. H-89 was used to test the role of PKA in maintenance of basal $I_{Ca,L}$. OVx myocytes still showed higher peak $I_{Ca,L}$ compared with Sham and OVx+E in the presence of H-89. Sham and OVx+E groups had similar peak $I_{Ca,L}$ with H-89 treatment. Thus, we suspect kinases including PKA which support the basal activity of L-type Ca^{2+} channel may work in different ways or have differential activity between Sham, OVx and OVx+E groups.

7.5.5 EADs and DADs

A key finding in this chapter was the observation that OVx myocytes had higher frequencies of EADs and a greater percentage of these cells showed DADs and DAD-induced triggered extra beats during ISO challenge. Significantly fewer pro-arrhythmic events were observed in myocytes isolated from OVx GPs with 17β-oestradiol supplementation. To the best of our knowledge, this is the first ISO challenge experiment to induce EADs/DADs in cardiomyocytes from ovariectomised animals. EADs are likely to occur when a proportion of Ca^{2+} channels reactivate or fail to inactivate, especially in the

case of increased window current[81]. Late phase EADs may share the same underlying mechanisms as DADs which are SR Ca^{2+} overload and spontaneous Ca^{2+} release[327]. Adrenergic stimulation-induced EADs are regarded as the underlying mechanism of torsades de pointes ventricular tachycardia and sudden death in patients with idiopathic LQTS[328]. Our observations may also help explain an *in vivo* whole heart study showing increase in susceptibility to adrenergic stimulation-induced arrhythmias in ovariectomised rats compared with gonad-intact animals[187]

7.5.6 Comparing Ca^{2+} handling in ovariectomised animal models

Table 7-4 summarises the changes in cardiac myocyte Ca^{2+} handling in ovariectomised animal models. We have reported an increased peak $I_{Ca,L}$ in OVx that is in good agreement with effects seen in rat and mouse OVx models[318,321]. The mRNA expression of L-type Ca^{2+} channel was unaltered following OVx; a finding similar to Fares *et al* in the rat[318] but it is uncertain if L-type Ca^{2+} channel protein expression changes[317,318]. We suggest the increased $I_{Ca,L}$ may result from the change in phosphorylation status of the channel. Further research using PKA/CaMKII inhibitors is required to assess their role in L-type Ca^{2+} channel phosphorylation.

Most studies of the effects of OVx report increased Ca^{2+} transient amplitudes[184,186,188,318,321] although discrepancies exist[190,329]. OVx in the GP speeds the decay of the Ca^{2+} transient and our results suggest that this is due to faster Ca^{2+} removal via NCX. While mRNA and protein expression of NCX were unaltered in most studies[184,318], there is one report of increased activity of NCX resulting from PKA phosphorylation[184]. The rate constant representing SERCA function remained unaltered following OVx implying unchanged Ca^{2+} uptake into the SR but the expression and regulation of SERCA seems to vary among studies[184,185,317,318,329,330].

We report an increased spark frequency, amplitudes and mass in the OVx group, which support similar reports in the mouse which is more reliant on SR Ca^{2+} release than the GP[186,318]. All these effects following OVx could be reversed with oestradiol supplementation confirming that it is the withdrawal of oestrogen that mediates the changes in Ca^{2+} regulation. In this study we have used an ISO challenge to assess if OVx imparts a pro-arrhythmic substrate. OVx myocytes had more sparks and waves following the ISO challenges compared with Sham and OVx+E cells. Furthermore, these cells had a higher frequency of EADs and a higher percentage of DADs and DAD-induced triggered extra beats. To further explore the pro-arrhythmic mechanism, the inactivation gating of L-type Ca^{2+} channel was investigated and was found to shift towards a more positive E_m with larger window current, allowing a higher probability of reactivation of L-type Ca^{2+} channel. These novel findings

may help better our understanding and provide new insights for the mechanism regarding to postmenopausal arrhythmia.

OVx animal	Guinea pig (present study)	Rat		Mouse		Rabbit
Include oestradiol supplement experiment	**Yes**	**Yes**	**No**	**Yes**	**No**	**Yes**
Peak $I_{Ca,L}$	↑ mRNA↔	A↑, with PKAI↔[321] WB↑[317] mRNA↔[317]			↑[318] ↔[186] WB↓[318]	Epicardium↓[331] Endocardium↔[331] Dispersion↓[331]
PKA		E↑[184], A↑[321]				
CaMKIIδ and phosphorylated CaMKII		WB↑[196]				
SR Ca^{2+} content	↑				↑[186,318]	
Ca^{2+} transient parameters						
Amplitudes	↑	↑[184,188,321] ↓[190]		↓[329]	↑[186,318]	
TTP	↔				↓[318]	
Rate constant	↑	↑[184,188]		↓[329]	↑[186,318]	
Fractional SR Ca^{2+} release	↑				↔[186,318]	
SERCA	R↔	A↔[184], ↓[185] WB↔[184,317], ↓[185] mRNA↔[317], ↓[185] PLB↔[185,317]	WB↓[330] PLB↔[330]	WB↓[329]	WB↔[318]	
NCX	R↑	A↑, with PKAI↔[184] RC↑[184] WB↔[184], ↓[317] mRNA↔[317]			WB↔[318]	
RyR2		A↑, with PKAI↔[184] WB↔[317]				
Spark frequency	↑				↑[186,318]	
Spark amplitude	↑				↑[186]	
Spark mass	↑				↑[318] ↔[186]	
Wave frequency	↑					
ISO induced EADs, DADs.	↑					

A=Activity, E=Expression of fluorescence intensity, WB=Western blot, R=Rate constant, RC=Relaxation contribution

↑: increase, ↔: no difference, ↓: decrease. Compared with Sham group.

Table 7-4. Changes in cardiomyocyte Ca^{2+} handling in ovariectomised animal models.

7.5.7 Myofilament Ca^{2+} sensitivity

Our data also showed a decrease in *in vivo* fractional shortening and an increase in LVIDd and LVIDs in the OVx group compared with the ovary-intact sham group, observations that are difficult to reconcile with increased Ca^{2+} current and SR Ca^{2+} content. A possible explanation is that there are changes to myofilament Ca^{2+} sensitivity in OVx hearts. Ca^{2+} desensitisation and/or decreased ATPase activity has been observed in *in vitro* studies of TnT mutant proteins[332-335] and accompanies many dilated cardiomyopathy phenotypes[332] that show decreases in *in vivo* fractional shortening yet increases to the Ca^{2+} transient as found in this chapter. A deficiency of female sex hormones alters the cardiac contractile machinery[304,308,336] but the few studies that have been done in rats present an ambiguous picture of the effects of OVx[310,337].

7.6 Conclusions

This chapter addressed the hypothesis that long-term deficiency of ovarian hormones alters cellular Ca^{2+} handling mechanisms in the heart resulting in the formation of a pro-arrhythmic substrate. We also tested if oestrogen supplementation to ovariectomised GPs reverses any alterations to cardiac Ca^{2+} handling and rescues pro-arrhythmic behaviour. OVx had detrimental effects on Ca^{2+} regulation in GP cardiac myocytes. The dysregulation of Ca^{2+} handling contributes to higher frequency of spontaneous or triggered SR Ca^{2+} release events. With β-adrenergic stimulation, the probability of EADs/DADs formation and DAD-induced triggered extra beats were higher in OVx group. These findings suggest long-term absence of ovarian hormones lead to adverse changes in Ca^{2+} handling mechanisms that may cause the formation of a more pro-arrhythmic substrate. 17β-oestradiol replacement prevented these changes.

8 THE ROLE OF OESTROGEN IN Ca^{2+} AND Na^{+} REGULATION IN PRESSURE-OVERLOAD HEART FAILURE FEMALE GUINEA PIGS

8.1 Aims

- To assess if long-term deprivation of ovarian hormones alters intracellular Ca^{2+} and Na^{+} regulation in a pressure-overload GP model.
- To test if oestrogen supplementation confers cardiac protection and modulates calcium handling and Na^{+} regulation in the ovariectomised aortic-constricted HF GP.

8.2 Introduction

Sex disparities appear in clinical data on the progression of cardiac hypertrophy towards HF[338]. The Framingham study revealed that the prognosis in women is significantly better than in men after the onset of HF[171]. In advanced HF, females still have a mortality advantage[172]. Animal studies reported the protective role of oestrogen in cardiac hypertrophy and HF[176,195,206]. Clinical evidence suggests that oestrogen is linked to cardiovascular protection in premenopausal women[158,175,178,339]. Pathways, including calcium handling, NOS, and regulation of collagen may be involved in the oestrogen-related protective effect[179]. However, the use of HRT failed to reduce the risk of cardiovascular events and may have detrimental effects on cardiovascular function[175,192]. The underlying mechanisms, especially the role of oestrogen in Ca^{2+} and Na^{+} regulation, and E-C coupling are not clear[167-170]. In this chapter, we used female AC GPs that had initially undergone an OVx to assess the relationship of long-term absence of oestrogen and pressure-overload HF on intracellular Ca^{2+} and Na^{+} regulation. In addition, selected female ACOVx GPs were supplemented with 17β-oestradiol to help clarify the proposed beneficial role of oestrogen on key features of intracellular Ca^{2+} and Na^{+} regulation.

8.3 Methods

8.3.1 AC combined with OVx GP model and *in vivo* echocardiography study

The pressure-overload AC combined with OVx GP model was detailed in section 2.1.3, and *in vivo* M-mode echocardiography measurements were described in section 2.2.

8.3.2 Myocytes isolation and electrophysiological measurement

Experiments were performed on single cardiac myocytes isolated from sham, AC or AC combined with OVx with or without 17β-oestradiol supplementation in female GPs at operation 150 D

(categorised as F-150Sham, F-150AC, F-150ACOV and F-150ACOV+E, respectively) according to the methods described in section 2.3.1. Techniques and protocols for electrophysiology measurements including APD, $I_{Ca,L}$, Ca^{2+} transient, SR Ca^{2+} content, spontaneous Ca^{2+} sparks, Na^{+}/K^{+} ATPase current and reactivation, and $I_{Na,L}$ were detailed in sections 2.4 and 2.5.

8.3.3 Serum oestradiol level

17β-oestradiol pellet implantation and serum oestradiol ELISA test were described in section 2.1.4 and 7.3.2.1, respectively.

8.3.4 Statistical Analysis

Data acquisition, processing, statistical analysis and expression of statistical significance were detailed in section 2.7.

8.4 Results

8.4.1 General physical characteristics

BW remained unchanged across all experimental groups (Fig. 8-1. A). F-150ACOV had increased HW/BW ratio compared with F-150AC by an average of 11 % and F-150ACOV+E by an average of 14 %. F-150AC and F-150ACOV+E had similar HW/BW ratio (Fig. 8-1. B). F-150ACOV showed increased LW/BW compared with F-150AC by 17 % (Fig. 8-1. C). There was no difference in LW/BW between F-150AC and F-150ACOV+E groups (Fig. 8-1. C). Average uterine weight (UW) was significantly lower in the combined AC-OVx group, at 0.4 ± 0.1 g compared with F-150AC, at 1.6 ± 0.4 g and the oestradiol supplement group, at 4.3 ± 0.6 g (Fig. 8-1. D). Average serum oestradiol levels were significantly lower in F-150ACOV, at 4.0 ± 1.9 pg/mL compared with F-150Sham, at 7.8 ± 4.4 pg/mL, F-150AC, at 8.2 ± 3.6 pg/mL and F-150ACOV+E, at 30.1 ± 10.0 pg/mL (Fig. 8-1. E).

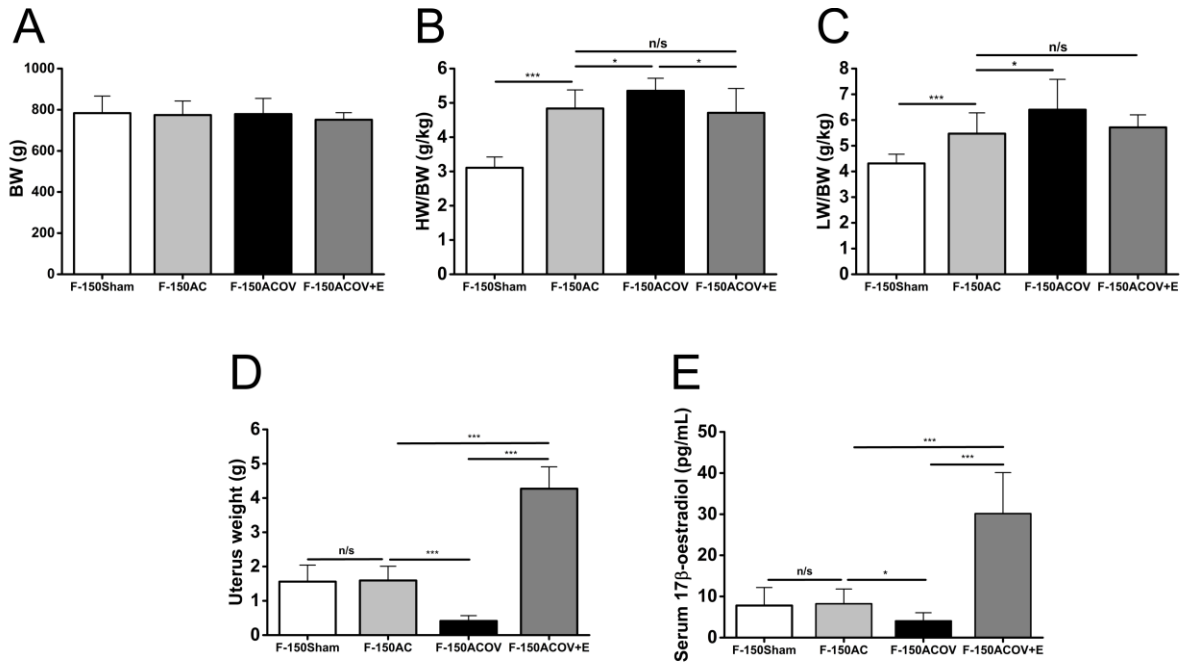

Figure 8-1. Assessing general physical characteristics.

*A: F-150Sham, F-150AC, F-150ACOV and F-150ACOV+E had similar BW. B: Mean F-150ACOV HW/BW ratios increased by 11 % and 14 % compared with the mean values for F-150AC and F-150ACOV+E groups, respectively. The mean HW/BW ratios for F-150AC and F-150ACOV+E were no different. C: Mean LW/BW for F-150ACOV was increased by 17 % compared with F-150AC. Mean LW/BW ratios were no different between F-150ACOV+E and F-150AC. D: Mean UW was significantly reduced in the AC combined with OVx group, at 0.4 ± 0.1 g compared with F-150AC, at 1.6 ± 0.4 g and F-150ACOV+E, at 4.3 ± 0.6 g (Fig. 8-1. B). (F-150Sham, n=15; F-150AC, n=13; F-150ACOV, n=10; F-150ACOV+E, n=7; n=GP numbers; Student's t-test, n/s: p>0.05 *p<0.05, ***p<0.001). E: The average serum oestradiol level was significantly reduced in F-150ACOV, at 4.0 ± 1.9 pg/mL compared with F-150AC, at 8.2 ± 3.6 pg/mL and the 17β-oestradiol supplemented group, at 30.1 ± 10.0 pg/mL (F-150Sham, n=9; F-150AC, n=9; F-150ACOV, n=6; F-150ACOV+E, n=6; n=GP numbers; one-way ANOVA with a Fisher post-hoc test, n/s: p>0.05, *p<0.05, ***p<0.001).*

8.4.2 *In vivo* M-mode echocardiography

While F-150AC, F-150ACOV and F-150ACOV+E had similar average LVIDd, F-150ACOV had wider average LVIDs compared with F-150AC, by 14 % and F-150ACOV+E, by 17 % (Fig. 8-2. A & B). There were no differences in LVIDs between F-150AC and F-150ACOV+E (Fig. 8-2. A & B). In chapter 6 it was reported that F-150AC had reduced FS compared with F-150Sham. In this chapter, the F-150ACOV group showed a further reduction in FS compared with F-150AC and F-150ACOV+E, by 14 % and 13 %, at 39.6 ± 3.3 % (Fig. 8-2. C). The 17β-oestradiol supplemented group, F-150ACOV+E, had similar FS to F-150AC (Fig. 8-2. C).

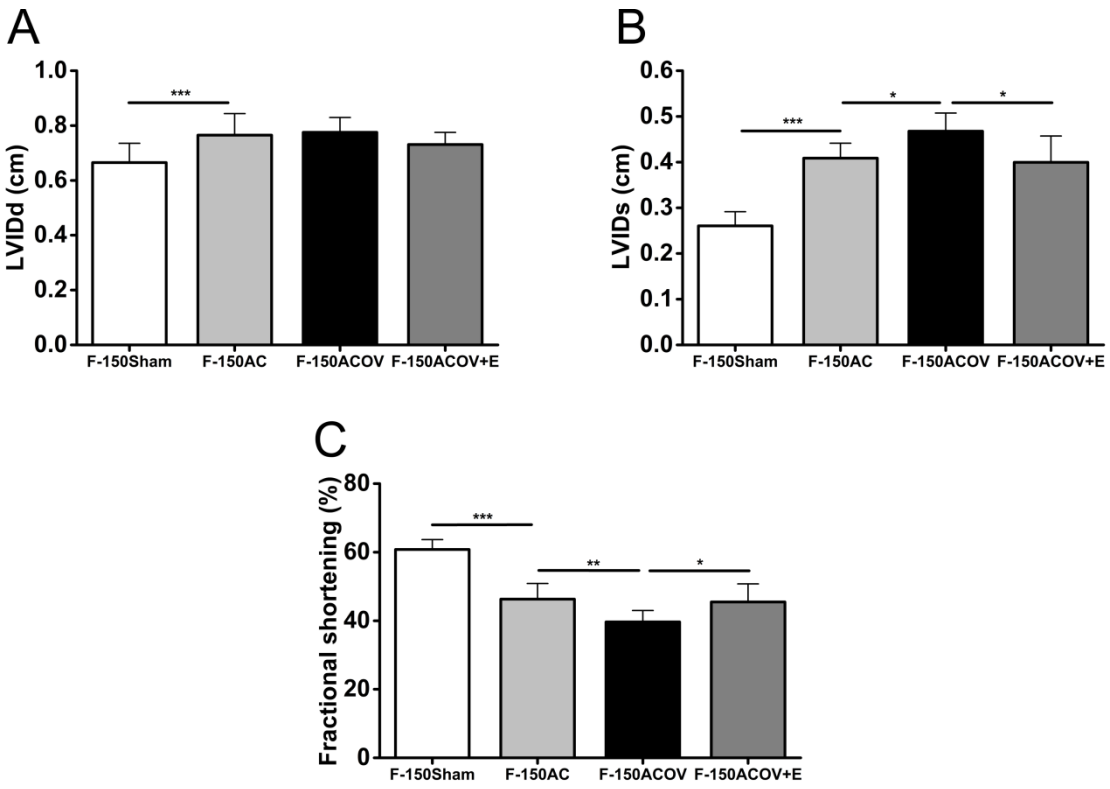

Figure 8-2. *In vivo* echocardiography study.

*A & B: The LVIDd between F-150AC, F-150ACOV and F-150ACOV+E was similar. The LVIDs in F-150ACOV was however 14 % and 17 % larger compared with F-150AC and F-150ACOV+E, respectively. F-150AC and F-150ACOV+E had similar LVIDs. C: F-150ACOV showed a 14 % and 13 % further reduction in FS, respectively, at 39.6 ± 3.3 % compared with F-150AC and F-150ACOV+E. F-150ACOV+E, the oestradiol supplemented group, had similar FS compared with F-150AC (F-150Sham, n=15; F-150AC, n=13; F-150ACOV, n=10; F-150ACOV+E, n=7; n=GP numbers; one-way ANOVA with a Fisher post-hoc test, n/s: p>0.05, *p<0.05, **p<0.01, ***p<0.001).*

8.4.3 APD

As can be seen in Figure 8-3, the average APD_{90} was prolonged in the three AC-operated groups, F-150AC by 27 %, F-150ACOV by 31 % and F-150ACOV+E by 18 %, compared with age-matched F-150Sham group. Compared with F-150AC, F-150ACOV had similar APD_{90}. F-150ACOV+E also had similar APD_{90} compared with F-150AC but showed shorter APD_{90} by 11 % compared with F-150ACOV.

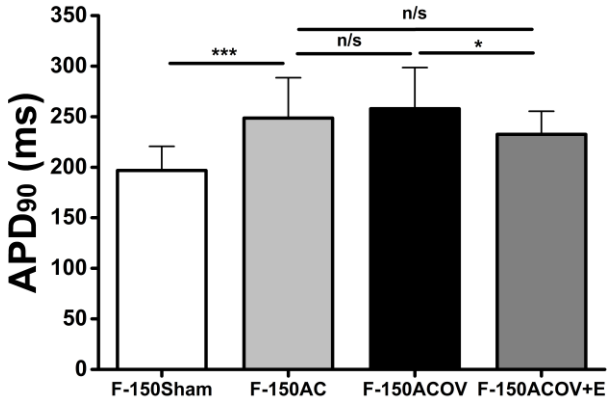

Figure 8-3. APD in sham, AC and AC combined with OVx female GPs.

*AC-operated groups, F-150AC, F-150ACOV and F-150ACOV+E, had significantly prolonged APD_{90} compared with the age-matched F-150Sham group. F-150ACOV had a similar APD_{90} compared with F-150AC. The APD_{90} was also similar in F-150ACOV+E compared with F-150AC but had an 11 % shorter APD_{90} compared with F-150ACOV (F-150Sham, n=43/5; F-150AC, n=33/3; F-150ACOV, n=46/3; F-150ACOV+E, n=34/3; one-way ANOVA with a Fisher post-hoc test, n/s: p>0.05, **p<0.01, ***p<0.001).*

8.4.4 Cell capacitances

Mean cell capacitances of F-150Sham, F-150AC, F-150ACOV and F-150ACOV+E were 173.2 ± 41.9, 241.6 ± 56.1, 291.7 ± 65.3, and 270.4 ± 73.7 pF, respectively (F-150Sham, n=125; F-150AC, n=107; F-150ACOV, n=122; F-150ACOV+E, n=92). F-150ACOV had larger cell capacitance compared with F-150AC and F-150ACOV+E (***p<0.001 and **p<0.01, respectively). F-150ACOV+E showed larger cell capacitance compared with F-150AC (***p<0.001). One-way ANOVA with a Fisher post-hoc test was used.

8.4.5 Ca^{2+} regulation in sham, AC and AC combined with OVx GPs

8.4.5.1 $I_{Ca,L}$

In chapter 4 we reported that peak $I_{Ca,L}$ remained unchanged between 150Sham and 150AC group. In this chapter we investigated if OVx alters peak $I_{Ca,L}$ in AC-operated GPs. When compared with F-150AC, both F-150ACOV and F-150ACOV+E had unchanged peak $I_{Ca,L}$ (Fig. 8-4).

We further investigated the decay phase time constants tau 1 and tau 2 of peak $I_{Ca,L}$ to probe any potential changes in inactivation kinetics. Figure 8-5 showed F-150AC had prolonged tau 1 and tau 2 compared with F-150Sham. F-150ACOV showed no difference in tau 1 or tau 2 compared with F-150AC. The oestradiol supplemented group F-150ACOV+E also had similar tau 1 and tau 2 to F-150AC.

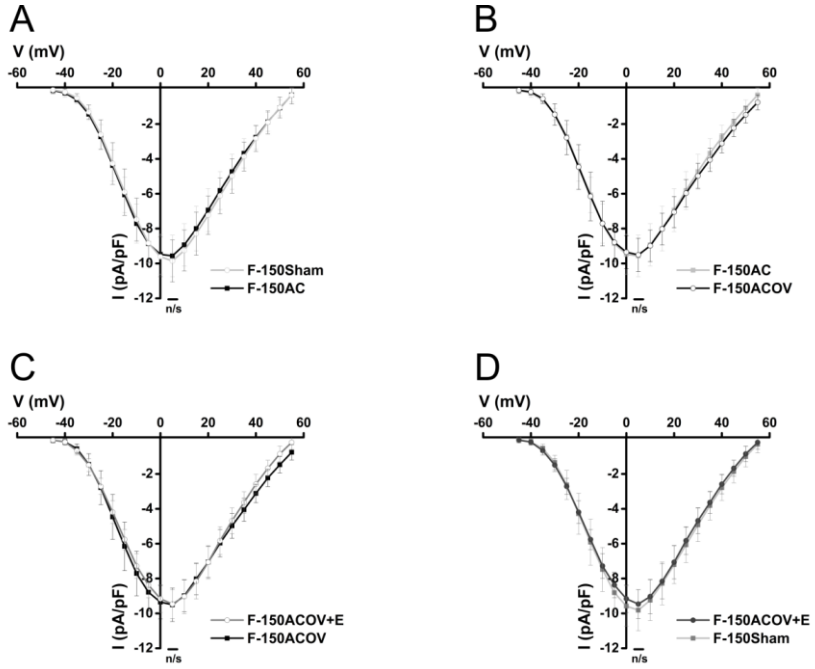

Figure 8-4. Comparing the I-V relationship of L-type Ca^{2+} channel between sham, AC or AC+OVx operated female GPs.

A: F-150AC showed no difference in maximal peak $I_{Ca,L}$ at 5 mV compared with F-150Sham. B, C & D: Both F-150ACOV and F-150ACOV+E had unaltered maximal peak $I_{Ca,L}$ at 5 mV compared with F-150AC. F-150ACOV+E also had similar $I_{Ca,L}$ compared with F-150Sham group (F-150Sham, n=40/5; F-150AC, n=17/3; F-150ACOV, n=32/3; F-150ACOV+E, n=22/3; one-way ANOVA with a Fisher post-hoc test, n/s: p>0.05).

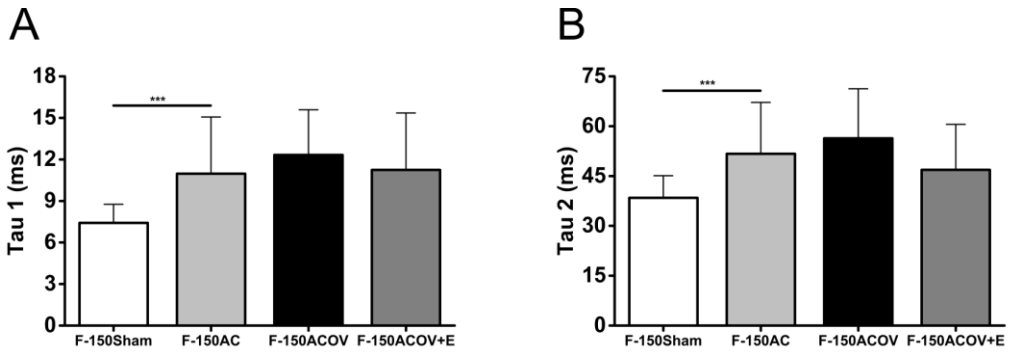

Figure 8-5. Comparing time constants for decay phase of peak $I_{Ca,L}$ in sham, AC, ACOV and ACOV+E-operated female GPs.

F-150AC had prolonged tau 1 and tau 2, by 48 % and 35 %, respectively, compared with F-150Sham. F-150ACOV showed no difference in tau 1 or tau 2 compared with F-150AC. The oestradiol supplemented group, F-150ACOV+E, also had a similar tau 1 and tau 2 to F-150AC (F-150Sham, n=40/5; F-150AC, n=17/3; F-150ACOV, n=32/3; F-150ACOV+E, n=22/3; one-way ANOVA with a Fisher post-hoc test, n/s: p>0.05).

8.4.5.2 Ca^{2+} transient

The F-150AC group had an average 31 % reduction in Ca^{2+} transient amplitudes compared with F-150Sham (Figure 8-6). F-150ACOV had a further average 10 % reduction in Ca^{2+} transient amplitudes compared with F-150AC. However, the oestradiol supplemented group had similar Ca^{2+} transient amplitudes to F-150AC. In figure 8-7, it is shown that F-150AC had an average 29 % slower Ca^{2+} transient decay rate constant compared with F-150Sham. Furthermore, F-150ACOV showed an additional average 13 % slower decay rate constant compared with F-150AC group. The F-150ACOV+E decay rate constant was unaltered compared with F-150AC.

In Figure 8-8. A & B, as previously shown, F-150AC had a reduced rate constant of SERCA compared with the age-matched sham group, resulting in similar contributions to Ca^{2+} removal between SERCA and NCX in the F-150AC group. The AC with OVx group F-150ACOV had further 20 % reduced rate constant of SERCA and unchanged rate constant of NCX compared with F-150AC, which suggests that NCX contributes relatively more to Ca^{2+} removal compared with SERCA in F-150ACOV group (Fig. 8-8. C & D). The oestradiol supplemented group showed no difference in the rate constants of SERCA and NCX and the corresponding contribution to Ca^{2+} removal compared with F-150AC group (Fig. 8-8. E & F). Fractional Ca^{2+} release increased in F-150AC compared with F-150Sham, but in general, there were no differences in fractional release compared between F-150AC, F-150ACOV, and F-150ACOV+E groups.

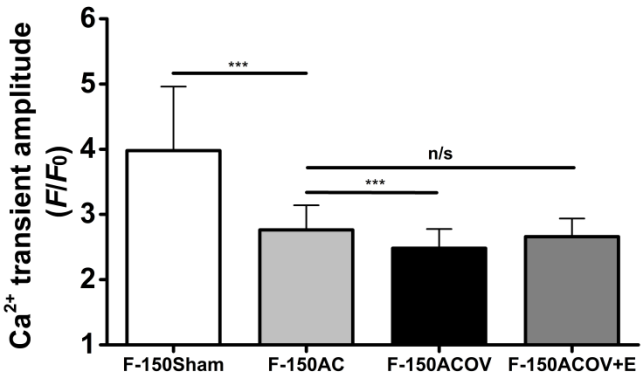

Figure 8-6. Ca^{2+} transient amplitudes in sham, AC, and AC with OVx female GPs.

*F-150AC group had a 31 % reduction in Ca^{2+} transient amplitudes compared with F-150Sham. F-150ACOV had an additional 10 % reduction in Ca^{2+} transient amplitudes compared with F-150AC. The oestradiol supplemented group had similar Ca^{2+} transient amplitudes to F-150AC (F-150Sham, n=44/3; F-150AC, n=47/3; F-150ACOV, n=31/3; F-150ACOV+E, n=21/2; one-way ANOVA with a Fisher post-hoc test; n/s: p>0.05, ***p<0.001).*

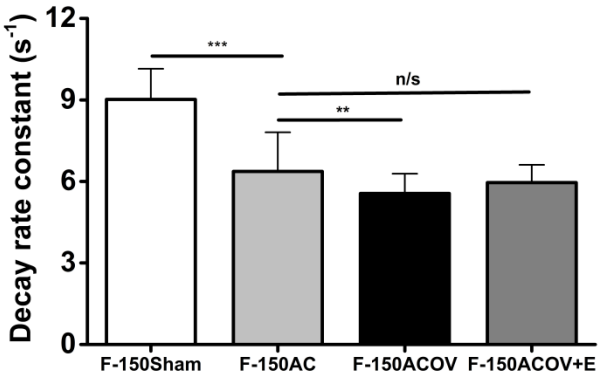

Figure 8-7. Rate constants for the decay of Ca^{2+} transients in sham, AC, and AC with OVx female GPs.

*F-150AC had a 29 % slower Ca^{2+} transient decay rate constant compared with F-150Sham. In the AC with OVx group, F-150ACOV, the average decay rate constant was 13 % slower compared with F-150AC. With oestradiol supplementation, F-150ACOV+E showed no difference in decay rate constant compared with F-150AC (F-150Sham, n=27/2; F-150AC, n=41/2; F-150ACOV, n=31/3; F-150ACOV+E, n=21/2; one-way ANOVA with a Fisher post-hoc test, n/s: p>0.05, **p<0.01, ***p<0.001).*

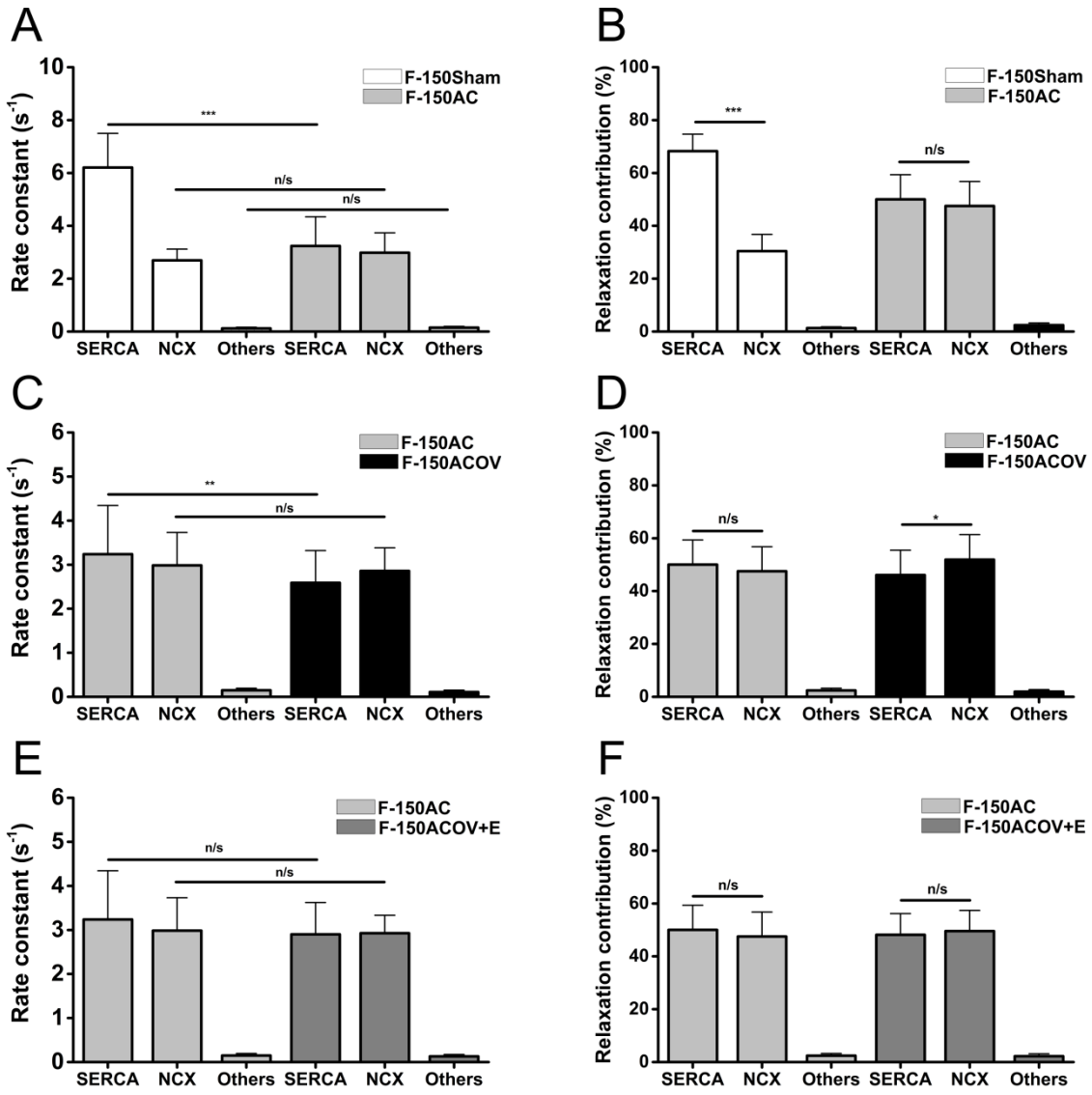

Figure 8-8. Rate constants and contributions of of SERCA, NCX and other slower components to cytosolic Ca^{2+} efflux ("relaxtion contribution") in sham, AC, and AC with OVx female GPs.

*A & B: Rate constants and relaxation contributions between F-150Sham and F-150AC groups. C & D: Rate constants and relaxation contributions between F-150AC and F-150ACOV groups. E & F: Rate constants and relaxation contributions between F-150AC and F-150ACOV+E groups (F-150Sham, n=27/2; F-150AC, n=41/2; F-150ACOV, n=31/3; F-150ACOV+E, n=21/2; one-way ANOVA with a Fisher post-hoc test; n/s: p>0.05, *p<0.05, **p<0.01, ***p<0.001).*

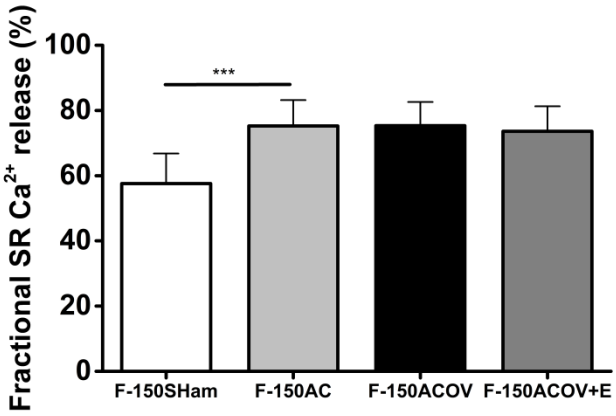

Figure 8-9. Fractional SR Ca^{2+} release in sham, AC, and AC and OVx female GPs.

*F-150AC had larger fractional SR Ca^{2+} release compared with F-150Sham. Fractional SR Ca^{2+} release was unaltered between F-150AC, F-150ACOV, and F-150ACOV+E groups (F-150Sham, n=46/5; F-150AC, n=33/3; F-150ACOV, n=24/3; F-150ACOV+E, n=21/2; one-way ANOVA with a Fisher post-hoc test, n/s: p>0.05, ***p<0.001).*

8.4.5.3 SR Ca^{2+} content

The effect of supplementation with oestradiol to OVx GPs with AC on SR Ca^{2+} content was assessed. In the F-150AC group, SR Ca^{2+} content decreased by an average of 41 % compared with the F-150Sham group (Fig. 8-10). The F-150ACOV group had a 13 % lower SR Ca^{2+} content compared with F-150AC, and oestrogen supplementation increased SR content so that the F-150ACOV+E group had similar SR Ca^{2+} content compared with F-150AC.

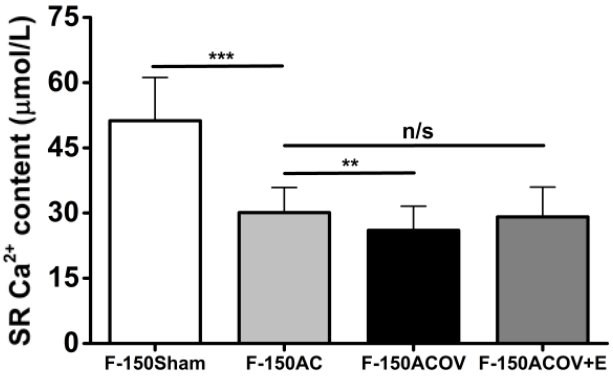

Figure 8-10. SR Ca^{2+} content in sham, AC, and AC with OVx female GPs.

*F-150AC had a 41 % decrease in SR Ca^{2+} content compared with F-150Sham. F-150ACOV had a 13 % lower SR Ca^{2+} content compared with F-150AC, but F-150ACOV+E SR Ca^{2+} content was unaltered compared with F-150AC (F-150Sham, n=33/3; F-150AC, n=34/4; F-150ACOV, n=42/3; F-150ACOV+E, n=29/3; one-way ANOVA with a Fisher post-hoc test, n/s: p>0.05, **p<0.01, ***p<0.001).*

8.4.5.4 Spontaneous Ca^{2+} sparks and spark-mediated SR leak

AC in females (F-150AC) resulted in a higher frequency of spontaneous Ca^{2+} sparks compared with sham-operated animals (F-150Sham) (Fig. 8-11 A). OVx and AC (F-150ACOV) produced a further increase in the mean spark frequency compared with F-150AC. Oestrogen supplementation (F-150ACOV+E) reversed this increase in spark frequency so the mean frequency values were similar to the F-150AC group. Spark amplitudes were greater in F-150ACOV compared with F-150AC, F-150Sham and F-150OV+E (Fig. 8-11. B). Spark mass was greater in F-150ACOV compared with F-150AC and F-150ACOV+E groups (Fig. 8-11. C). The calculated spark-mediated SR leak was greatest in AC combined with OVx operated group (Fig. 8-11. D).

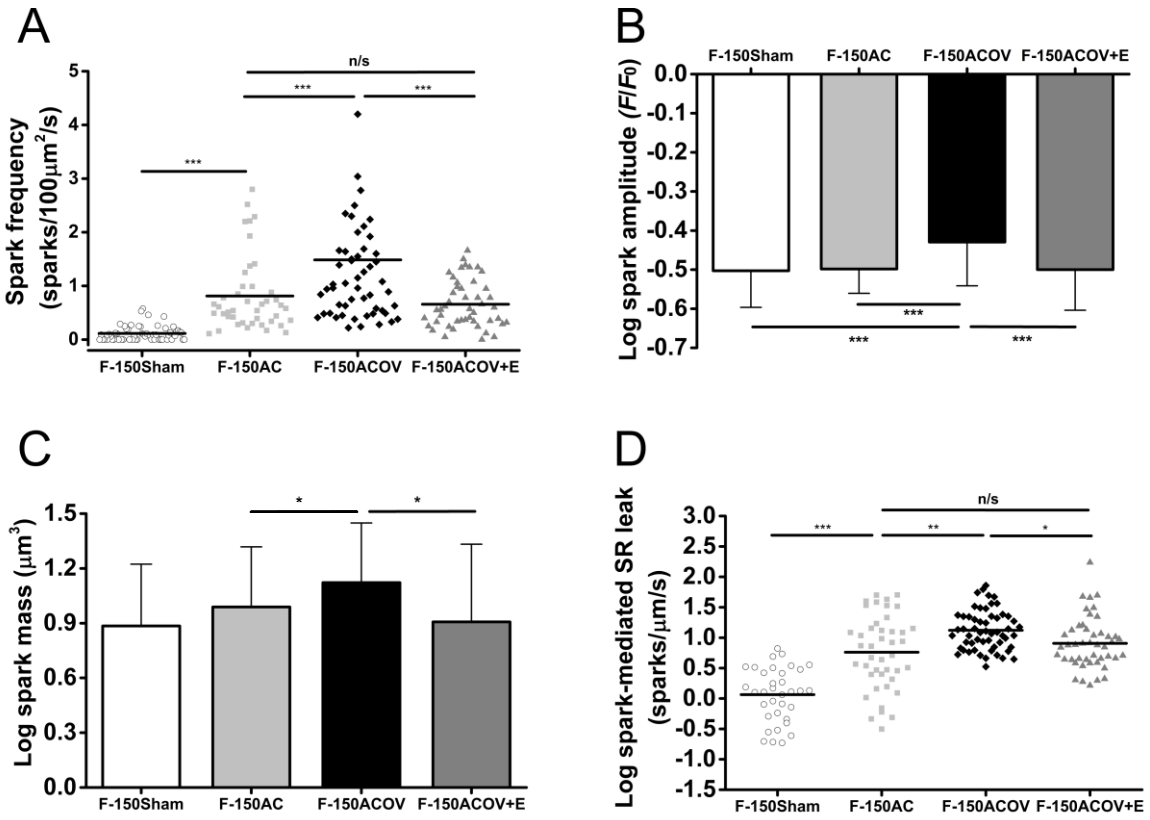

Figure 8-11. Spontaneous Ca^{2+} sparks and spark-mediated SR leak in sham, AC, and AC with OVx female GPs.

*A: F-150AC had a higher frequency of spontaneous Ca^{2+} sparks compared with F-150Sham. F-150ACOV had relatively higher frequency of spontaneous Ca^{2+} sparks compared with F-150AC. F-150ACOV+E and F-150AC had similar frequencies of spontaneous Ca^{2+} sparks. B: Spark amplitudes. C: Spark mass. D: The calculated spark-mediated SR leak was greatest in the F-150ACOV group (F-150Sham, n=57/5; F-150AC, n=43/3; F-150ACOV, n=56/4; F-150ACOV+E, n=47/3; one-way ANOVA with a Fisher post-hoc test, n/s: p>0.05, *p<0.05, **p<0.01, ***p<0.001).*

8.4.6 Na^+ regulation in sham, AC or AC combined with OVx GPs

8.4.6.1 Na^+/K^+ ATPase current and corresponding Na^+ extrusion rate

In chapter 5 we demonstrated both Na^+/K^+ ATPase steady-state current and reactivated Na^+/K^+ ATPase-mediated Na^+ extrusion rate markedly declined in the HF group compared with the age-matched sham group. When combined with OVx the AC group showed a 13 % further reduction in Na^+/K^+ ATPase current and a 19 % reduction in the Na^+ extrusion rate compared with the HF group (Fig 8-12. A & B). Oestradiol supplementation results in a return of mean values of steady-state current and extrusion rate to those of the HF group (Fig. 8-12. A & B).

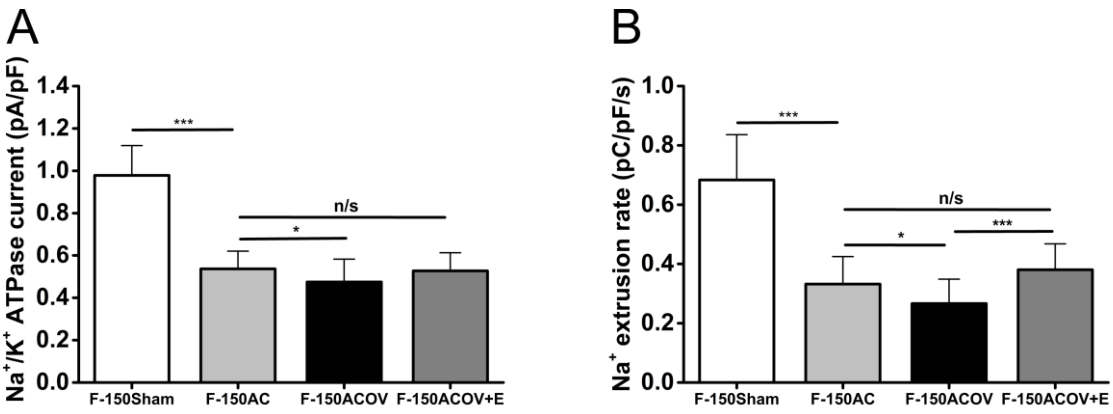

Figure 8-12. Na^+/K^+ ATPase current and reactivated Na^+/K^+ ATPase-mediated Na^+ extrusion rate sham, AC, and AC with OVx female GPs.

*A & B: Both Na^+/K^+ ATPase current and reactivated Na^+/K^+ ATPase-mediated Na^+ extrusion rate markedly declined in the HF group compared with the age-match sham group. OVx produced a further reductions in Na^+/K^+ ATPase current and Na^+ extrusion rate compared with F-150AC and these effects were reversed by oestradiol supplementation (F-150Sham, n=22/2; F-150AC, n=19/3; F-150ACOV, n=25/2; F-150ACOV+E, n=27/2; one-way ANOVA with a Fisher post-hoc test; n/s: p>0.05, *p<0.05, ***p<0.001).*

8.4.6.2 $I_{Na,L}$ density, associated Na^+ influx and late Na^+ current decay kinetics

While F-150ACOV had a 17 % larger $I_{Na,L}$ and 15 % greater $I_{Na,L}$-related Na^+ influx compared with F-150AC, supplementing OVx GPs with oestradiol resulted in a similar $I_{Na,L}$ and corresponding Na^+ influx compared with F-150AC (Fig. 8-13. A & B). The time constant of $I_{Na,L}$ decay remained unchanged between AC, AC combined with OVx and the oestradiol supplemented groups (Fig. 8-13. C).

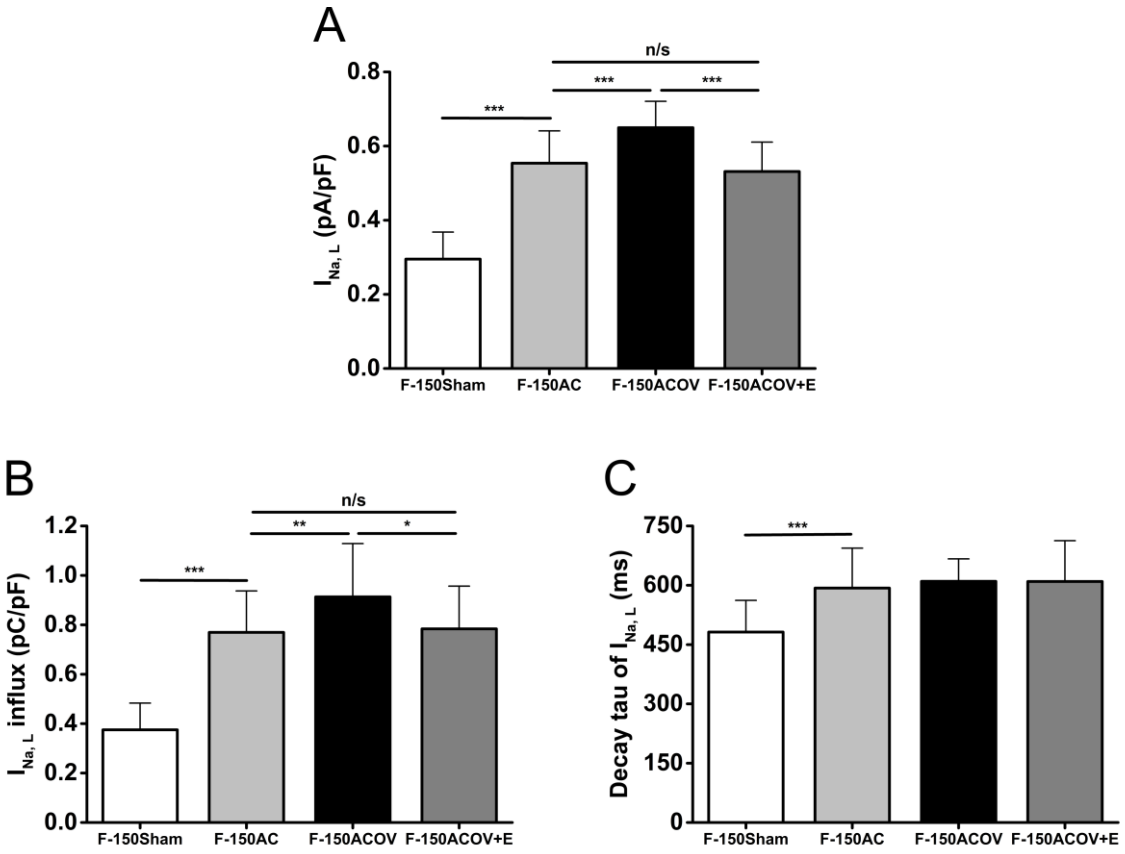

Figure 8-13. $I_{Na,L}$, the corresponding Na^+ influx, and the decay tau in sham, AC, and AC with OVx female GPs.

*A: The amplitude of the late Na^+ current in the four experimental groups (sham-operated, AC, AC+OVx and AC+OVx with oestrogen supplementation. B: The ranolazine-sensitive change transfer associated with the clamp step as outlined in the Methods section. F-150ACOV had a 15 % greater $I_{Na,L}$-related Na^+ influx compared with F-150AC. The oestradiol supplemented group had similar Na^+ influx compared with F-150AC. C: The decay time constant of $I_{Na,L}$ remained unchanged between F-150AC, F-150ACOV and oestradiol supplemented group, F-150OVAC+E (F-150Sham, n=31/3; F-150AC, n=25/3; F-150ACOV, n=23/3; F-150ACOV+E, n=21/3; one-way ANOVA with a Fisher post-hoc test, n/s: p>0.05, *p<0.05, ***p<0.001).*

8.5 Discussion

This chapter detailed the changes in Ca^{2+} and Na^{+} regulation between female AC HF and AC combined with OVx operation HF group to assess if long-term deprivation of ovarian hormone alters intracellular Ca^{2+} and Na^{+} regulation in the pressure-overload HF model. Here we further investigated the effect of oestrogen supplementation to AC combined with OVx operated GPs to assess if oestradiol confers cardiac protection against AC stress.

8.5.1 Physical characteristics and cardiac function in AC and ACOVx GPs

In chapter 6 we revealed that the female AC group had a smaller reduction in FS compared with the male AC group at the HF stage. The combination of AC and OVx produces a greater reduction in FS compared with female AC only GPs and this adverse effect appears to be reversed with supplementation of oestradiol. This suggests that oestrogen may play a modulatory role in the maintenance of global cardiac function following pressure-overload in female GPs in line with other studies imposing pressure-overload the rat or mouse[197,340-343]. Given that the female AC group with ovaries intact experienced a smaller decline in FS than males, this data support the idea that oestrogen may play a role in attenuating the hypertrophic response to pressure-overload and also may provide modulatory support to cardiac function following OVx. Distinct from the approaches taken from previous pressure-overload animal studies, including regulation of gene expression, MAPK pathway, NOS signalling, regulation of caveolin-3 and cardiac inflammation and oxidative stress, we focused on investigating the changes in Ca^{2+} and Na^{+} regulation – both fundamentally involved in the E-C coupling of cardiomyocytes – to explore how the underlying mechanisms in their regulation might be affected following OVx and pressure-overload.

8.5.2 Action potential and Ca^{2+} handling in AC and ACOVx GPs

8.5.2.1 APD

Prolongation of APD is commonly observed in HF models and can be viewed as the overall outcome of remodelling of ionic currents in response to HF[344]. In chapter 6 we reported that males and females had similar prolonged APD_{90} at the HF stage. In this chapter we also showed that AC and ACOVx hand similar prolonged APD_{90} compared with age-matched sham. While oestradiol supplemented group had shorter APD compared with ACOVx, the APD remained unchanged compared with AC group. Thus, long-term deprivation of ovarian hormone may not have a significant influence on APD in AC GPs. In the non-disease condition, APD was not altered following OVx in mice[318]. In physiological conditions, oestrogen has been shown to decrease outward K^{+} current, such as I_{Kr} and I_{K1}, resulting in prolongation of APD[225,227,345]. In pathophysiological condition such cardiac hypertrophy and HF, however, oestrogen appears to be able to influence cardiac

remodelling and modulate genomic responses and E-C coupling and so may provide an improvement in tolerance against pressure-overload heart disease[197,207,211,214,309]. This may be mediated via the ER β axis, NOS signalling and Akt pathway, which may provide protective effects against pressure-overload heart disease[197,207,211,214,309]. Oestradiol supplementation improved Ca^{2+} handling, which we will discuss in later sections, thus shortened APD may be a consquence of the improved Ca^{2+} regulation compared with ACOVx.

8.5.2.2 Ca^{2+} handling

Our data showed OVx did not affect peak $I_{Ca,L}$ or the inactivation rates of the current in AC GPs. Thus long-term deprivation of ovarian hormone may not alter $I_{Ca,L}$ following pressure-overload. This current provides the trigger for Ca^{2+} release yet in the pathophysiological state appears unaffected by oestrogen. In contrast, in chapter 7, we reported that peak $I_{Ca,L}$ was increased after OVx, and this effect was suggested to be associated with increased basal phosphorylation of L-type Ca^{2+} channel[196,321]. The modulation mechanism of $I_{Ca,L}$ in OVx may be different from the ACOVx group that involves cardiac hypertrophy and HF. We suggest increased peak $I_{Ca,L}$ may be initially arise in ACOVx at an early HF stage. While the cell becomes more hypertrophic at HF stage, the density of $I_{Ca,L}$ could not keep the pace with the increased cell size; therefore increased peak $I_{Ca,L}$ was not observed at HF stage.

The Ca^{2+} transient amplitudes and their rates of decay were further reduced in the ACOVx group compared with the AC group. The slower Ca^{2+} transient decay rate constant resulted from a further slowing of SERCA function. As a result, NCX contributed more to cytosolic Ca^{2+} efflux in the ACOVx group. Down-regulation of SERCA/PLB has been documented in numerous HF studies[92,93,95,98], and has been the focus of gene-target therapy that aims to restore the expression of the SERCA/PLB to improve Ca^{2+} cycling and cardiac function[94,98,346]. The ACOVx group showed a further reduction in Ca^{2+} uptake by SERCA, which suggested that OVx may have influence on the function of SERCA or PLB in pathophysiological overload. A decrease in mRNA or protein expression of SERCA has been shown in OVx rat studies[185,330], which was in agreement with the reduction of relative mRNA expression of SERCA in OVx GPS reported in chapter 7. We therefore suspect that the further reduction in Ca^{2+} uptake of SERCA may be related to an enhanced down-regulation of SERCA in ACOVx group. The ACOVx group also had a smaller SR Ca^{2+} content compared with AC group, which may contribute to the smaller Ca^{2+} transient amplitudes.

The spark-mediated SR leak was greater in the dual-surgery group compared with AC group. Thus, the smaller SR Ca^{2+} content may result from the further reduction in Ca^{2+} uptake of SERCA and

greater SR Ca^{2+} leak. The increased SR Ca^{2+} leak in ACOVx may also contribute to more accumulation of $[Ca^{2+}]_i$, leading to worse diastolic dysfunction[274], and more arrhythmogenic[274,275] compared with AC group.

As discussed in chapter 4, the phosphorylation of RyR2 by CaMKII has been shown to increase diastolic SR Ca^{2+} leak[110,271,272]. CaMKIIδ and phosphorylated CaMKII were found up-regulated in an ovariectomised rat model[196], which additionally suggests that oestrogen supplementation could suppress CaMKII activity. We suggest the activity of CaMKII may be up-regulated in the ACOVx GPs, resulting in enhanced phosphorylation of RyR2 and subsequent higher leak. These adverse effects were not observed in ACOVx given oestradiol supplementation, supporting the notion that oestrogen has a cardioprotective effect by modulating Ca^{2+} regulation. The ACOVx had similar dysregulation of Ca^{2+} handling and reduction in FS compared with the male AC group. Both experienced more detrimental outcomes during progression of the disease compared with the female AC group (i.e. with intact ovaries). This observation also provides support for there being some cardioprotective role of oestrogen in pressure-overload heart disease.

8.5.3 Na^+/K^+ ATPase current and function, and $I_{Na,L}$

Myocytes from ACOVx had a further reduction in Na^+/K^+ ATPase current and reactivated Na^+/K^+ ATPase mediated Na^+ extrusion rate. The reduced function of the Na^+/K^+ ATPase may be a response to dysregulation of Ca^{2+}, as we know reduced function of Na^+/K^+ ATPase can elevate $[Na^+]_i$ which in turn influences NCX operation[32]. Alternatively, OVx may influence the expression of Na^+/K^+ ATPase or affect the phosphorylation of PLM. Further research is required of this understudied field. The ACOVx group also had a larger $I_{Na,L}$ compared with the AC group. This could be due to an up-regulation of CaMKII following OVx[196], which was shown to phosphorylate $Na_v1.5$ at Ser-571, causing increased $I_{Na,L}$ in a transgenic mouse model[142]. Again, oestradiol supplementation reversed these potentially adverse effects, supporting the hypothesis that oestrogen may modulate Na^+ regulation following AC.

Oestradiol was reported to increase α2 mRNA expression in rats although the study used arterial tissue[299]. Oestradiol may modulate Na^+/K^+ ATPase function by regulating the expression of Na^+/K^+ ATPase as reduced Na^+/K^+ ATPase protein expression and activity were found in human HF[90]. Therefore, reduced protein expression of the Na^+/K^+ ATPase could be another possible factor for the reduced Na^+/K^+ ATPase function of the ACOVx group but there is lack of evidence from our data and also from other studies in this field. The ACOVx group had more dysregulation of Ca^{2+} handling and reduced FS compared with female AC group. Therefore, the more reduced Na^+/K^+ ATPase function

and enhanced $I_{Na,L}$ may be a cause for the more dysregulated Ca^{2+} and FS. To the best of our knowledge, this is the first study to test the role of oestrogen in Na^+/K^+ ATPase and $I_{Na,L}$ in a ACOVx GP model. Further investigations, including proteomic or genomic studies of Na^+/K^+ ATPase are required to explore the mechanisms involved. In addition, further investigation is required to assess the role of CaMKII-mediated phosphorylation in the effect of long-term absence of ovarian hormones and oestradiol supplementation on cardiac hypertrophy and HF, which would provide a clearer picture of the mechanism.

8.6 Conclusions

Long-term deprivation of ovarian hormones altered Ca^{2+} and Na^+ regulation in pressure-overload HF, leading to more impaired cardiac function. Myocytes from ACOVx group had more detrimental Ca^{2+} handling, including smaller and slower Ca^{2+} transients and more reduced SR Ca^{2+} content, which explained the more reduced cardiac function in ACOVX compared with AC. The slower Ca^{2+} uptake by SERCA, together with greater SR Ca^{2+} leak leaded to less SR Ca^{2+} content in ACOVx compared with AC group. The greater SR Ca^{2+} leak may lead to more increased $[Ca^{2+}]_i$, causing worse diastolic dysfunction and could be more arrhythmogenic in ACOVx compared with AC. OVx influenced Na^+ regulation in AC HF, and showed a further reduction in Na^+/K^+ ATPase current and function and greater $I_{Na,L}$. The effects were reversed in the ACOVx GPs with oestradiol supplementation. CaMKII-mediated phosphorylation may play a role in the effect of long-term absence of ovarian hormones and oestradiol supplementation on cardiac hypertrophy and HF; therefore, further investigation is needed.

9 GENERAL DISCUSSION

Sex differences exist in the development of cardiac hypertrophy and the subsequent progression to HF in response to CVD[174,200,217,345,347,348]. While females seem to be more resistant to the development of cardiac hypertrophy and have a better survival in HF compared with males[167-172], the underlying mechanisms, especially the cardioprotective effect of oestrogen, is not clear and, indeed, remains controversial after HRT was demonstrated not to have cardiovascular benefit[192]. Therefore further investigation is required to clarify the effect of ovarian hormones on cardiac function and elucidate underlying mechanisms and this was one of the aims of the work detailed in this thesis. The first series of experiments in the thesis aimed to investigate differential changes in cardiac cell Ca^{2+} handling and Na^{+} regulation during the progression and development of cardiac hypertrophy to HF between the sexes using constriction of the ascending aorta in the GP to cause pressure-overload on the heart. The second series of experiments used OVx of GPs , which mimics a postmenopausal state, to investigate the effect of long-term absence of ovarian hormones on cardiac cell Ca^{2+} handling and Na^{+} regulation and explore underlying mechanisms, particularly those could be associated with pro-arrhythmia. Finally, a combination of AC combined with OVx was used to assess if ovarian hormones withdrawal worsens and accelerates the progression to HF. This tests the hypothesis that postmenopausal women lose a cardioprotective effect derived from ovarian hormones. 17β-oestradiol was supplemented to selected OVx GPs to assess the specific effects of oestrogen on the progression of the disease state.

9.1 Overview of key findings

9.1.1 The aortic-constricted GP model

We successfully established a pressure-overload GP model, which presented clear transition from cardiac hypertrophy to HF following AC surgery. The GPs initially adapted and compensated for the pressure-overload at 60 days, then this compensation started to fail and they transitioned towards decompensated HF around 150 days after surgery. *In vivo* fractional shortening of whole heart was unaltered though HW/BW was increased at the compensatory stage, whereas decompensated HF was characterised by a marked reduction in FS and increased HW/BW and LW/BW ratios.

9.1.1.1 Compensated cardiac hypertrophy

The cell compensation mechanisms in cardiac hypertrophy were explored using AC GPs at 60 days when the animals presented with the cardiac hypertrophy phenotype. The density and inactivation kinetics of $I_{Ca,L}$ remained unchanged so the prolongation of APD at this stage was suggested to be associated with increased Na^{+} influx via $I_{Na,L}$ or decreased outward I_K. The former was investigated, the latter was not. Larger cell Ca^{2+} transient amplitudes, greater SR Ca^{2+} content and higher

fractional SR Ca^{2+} release were observed and thought to be the underlying reasons for compensation of the whole heart . Notably the Ca^{2+} transient decay rates, and the function of SERCA and NCX remained unchanged. The function of the Na^+/K^+ ATPase started to decline at this stage. We demonstrated that partially inhibiting the Na^+/K^+ ATPase using strophanthidin to a level that mimicked the pathophysiological decline in current, increased Ca^{2+} transient amplitudes and SR Ca^{2+} content in sham cardiomyocytes. This suggested that the decline in Na^+/K^+ ATPase current and function reported at this stage, which would be expected to elevate $[Na^+]_i$, may act as a compensatory mechanism to induce inotropy by increasing Ca^{2+} influx via reverse-mode NCX. The protein expression of Na^+/K^+ ATPase α1 isoform was decreased but PLM and phosphorylated PLM at Ser-68 were unaltered, suggesting that the decline in Na^+/K^+ ATPase function was a consequence of decreased Na^+/K^+ ATPase protein expression. Furthermore, enhanced $I_{Na,L}$ was reported in myocytes from hypertrophied hearts, which may not only contribute to prolongation of the AP, but increase $[Na^+]_i$ that in turn results in more Ca^{2+} influx via NCX.

While the function of SERCA and NCX remained unaltered, declined Na^+/K^+ ATPase function and enhanced $I_{Na,L,}$ expecting to elevated $[Na^+]_i$[114,125], produced an inotropic effect at this stage.

9.1.1.2 Decompensated HF

At 150 days after AC, the animals developed decompensated HF indicated by a severe decline in heart function and congested lungs. APD was significantly prolonged at this stage. The peak $I_{Ca,L}$ still remained unchanged, analogous to the compensatory stage, but the inactivation of the $I_{Ca,L}$ slowed implying an increase in Ca^{2+} influx. There was a further decline in Na^+/K^+ ATPase function and further enhancement of $I_{Na,L}$. These changes would raise $[Na^+]_i$ even more and provide more Ca^{2+} influx via NCX. However, the relative contributions of SERCA and NCX to Ca^{2+} efflux were found to change at this stage. There was a decrease in the Ca^{2+} uptake function of SERCA and an up-regulation of Ca^{2+} removal from the cells by NCX. These changes can help to explain the reduction in SR Ca^{2+} content and Ca^{2+} transient and, as a result, whole heart FS was greatly reduced. The higher spark frequency and greater spark-mediated SR leak occurring at this stage may contribute to the depletion of SR Ca^{2+} and may increase diastolic $[Ca^{2+}]_i$ so that filling is impaired, diastolic dysfunction appears and a pro-arrhythmic substrate is favoured[274,275]. The decline in Na^+/K^+ ATPase current and function was accompanied by a decrease in α1 protein expression assessed by Western blot and by immunofluorescence. The decline in Na^+/K^+ ATPase function and increased $I_{Na,L}$ will contribute to the accumulation of $[Na^+]_i$ that has been measured in this model of HF.

9.1.2 Sex differences in AC progress

Having established an AC GP model which showed cardiac hypertrophy and HF phenotypes we then compared how males and females responded at the two stages to explore if sex plays a role in the progression to HF.

9.1.2.1 Sex differences in compensated cardiac hypertrophy

At this stage, both sexes had unaltered FS with increased HW/BW ratio. Similar prolongation of APD_{90} appeared in both sexes. Both sexes also had unchanged peak $I_{Ca,L}$ and its decay kinetics. While males showed larger Ca^{2+} transient amplitudes and greater SR Ca^{2+} content at the cardiac hypertrophy stage, females did not. The Ca^{2+} transient decay rate and the function of SERCA and NCX remained unaltered at this stage between sexes. Both sexes showed significant reductions in Na^+/K^+ ATPase current and function at this compensated stage but male current and function declined more compared with females. Both sexes also had significantly increased $I_{Na,L}$ but with unchanged decay kinetics.

Sex differences therefore may exist in $[Na^+]_i$ accumulation in the face of CVD[301].

9.1.2.2 Sex differences in decompensated HF

When entering decompensated HF state, males showed larger LW/BW ratios and less whole heart *in vivo* FS compared with females. Both sexes had markedly prolonged APD_{90}. Both sexes showed unaltered peak $I_{Ca,L}$ but prolonged inactivation. Smaller Ca^{2+} transient amplitudes and SR Ca^{2+} content in males could explain the poorer FS compared with females. The slower Ca^{2+} uptake function of SERCA in males not only contributed to the slower Ca^{2+} transient decay but resulted in less SR Ca^{2+} content compared with females. Males had higher spontaneous Ca^{2+} spark frequencies compared with females, suggesting the SR in males may tend to be leakier in HF. The Na^+/K^+ ATPase current and function were markedly reduced in both genders, with males having a larger reduction in Na^+/K^+ ATPase current compared with females. The marked increase in $I_{Na,L}$ with prolonged decay rate was sex-independent at the HF stage.

In summary, in males the Ca^{2+} handling and Na^+/K^+ ATPase current and function at the HF stage appears more dysfunctional compared with females.

9.1.3 Effect of OVx on Ca^{2+} handling

The OVx GP mimics a postmenopausal state. This group of animals had larger Ca^{2+} transients, faster Ca^{2+} transient decay with up-regulated NCX function, and greater fractional SR Ca^{2+} release. Relative mRNA expression of SERCA was reduced in OVx but partially restored after oestradiol

supplementation. The mRNA expression of NCX remained unaltered. The OVx group also had larger peak $I_{Ca,L}$ with channel inactivation shifting to more positive membrane potentials creating a larger "window" current, which may be associated with increased basal phosphorylation of the channel[196,349]. The amount of mRNA coding for $Ca_v1.2$ α1c and β2 subunits remained unaltered. SR Ca^{2+} stores were greater in the OVx group and these cells showed a higher frequency of Ca^{2+} sparks and waves and shorter wave-free intervals. OVx myocytes had higher frequencies of EADs and a greater percentage of these cells showed DADs and DAD-induced triggered extra beats following exposure to β-adrenergic stimulation compared with sham. The altered Ca^{2+} regulation of the OVx group was not observed in the OVx+E group.

These findings suggest that long-term deprivation of ovarian hormones in GP leads to changes in myocyte Ca^{2+} handling mechanisms which could produce pro-arrhythmic substrates. 17β-oestradiol replacement prevented these adverse effects suggesting a modulatory role of oestrogen in Ca^{2+} handling.

9.1.4 Effect of OVx on decompensated HF

AC combined with OVx in females was used to test if females lose their better adaptation to pressure-overload than males following long-term ovarian hormone withdrawal. FS was significantly reduced with higher HW/BW and LW/BW ratios in the ACOVx group compared with female AC. The ACOVx group had prolonged APD_{90} similar to that of the female AC group. OVx did not alter peak $I_{Ca,L}$ and inactivation kinetics in AC. The ACOVx group had a larger decline in Ca^{2+} transient amplitudes and SR Ca^{2+} content than the AC females, leading to a more reduced systolic cardiac function. There was more impaired Ca^{2+} uptake function of SERCA in the ACOVX group compared with the AC group which resulted in more prolonged Ca^{2+} transient decay. The ACOVx group also had an increased frequency of spontaneous Ca^{2+} sparks together with greater spark-mediated SR leak compared with the AC group and these changes may contribute to the depletion of SR Ca^{2+} content and may also increase diastolic $[Ca^{2+}]_i$ thus exacerbating diastolic dysfunction and creating a more arrhythmogenic substrate[107,275]. There was reduced Na^+/K^+ ATPase current combined with poorer function in ACOVx group compared with the AC group. The ACOVx group also had larger $I_{Na,L}$ and $I_{Na,L}$-related Na^+ influx compared with the female AC group.

In summary, long-term deprivation of ovarian hormones worsened Ca^{2+} and Na^+ regulation in AC HF GPs. Supplementing ACOVx animals with oestradiol reversed these detrimental effects suggesting that 17β-oestradiol plays an important role in ionic regulation and may offer putative cardiac protection.

9.2 Future direction

This thesis has described a diverse range of changes in *in vivo* and cellular ionic parameters in response to pressure-overload in both male and female GPs. Unequivocally, the work presented here has highlighted areas which require further attention and future investigation. It would be beneficial to measure changes in $[Na^+]_i$ at both the hypertrophy and HF stages to see if there are differences between sexes. $[Na^+]_i$ may be an important link in the transition from compensation to decompensation. The decline in Na^+/K^+ ATPase function and enhanced $I_{Na,L}$ are presumed to contribute towards $[Na^+]_i$ accumulation, however little is known whether there is a positive feedback mechanism between the two proteins. Hoyer *et al*, reported a ouabain-induced increase of $I_{Na,L}$, which was reversed by a CaMKII inhibitor[283], suggesting that the interaction may be dependent on CaMKII.

Future work must also be directed towards using a multi-cellular layer approach. Investigating cardiac slices from the six intervention groups and comparing them with their age-matched sham group would provide valuable structural remodelling and conduction data during disease progression. In addition, whole heart investigation using optical mapping would be ideal to provide more direct whole organ evidence of arrhythmia occurrence in the experimental animals.

The experiments did not carry out OVx combined with AC GP at the cardiac hypertrophy stage, so it would be constructive to complete our knowledge of this experimental group to obtain a more compete view of the effect of OVx at the compensated stage.

Further exploration of the proposed beneficial role of 17β-oestradiol by teasing out the specific pathways involved in oestradiol signalling via ERs (ER α and ER β) and the G protein-coupled ER 1 (GPER)[350], would offer future therapeutic insight for selective drug targeting.

10 BIBLIOGRAPHY

1. Bers D. Excitation-contraction coupling and cardiac contractile force. Springer Science & Business Media; 2001.
2. MacLeod KT. An essential introduction to cardiac electrophysiology. 2014.
3. Grant AO. Cardiac Ion Channels. *Circulation: Arrhythmia and Electrophysiology.* 2009;2(2):185-194.
4. Maltsev VA, Sabbah HN, Higgins RS, Silverman N, Lesch M, Undrovinas AI. Novel, ultraslow inactivating sodium current in human ventricular cardiomyocytes. *Circulation.* 1998;98(23):2545-2552.
5. Remme CA. Cardiac sodium channelopathy associated with SCN5A mutations: electrophysiological, molecular and genetic aspects. *The Journal of physiology.* Sep 01 2013;591(17):4099-4116.
6. Veerman CC, Wilde AA, Lodder EM. The cardiac sodium channel gene SCN5A and its gene product NaV1.5: Role in physiology and pathophysiology. *Gene.* Dec 01 2015;573(2):177-187.
7. Zaklyazminskaya E, Dzemeshkevich S. The role of mutations in the SCN5A gene in cardiomyopathies. *Biochimica et biophysica acta.* Jul 2016;1863(7 Pt B):1799-1805.
8. Findlay I. Is there an A-type K+ current in guinea pig ventricular myocytes? *American journal of physiology. Heart and circulatory physiology.* Feb 2003;284(2):H598-604.
9. Li GR, Yang B, Sun H, Baumgarten CM. Existence of a transient outward K(+) current in guinea pig cardiac myocytes. *American journal of physiology. Heart and circulatory physiology.* Jul 2000;279(1):H130-138.
10. Niwa N, Nerbonne JM. Molecular determinants of cardiac transient outward potassium current (I(to)) expression and regulation. *Journal of molecular and cellular cardiology.* Jan 2010;48(1):12-25.
11. Benitah JP, Alvarez JL, Gomez AM. L-type Ca(2+) current in ventricular cardiomyocytes. *Journal of molecular and cellular cardiology.* 2010;48(1):26-36.
12. Harvey RD, Hell JW. Cav1.2 signaling complexes in the heart. *Journal of molecular and cellular cardiology.* 2013;58:143-152.
13. Bodi I, Mikala G, Koch SE, Akhter SA, Schwartz A. The L-type calcium channel in the heart: the beat goes on. *The Journal of clinical investigation.* 2005;115(12):3306-3317.
14. Hidalgo P, Neely A. Multiplicity of protein interactions and functions of the voltage-gated calcium channel beta-subunit. *Cell calcium.* 2007;42(4-5):389-396.
15. Hartzell HC. Regulation of cardiac ion channels by catecholamines, acetylcholine and second messenger systems. *Progress in biophysics and molecular biology.* 1988;52(3):165-247.
16. Yan X, Gao S, Tang M, Xi J, Gao L, Zhu M, Luo H, Hu X, Zheng Y, Hescheler J, Liang H. Adenylyl cyclase/cAMP-PKA-mediated phosphorylation of basal L-type Ca(2+) channels in mouse embryonic ventricular myocytes. *Cell calcium.* 2011;50(5):433-443.
17. Lemke T, Welling A, Christel CJ, Blaich A, Bernhard D, Lenhardt P, Hofmann F, Moosmang S. Unchanged beta-adrenergic stimulation of cardiac L-type calcium channels in Cav1.2 phosphorylation site S1928A mutant mice. *The Journal of biological chemistry.* 2008;283(50):34738-34744.
18. Fu Y, Westenbroek RE, Scheuer T, Catterall WA. Basal and beta-adrenergic regulation of the cardiac calcium channel CaV1.2 requires phosphorylation of serine

1700. *Proceedings of the National Academy of Sciences of the United States of America.* Nov 18 2014;111(46):16598-16603.
19. Buraei Z, Yang J. Structure and function of the beta subunit of voltage-gated Ca(2+) channels. *Biochimica et biophysica acta.* 2013;1828(7):1530-1540.
20. Findlay I. Physiological modulation of inactivation in L-type Ca(2+) channels: one switch. *The Journal of physiology.* 2004;554(Pt 2):275-283.
21. MacLeod K. *An essential introduction to cardiac electrophysiology.* London, UK: Imperial College Press; 2014.
22. Ravens U, Wettwer E. Ultra-rapid delayed rectifier channels: molecular basis and therapeutic implications. *Cardiovasc Res.* Mar 1 2011;89(4):776-785.
23. Sanguinetti MC. HERG1 channelopathies. *Pflugers Archiv : European journal of physiology.* Jul 2010;460(2):265-276.
24. Jespersen T, Grunnet M, Olesen SP. The KCNQ1 potassium channel: from gene to physiological function. *Physiology.* Dec 2005;20:408-416.
25. Ward OC. The electrocardiographic abnormality in familial cardiac arrhythmia. *Irish journal of medical science.* Nov 1966;6(491):553-557.
26. Spector PS, Curran ME, Zou A, Keating MT, Sanguinetti MC. Fast inactivation causes rectification of the I_{Kr} channel. *The Journal of general physiology.* 1996;107(5):611-619.
27. Dhamoon AS, Jalife J. The inward rectifier current (I_{K1}) controls cardiac excitability and is involved in arrhythmogenesis. *Heart rhythm.* 2005;2(3):316-324.
28. Mackiewicz U, Lewartowski B. Temperature dependent contribution of Ca(2+) transporters to relaxation in cardiac myocytes: important role of sarcolemmal Ca(2+) ATPase. *Journal of physiology and pharmacology : an official journal of the Polish Physiological Society.* 2006;57(1):3-15.
29. Shattock MJ. Phospholemman: its role in normal cardiac physiology and potential as a druggable target in disease. *Current opinion in pharmacology.* 2009;9(2):160-166.
30. Bassani RA, Bassani JW, Bers DM. Mitochondrial and sarcolemmal Ca(2+) transport reduce [Ca2+]i during caffeine contractures in rabbit cardiac myocytes. *The Journal of physiology.* 1992;453:591-608.
31. Ginsburg KS, Weber CR, Bers DM. Cardiac Na/Ca exchanger: dynamics of Ca(2+)-dependent activation and deactivation in intact myocytes. *The Journal of physiology.* 2013;591(8):2067-2086.
32. Verdonck F, Volders PG, Vos MA, Sipido KR. Intracellular Na(+) and altered Na(+) transport mechanisms in cardiac hypertrophy and failure. *Journal of molecular and cellular cardiology.* 2003;35(1):5-25.
33. Aronsen JM, Skogestad J, Lewalle A, Louch WE, Hougen K, Stokke MK, Swift F, Niederer S, Smith NP, Sejersted OM, Sjaastad I. Hypokalaemia induces Ca(2+) overload and Ca(2+) waves in ventricular myocytes by reducing Na/K ATPase alpha2 activity. *The Journal of physiology.* 2015;593(6):1509-1521.
34. Philipson KD, Nicoll DA. Sodium-calcium exchange: a molecular perspective. *Annual review of physiology.* 2000;62:111-133.
35. Cheng H, Lederer WJ, Cannell MB. Calcium sparks: elementary events underlying excitation-contraction coupling in heart muscle. *Science.* 1993;262(5134):740-744.
36. Shiferaw Y, Aistrup GL, Wasserstrom JA. Intracellular Ca(2+) waves, afterdepolarizations, and triggered arrhythmias. *Cardiovascular research.* 2012;95(3):265-268.
37. Gyorke S, Gyorke I, Terentyev D, Viatchenko-Karpinski S, Williams SC. Modulation of sarcoplasmic reticulum calcium release by calsequestrin in cardiac myocytes. *Biological research.* 2004;37(4):603-607.

38. Gyorke I, Gyorke S. Regulation of the cardiac ryanodine receptor channel by luminal Ca(2+) involves luminal Ca(2+) sensing sites. *Biophysical journal.* 1998;75(6):2801-2810.
39. Chen W, Wang R, Chen B, Zhong X, Kong H, Bai Y, Zhou Q, Xie C, Zhang J, Guo A, Tian X, Jones PP, O'Mara ML, Liu Y, Mi T, Zhang L, Bolstad J, Semeniuk L, Cheng H, Zhang J, Chen J, Tieleman DP, Gillis AM, Duff HJ, Fill M, Song LS, Chen SR. The ryanodine receptor store-sensing gate controls Ca(2+) waves and Ca(2+) triggered arrhythmias. *Nature medicine.* 2014;20(2):184-192.
40. Wehrens XH, Lehnart SE, Reiken SR, Marks AR. Ca/calmodulin-dependent protein kinase II phosphorylation regulates the cardiac ryanodine receptor. *Circulation research.* 2004;94(6):e61-70.
41. Satoh H, Blatter LA, Bers DM. Effects of [Ca2+]i, SR Ca(2+) load, and rest on Ca(2+) spark frequency in ventricular myocytes. *The American journal of physiology.* 1997;272(2 Pt 2):H657-668.
42. Jiang D, Xiao B, Yang D, Wang R, Choi P, Zhang L, Cheng H, Chen SR. RyR2 mutations linked to ventricular tachycardia and sudden death reduce the threshold for store-overload-induced Ca(2+) release (SOICR). *Proceedings of the National Academy of Sciences of the United States of America.* 2004;101(35):13062-13067.
43. Kanai R, Ogawa H, Vilsen B, Cornelius F, Toyoshima C. Crystal structure of a Na(+) bound Na/K ATPase preceding the E1P state. *Nature.* 2013;502(7470):201-206.
44. Sweadner KJ, Herrera VL, Amato S, Moellmann A, Gibbons DK, Repke KR. Immunologic identification of Na/K ATPase isoforms in myocardium. Isoform change in deoxycorticosterone acetate-salt hypertension. *Circulation research.* 1994;74(4):669-678.
45. Gao J, Mathias RT, Cohen IS, Baldo GJ. Two functionally different Na/K pumps in cardiac ventricular myocytes. *The Journal of general physiology.* 1995;106(5):995-1030.
46. James PF, Grupp IL, Grupp G, Woo AL, Askew GR, Croyle ML, Walsh RA, Lingrel JB. Identification of a specific role for the Na/K ATPase alpha 2 isoform as a regulator of calcium in the heart. *Molecular cell.* 1999;3(5):555-563.
47. Zahler R, Gilmore-Hebert M, Baldwin JC, Franco K, Benz EJ, Jr. Expression of alpha isoforms of the Na,K-ATPase in human heart. *Biochimica et biophysica acta.* Jul 4 1993;1149(2):189-194.
48. Swift F, Tovsrud N, Enger UH, Sjaastad I, Sejersted OM. The Na/K ATPase alpha2-isoform regulates cardiac contractility in rat cardiomyocytes. *Cardiovascular research.* 2007;75(1):109-117.
49. Despa S, Bers DM. Functional analysis of Na/K ATPase isoform distribution in rat ventricular myocytes. *American journal of physiology. Cell physiology.* 2007;293(1):C321-327.
50. Dostanic I, Schultz Jel J, Lorenz JN, Lingrel JB. The alpha 1 isoform of Na/K ATPase regulates cardiac contractility and functionally interacts and co-localizes with the Na/Ca exchanger in heart. *The Journal of biological chemistry.* 2004;279(52):54053-54061.
51. Swift F, Tovsrud N, Sjaastad I, Sejersted OM, Niggli E, Egger M. Functional coupling of alpha(2)-isoform Na/K ATPase and Ca(2+) extrusion through the Na/Ca exchanger in cardiomyocytes. *Cell calcium.* 2010;48(1):54-60.
52. Levi AJ. The effect of strophanthidin on action potential, calcium current and contraction in isolated guinea-pig ventricular myocytes. *The Journal of physiology.* 1991;443:1-23.

53. Shattock MJ, Matsuura H. Measurement of Na/K pump current in isolated rabbit ventricular myocytes using the whole-cell voltage-clamp technique. Inhibition of the pump by oxidant stress. *Circulation research.* 1993;72(1):91-101.
54. Nakao M, Gadsby DC. [Na+] and [K+] dependence of the Na/K pump current-voltage relationship in guinea pig ventricular myocytes. *The Journal of general physiology.* 1989;94(3):539-565.
55. Glitsch HG. Electrophysiology of the Na/K ATPase in cardiac cells. *Physiol Rev.* 2001;81(4):1791-1826.
56. Bers DM. *Excitation-contraction coupling and cardiac contractile force.* 2nd ed. Dordrecht ; Boston: Kluwer Academic Publishers; 2001.
57. Hong T, Shaw RM. Cardiac T-Tubule Microanatomy and Function. *Physiol Rev.* 2017;97(1):227-252.
58. Fawcett DW, McNutt NS. THE ULTRASTRUCTURE OF THE CAT MYOCARDIUM. *I. Ventricular Papillary Muscle.* 1969;42(1):1-45.
59. Amsellem J, Delorme R, Souchier C, Ojeda C. Transverse-axial tubular system in guinea pig ventricular cardiomyocyte: 3D reconstruction, quantification and its possible role in K(+) accumulation-depletion phenomenon in single cells. *Biology of the cell.* 1995;85(1):43-54.
60. Soeller C, Cannell MB. Examination of the transverse tubular system in living cardiac rat myocytes by 2-photon microscopy and digital image-processing techniques. *Circulation research.* 1999;84(3):266-275.
61. Guo A, Zhang C, Wei S, Chen B, Song LS. Emerging mechanisms of T-tubule remodelling in heart failure. *Cardiovascular research.* 2013;98(2):204-215.
62. Hong T, Yang H, Zhang SS, Cho HC, Kalashnikova M, Sun B, Zhang H, Bhargava A, Grabe M, Olgin J, Gorelik J, Marban E, Jan LY, Shaw RM. Cardiac BIN1 folds T-tubule membrane, controlling ion flux and limiting arrhythmia. *Nature medicine.* 2014;20(6):624-632.
63. Fu Y, Hong T. BIN1 regulates dynamic t-tubule membrane. *Biochimica et biophysica acta.* 2016;1863(7 Pt B):1839-1847.
64. Gorelik J, Wright PT, Lyon AR, Harding SE. Spatial control of the βAR system in heart failure: the transverse tubule and beyond. *Cardiovascular research.* 2013;98(2):216-224.
65. Mohler PJ, Davis JQ, Bennett V. Ankyrin-B Coordinates the Na/K ATPase, Na/Ca Exchanger, and InsP(3) Receptor in a Cardiac T-Tubule/SR Microdomain. *PLoS Biology.* 2005;3(12):e423.
66. Mozaffarian D, Benjamin EJ, Go AS, Arnett DK, Blaha MJ, Cushman M, Das SR, de Ferranti S, Despres JP, Fullerton HJ, Howard VJ, Huffman MD, Isasi CR, Jimenez MC, Judd SE, Kissela BM, Lichtman JH, Lisabeth LD, Liu S, Mackey RH, Magid DJ, McGuire DK, Mohler ER, 3rd, Moy CS, Muntner P, Mussolino ME, Nasir K, Neumar RW, Nichol G, Palaniappan L, Pandey DK, Reeves MJ, Rodriguez CJ, Rosamond W, Sorlie PD, Stein J, Towfighi A, Turan TN, Virani SS, Woo D, Yeh RW, Turner MB. Heart Disease and Stroke Statistics-2016 Update: A Report From the American Heart Association. *Circulation.* 2016;133(4):e38-360.
67. MacLeod KT. Recent advances in understanding cardiac contractility in health and disease. *F1000Research.* 2016;5.
68. Bers DM. Calcium cycling and signaling in cardiac myocytes. *Annual review of physiology.* 2008;70:23-49.
69. Milani RV, Drazner MH, Lavie CJ, Morin DP, Ventura HO. Progression from concentric left ventricular hypertrophy and normal ejection fraction to left ventricular dysfunction. *The American journal of cardiology.* 2011;108(7):992-996.

70. Sugden PH, Clerk A. Activation of the small GTP-binding protein Ras in the heart by hypertrophic agonists. *Trends in cardiovascular medicine.* 2000;10(1):1-8.
71. Molkentin JD. Calcineurin and beyond: cardiac hypertrophic signaling. *Circulation research.* 2000;87(9):731-738.
72. Bers DM, Despa S, Bossuyt J. Regulation of Ca(2+) and Na(+) in normal and failing cardiac myocytes. *Annals of the New York Academy of Sciences.* 2006;1080:165-177.
73. Louch WE, Hake J, Jolle GF, Mork HK, Sjaastad I, Lines GT, Sejersted OM. Control of Ca2+ release by action potential configuration in normal and failing murine cardiomyocytes. *Biophysical journal.* Sep 8 2010;99(5):1377-1386.
74. Beuckelmann DJ, Nabauer M, Erdmann E. Intracellular calcium handling in isolated ventricular myocytes from patients with terminal heart failure. *Circulation.* Mar 1992;85(3):1046-1055.
75. Beuckelmann DJ, Nabauer M, Erdmann E. Alterations of K+ currents in isolated human ventricular myocytes from patients with terminal heart failure. *Circ Res.* Aug 1993;73(2):379-385.
76. Kaab S, Nuss HB, Chiamvimonvat N, O'Rourke B, Pak PH, Kass DA, Marban E, Tomaselli GF. Ionic mechanism of action potential prolongation in ventricular myocytes from dogs with pacing-induced heart failure. *Circ Res.* Feb 1996;78(2):262-273.
77. Kaab S, Dixon J, Duc J, Ashen D, Nabauer M, Beuckelmann DJ, Steinbeck G, McKinnon D, Tomaselli GF. Molecular basis of transient outward potassium current downregulation in human heart failure: a decrease in Kv4.3 mRNA correlates with a reduction in current density. *Circulation.* Oct 6 1998;98(14):1383-1393.
78. Nabauer M, Beuckelmann DJ, Uberfuhr P, Steinbeck G. Regional differences in current density and rate-dependent properties of the transient outward current in subepicardial and subendocardial myocytes of human left ventricle. *Circulation.* Jan 1 1996;93(1):168-177.
79. Janse MJ. Electrophysiological changes in heart failure and their relationship to arrhythmogenesis. *Cardiovascular research.* 2004;61(2):208-217.
80. Eisner D, Bode E, Venetucci L, Trafford A. Calcium flux balance in the heart. *Journal of molecular and cellular cardiology.* 2013;58:110-117.
81. Weiss JN, Garfinkel A, Karagueuzian HS, Chen PS, Qu Z. Early afterdepolarizations and cardiac arrhythmias. *Heart rhythm.* 2010;7(12):1891-1899.
82. Wickenden AD, Kaprielian R, Kassiri Z, Tsoporis JN, Tsushima R, Fishman GI, Backx PH. The role of action potential prolongation and altered intracellular calcium handling in the pathogenesis of heart failure. *Cardiovascular research.* 1998;37(2):312-323.
83. Piacentino V, 3rd, Weber CR, Chen X, Weisser-Thomas J, Margulies KB, Bers DM, Houser SR. Cellular basis of abnormal calcium transients of failing human ventricular myocytes. *Circulation research.* 2003;92(6):651-658.
84. Hobai IA, O'Rourke B. Decreased sarcoplasmic reticulum calcium content is responsible for defective excitation-contraction coupling in canine heart failure. *Circulation.* 2001;103(11):1577-1584.
85. Mukherjee R, Spinale FG. L-type calcium channel abundance and function with cardiac hypertrophy and failure: a review. *Journal of molecular and cellular cardiology.* 1998;30(10):1899-1916.
86. Terracciano CM, Harding SE, Adamson D, Koban M, Tansley P, Birks EJ, Barton PJ, Yacoub MH. Changes in sarcolemmal Ca(2+) entry and sarcoplasmic reticulum Ca(2+) content in ventricular myocytes from patients with end-stage heart failure

following myocardial recovery after combined pharmacological and ventricular assist device therapy. *European heart journal.* 2003;24(14):1329-1339.
87. Pogwizd SM, Schlotthauer K, Li L, Yuan W, Bers DM. Arrhythmogenesis and contractile dysfunction in heart failure: Roles of sodium-calcium exchange, inward rectifier potassium current, and residual beta-adrenergic responsiveness. *Circulation research.* 2001;88(11):1159-1167.
88. Winslow RL, Rice J, Jafri S, Marban E, O'Rourke B. Mechanisms of altered excitation-contraction coupling in canine tachycardia-induced heart failure, II: model studies. *Circulation research.* 1999;84(5):571-586.
89. Despa S, Bers DM. Na(+) transport in the normal and failing heart - remember the balance. *Journal of molecular and cellular cardiology.* 2013;61:2-10.
90. Schwinger RH, Wang J, Frank K, Muller-Ehmsen J, Brixius K, McDonough AA, Erdmann E. Reduced sodium pump alpha1, alpha3, and beta1-isoform protein levels and Na/K ATPase activity but unchanged Na/Ca exchanger protein levels in human heart failure. *Circulation.* 1999;99(16):2105-2112.
91. Gupta RC, Mishra S, Wang M, Jiang A, Rastogi S, Rousso B, Mika Y, Sabbah HN. Cardiac contractility modulation electrical signals normalize activity, expression, and phosphorylation of the Na/Ca exchanger in heart failure. *Journal of cardiac failure.* 2009;15(1):48-56.
92. Kiss E, Ball NA, Kranias EG, Walsh RA. Differential changes in cardiac phospholamban and sarcoplasmic reticular Ca(2+) ATPase protein levels. Effects on Ca(2+) transport and mechanics in compensated pressure-overload hypertrophy and congestive heart failure. *Circulation research.* 1995;77(4):759-764.
93. Qi M, Shannon TR, Euler DE, Bers DM, Samarel AM. Downregulation of sarcoplasmic reticulum Ca(2+) ATPase during progression of left ventricular hypertrophy. *The American journal of physiology.* 1997;272(5 Pt 2):H2416-2424.
94. Byrne MJ, Power JM, Preovolos A, Mariani JA, Hajjar RJ, Kaye DM. Recirculating cardiac delivery of AAV2/1SERCA2a improves myocardial function in an experimental model of heart failure in large animals. *Gene therapy.* 2008;15(23):1550-1557.
95. Arai M, Suzuki T, Nagai R. Sarcoplasmic reticulum genes are upregulated in mild cardiac hypertrophy but downregulated in severe cardiac hypertrophy induced by pressure overload. *Journal of molecular and cellular cardiology.* 1996;28(8):1583-1590.
96. Feldman AM, Weinberg EO, Ray PE, Lorell BH. Selective changes in cardiac gene expression during compensated hypertrophy and the transition to cardiac decompensation in rats with chronic aortic banding. *Circulation research.* 1993;73(1):184-192.
97. Huang B, Wang S, Qin D, Boutjdir M, El-Sherif N. Diminished basal phosphorylation level of phospholamban in the postinfarction remodeled rat ventricle: role of beta-adrenergic pathway, G(i) protein, phosphodiesterase, and phosphatases. *Circulation research.* 1999;85(9):848-855.
98. Papolos A, Frishman WH. Sarcoendoplasmic reticulum calcium transport ATPase 2a: a potential gene therapy target in heart failure. *Cardiology in review.* 2013;21(3):151-154.
99. Greenberg B, Yaroshinsky A, Zsebo KM, Butler J, Felker GM, Voors AA, Rudy JJ, Wagner K, Hajjar RJ. Design of a Phase 2b Trial of Intracoronary Administration of AAV1/SERCA2a in Patients With Advanced Heart Failure: The CUPID 2 Trial (Calcium Up-Regulation by Percutaneous Administration of Gene Therapy in Cardiac Disease Phase 2b). *JACC. Heart failure.* 2014;2(1):84-92.

100. Prunier F, Kawase Y, Gianni D, Scapin C, Danik SB, Ellinor PT, Hajjar RJ, Del Monte F. Prevention of ventricular arrhythmias with sarcoplasmic reticulum Ca(2+) ATPase pump overexpression in a porcine model of ischemia reperfusion. *Circulation.* 2008;118(6):614-624.
101. Greenberg B, Butler J, Felker GM, Ponikowski P, Voors AA, Desai AS, Barnard D, Bouchard A, Jaski B, Lyon AR, Pogoda JM, Rudy JJ, Zsebo KM. Calcium upregulation by percutaneous administration of gene therapy in patients with cardiac disease (CUPID 2): a randomised, multinational, double-blind, placebo-controlled, phase 2b trial. *Lancet.* 2016;387(10024):1178-1186.
102. Rincon MY, VandenDriessche T, Chuah MK. Gene therapy for cardiovascular disease: advances in vector development, targeting, and delivery for clinical translation. *Cardiovascular research.* 2015;108(1):4-20.
103. Hasenfuss G. Alterations of calcium-regulatory proteins in heart failure. *Cardiovascular research.* 1998;37(2):279-289.
104. Pogwizd SM, Qi M, Yuan W, Samarel AM, Bers DM. Upregulation of Na/Ca exchanger expression and function in an arrhythmogenic rabbit model of heart failure. *Circulation research.* 1999;85(11):1009-1019.
105. Studer R, Reinecke H, Bilger J, Eschenhagen T, Bohm M, Hasenfuss G, Just H, Holtz J, Drexler H. Gene expression of the cardiac Na/Ca exchanger in end-stage human heart failure. *Circulation research.* 1994;75(3):443-453.
106. Hasenfuss G, Schillinger W, Lehnart SE, Preuss M, Pieske B, Maier LS, Prestle J, Minami K, Just H. Relationship between Na/Ca exchanger protein levels and diastolic function of failing human myocardium. *Circulation.* 1999;99(5):641-648.
107. Shannon TR, Pogwizd SM, Bers DM. Elevated sarcoplasmic reticulum Ca(2+) leak in intact ventricular myocytes from rabbits in heart failure. *Circulation research.* 2003;93(7):592-594.
108. Wehrens XH, Lehnart SE, Reiken S, Vest JA, Wronska A, Marks AR. Ryanodine receptor/calcium release channel PKA phosphorylation: a critical mediator of heart failure progression. *Proceedings of the National Academy of Sciences of the United States of America.* 2006;103(3):511-518.
109. Marx SO, Reiken S, Hisamatsu Y, Jayaraman T, Burkhoff D, Rosemblit N, Marks AR. PKA phosphorylation dissociates FKBP12.6 from the calcium release channel (ryanodine receptor): defective regulation in failing hearts. *Cell.* May 12 2000;101(4):365-376.
110. Ai X, Curran JW, Shannon TR, Bers DM, Pogwizd SM. Ca/calmodulin-dependent protein kinase modulates cardiac ryanodine receptor phosphorylation and sarcoplasmic reticulum Ca(2+) leak in heart failure. *Circulation research.* 2005;97(12):1314-1322.
111. Horvath B, Banyasz T, Jian Z, Hegyi B, Kistamas K, Nanasi PP, Izu LT, Chen-Izu Y. Dynamics of the late Na(+) current during cardiac action potential and its contribution to afterdepolarizations. *Journal of molecular and cellular cardiology.* 2013;64:59-68.
112. Chorvatova A, Snowdon R, Hart G, Hussain M. Effects of pressure overload-induced hypertrophy on TTX-sensitive inward currents in guinea pig left ventricle. *Molecular and cellular biochemistry.* 2004;261(1-2):217-226.
113. Aistrup GL, Gupta DK, Kelly JE, O'Toole MJ, Nahhas A, Chirayil N, Misener S, Beussink L, Singh N, Ng J, Reddy M, Mongkolrattanothai T, El-Bizri N, Rajamani S, Shryock JC, Belardinelli L, Shah SJ, Wasserstrom JA. Inhibition of the late sodium current slows t-tubule disruption during the progression of hypertensive heart disease in the rat. *American journal of physiology. Heart and circulatory physiology.* 2013;305(7):H1068-1079.

114. Gray RP, McIntyre H, Sheridan DS, Fry CH. Intracellular sodium and contractile function in hypertrophied human and guinea-pig myocardium. *Pflugers Archiv : European journal of physiology.* 2001;442(1):117-123.
115. Jelicks LA, Siri FM. Effects of hypertrophy and heart failure on [Na+]i in pressure-overloaded guinea pig heart. *American journal of hypertension.* 1995;8(9):934-943.
116. Despa S, Islam MA, Weber CR, Pogwizd SM, Bers DM. Intracellular Na(+) concentration is elevated in heart failure but Na/K pump function is unchanged. *Circulation.* 2002;105(21):2543-2548.
117. Pieske B, Maier LS, Piacentino V, 3rd, Weisser J, Hasenfuss G, Houser S. Rate dependence of [Na+]i and contractility in nonfailing and failing human myocardium. *Circulation.* 2002;106(4):447-453.
118. Baartscheer A, Schumacher CA, van Borren MM, Belterman CN, Coronel R, Fiolet JW. Increased Na/H exchange activity is the cause of increased [Na+]i and underlies disturbed calcium handling in the rabbit pressure and volume overload heart failure model. *Cardiovascular research.* 2003;57(4):1015-1024.
119. Schillinger W, Teucher N, Christians C, Kohlhaas M, Sossalla S, Van Nguyen P, Schmidt AG, Schunck O, Nebendahl K, Maier LS, Zeitz O, Hasenfuss G. High intracellular Na(+) preserves myocardial function at low heart rates in isolated myocardium from failing hearts. *European journal of heart failure.* 2006;8(7):673-680.
120. Fisch C, Knoebel SB. Digitalis cardiotoxicity. *Journal of the American College of Cardiology.* 1985;5(5 Suppl A):91a-98a.
121. Pitt B. Whither withering? The role of digoxin in patients with heart failure due to systolic left ventricular dysfunction in sinus rhythm. *Journal of cardiac failure.* 2006;12(5):347-348.
122. Allen PD, Schmidt TA, Marsh JD, Kjeldsen K. Na/K ATPase expression in normal and failing human left ventricle. *Basic research in cardiology.* 1992;87 Suppl 1:87-94.
123. Bossuyt J, Ai X, Moorman JR, Pogwizd SM, Bers DM. Expression and phosphorylation of the Na(+) pump regulatory subunit phospholemman in heart failure. *Circulation research.* 2005;97(6):558-565.
124. Trouve P, Carre F, Belikova I, Leclercq C, Dakhli T, Soufir L, Coquard I, Ramirez-Gil J, Charlemagne D. Na/K ATPase alpha2-isoform expression in guinea pig hearts during transition from compensation to decompensation. *American journal of physiology. Heart and circulatory physiology.* 2000;279(4):H1972-1981.
125. Verdonck F, Volders PG, Vos MA, Sipido KR. Increased Na(+) concentration and altered Na/K pump activity in hypertrophied canine ventricular cells. *Cardiovascular research.* 2003;57(4):1035-1043.
126. Semb SO, Lunde PK, Holt E, Tonnessen T, Christensen G, Sejersted OM. Reduced myocardial Na/K pump capacity in congestive heart failure following myocardial infarction in rats. *Journal of molecular and cellular cardiology.* 1998;30(7):1311-1328.
127. Louch WE, Hougen K, Mork HK, Swift F, Aronsen JM, Sjaastad I, Reims HM, Roald B, Andersson KB, Christensen G, Sejersted OM. Sodium accumulation promotes diastolic dysfunction in end-stage heart failure following SERCA2a knockout. *The Journal of physiology.* 2010;588(Pt 3):465-478.
128. Boguslavskyi A, Pavlovic D, Aughton K, Clark JE, Howie J, Fuller W, Shattock MJ. Cardiac hypertrophy in mice expressing unphosphorylatable phospholemman. *Cardiovascular research.* 2014;104(1):72-82.
129. El-Armouche A, Wittkopper K, Fuller W, Howie J, Shattock MJ, Pavlovic D. Phospholemman-dependent regulation of the cardiac Na/K ATPase activity is

modulated by inhibitor-1 sensitive type-1 phosphatase. *FASEB journal : official publication of the Federation of American Societies for Experimental Biology.* 2011;25(12):4467-4475.
130. Kiyosue T, Arita M. Late sodium current and its contribution to action potential configuration in guinea pig ventricular myocytes. *Circulation research.* 1989;64(2):389-397.
131. Noble D, Noble PJ. Late sodium current in the pathophysiology of cardiovascular disease: consequences of sodium–calcium overload. *Heart.* 2006;92(Suppl 4):iv1-iv5.
132. Valdivia CR, Chu WW, Pu J, Foell JD, Haworth RA, Wolff MR, Kamp TJ, Makielski JC. Increased late sodium current in myocytes from a canine heart failure model and from failing human heart. *Journal of molecular and cellular cardiology.* 2005;38(3):475-483.
133. Maier LS. New treatment options for late Na(+) current, arrhythmias, and diastolic dysfunction. *Current heart failure reports.* 2012;9(3):183-191.
134. Sossalla S, Wagner S, Rasenack EC, Ruff H, Weber SL, Schondube FA, Tirilomis T, Tenderich G, Hasenfuss G, Belardinelli L, Maier LS. Ranolazine improves diastolic dysfunction in isolated myocardium from failing human hearts--role of late sodium current and intracellular ion accumulation. *Journal of molecular and cellular cardiology.* 2008;45(1):32-43.
135. Zaza A, Belardinelli L, Shryock JC. Pathophysiology and pharmacology of the cardiac "late sodium current.". *Pharmacology & therapeutics.* 2008;119(3):326-339.
136. Linz KW, Meyer R. Control of L-type calcium current during the action potential of guinea-pig ventricular myocytes. *The Journal of physiology.* 1998;513 (Pt 2):425-442.
137. Banyasz T, Horvath B, Jian Z, Izu LT, Chen-Izu Y. Profile of L-type Ca(2+) current and Na/Ca exchange current during cardiac action potential in ventricular myocytes. *Heart rhythm.* 2012;9(1):134-142.
138. Maltsev VA, Undrovinas A. Late sodium current in failing heart: friend or foe? *Progress in biophysics and molecular biology.* Jan-Apr 2008;96(1-3):421-451.
139. Undrovinas NA, Maltsev VA, Belardinelli L, Sabbah HN, Undrovinas A. Late sodium current contributes to diastolic cell Ca(2+) accumulation in chronic heart failure. *The journal of physiological sciences : JPS.* 2010;60(4):245-257.
140. Coppini R, Ferrantini C, Yao L, Fan P, Del Lungo M, Stillitano F, Sartiani L, Tosi B, Suffredini S, Tesi C, Yacoub M, Olivotto I, Belardinelli L, Poggesi C, Cerbai E, Mugelli A. Late sodium current inhibition reverses electromechanical dysfunction in human hypertrophic cardiomyopathy. *Circulation.* 2013;127(5):575-584.
141. Maltsev VA, Reznikov V, Undrovinas NA, Sabbah HN, Undrovinas A. Modulation of late sodium current by Ca(2+), calmodulin, and CaMKII in normal and failing dog cardiomyocytes: similarities and differences. *American journal of physiology. Heart and circulatory physiology.* 2008;294(4):H1597-1608.
142. Glynn P, Musa H, Wu X, Unudurthi SD, Little S, Qian L, Wright PJ, Radwanski PB, Gyorke S, Mohler PJ, Hund TJ. Voltage-Gated Sodium Channel Phosphorylation at Ser-571 Regulates Late Current, Arrhythmia, and Cardiac Function In Vivo. *Circulation.* 2015;132(7):567-577.
143. Koval OM, Snyder JS, Wolf RM, Pavlovicz RE, Glynn P, Curran J, Leymaster ND, Dun W, Wright PJ, Cardona N, Qian L, Mitchell CC, Boyden PA, Binkley PF, Li C, Anderson ME, Mohler PJ, Hund TJ. Ca/calmodulin-dependent protein kinase II-based regulation of voltage-gated Na(+) channel in cardiac disease. *Circulation.* 2012;126(17):2084-2094.
144. Antzelevitch C, Belardinelli L, Zygmunt AC, Burashnikov A, Di Diego JM, Fish JM, Cordeiro JM, Thomas G. Electrophysiological effects of ranolazine, a novel

antianginal agent with antiarrhythmic properties. *Circulation.* Aug 24 2004;110(8):904-910.
145. Kohlhaas M, Liu T, Knopp A, Zeller T, Ong MF, Bohm M, O'Rourke B, Maack C. Elevated cytosolic Na(+) increases mitochondrial formation of reactive oxygen species in failing cardiac myocytes. *Circulation.* 2010;121(14):1606-1613.
146. Maack C, Cortassa S, Aon MA, Ganesan AN, Liu T, O'Rourke B. Elevated cytosolic Na(+) decreases mitochondrial Ca(2+) uptake during excitation-contraction coupling and impairs energetic adaptation in cardiac myocytes. *Circulation research.* 2006;99(2):172-182.
147. Bay J, Kohlhaas M, Maack C. Intracellular Na(+) and cardiac metabolism. *Journal of molecular and cellular cardiology.* 2013;61:20-27.
148. Liao Y, Cooper RS, Mensah GA, McGee DL. Left ventricular hypertrophy has a greater impact on survival in women than in men. *Circulation.* 1995;92(4):805-810.
149. Liu T, Takimoto E, Dimaano VL, DeMazumder D, Kettlewell S, Smith G, Sidor A, Abraham TP, O'Rourke B. Inhibiting mitochondrial Na/Ca exchange prevents sudden death in a Guinea pig model of heart failure. *Circulation research.* 2014;115(1):44-54.
150. Yusuf S, Pitt B, Davis CE, Hood WB, Cohn JN. Effect of enalapril on survival in patients with reduced left ventricular ejection fractions and congestive heart failure. *The New England journal of medicine.* 1991;325(5):293-302.
151. Hool LC, Whalley DW, Doohan MM, Rasmussen HH. Angiotensin-converting enzyme inhibition, intracellular Na(+), and Na/K pumping in cardiac myocytes. *The American journal of physiology.* 1995;268(2 Pt 1):C366-375.
152. Maron BJ, Ferrans VJ, Roberts WC. Ultrastructural features of degenerated cardiac muscle cells in patients with cardiac hypertrophy. *The American journal of pathology.* Jun 1975;79(3):387-434.
153. Ibrahim M, Terracciano CM. Reversibility of T-tubule remodelling in heart failure: mechanical load as a dynamic regulator of the T-tubules. *Cardiovascular research.* 2013;98(2):225-232.
154. Hong TT, Smyth JW, Gao D, Chu KY, Vogan JM, Fong TS, Jensen BC, Colecraft HM, Shaw RM. BIN1 localizes the L-type calcium channel to cardiac T-tubules. *PLoS Biol.* 2010;8(2):e1000312.
155. Ibrahim M, Siedlecka U, Buyandelger B, Harada M, Rao C, Moshkov A, Bhargava A, Schneider M, Yacoub MH, Gorelik J, Knoll R, Terracciano CM. A critical role for Telethonin in regulating t-tubule structure and function in the mammalian heart. *Human molecular genetics.* 2013;22(2):372-383.
156. Galbiati F, Engelman JA, Volonte D, Zhang XL, Minetti C, Li M, Hou H, Jr., Kneitz B, Edelmann W, Lisanti MP. Caveolin-3 null mice show a loss of caveolae, changes in the microdomain distribution of the dystrophin-glycoprotein complex, and t-tubule abnormalities. *The Journal of biological chemistry.* 2001;276(24):21425-21433.
157. Schirmer SH, Hohl M, Bohm M. Gender differences in heart failure: paving the way towards personalized medicine? *European heart journal.* 2010;31(10):1165-1167.
158. Perez-Lopez FR, Larrad-Mur L, Kallen A, Chedraui P, Taylor HS. Gender differences in cardiovascular disease: hormonal and biochemical influences. *Reproductive sciences.* 2010;17(6):511-531.
159. Roger VL, Go AS, Lloyd-Jones DM, Adams RJ, Berry JD, Brown TM, Carnethon MR, Dai S, de Simone G, Ford ES, Fox CS, Fullerton HJ, Gillespie C, Greenlund KJ, Hailpern SM, Heit JA, Ho PM, Howard VJ, Kissela BM, Kittner SJ, Lackland DT, Lichtman JH, Lisabeth LD, Makuc DM, Marcus GM, Marelli A, Matchar DB, McDermott MM, Meigs JB, Moy CS, Mozaffarian D, Mussolino ME, Nichol G, Paynter NP, Rosamond WD, Sorlie PD, Stafford RS, Turan TN, Turner MB, Wong

ND, Wylie-Rosett J. Heart disease and stroke statistics--2011 update: a report from the American Heart Association. *Circulation.* 2011;123(4):e18-e209.
160. Cleland JG, Swedberg K, Follath F, Komajda M, Cohen-Solal A, Aguilar JC, Dietz R, Gavazzi A, Hobbs R, Korewicki J, Madeira HC, Moiseyev VS, Preda I, van Gilst WH, Widimsky J, Freemantle N, Eastaugh J, Mason J, Study Group on Diagnosis of the Working Group on Heart Failure of the European Society of C. The EuroHeart Failure survey programme--a survey on the quality of care among patients with heart failure in Europe. Part 1: patient characteristics and diagnosis. *European heart journal.* 2003;24(5):442-463.
161. Nieminen MS, Harjola VP, Hochadel M, Drexler H, Komajda M, Brutsaert D, Dickstein K, Ponikowski P, Tavazzi L, Follath F, Lopez-Sendon JL. Gender related differences in patients presenting with acute heart failure. Results from EuroHeart Failure Survey II. *European journal of heart failure.* 2008;10(2):140-148.
162. Gori M, Lam CS, Gupta DK, Santos AB, Cheng S, Shah AM, Claggett B, Zile MR, Kraigher-Krainer E, Pieske B, Voors AA, Packer M, Bransford T, Lefkowitz M, McMurray JJ, Solomon SD. Sex-specific cardiovascular structure and function in heart failure with preserved ejection fraction. *European journal of heart failure.* 2014.
163. The survival of patients with heart failure with preserved or reduced left ventricular ejection fraction: an individual patient data meta-analysis. *European heart journal.* 2012;33(14):1750-1757.
164. Lenzen MJ, Rosengren A, Scholte op Reimer WJ, Follath F, Boersma E, Simoons ML, Cleland JG, Komajda M. Management of patients with heart failure in clinical practice: differences between men and women. *Heart.* 2008;94(3):e10.
165. Alehagen U, Ericsson A, Dahlstrom U. Are there any significant differences between females and males in the management of heart failure? Gender aspects of an elderly population with symptoms associated with heart failure. *Journal of cardiac failure.* 2009;15(6):501-507.
166. Jimenez-Navarro MF, Ramirez-Marrero MA, Anguita-Sanchez M, Castillo JC. Influence of gender on long-term prognosis of patients with chronic heart failure seen in heart failure clinics. *Clinical cardiology.* 2010;33(3):E13-18.
167. Shin JJ, Hamad E, Murthy S, Pina IL. Heart failure in women. *Clinical cardiology.* 2012;35(3):172-177.
168. Hsich EM, Pina IL. Heart failure in women: a need for prospective data. *Journal of the American College of Cardiology.* 2009;54(6):491-498.
169. Rho RW, Patton KK, Poole JE, Cleland JG, Shadman R, Anand I, Maggioni AP, Carson PE, Swedberg K, Levy WC. Important differences in mode of death between men and women with heart failure who would qualify for a primary prevention implantable cardioverter-defibrillator. *Circulation.* 2012;126(20):2402-2407.
170. Rodriguez F, Wang Y, Johnson CE, Foody JM. National patterns of heart failure hospitalizations and mortality by sex and age. *Journal of cardiac failure.* 2013;19(8):542-549.
171. Ho KK, Anderson KM, Kannel WB, Grossman W, Levy D. Survival after the onset of congestive heart failure in Framingham Heart Study subjects. *Circulation.* 1993;88(1):107-115.
172. Adams KF, Jr., Sueta CA, Gheorghiade M, O'Connor CM, Schwartz TA, Koch GG, Uretsky B, Swedberg K, McKenna W, Soler-Soler J, Califf RM. Gender differences in survival in advanced heart failure. Insights from the FIRST study. *Circulation.* 1999;99(14):1816-1821.

173. Greiten LE, Holditch SJ, Arunachalam SP, Miller VM. Should there be sex-specific criteria for the diagnosis and treatment of heart failure? *Journal of cardiovascular translational research.* 2014;7(2):139-155.
174. Barsheshet A, Brenyo A, Goldenberg I, Moss AJ. Sex-related differences in patients' responses to heart failure therapy. *Nature reviews. Cardiology.* 2012;9(4):234-242.
175. Murphy E. Estrogen signaling and cardiovascular disease. *Circulation research.* 2011;109(6):687-696.
176. Wang YC, Xiao XL, Li N, Yang D, Xing Y, Huo R, Liu MY, Zhang YQ, Dong DL. Oestrogen inhibits BMP4-induced BMP4 expression in cardiomyocytes: a potential mechanism of oestrogen-mediated protection against cardiac hypertrophy. *British journal of pharmacology.* 2015;172(23):5586-5595.
177. Bell JR, Bernasochi GB, Varma U, Raaijmakers AJ, Delbridge LM. Sex and sex hormones in cardiac stress--mechanistic insights. *The Journal of steroid biochemistry and molecular biology.* 2013;137:124-135.
178. Mendelsohn ME, Karas RH. The protective effects of estrogen on the cardiovascular system. *The New England journal of medicine.* 1999;340(23):1801-1811.
179. Regitz-Zagrosek V, Oertelt-Prigione S, Seeland U, Hetzer R. Sex and Gender Differences in Myocardial Hypertrophy and Heart Failure. *Circulation Journal.* 2010;74(7):1265-1273.
180. Wang Y, Wang Q, Zhao Y, Gong D, Wang D, Li C, Zhao H. Protective effects of estrogen against reperfusion arrhythmias following severe myocardial ischemia in rats. *Circulation journal : official journal of the Japanese Circulation Society.* 2010;74(4):634-643.
181. Sourander L, Rajala T, Raiha I, Makinen J, Erkkola R, Helenius H. Cardiovascular and cancer morbidity and mortality and sudden cardiac death in postmenopausal women on oestrogen replacement therapy (ERT). *Lancet.* 1998;352(9145):1965-1969.
182. Dogan M, Yiginer O, Uz O, Kucuk U, Degirmencioglu G, Isilak Z, Uzun M, Davulcu E. The Effects of Female Sex Hormones on Ventricular Premature Beats and Repolarization Parameters in Physiological Menstrual Cycle. *Pacing and clinical electrophysiology : PACE.* 2016;39(5):418-426.
183. Hu X, Wang J, Xu C, He B, Lu Z, Jiang H. Effect of oestrogen replacement therapy on idiopathic outflow tract ventricular arrhythmias in postmenopausal women. *Archives of cardiovascular diseases.* 2011;104(2):84-88.
184. Kravtsov GM, Kam KW, Liu J, Wu S, Wong TM. Altered Ca(2+) handling by ryanodine receptor and Na/Ca exchange in the heart from ovariectomized rats: role of protein kinase A. *American journal of physiology. Cell physiology.* 2007;292(5):C1625-1635.
185. Bupha-Intr T, Wattanapermpool J. Regulatory role of ovarian sex hormones in calcium uptake activity of cardiac sarcoplasmic reticulum. *American journal of physiology. Heart and circulatory physiology.* 2006;291(3):H1101-1108.
186. Fares E, Parks RJ, Macdonald JK, Egar JM, Howlett SE. Ovariectomy enhances SR Ca(2+) release and increases Ca(2+) spark amplitudes in isolated ventricular myocytes. *Journal of molecular and cellular cardiology.* 2012;52(1):32-42.
187. Teplitz L, Igic R, Berbaum ML, Schwertz DW. Sex differences in susceptibility to epinephrine-induced arrhythmias. *Journal of cardiovascular pharmacology.* 2005;46(4):548-555.
188. Curl CL, Wendt IR, Canny BJ, Kotsanas G. Effects of ovariectomy and 17beta-oestradiol replacement on [Ca2+]i in female rat cardiac myocytes. *Clinical and experimental pharmacology & physiology.* 2003;30(7):489-494.

189. Wu Q, Zhao Z, Sun H, Hao YL, Yan CD, Gu SL. Oestrogen changed cardiomyocyte contraction and beta-adrenoceptor expression in rat hearts subjected to ischaemia-reperfusion. *Experimental physiology.* 2008;93(9):1034-1043.
190. Bupha-Intr T, Wattanapermpool J, Pena JR, Wolska BM, Solaro RJ. Myofilament response to Ca(2+) and Na/H exchanger activity in sex hormone-related protection of cardiac myocytes from deactivation in hypercapnic acidosis. *American journal of physiology. Regulatory, integrative and comparative physiology.* 2007;292(2):R837-843.
191. Ren J, Hintz KK, Roughead ZK, Duan J, Colligan PB, Ren BH, Lee KJ, Zeng H. Impact of estrogen replacement on ventricular myocyte contractile function and protein kinase B/Akt activation. *American journal of physiology. Heart and circulatory physiology.* 2003;284(5):H1800-1807.
192. Rossouw JE, Anderson GL, Prentice RL, LaCroix AZ, Kooperberg C, Stefanick ML, Jackson RD, Beresford SA, Howard BV, Johnson KC, Kotchen JM, Ockene J. Risks and benefits of estrogen plus progestin in healthy postmenopausal women: principal results From the Women's Health Initiative randomized controlled trial. *JAMA : the journal of the American Medical Association.* 2002;288(3):321-333.
193. Schierbeck LL, Rejnmark L, Tofteng CL, Stilgren L, Eiken P, Mosekilde L, Kober L, Jensen JE. Effect of hormone replacement therapy on cardiovascular events in recently postmenopausal women: randomised trial. *BMJ (Clinical research ed.).* 2012;345:e6409.
194. Skavdahl M, Steenbergen C, Clark J, Myers P, Demianenko T, Mao L, Rockman HA, Korach KS, Murphy E. Estrogen receptor-beta mediates male-female differences in the development of pressure overload hypertrophy. *American journal of physiology. Heart and circulatory physiology.* 2005;288(2):H469-476.
195. Xin HB, Senbonmatsu T, Cheng DS, Wang YX, Copello JA, Ji GJ, Collier ML, Deng KY, Jeyakumar LH, Magnuson MA, Inagami T, Kotlikoff MI, Fleischer S. Oestrogen protects FKBP12.6 null mice from cardiac hypertrophy. *Nature.* 2002;416(6878):334-338.
196. Ma Y, Cheng WT, Wu S, Wong TM. Oestrogen confers cardioprotection by suppressing Ca/calmodulin-dependent protein kinase II. *British journal of pharmacology.* 2009;157(5):705-715.
197. Kararigas G, Fliegner D, Gustafsson JA, Regitz-Zagrosek V. Role of the estrogen/estrogen-receptor-beta axis in the genomic response to pressure overload-induced hypertrophy. *Physiological genomics.* 2011;43(8):438-446.
198. Bernardo BC, Weeks KL, Pretorius L, McMullen JR. Molecular distinction between physiological and pathological cardiac hypertrophy: experimental findings and therapeutic strategies. *Pharmacology & therapeutics.* 2010;128(1):191-227.
199. Odening KE, Koren G. How do sex hormones modify arrhythmogenesis in long QT syndrome? Sex hormone effects on arrhythmogenic substrate and triggered activity. *Heart rhythm.* 2014;11(11):2107-2115.
200. Carroll JD, Carroll EP, Feldman T, Ward DM, Lang RM, McGaughey D, Karp RB. Sex-associated differences in left ventricular function in aortic stenosis of the elderly. *Circulation.* 1992;86(4):1099-1107.
201. Petrov G, Regitz-Zagrosek V, Lehmkuhl E, Krabatsch T, Dunkel A, Dandel M, Dworatzek E, Mahmoodzadeh S, Schubert C, Becher E, Hampl H, Hetzer R. Regression of myocardial hypertrophy after aortic valve replacement: faster in women? *Circulation.* 2010;122(11 Suppl):S23-28.
202. Petrie MC, Dawson NF, Murdoch DR, Davie AP, McMurray JJV. Failure of Women's Hearts. *Circulation.* 1999;99(17):2334-2341.

203. Fliegner D, Schubert C, Penkalla A, Witt H, Kararigas G, Dworatzek E, Staub E, Martus P, Ruiz Noppinger P, Kintscher U, Gustafsson JA, Regitz-Zagrosek V. Female sex and estrogen receptor-beta attenuate cardiac remodeling and apoptosis in pressure overload. *American journal of physiology. Regulatory, integrative and comparative physiology.* 2010;298(6):R1597-1606.
204. Scantlebury DC, Borlaug BA. Why are women more likely than men to develop heart failure with preserved ejection fraction? *Current opinion in cardiology.* 2011;26(6):562-568.
205. Blenck CL, Harvey PA, Reckelhoff JF, Leinwand LA. The Importance of Biological Sex and Estrogen in Rodent Models of Cardiovascular Health and Disease. *Circulation research.* 2016;118(8):1294-1312.
206. Weinberg EO, Thienelt CD, Katz SE, Bartunek J, Tajima M, Rohrbach S, Douglas PS, Lorell BH. Gender differences in molecular remodeling in pressure overload hypertrophy. *Journal of the American College of Cardiology.* 1999;34(1):264-273.
207. Bhuiyan MS, Shioda N, Fukunaga K. Ovariectomy augments pressure overload-induced hypertrophy associated with changes in Akt and nitric oxide synthase signaling pathways in female rats. *American journal of physiology. Endocrinology and metabolism.* 2007;293(6):E1606-1614.
208. Witt H, Schubert C, Jaekel J, Fliegner D, Penkalla A, Tiemann K, Stypmann J, Roepcke S, Brokat S, Mahmoodzadeh S, Brozova E, Davidson MM, Ruiz Noppinger P, Grohe C, Regitz-Zagrosek V. Sex-specific pathways in early cardiac response to pressure overload in mice. *Journal of molecular medicine.* 2008;86(9):1013-1024.
209. Cross HR, Lu L, Steenbergen C, Philipson KD, Murphy E. Overexpression of the cardiac Na/Ca exchanger increases susceptibility to ischemia/reperfusion injury in male, but not female, transgenic mice. *Circulation research.* 1998;83(12):1215-1223.
210. Wei SK, McCurley JM, Hanlon SU, Haigney MC. Gender differences in Na/Ca exchanger current and beta-adrenergic responsiveness in heart failure in pig myocytes. *Annals of the New York Academy of Sciences.* 2007;1099:183-189.
211. Iorga A, Li J, Sharma S, Umar S, Bopassa JC, Nadadur RD, Centala A, Ren S, Saito T, Toro L, Wang Y, Stefani E, Eghbali M. Rescue of Pressure Overload-Induced Heart Failure by Estrogen Therapy. *Journal of the American Heart Association.* 2016;5(1).
212. Vittone L, Mundina-Weilenmann C, Said M, Ferrero P, Mattiazzi A. Time course and mechanisms of phosphorylation of phospholamban residues in ischemia-reperfused rat hearts. Dissociation of phospholamban phosphorylation pathways. *Journal of molecular and cellular cardiology.* 2002;34(1):39-50.
213. Cross HR, Kranias EG, Murphy E, Steenbergen C. Ablation of PLB exacerbates ischemic injury to a lesser extent in female than male mice: protective role of NO. *American journal of physiology. Heart and circulatory physiology.* 2003;284(2):H683-690.
214. Dash R, Schmidt AG, Pathak A, Gerst MJ, Biniakiewicz D, Kadambi VJ, Hoit BD, Abraham WT, Kranias EG. Differential regulation of p38 mitogen-activated protein kinase mediates gender-dependent catecholamine-induced hypertrophy. *Cardiovascular research.* 2003;57(3):704-714.
215. Sande JB, Sjaastad I, Hoen IB, Bokenes J, Tonnessen T, Holt E, Lunde PK, Christensen G. Reduced level of Ser-16 phosphorylated phospholamban in the failing rat myocardium: a major contributor to reduced SERCA2 activity. *Cardiovascular research.* 2002;53(2):382-391.

216. Dash R, Frank KF, Carr AN, Moravec CS, Kranias EG. Gender influences on sarcoplasmic reticulum Ca(2+) handling in failing human myocardium. *Journal of molecular and cellular cardiology.* 2001;33(7):1345-1353.
217. Fischer TH, Herting J, Eiringhaus J, Pabel S, Hartmann NH, Ellenberger D, Friedrich M, Renner A, Gummert J, Maier LS, Zabel M, Hasenfuss G, Sossalla S. Sex-dependent alterations of Ca(2+) cycling in human cardiac hypertrophy and heart failure. *Europace : European pacing, arrhythmias, and cardiac electrophysiology : journal of the working groups on cardiac pacing, arrhythmias, and cardiac cellular electrophysiology of the European Society of Cardiology.* 2016;18(9):1440-1448.
218. Holzem KM, Madden EJ, Efimov IR. Human cardiac systems electrophysiology and arrhythmogenesis: iteration of experiment and computation. *Europace : European pacing, arrhythmias, and cardiac electrophysiology : journal of the working groups on cardiac pacing, arrhythmias, and cardiac cellular electrophysiology of the European Society of Cardiology.* 2014;16 Suppl 4:iv77-iv85.
219. Luo CH, Rudy Y. A model of the ventricular cardiac action potential. Depolarization, repolarization, and their interaction. *Circulation research.* 1991;68(6):1501-1526.
220. Taggart MJ, Hume R, Lartey J, Johnson M, Tong WC, Macleod KT. Cardiac remodelling during pregnancy: whither the guinea pig? *Cardiovascular research.* 2014;104(1):226-227.
221. Mitchell BF, Taggart MJ. Are animal models relevant to key aspects of human parturition? *American journal of physiology. Regulatory, integrative and comparative physiology.* 2009;297(3):R525-545.
222. Hasenfuss G. Animal models of human cardiovascular disease, heart failure and hypertrophy. *Cardiovascular research.* 1998;39(1):60-76.
223. Kingsbury MP, Huang W, Giuliatti S, Turner M, Hunter R, Parker K, Sheridan DJ. Investigation of distal aortic compliance and vasodilator responsiveness in heart failure due to proximal aortic stenosis in the guinea pig. *Clinical science (London, England : 1979).* 1999;96(3):241-251.
224. Gomes AC, Falcao-Pires I, Pires AL, Bras-Silva C, Leite-Moreira AF. Rodent models of heart failure: an updated review. *Heart failure reviews.* 2013;18(2):219-249.
225. James AF, Choisy SC, Hancox JC. Recent advances in understanding sex differences in cardiac repolarization. *Progress in biophysics and molecular biology.* 2007;94(3):265-319.
226. Petanceska SS, Nagy V, Frail D, Gandy S. Ovariectomy and 17beta-estradiol modulate the levels of Alzheimer's amyloid beta peptides in brain. *Neurology.* 2000;54(12):2212-2217.
227. James AF, Arberry LA, Hancox JC. Gender-related differences in ventricular myocyte repolarization in the guinea pig. *Basic research in cardiology.* 2004;99(3):183-192.
228. Thompson LP, Pinkas G, Weiner CP. Chronic 17beta-Estradiol Replacement Increases Nitric Oxide-Mediated Vasodilation of Guinea Pig Coronary Microcirculation. *Circulation.* 2000;102(4):445-451.
229. MacLeod KT, Harding SE. Effects of phorbol ester on contraction, intracellular pH and intracellular Ca(2+) in isolated mammalian ventricular myocytes. *The Journal of physiology.* 1991;444:481-498.
230. Egdell RM, MacLeod KT. Calcium extrusion during aftercontractions in cardiac myocytes: the role of the Na/Ca exchanger in the generation of the transient inward current. *Journal of molecular and cellular cardiology.* 2000;32(1):85-93.

231. Liew R, Stagg MA, MacLeod KT, Collins P. Acute actions of 3 alpha-hydroxy-tibolone on factors influencing contraction in guinea-pig ventricular myocytes. *European journal of pharmacology.* 2004;484(2-3):141-145.
232. Hamill OP, Marty A, Neher E, Sakmann B, Sigworth FJ. Improved patch-clamp techniques for high-resolution current recording from cells and cell-free membrane patches. *Pflugers Archiv : European journal of physiology.* 1981;391(2):85-100.
233. Terracciano CM, MacLeod KT. Measurements of Ca(2+) entry and sarcoplasmic reticulum Ca(2+) content during the cardiac cycle in guinea pig and rat ventricular myocytes. *Biophysical journal.* 1997;72(3):1319-1326.
234. De Ferrari GM, Viola MC, D'Amato E, Antolini R, Forti S. Distinct patterns of calcium transients during early and delayed afterdepolarizations induced by isoproterenol in ventricular myocytes. *Circulation.* 1995;91(10):2510-2515.
235. Bassani JW, Yuan W, Bers DM. Fractional SR Ca(2+) release is regulated by trigger Ca(2+) and SR Ca(2+) content in cardiac myocytes. *The American journal of physiology.* 1995;268(5 Pt 1):C1313-1319.
236. Egdell RM, De Souza AI, Macleod KT. Relative importance of SR load and cytoplasmic calcium concentration in the genesis of aftercontractions in cardiac myocytes. *Cardiovascular research.* 2000;47(4):769-777.
237. Brini M, Carafoli E. The plasma membrane Ca(2+) ATPase and the plasma membrane sodium calcium exchanger cooperate in the regulation of cell calcium. *Cold Spring Harbor perspectives in biology.* 2011;3(2).
238. Toischer K, Hartmann N, Wagner S, Fischer TH, Herting J, Danner BC, Sag CM, Hund TJ, Mohler PJ, Belardinelli L, Hasenfuss G, Maier LS, Sossalla S. Role of late sodium current as a potential arrhythmogenic mechanism in the progression of pressure-induced heart disease. *Journal of molecular and cellular cardiology.* 2013;61:111-122.
239. Aiba T, Hesketh GG, Liu T, Carlisle R, Villa-Abrille MC, O'Rourke B, Akar FG, Tomaselli GF. Na+ channel regulation by Ca2+/calmodulin and Ca2+/calmodulin-dependent protein kinase II in guinea-pig ventricular myocytes. *Cardiovascular research.* Feb 01 2010;85(3):454-463.
240. Li GR, Lau CP, Shrier A. Heterogeneity of sodium current in atrial vs epicardial ventricular myocytes of adult guinea pig hearts. *Journal of molecular and cellular cardiology.* Sep 2002;34(9):1185-1194.
241. Muramatsu H, Kiyosue T, Arita M, Ishikawa T, Hidaka H. Modification of cardiac sodium current by intracellular application of cAMP. *Pflugers Archiv : European journal of physiology.* Jan 1994;426(1-2):146-154.
242. Sikkel MB, Collins TP, Rowlands C, Shah M, O'Gara P, Williams AJ, Harding SE, Lyon AR, MacLeod KT. Flecainide reduces Ca(2+) spark and wave frequency via inhibition of the sarcolemmal sodium current. *Cardiovascular research.* 2013;98(2):286-296.
243. Picht E, Zima AV, Blatter LA, Bers DM. SparkMaster: automated calcium spark analysis with ImageJ. *American journal of physiology. Cell physiology.* 2007;293(3):C1073-1081.
244. Hollingworth S, Peet J, Chandler WK, Baylor SM. Calcium sparks in intact skeletal muscle fibers of the frog. *The Journal of general physiology.* 2001;118(6):653-678.
245. Shimizu I, Minamino T. Physiological and pathological cardiac hypertrophy. *Journal of molecular and cellular cardiology.* 2016;97:245-262.
246. Burchfield JS, Xie M, Hill JA. Pathological ventricular remodeling: mechanisms: part 1 of 2. *Circulation.* 2013;128(4):388-400.

247. Francis GS, McDonald KM, Cohn JN. Neurohumoral activation in preclinical heart failure. Remodeling and the potential for intervention. *Circulation.* 1993;87(5 Suppl):Iv90-96.
248. Carey PA, Turner M, Fry CH, Sheridan DJ. Reduced anisotropy of action potential conduction in left ventricular hypertrophy. *Journal of cardiovascular electrophysiology.* 2001;12(7):830-835.
249. Naqvi RU, Macleod KT. Effect of hypertrophy on mechanisms of relaxation in isolated cardiac myocytes from guinea pig. *The American journal of physiology.* 1994;267(5 Pt 2):H1851-1861.
250. Monnet E, Chachques JC. Animal models of heart failure: what is new? *The Annals of thoracic surgery.* 2005;79(4):1445-1453.
251. Frohlich ED, Susic D. Pressure overload. *Heart failure clinics.* 2012;8(1):21-32.
252. Carabello BA. Aortic stenosis: from pressure overload to heart failure. *Heart failure clinics.* 2006;2(4):435-442.
253. Despa S, Vigmond E. From Single Myocyte to Whole Heart: The Intricate Dance of Electrophysiology and Modeling. *Circulation research.* 2016;118(2):184-186.
254. Sah R, Ramirez RJ, Kaprielian R, Backx PH. Alterations in action potential profile enhance excitation-contraction coupling in rat cardiac myocytes. *The Journal of physiology.* May 15 2001;533(Pt 1):201-214.
255. Volk T, Nguyen TH, Schultz JH, Faulhaber J, Ehmke H. Regional alterations of repolarizing K(+) currents among the left ventricular free wall of rats with ascending aortic stenosis. *The Journal of physiology.* 2001;530(Pt 3):443-455.
256. Priebe L, Beuckelmann DJ. Simulation study of cellular electric properties in heart failure. *Circulation research.* 1998;82(11):1206-1223.
257. Ryder KO, Bryant SM, Hart G. Membrane current changes in left ventricular myocytes isolated from guinea pigs after abdominal aortic coarctation. *Cardiovascular research.* 1993;27(7):1278-1287.
258. Naqvi RU, Tweedie D, MacLeod KT. Evidence for the action potential mediating the changes to contraction observed in cardiac hypertrophy in the rabbit. *International journal of cardiology.* 2001;77(2-3):189-206.
259. Ouadid H, Albat B, Nargeot J. Calcium currents in diseased human cardiac cells. *Journal of cardiovascular pharmacology.* 1995;25(2):282-291.
260. Aimond F, Alvarez JL, Rauzier JM, Lorente P, Vassort G. Ionic basis of ventricular arrhythmias in remodeled rat heart during long-term myocardial infarction. *Cardiovascular research.* 1999;42(2):402-415.
261. Bito V, Heinzel FR, Biesmans L, Antoons G, Sipido KR. Crosstalk between L-type Ca(2+) channels and the sarcoplasmic reticulum: alterations during cardiac remodelling. *Cardiovascular research.* 2008;77(2):315-324.
262. Kobrinsky E, Tiwari S, Maltsev VA, Harry JB, Lakatta E, Abernethy DR, Soldatov NM. Differential role of the alpha1C subunit tails in regulation of the Cav1.2 channel by membrane potential, beta subunits, and Ca(2+) ions. *The Journal of biological chemistry.* 2005;280(13):12474-12485.
263. Blaich A, Welling A, Fischer S, Wegener JW, Kostner K, Hofmann F, Moosmang S. Facilitation of murine cardiac L-type Ca(2+) channel is modulated by calmodulin kinase II-dependent phosphorylation of S1512 and S1570. *Proceedings of the National Academy of Sciences of the United States of America.* 2010;107(22):10285-10289.
264. Lips DJ, deWindt LJ, van Kraaij DJW, Doevendans PA. Molecular determinants of myocardial hypertrophy and failure: alternative pathways for beneficial and maladaptive hypertrophy. *European heart journal.* 2003;24(10):883-896.

265. Ottolia M, Torres N, Bridge JH, Philipson KD, Goldhaber JI. Na/Ca exchange and contraction of the heart. *Journal of molecular and cellular cardiology.* 2013;61:28-33.
266. Luo M, Anderson ME. Mechanisms of altered Ca(2+) handling in heart failure. *Circulation research.* 2013;113(6):690-708.
267. Ablorh NA, Dong X, James ZM, Xiong Q, Zhang J, Thomas DD, Karim CB. Synthetic phosphopeptides enable quantitation of the content and function of the four phosphorylation states of phospholamban in cardiac muscle. *The Journal of biological chemistry.* 2014;289(42):29397-29405.
268. Schillinger W, Janssen PM, Emami S, Henderson SA, Ross RS, Teucher N, Zeitz O, Philipson KD, Prestle J, Hasenfuss G. Impaired contractile performance of cultured rabbit ventricular myocytes after adenoviral gene transfer of Na/Ca exchanger. *Circulation research.* 2000;87(7):581-587.
269. Fischer TH, Herting J, Tirilomis T, Renner A, Neef S, Toischer K, Ellenberger D, Forster A, Schmitto JD, Gummert J, Schondube FA, Hasenfuss G, Maier LS, Sossalla S. Ca/calmodulin-dependent protein kinase II and protein kinase A differentially regulate sarcoplasmic reticulum Ca(2+) leak in human cardiac pathology. *Circulation.* 2013;128(9):970-981.
270. Kohlhaas M, Zhang T, Seidler T, Zibrova D, Dybkova N, Steen A, Wagner S, Chen L, Brown JH, Bers DM, Maier LS. Increased sarcoplasmic reticulum calcium leak but unaltered contractility by acute CaMKII overexpression in isolated rabbit cardiac myocytes. *Circulation research.* 2006;98(2):235-244.
271. Maier LS, Zhang T, Chen L, DeSantiago J, Brown JH, Bers DM. Transgenic CaMKIIdeltaC overexpression uniquely alters cardiac myocyte Ca(2+) handling: reduced SR Ca(2+) load and activated SR Ca(2+) release. *Circulation research.* 2003;92(8):904-911.
272. Sag CM, Wadsack DP, Khabbazzadeh S, Abesser M, Grefe C, Neumann K, Opiela MK, Backs J, Olson EN, Brown JH, Neef S, Maier SK, Maier LS. Calcium/calmodulin-dependent protein kinase II contributes to cardiac arrhythmogenesis in heart failure. *Circulation. Heart failure.* 2009;2(6):664-675.
273. Maier LS, Bers DM. Role of Ca/calmodulin-dependent protein kinase (CaMK) in excitation-contraction coupling in the heart. *Cardiovascular research.* 2007;73(4):631-640.
274. Bers DM. Cardiac sarcoplasmic reticulum calcium leak: basis and roles in cardiac dysfunction. *Annual review of physiology.* 2014;76:107-127.
275. Bers DM, Eisner DA, Valdivia HH. Sarcoplasmic reticulum Ca(2+) and heart failure: roles of diastolic leak and Ca(2+) transport. *Circulation research.* 2003;93(6):487-490.
276. Swift F, Birkeland JA, Tovsrud N, Enger UH, Aronsen JM, Louch WE, Sjaastad I, Sejersted OM. Altered Na/Ca exchanger activity due to downregulation of Na/K ATPase alpha2-isoform in heart failure. *Cardiovascular research.* 2008;78(1):71-78.
277. Dostanic I, Schultz Jel J, Lorenz JN, Lingrel JB. The alpha 1 isoform of Na,K-ATPase regulates cardiac contractility and functionally interacts and co-localizes with the Na/Ca exchanger in heart. *The Journal of biological chemistry.* Dec 24 2004;279(52):54053-54061.
278. Dostanic I, Lorenz JN, Schultz Jel J, Grupp IL, Neumann JC, Wani MA, Lingrel JB. The alpha2 isoform of Na/K ATPase mediates ouabain-induced cardiac inotropy in mice. *The Journal of biological chemistry.* 2003;278(52):53026-53034.
279. Correll RN, Eder P, Burr AR, Despa S, Davis J, Bers DM, Molkentin JD. Overexpression of the Na/K ATPase alpha2 but not alpha1 isoform attenuates pathological cardiac hypertrophy and remodeling. *Circulation research.* 2014;114(2):249-256.

280. Swift F, Birkeland JA, Tovsrud N, Enger UH, Aronsen JM, Louch WE, Sjaastad I, Sejersted OM. Altered Na+/Ca2+-exchanger activity due to downregulation of Na+/K+-ATPase alpha2-isoform in heart failure. *Cardiovascular research.* Apr 1 2008;78(1):71-78.
281. Fedida D, Orth PM, Hesketh JC, Ezrin AM. The role of late I and antiarrhythmic drugs in EAD formation and termination in Purkinje fibers. *Journal of cardiovascular electrophysiology.* 2006;17 Suppl 1:S71-s78.
282. Guo D, Yu M, Liu Q, Cox RH, Liu T, Yan GX. Ventricular hypertrophy amplifies transmural dispersion of repolarization by preferentially increasing the late sodium current in endocardium. *Journal of electrocardiology.* 2014;47(5):642-648.
283. Hoyer K, Song Y, Wang D, Phan D, Balschi J, Ingwall JS, Belardinelli L, Shryock JC. Reducing the late sodium current improves cardiac function during sodium pump inhibition by ouabain. *The Journal of pharmacology and experimental therapeutics.* 2011;337(2):513-523.
284. Sapia L, Palomeque J, Mattiazzi A, Petroff MV. Na/K ATPase inhibition by ouabain induces CaMKII-dependent apoptosis in adult rat cardiac myocytes. *Journal of molecular and cellular cardiology.* 2010;49(3):459-468.
285. Frazier CG, Alexander KP, Newby LK, Anderson S, Iverson E, Packer M, Cohn J, Goldstein S, Douglas PS. Associations of gender and etiology with outcomes in heart failure with systolic dysfunction: a pooled analysis of 5 randomized control trials. *Journal of the American College of Cardiology.* 2007;49(13):1450-1458.
286. Fujimoto N, Borlaug BA, Lewis GD, Hastings JL, Shafer KM, Bhella PS, Carrick-Ranson G, Levine BD. Hemodynamic responses to rapid saline loading: the impact of age, sex, and heart failure. *Circulation.* 2013;127(1):55-62.
287. Peters RW, Gold MR. The influence of gender on arrhythmias. *Cardiology in review.* 2004;12(2):97-105.
288. Piro M, Della Bona R, Abbate A, Biasucci LM, Crea F. Sex-related differences in myocardial remodeling. *Journal of the American College of Cardiology.* 2010;55(11):1057-1065.
289. Sims C, Reisenweber S, Viswanathan PC, Choi BR, Walker WH, Salama G. Sex, age, and regional differences in L-type calcium current are important determinants of arrhythmia phenotype in rabbit hearts with drug-induced long QT type 2. *Circulation research.* 2008;102(9):e86-100.
290. Mason SA, MacLeod KT. Cardiac action potential duration and calcium regulation in males and females. *Biochemical and biophysical research communications.* 2009;388(3):565-570.
291. Liew R, Stagg MA, Chan J, Collins P, MacLeod KT. Gender determines the acute actions of genistein on intracellular calcium regulation in the guinea-pig heart. *Cardiovascular research.* 2004;61(1):66-76.
292. Wasserstrom JA, Kapur S, Jones S, Faruque T, Sharma R, Kelly JE, Pappas A, Ho W, Kadish AH, Aistrup GL. Characteristics of intracellular Ca(2+) cycling in intact rat heart: a comparison of sex differences. *American journal of physiology. Heart and circulatory physiology.* 2008;295(5):H1895-1904.
293. Gottdiener JS, Arnold AM, Aurigemma GP, Polak JF, Tracy RP, Kitzman DW, Gardin JM, Rutledge JE, Boineau RC. Predictors of congestive heart failure in the elderly: the Cardiovascular Health Study. *Journal of the American College of Cardiology.* 2000;35(6):1628-1637.
294. Blenck CL, Harvey PA, Reckelhoff JF, Leinwand LA. The importance of biological sex and estrogen in rodent models of cardiovascular health and disease. *Circulation research.* 2016;118(8):1294-1312.

295. Saito T, Ciobotaru A, Bopassa JC, Toro L, Stefani E, Eghbali M. Estrogen contributes to gender differences in mouse ventricular repolarization. *Circulation research.* 2009;105(4):343-352.
296. MacDonald JK, Pyle WG, Reitz CJ, Howlett SE. Cardiac contraction, calcium transients, and myofilament calcium sensitivity fluctuate with the estrous cycle in young adult female mice. *American journal of physiology. Heart and circulatory physiology.* 2014;306(7):H938-953.
297. Leblanc N, Chartier D, Gosselin H, Rouleau JL. Age and gender differences in excitation-contraction coupling of the rat ventricle. *The Journal of physiology.* 1998;511 (Pt 2):533-548.
298. Farrell SR, Ross JL, Howlett SE. Sex differences in mechanisms of cardiac excitation-contraction coupling in rat ventricular myocytes. *American journal of physiology. Heart and circulatory physiology.* 2010;299(1):H36-45.
299. Palacios J, Marusic ET, Lopez NC, Gonzalez M, Michea L. Estradiol-induced expression of Na/K ATPase catalytic isoforms in rat arteries: gender differences in activity mediated by nitric oxide donors. *American journal of physiology. Heart and circulatory physiology.* 2004;286(5):H1793-1800.
300. Cerbai E, Barbieri M, Li Q, Mugelli A. Ionic basis of action potential prolongation of hypertrophied cardiac myocytes isolated from hypertensive rats of different ages. *Cardiovascular research.* 1994;28(8):1180-1187.
301. Imahashi K, London RE, Steenbergen C, Murphy E. Male/female differences in intracellular Na(+) regulation during ischemia/reperfusion in mouse heart. *Journal of molecular and cellular cardiology.* 2004;37(3):747-753.
302. Fekete A, Vannay A, Ver A, Vasarhelyi B, Muller V, Ouyang N, Reusz G, Tulassay T, Szabo AJ. Sex differences in the alterations of Na/K ATPase following ischaemia-reperfusion injury in the rat kidney. *The Journal of physiology.* 2004;555(Pt 2):471-480.
303. Vlkovicova J, Javorkova V, Pechanova O, Vrbjar N. Gender difference in functional properties of Na/K ATPase in the heart of spontaneously hypertensive rats. *Life Sci.* 2005;76(9):971-982.
304. Ribeiro RF, Jr., Pavan BM, Potratz FF, Fiorim J, Simoes MR, Dias FM, Lima FL, Fernandes AA, Vassallo DV, Stefanon I. Myocardial contractile dysfunction induced by ovariectomy requires AT1 receptor activation in female rats. *Cellular physiology and biochemistry : international journal of experimental cellular physiology, biochemistry, and pharmacology.* 2012;30(1):1-12.
305. Lujan HL, Dicarlo SE. Sex differences to myocardial ischemia and beta-adrenergic receptor blockade in conscious rats. *American journal of physiology. Heart and circulatory physiology.* 2008;294(4):H1523-1529.
306. Gillis AM. Atrial Fibrillation and Ventricular Arrhythmias: Sex Differences in Electrophysiology, Epidemiology, Clinical Presentation, and Clinical Outcomes. *Circulation.* 2017;135(6):593-608.
307. Stock EO, Redberg R. Cardiovascular disease in women. *Current problems in cardiology.* 2012;37(11):450-526.
308. Paigel AS, Ribeiro Junior RF, Fernandes AA, Targueta GP, Vassallo DV, Stefanon I. Myocardial contractility is preserved early but reduced late after ovariectomy in young female rats. *Reproductive Biology and Endocrinology.* 2011;9(1):54.
309. Zhao Z, Wang H, Jessup JA, Lindsey SH, Chappell MC, Groban L. Role of estrogen in diastolic dysfunction. *American journal of physiology. Heart and circulatory physiology.* 2014;306(5):H628-640.

310. Pandit S, Woranush W, Wattanapermpool J, Bupha-Intr T. Significant role of female sex hormones in cardiac myofilament activation in angiotensin II-mediated hypertensive rats. *The journal of physiological sciences : JPS.* 2014;64(4):269-277.
311. Huang H, Priori SG, Napolitano C, O'Leary ME, Chahine M. Y1767C, a novel *SCN5A* mutation, induces a persistent Na(+) current and potentiates ranolazine inhibition of $Na_v1.5$ channels. *American Journal of Physiology - Heart and Circulatory Physiology.* 2011;300(1):H288-H299.
312. Szabo B, Sweidan R, Rajagopalan CV, Lazzara R. Role of Na/Ca exchange current in Cs(+)-induced early afterdepolarizations in Purkinje fibers. *Journal of cardiovascular electrophysiology.* 1994;5(11):933-944.
313. Livak KJ, Schmittgen TD. Analysis of relative gene expression data using real-time quantitative PCR and the 2(-Delta Delta C(T)) Method. *Methods (San Diego, Calif.).* 2001;25(4):402-408.
314. Bers DM, Morotti S. Ca(2+) current facilitation is CaMKII-dependent and has arrhythmogenic consequences. *Frontiers in pharmacology.* 2014;5:144.
315. Zhang X, Ai X, Nakayama H, Chen B, Harris DM, Tang M, Xie Y, Szeto C, Li Y, Li Y, Zhang H, Eckhart AD, Koch WJ, Molkentin JD, Chen X. Persistent increases in Ca(2+) influx through Cav1.2 shortens action potential and causes Ca(2+) overload-induced afterdepolarizations and arrhythmias. *Basic research in cardiology.* 2016;111(1):4.
316. Shannon TR, Ginsburg KS, Bers DM. Potentiation of fractional sarcoplasmic reticulum calcium release by total and free intra-sarcoplasmic reticulum calcium concentration. *Biophysical journal.* 2000;78(1):334-343.
317. Chu SH, Goldspink P, Kowalski J, Beck J, Schwertz DW. Effect of estrogen on calcium-handling proteins, beta-adrenergic receptors, and function in rat heart. *Life Sci.* 2006;79(13):1257-1267.
318. Fares E, Pyle WG, Ray G, Rose RA, Denovan-Wright EM, Chen RP, Howlett SE. The impact of ovariectomy on calcium homeostasis and myofilament calcium sensitivity in the aging mouse heart. *PloS one.* 2013;8(9):e74719.
319. Guo T, Gillespie D, Fill M. Ryanodine receptor current amplitude controls Ca(2+) sparks in cardiac muscle. *Circulation research.* 2012;111(1):28-36.
320. Venetucci LA, Trafford AW, O'Neill SC, Eisner DA. The sarcoplasmic reticulum and arrhythmogenic calcium release. *Cardiovascular research.* 2008;77(2):285-292.
321. Kam KW, Kravtsov GM, Liu J, Wong TM. Increased PKA activity and its influence on isoprenaline-stimulated L-type Ca(2+) channels in the heart from ovariectomized rats. *British journal of pharmacology.* 2005;144(7):972-981.
322. Patterson E, Ma L, Szabo B, Robinson CP, Thadani U. Ovariectomy and estrogen-induced alterations in myocardial contractility in female rabbits: role of the L-type calcium channel. *The Journal of pharmacology and experimental therapeutics.* 1998;284(2):586-591.
323. Tharp DL, Ivey JR, Shaw RL, Bowles DK. Ovariectomy increases L-type Ca(2+) channel activity in porcine coronary smooth muscle. *Menopause (New York, N.Y.).* 2014;21(6):661-668.
324. Yuan W, Bers DM. Ca(2+)-dependent facilitation of cardiac Ca(2+) current is due to Ca/calmodulin-dependent protein kinase. *The American journal of physiology.* 1994;267(3 Pt 2):H982-993.
325. Yuan W, Bers DM. Protein kinase inhibitor H-89 reverses forskolin stimulation of cardiac L-type calcium current. *The American journal of physiology.* 1995;268(3 Pt 1):C651-659.

326. Guo J, Duff HJ. Calmodulin kinase II accelerates L-type Ca(2+) current recovery from inactivation and compensates for the direct inhibitory effect of [Ca2+]i in rat ventricular myocytes. *The Journal of physiology.* 2006;574(Pt 2):509-518.
327. Volders PGA, Kulcsár A, Vos MA, Sipido KR, Wellens HJJ, Lazzara R, Szabo B. Similarities between early and delayed afterdepolarizations induced by isoproterenol in canine ventricular myocytes. *Cardiovascular research.* 1997;34(2):348-359.
328. Priori SG, Napolitano C, Schwartz PJ. Electrophysiologic mechanisms involved in the development of torsades de pointes. *Cardiovascular drugs and therapy.* 1991;5(1):203-212.
329. Turdi S, Huff AF, Pang J, He EY, Chen X, Wang S, Chen Y, Zhang Y, Ren J. 17beta-estradiol attenuates ovariectomy-induced changes in cardiomyocyte contractile function via activation of AMP-activated protein kinase. *Toxicology letters.* 2015;232(1):253-262.
330. Bupha-Intr T, Laosiripisan J, Wattanapermpool J. Moderate intensity of regular exercise improves cardiac SR Ca(2+) uptake activity in ovariectomized rats. *Journal of applied physiology (Bethesda, Md. : 1985).* 2009;107(4):1105-1112.
331. Pham TV, Robinson RB, Danilo P, Jr., Rosen MR. Effects of gonadal steroids on gender-related differences in transmural dispersion of L-type calcium current. *Cardiovascular research.* Feb 15 2002;53(3):752-762.
332. Willott RH, Gomes AV, Chang AN, Parvatiyar MS, Pinto JR, Potter JD. Mutations in Troponin that cause HCM, DCM AND RCM: what can we learn about thin filament function? *Journal of molecular and cellular cardiology.* 2010;48(5):882-892.
333. Lu QW, Morimoto S, Harada K, Du CK, Takahashi-Yanaga F, Miwa Y, Sasaguri T, Ohtsuki I. Cardiac troponin T mutation R141W found in dilated cardiomyopathy stabilizes the troponin T-tropomyosin interaction and causes a Ca(2+) desensitization. *Journal of molecular and cellular cardiology.* 2003;35(12):1421-1427.
334. Sommese RF, Nag S, Sutton S, Miller SM, Spudich JA, Ruppel KM. Effects of troponin T cardiomyopathy mutations on the calcium sensitivity of the regulated thin filament and the actomyosin cross-bridge kinetics of human beta-cardiac myosin. *PloS one.* 2013;8(12):e83403.
335. Ramratnam M, Salama G, Sharma RK, Wang DW, Smith SH, Banerjee SK, Huang XN, Gifford LM, Pruce ML, Gabris BE, Saba S, Shroff SG, Ahmad F. Gene-Targeted Mice with the Human Troponin T R141W Mutation Develop Dilated Cardiomyopathy with Calcium Desensitization. *PloS one.* 2016;11(12):e0167681.
336. Wattanapermpool J. Increase in calcium responsiveness of cardiac myofilament activation in ovariectomized rats. *Life Sci.* 1998;63(11):955-964.
337. Wattanapermpool J, Reiser PJ. Differential effects of ovariectomy on calcium activation of cardiac and soleus myofilaments. *The American journal of physiology.* 1999;277(2 Pt 2):H467-473.
338. Klempfner R, Koifman E, Goldenberg I, Hamdan A, Tofler GH, Kopel E. The Israel Nationwide Heart Failure Survey: Sex Differences in Early and Late Mortality for Hospitalized Heart Failure Patients. *Journal of cardiac failure.* 2013.
339. Murphy E, Steenbergen C. Gender-based differences in mechanisms of protection in myocardial ischemia-reperfusion injury. *Cardiovascular research.* 2007;75(3):478-486.
340. Cui YH, Tan Z, Fu XD, Xiang QL, Xu JW, Wang TH. 17beta-estradiol attenuates pressure overload-induced myocardial hypertrophy through regulating caveolin-3 protein in ovariectomized female rats. *Molecular biology reports.* 2011;38(8):4885-4892.

341. Tagashira H, Bhuiyan S, Shioda N, Fukunaga K. Distinct cardioprotective effects of 17beta-estradiol and dehydroepiandrosterone on pressure overload-induced hypertrophy in ovariectomized female rats. *Menopause (New York, N.Y.).* 2011;18(12):1317-1326.
342. van Eickels M, Grohe C, Cleutjens JP, Janssen BJ, Wellens HJ, Doevendans PA. 17beta-estradiol attenuates the development of pressure-overload hypertrophy. *Circulation.* 2001;104(12):1419-1423.
343. Mori T, Kai H, Kajimoto H, Koga M, Kudo H, Takayama N, Yasuoka S, Anegawa T, Kai M, Imaizumi T. Enhanced cardiac inflammation and fibrosis in ovariectomized hypertensive rats: a possible mechanism of diastolic dysfunction in postmenopausal women. *Hypertension research : official journal of the Japanese Society of Hypertension.* 2011;34(4):496-502.
344. Coronel R, Wilders R, Verkerk AO, Wiegerinck RF, Benoist D, Bernus O. Electrophysiological changes in heart failure and their implications for arrhythmogenesis. *Biochimica et biophysica acta.* 2013;1832(12):2432-2441.
345. Tadros R, Ton AT, Fiset C, Nattel S. Sex differences in cardiac electrophysiology and clinical arrhythmias: epidemiology, therapeutics, and mechanisms. *The Canadian journal of cardiology.* 2014;30(7):783-792.
346. Dieterle T, Meyer M, Gu Y, Belke DD, Swanson E, Iwatate M, Hollander J, Peterson KL, Ross J, Jr., Dillmann WH. Gene transfer of a phospholamban-targeted antibody improves calcium handling and cardiac function in heart failure. *Cardiovascular research.* 2005;67(4):678-688.
347. Regitz-Zagrosek V, Seeland U. Sex and gender differences in myocardial hypertrophy and heart failure. *Wiener medizinische Wochenschrift (1946).* 2011;161(5-6):109-116.
348. Mullens W, Abrahams Z, Sokos G, Francis GS, Starling RC, Young JB, Taylor DO, Wilson Tang WH. Gender differences in patients admitted with advanced decompensated heart failure. *The American journal of cardiology.* 2008;102(4):454-458.
349. Kam KWL, Kravtsov GM, Liu J, Wong TM. Increased PKA activity and its influence on isoprenaline-stimulated L-type Ca(2+) channels in the heart from ovariectomized rats. *British journal of pharmacology.* 2005;144(7):972-981.
350. Prossnitz ER, Barton M. The G protein-coupled estrogen receptor GPER in health and disease. *Nature reviews. Endocrinology.* 2011;7(12):715-726.

11 APPENDIX

11.1 Publications and abstract related to this thesis

Publications

1. Michael J. Shattock, Kyung Chan Park, **Hsiang-Yu Yang**, Angela W. C. Lee, Steven Niederer, Kenneth T. MacLeod, James Winter. Restitution slope is principally determined by steady-state action potential duration. Cardiovasc Res (2017) 113 (7): 817-828.
2. **Hsiang-Yu Yang**, Jahn M. Firth, Alice J. Francis, Anita Alvarez-Laviada, Kenneth T. MacLeod. The effect of ovariectomy on intracellular calcium (Ca^{2+}) regulation in guinea pig cardiomyocytes. Accepted by AJP - Heart and Circulatory Physiology, 2nd Aug 17.
3. Christina T Rowlands, Thomas Owen, Saheed Lawal, Shuangyi Cao, Samata S Pandey, **Hsiang-Yu Yang**, Weihua Song, Ross Wilkinson, Anita Alvarez-Laviada, Katja Gehmlich, Steven B Marston, Kenneth T MacLeod. Age and strain related aberrant Ca^{2+} release is associated with sudden cardiac death in the ACTC E99K mouse model of hypertrophic cardiomyopathy. Accepted by AJP - Heart and Circulatory Physiology, 30th Aug 17
4. Ke H-Y, **Yang HY**, Collins TP, Alvarez-Laviada A, Surendran H, Firth JM, Francis AJ, MacLeod KT. Changes in cellular Ca^{2+} and Na^{+} regulation during the progression towards heart failure. *In preparation.*

Abstract

1. **Hsiang-Yu Yang**, Jahn M. Firth, Alice J. Francis, Anita Alvarez-Laviada, Kenneth T. MacLeod. The Effect of Ovariectomy on Calcium (Ca^{2+}) Handling in Guinea Pig Cardiomyocytes. Biophysical Journal 2017, Vol. 112, Issue 3, Supplement 1, p101a.